

ACS SYMPOSIUM SERIES **935**

Advances in Biopolymers

Molecules, Clusters, Networks, and Interactions

Marshall L. Fishman, Editor

Agricultural Research Service, U.S. Department of Agriculture

Phoebe X. Qi, Editor

Agricultural Research Service, U.S. Department of Agriculture

Louise Wicker, Editor

University of Georgia

**Sponsored by the
ACS Division of Agricultural and Food Chemistry, Inc.**



American Chemical Society, Washington, DC



Library of Congress Cataloging-in-Publication Data

American Chemical Society. Meeting (228th : 2004 : Philadelphia, Pa.)

Advances in biopolymers : molecules, clusters, networks, and interactions / Marshall L. Fishman, editor, Phoebe X. Qi, editor, Louise Wicker, editor.

p. cm.—(ACS symposium series ; 935)

“Developed from a symposium sponsored by the ACS Division of Agricultural and Food Chemistry, Inc. at the 228th National Meeting of the American Chemical Society, Philadelphia, Pennsylvania, August 22–26, 2004”—T.p. verso.

“Sponsored by the ACS Division of Agricultural and Food Chemistry, Inc.

Includes bibliographical references and index.

ISBN-13: 978-0-8412-3959-3 (alk. paper)

ISBN-10: 0-8412-3959-2 (alk. paper)

I. Biopolymers—Congresses.

I. Fishman, Marshall L., 1937– II. Qi, Phoebe X. III. Wicker, Louise. IV. American Chemical Society. Division of Agricultural and food Chemistry, Inc. V. Title. VI Series

QP801.B69A44 2004
661'.8—dc22

2006042721

The paper used in this publication meets the minimum requirements of American National Standard for Information Sciences—Permanence of Paper for Printed Library Materials, ANSI Z39.48–1984.

Copyright © 2006 American Chemical Society

Distributed by Oxford University Press

All Rights Reserved. Reprographic copying beyond that permitted by Sections 107 or 108 of the U.S. Copyright Act is allowed for internal use only, provided that a per-chapter fee of \$33.00 plus \$0.75 per page is paid to the Copyright Clearance Center, Inc., 222 Rosewood Drive, Danvers, MA 01923, USA. Republication or reproduction for sale of pages in this book is permitted only under license from ACS. Direct these and other permission requests to ACS Copyright Office, Publications Division, 1155 16th Street, N.W., Washington, DC 20036.

The citation of trade names and/or names of manufacturers in this publication is not to be construed as an endorsement or as approval by ACS of the commercial products or services referenced herein; nor should the mere reference herein to any drawing, specification, chemical process, or other data be regarded as a license or as a conveyance of any right or permission to the holder, reader, or any other person or corporation, to manufacture, reproduce, use, or sell any patented invention or copyrighted work that may in any way be related thereto. Registered names, trademarks, etc., used in this publication, even without specific indication thereof, are not to be considered unprotected by law.

PRINTED IN THE UNITED STATES OF AMERICA

Foreword

The ACS Symposium Series was first published in 1974 to provide a mechanism for publishing symposia quickly in book form. The purpose of the series is to publish timely, comprehensive books developed from ACS sponsored symposia based on current scientific research. Occasionally, books are developed from symposia sponsored by other organizations when the topic is of keen interest to the chemistry audience.

Before agreeing to publish a book, the proposed table of contents is reviewed for appropriate and comprehensive coverage and for interest to the audience. Some papers may be excluded to better focus the book; others may be added to provide comprehensiveness. When appropriate, overview or introductory chapters are added. Drafts of chapters are peer-reviewed prior to final acceptance or rejection, and manuscripts are prepared in camera-ready format.

As a rule, only original research papers and original review papers are included in the volumes. Verbatim reproductions of previously published papers are not accepted.

ACS Books Department

Preface

The necessity to better understand the functionality and nutrition of biopolymers in foods, to replace synthetic macromolecules with polymers derived from natural resources and to develop a sustainable economy has been an impetus for research on structure–function relationships and applications for these natural materials. Because of their ability to aggregate, associate, interact, and form networks, systems containing biopolymers are extremely complex and elucidating structure–function relationships in these systems is difficult. This symposium series book covers selected recent research and developments involving elucidation of networks, protein–polysaccharide interactions; and isolation, characterization, modification, and applications of biopolymers.

During the last half of the twentieth century, science has made incredible strides in instrumentation and computation. These developments have enabled scientists to investigate increasingly more complex systems. Undoubtedly, biological systems are among the most complex. As a result of these breakthroughs, information involving biopolymer aggregation, association, interactions, and network formation has escalated.

Research on the structure and function of biopolymers is being conducted by a multidisciplinary group of scientists. This book and the symposium upon which it was based were organized to engage and bring together leading scientists and technologists who are interested in or performing research in the structure and function of biopolymers. It is intended to advance this field of research by promoting the interchange of sound research ideas by a gathering of scientists with diverse interests and expertise who might not interact.

This book covers selected research on proteins and polysaccharides; therefore, there are separate overview chapters on proteins and polysaccharides. The chapter on proteins (Chapter 1) presents a new view on protein structure and how it impacts on protein folding. As an example, it is suggested in the overview how this new view of protein folding could be used to produce enhanced dairy products. The polysaccharide overview chapter (Chapter 2) reviews the structural organization of polysaccharides

with respect to molecules clusters, networks, and interactions. State-of-the-art experimental techniques are described for measuring secondary and higher order polysaccharide structures. The above-mentioned structural organizations are illustrated with various polysaccharides. In addition to the overviews, the book is divided into sections on protein structure and function, polysaccharide structure and function, and novel applications of biopolymers. The protein section deals with protein structures as they pertain to their use and potential use in leather tanning, medical devices, synthetic biofabrication materials, and natural food products. Also in this section, there is a chapter in which the mechanism of enzymatic repair of DNA is explored. The polysaccharide section has chapters on starch, pectin, and gum arabic. One chapter on starch describes how the structure of its major constituent polysaccharide, amylopectin, dictates starch granule structure whereas a second chapter describes how the architecture of the granule in combination with reaction conditions influence chemical derivatization within the starch granule. A third chapter on starch describes characterization of supramolecular structures synthesized from fragments obtained by acid degradation of potato starch. These chapters should prove useful to those who are interested in developing new value-added products from starch. Pectin chapters include basic information on the structure of pectin in solution and in sugar acid gels determined by HPSEC with light scattering and viscometric detection, electron microscopy, and atomic force microscopy; extraction and characterization of pectin from novel sources; and characterization of pectins modified by pectinmethyl-esterase isoenzymes responsible for destabilization of orange juice cloud. Collectively, these studies provide basic information that is useful in developing new pectin-based value added products. The final chapter in this section describes the isolation and characterization of an arabinogalactan protein fraction from gum, which is responsible for a significant portion of the emulsifying ability of gum. This research opens the possibility of developing new highly effective emulsifying agents. In the final section, novel applications of biopolymers are discussed. These include biodegradable electronic components, some of which could respond to external stimuli such as changes in light or temperature. Also discussed in this section are biodegradable materials that are useful for bone and tissue regeneration, biodegradable, flame retardant coatings, and hydrogels comprised of peptides, which are cytocompatible, nontoxic to fibroblast cells and promote proliferation.

This book should be of interest to chemists, biochemists, food scientists, chemical engineers, biochemical engineers and plant scientists.

Also graduate students involved in research in the aforementioned areas would be interested in reading this book. The symposium upon which it was based was organized by the editors and held at the 228th American Chemical Society (ACS) National Meeting in Philadelphia, Pennsylvania in August 2004. Twenty oral presentations were given detailing the current knowledge and new developments concerning many agriculturally and nutritionally important biopolymers.

The editors offer their appreciation and gratitude to participants, authors, and reviewers of chapters, whose dedication to science and hard work made possible the symposium and the book. We also thank the ACS Division of Agricultural and Food Chemistry, Inc. for sponsoring the symposium. Furthermore we acknowledge the generous financial support of the ACS Division of Agricultural and Food Chemistry, Inc. and CPKelco.

Marshall L. Fishman

Eastern Regional Research Center
Agricultural Research Service
U.S. Department of Agriculture
600 East Mermaid Lane
Wyndmoor PA 19038

Phoebe X. Qi

Eastern Regional Research Center
Agricultural Research Service
U.S. Department of Agriculture
600 East Mermaid Lane
Wyndmoor PA 19038

Louise Wicker

Department of Food Science and Technology
University of Georgia
Athens GA 30602

Chapter 1

New Views of Protein Structure: Implications for Potential New Protein Structure–Function Relationships

Protein Structure and Functionality

H. M. Farrell, Jr.^{1*}, P. X. Qi¹, and V. N. Uversky^{2–4}

¹Eastern Regional Research Center, Agricultural Research Service,
U.S. Department of Agriculture, 600 East Mermaid Lane,
Wyndmoor, PA 19038

²Department of Biochemistry and Molecular Biology, School of Medicine,
Indiana University, Indianapolis, IN 46202

³Institute for Biological Instrumentation, Russian Academy of Sciences,
142292 Pushchino, Moscow Region, Russia

⁴Molecular Kinetics, 6201 La Pas Trail, Suite 160, Indianapolis, IN 46268

Recent advances in the field of protein chemistry have significantly enhanced our understanding of the possible intermediates which may occur during protein folding and unfolding. In particular, studies on α -lactalbumin have led to the theory that the molten globule state may be one possible intermediate in the folding of many proteins. The molten globule state is characterized by a compact structure, a high degree of hydration and side chain flexibility, a significant amount of native secondary structure but little tertiary structure, and the ability to react with chaperones. Other partially folded conformations (e.g., pre-molten globule) have also been found. Many proteins known as natively unfolded, intrinsically unstructured, or intrinsically disordered were shown to be highly flexible under physiological conditions. By taking advantage of this “new view” of protein folding, and applying these concepts to engineered macromolecules and food proteins, it may be possible to generate new and useful forms of proteins for the food ingredient, pharmaceutical and nanotechnological markets.

Introduction

The recent announcement that the human genome has been solved, represents not an end in itself, but a beginning. It is now the work of the protein chemists and structural biologists to translate this linear sequence information into the functional molecular shapes necessary to make significant breakthroughs in biological applications. This task is currently underway, and by the union experimental and theoretical protein studies, we may soon be able to fully understand how a protein structure relates to its biological function. Basic studies on the protein folding problem, are already producing a wealth of fundamental information (1-7). We must now render this information into new food and technological applications. It has long been known that changing protein structure can alter food functionality. We have often previously thought of these changes as all (completely unfolded) or nothing (completely native) events. The latest research, however, demonstrates a multiplicity of stages in protein folding (unfolding) pathways. The energy profiles suggest that these "molten globule" (1) and "pre-molten globule" states (7) may be stable under certain conditions. If this is the case, then a single whey protein such as α -lactalbumin may have a myriad of stable intermediate stages which could be "trapped" and thus provide the potential for new functional properties. Similar applications to the major milk proteins (the caseins) are urgently needed. As food protein chemists we must also recall that while native structure arises from sequence, processing treatment has the potential to transform native structure into non-native states. Furthermore, some proteins were shown to avoid complete folding, existing instead as dynamic ensembles of interconverting partially folded structures. This latter fact represents both a challenge and an opportunity, as denatured, or partially denatured proteins, may serve as either a problem or a potentially valuable food ingredient. Examples of these opportunities for the development of novel protein ingredients are given for α -lactalbumin (α -LA) as "food for thought".

Historical Background of Protein Folding

Historically, the central dogma of structural biology is the Anfinsen hypothesis: the linear primary sequence of amino acids of a protein codes for rather specific secondary structural elements, which in turn lead to protein folding and tertiary structure, and ultimately to quaternary structure for complex higher order systems (8). There has been considerable debate in recent years, folding and tertiary structure, and ultimately to quaternary structure for complex higher order systems (8). There has been considerable debate in recent years, not

so much on the veracity of the Anfinsen hypothesis, but on the details of the folding mechanisms which bring about protein structure. This debate arises, in part, because until very recently our best information on protein folding came from unfolding studies on small and relatively simple proteins (9). For example, the early studies on lysozyme, as summarized by Arai and Kuwajima (2), indicated a concerted mechanism by which loss of enzyme activity and loss of structure followed nearly similar curves. Figure 1 represents the typical sigmoidal curve found for lysozyme unfolding induced by guanidine HCl showing loss of structure; this was coincident with loss of enzymatic function (2). These and many other studies could be summarized in eq 1.

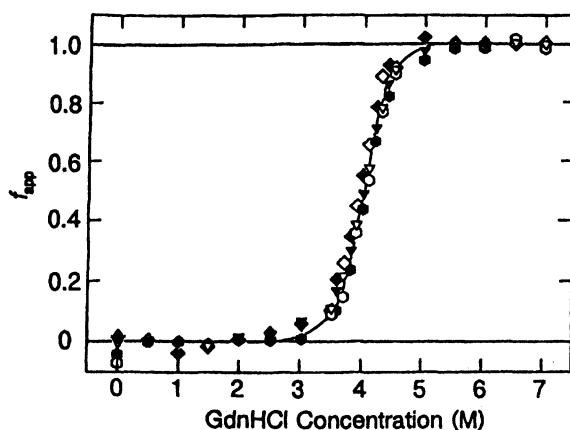


Figure 1. Guanidine HCl induced unfolding of lysozyme showing coincident loss of enzyme activity and of structure by as measured by f_{app} , the apparent fraction denatured. Open symbols represent NaCl only and closed represent NaCl + CaCl₂. Changes in CD were monitored at 289 nm (\square , Δ) 255 nm (\bullet , \circ) and 222 nm (\blacktriangledown , \triangledown). Data from Arai and Kuwajima (2) reproduced courtesy of Academic Press, San Diego, CA. Copyright 2000.

By inference, protein folding was thought to be the reverse reaction. Indeed the argument was made that kinetically the two processes might be microscopically reversible, and that the native state could represent a singular folded state with minimum potential energy.

α -Lactalbumin and the Molten Globule State

The "new view" of protein folding began to emerge, in part, from experimental observations on the milk Ca^{2+} -binding protein, α -lactalbumin (α -LA) (10, 11). Physical studies on this protein appeared to indicate that some measurable structural loss might occur at different stages in the unfolding process. Conventional Fourier transform infrared (FTIR) and far-UV circular dichroism (CD) spectroscopies are used to follow losses of secondary structural elements, but near-UV CD can also provide important information on protein tertiary structure. In a typical globular protein, steric restrictions as well as hydrogen bonding can limit the mobility of aromatic side chains such as Trp, Tyr and Phe, thus causing a near-UV CD spectra. Unrestricted rotation of aromatic groups does not in general give rise to a CD spectrum. Figure 2 shows that for guanidine denaturation of α -LA, loss of aromatic dichroism preceded loss of secondary structure. In a similar fashion the typical near-UV CD spectra of bovine α -LA is diminished at elevated temperatures (2) or low pH (11). The near-UV CD spectrum is significantly diminished at 50°C, whereas measures of changes in secondary structure reveal higher transition temperatures.

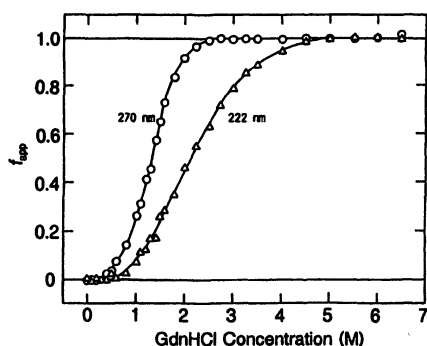


Figure 2. Guanidine HCl induced unfolding of α -LA; the f_{app} (fraction denatured) shows non-coincident loss of protein structure by CD. Loss of aromatic dichroism was measured at 270 nm (o); loss of α -helix was followed at 222 nm (Δ). Figure as credited in Figure 1.

Differential scanning calorimetry (DSC) studies of α -LA by Dolgikh *et al.* (11) showed that the denaturation temperature is about 60°C (Figure 3). When Ca^{2+} is removed from α -LA there is a loss of tertiary structural stability and the denaturation temperature lowers to about 20°C (Figure 3). Curiously, on acid denaturation at pH 2.0, much secondary structure is retained but a complete loss of the characteristic thermal transition of α -LA occurs (dotted line, Figure 3). The lack of coincidence of loss of aromatic CD and secondary structure began the search for a broader meaning of eq 1.

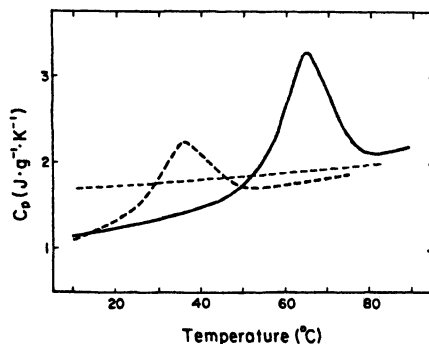


Figure 3. Dependence of partial heat capacity (C_p) on temperature for α -LA as holoprotein (—) apoprotein (dark dashed line) and acid denatured protein (flat, light dashed line). Data from Dolgikh et al. (12) reproduced courtesy of Springer-Verlag Heidelberg, Germany.

Friere and his colleagues (13) introduced the concept of 3D DSC by which the temperature of denaturation was studied as a function of guanidine concentration. Surprisingly, 1 M guanidine alleviated almost all of the typical enthalpic thermal transition found for α -LA in the absence of guanidine, yielding a DSC pattern similar to that found at pH 2.0 (Figure 3). From the data of Figure 2, it can be seen that at 1 M guanidine, there has been some change in the near-UV CD spectrum, but little change in secondary structure. Studies on many other proteins now reveal that multi-step mechanisms of protein unfolding may be the rule, rather than the exception (1, 14). The condition in which a partially denatured protein may exhibit a high degree of segmental motion (*i.e.*, loss of aromatic dichroism) while retaining a significant amount of secondary structure has been termed the molten globule state, but this too turns out to be an over simplification as we shall see.

Multi-State Unfolding of Globular Proteins and Pre-Molten Globule State

Subsequent studies revealed that the molten globule is a member of the realm of partially folded conformations as globular proteins may exist in at least four different conformations: native (ordered), molten globule, pre-molten globule, and unfolded (1, 7, 15). For example, using a combination of several spectroscopic techniques, such as intrinsic and ANS fluorescence, near- and far-UV CD spectra, with size exclusion chromatography it has been shown that the equilibrium GdmCl-induced unfolding of β -lactamase (16), carbonic anhydrase (17), creatine kinase (18), and NAD⁺-dependent DNA-ligase from *Thermus scotoductus* (19) is a sequential process, which involves the formation of at least

two partially folded intermediates, molten globule (MG) and pre-molten globule (PMG) states. Figure 4 summarizes the results of these studies for DNA-ligase and visualizes the four-state $N \leftrightarrow U$ transition by plotting fractions of molecules in all four states (N, MG, PMG, and U) as functions of GdmCl concentrations. The plot illustrates how the molten globule state appears in the first step of unfolding at the expense of native proteins, and how it transforms first into the pre-molten globule and then into the unfolded state (19).

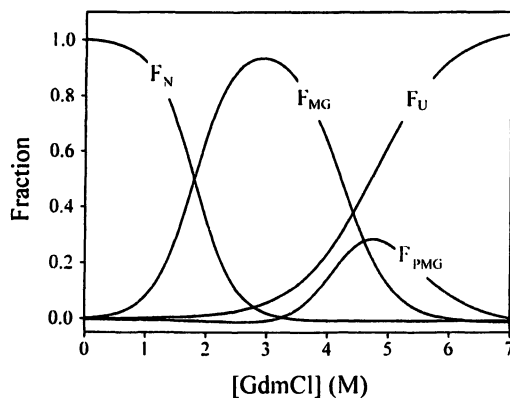


Figure 4. Multi-state guanidine HCl-induced unfolding of NAD⁺-dependent DNA-ligase from *Thermus scotoductus* presented in terms of the fractions of different conformations; f_N is fraction of molecules in the native state, f_{MG} the fraction in the molten-globule state, f_{PMG} the fraction in the pre-molten globule state and f_U the fraction in the unfolded state. The fractions of different conformations were calculated from changes induced by guanidine HCl in aromatic dichroism (ellipticity at 280 nm), secondary structure content (ellipticity at 220 nm), intrinsic fluorescence, ANS fluorescence and chromatographic behavior. Figure modified from Georlette et al. (19).

Major structural properties of the polypeptide chain in the molten globule and pre-molten globule conformations are outlined below. A protein molecule in the molten globule state has no (or only a trace of) rigid cooperatively melted tertiary structure; *i.e.*, it is denatured. Small-angle X-ray scattering showed that the protein molecule in this intermediate state has a globular structure typical of native globular proteins (20-25). 2D NMR showed that the protein molecule in the molten globule state might have native-like secondary structure and a native-like folding pattern (26-33). A considerable increase in the accessibility of a protein molecule to proteases was noted as a specific property of the molten globule state (34, 35). It has also been shown that a molten globule possesses high affinity to the hydrophobic fluorescence probes (such as 8-

anilinonaphthalene-1-sulfonate, ANS), and this behavior should be considered as a characteristic property of this intermediate state (36, 37). Finally, it has been established that the hydrodynamic radius of the molten globule state is only ~15% greater than that of the native state, which corresponds to the volume increase of ~50% (7, 38, 39).

The protein molecule in the pre-molten globule state is definitely denatured; *i.e.*, it has no rigid tertiary structure. It is characterized by a considerable secondary structure, although much less pronounced than that of the native or the molten globule protein. The protein molecule in the pre-molten globule state is considerably less compact than in the molten globule or native states, but it is still more compact than the random coil. The pre-molten globule can effectively interact with the hydrophobic fluorescent probe ANS, though essentially weaker than the molten globule does. This means that at least a part of the hydrophobic clusters of polypeptide chain accessible to the solvent is already formed in the pre-molten globule state. It has been also established that the pre-molten globule does not have globular structure, assuming that this conformation probably represents a “squeezed” and partially ordered form of a coil. Finally, it has been shown that the pre-molten globule is separated from the molten globule state by an all-or-none-transition, which represents an intramolecular analog of the first order phase transition (7, 39-41).

One of the most characteristic features of partially folded conformations is their combination of properties typical of native and completely unfolded states. In fact, in compact non-native conformation, such as the molten globule, a protein molecule preserves the main features of the native folding pattern, but has considerably increased flexibility. These properties appear almost ideal for a protein in a living cell, which must adjust itself to a large set of different conditions – in the cytoplasm, near or inside membranes, in cell organelles, etc. Some of these conditions are denaturing ones (1), assuming that non-folded states of globular proteins may be presented in a living cell and may be involved in a number of physiological processes (42-46).

As we shall see below, this knowledge accumulated as a result of exhaustive studies on protein folding played an important role in understanding the recently discovered phenomenon of protein intrinsic disorder and in structural classification of different natively non-folded proteins.

How Random is a Random Coil?

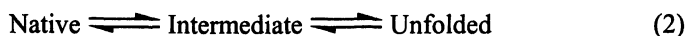
The next very important question is related to the structure of unfolded polypeptide chain. It has long been assumed that in the presence of high concentrations of strong denaturants proteins completely lose all elements of their tertiary and secondary structures, and become completely unfolded which resemble random coil. The unfolded state represents an ensemble of rapidly interchanging conformations, some of which are extended, and some more

compact. It is possible that when stabilizing interactions occur they induce a more populated ensemble of chain conformations, and, if such structures do exist in the unfolded state, they would probably guide the folding process and function as folding-initiation sites (47). It is important to mention that theoretical studies have shown that small preferences for native-like interactions in the unfolded state will substantially increase the probability of reaching the native state (48).

In agreement with these hypotheses a great many protein-folding studies revealed the presence of an assured residual structure even under the most severe denaturing conditions, such as high concentrations of strong denaturants. It has been unambiguously shown that the existence of profound residual structure might be considered as a general characteristic of the unfolded polypeptide chain under aggressively denaturing conditions (49-53). In other words, unfolded states of proteins exhibit behavior that is not random coil in nature, which is not surprising considering the complexity of polypeptide chains. In fact, it has been pointed out that a total lack of intra-residue interactions would be unexpected in the unfolded state, because certain (e.g., hydrophobic) side chains have high affinity for each other in a folded protein (54). In addition, some secondary structure within an unfolded protein could be expected due to the preferential distribution of phi and psi angles (55-57) and some residual hydrophobic interactions can also be present (54, 58). All this considerably restricts the conformational space of an unfolded polypeptide chain.

Energy Landscape Theory

The idea that a protein may unfold through a multi-step process in turn leads to the "new view" of protein folding, according to which, a significant amount of conformational space may be "sampled" by a polypeptide chain undergoing folding before it settles into a global energy minimum. It has been also suggested that several false minima may lay quite close or even somewhat remotely removed from the true global minimum. The important prediction here is that eq 1 can now be modified:



where the intermediate stage may be represented by a multiplicity of macroscopic states or ensembles. Studies on multistate protein unfolding further expand the nomenclature of eq 2 to include PMG, which energetically located above the MG state. PMG and MG may interconvert with each other and the totally unfolded (U) state. The complexity of this picture offers an enormous challenge to the study of protein folding. Conversely, a myriad of states in unfolding can represent an enormous opportunity for food protein chemists, as

stable folding intermediates or partially unfolded proteins may offer new food functionality. This is not to say that there are a limitless number of possible denatured conformational states for a protein or that the native state is without mobility or internal motion. So these concepts offer the possibility of generating new protein-based products with altered biological or nutraceutical activity or new food functionality.

Introducing Intrinsic Disorder Phenomenon

Many proteins have been shown to lack rigid 3-D structure under physiological conditions *in vitro*, existing instead as dynamic ensembles of interconverting structures. These proteins are known by different names, including intrinsically disordered, natively flexible, intrinsically unstructured, natively unfolded, etc. Intrinsic disorder here refers to a protein exists as a structural ensemble. In other words, in contrast to an ordered protein whose 3-D structure is relatively stable and Ramachandran angles vary slightly around their equilibrium positions with occasional cooperative conformational switches, intrinsically disordered proteins or regions exist as dynamic ensembles in which the atom positions and backbone Ramachandran angles vary significantly over time with no specific equilibrium values and typically undergo non-cooperative conformational changes (59). Both extended (random coil-like) regions with perhaps some fluctuating elements of secondary structure and collapsed (partially folded or molten globule-like) domains with poorly packed side chains are included in this view of intrinsic disorder (60).

As a reflection of this new view, Wright and Dyson (61) pointed out that the number of unfolded proteins being reported might require a reassessment of the structure/function paradigm. It is now recognized that many proteins, being intrinsically disordered (ID), are unable to form truly compact globular structures and may reside permanently in open states that resemble the molten globule state, *i.e.*, “native molten globules” (60). Other proteins may be intrinsically less compact and permanently reside in conformational space above the molten globule state. These latter proteins were classified as natively unfolded (NU) (62) and intrinsically unstructured proteins (IUP) (4). That is not to say that these proteins are disordered random coils, but rather pliable proteins whose structures, are indeed a requisite of their biological function (in accord with the Anfinsen hypothesis). In a series of studies, Uversky (5) also pointed out that a significant number of NU proteins do display residual structure and suggested two distinct classifications for them, coil-like (NU_{coil}) and PMG-like (NU_{PMG}). In addition he included several quantitative measurements for determining the states in which a protein may reside (5, 63).

Currently, the literature on intrinsically disordered proteins is virtually exploding (59, 61, 64, 65). This explosion is consistent with bioinformatics studies indicating that about 25 to 30% of eukaryotic proteins are mostly

disordered (66), that more than half of eukaryotic proteins have long regions of disorder (66, 67), and that more than 70% of signaling proteins have long disordered regions (68). It has been established that despite the fact that intrinsically disordered proteins fail to form fixed 3D-structures under physiological conditions, they carry out numerous important biological functions (61-63, 65, 68-70). For example, in a living organism, proteins are involved in complex interactions, which represent the mechanistic foundation for much of the organism's physiology and function. Regulation, recognition and cell signaling involve the coordinated actions of many players. To achieve this coordination, each participant must have a valid identification that is easily recognized by the others. For proteins, these identification signs are often within intrinsically disordered regions (59). Thus, intrinsically disordered regions are typically involved in regulation, signaling and control pathways in which interactions with multiple partners and high-specificity/ low-affinity interactions are often requisite. In this way, the functional diversity provided by disordered regions complements those of ordered protein regions.

Many protein-protein and protein-nucleic acid interactions involve coupled folding and binding of at least one of the partners (61, 63, 64, 68, 70). These function-associated conformational changes may be brought about by alterations in environmental or cellular conditions (e.g. disorder-to-order transition upon binding during signal transduction). Overall, it is suggested that the functions of disordered proteins may arise from a specific disorder form, an interconversion of disordered forms, or transitions between disordered and ordered conformations (69, 71).

Several laboratories base their research on intrinsic disorder and apply it to answer questions and identify mechanisms that the classical lock-and-key model alone could not answer. Function arises not only from strictly structured proteins, but also from disordered proteins and transitions between ordered and disordered in both directions. These observations resulted in the development of the Protein Trinity model (71), which suggests function ascends from three distinct states (ordered, molten globule and random coil) and transitions between them. This model has subsequently been expanded to include a fourth state (pre-molten globule) and transitions between all four states (5). Recently, more than 150 proteins have been identified as proteins that contain functional disordered regions, including proteins that are completely disordered, yet perform vital cellular roles (69, 72). Furthermore, twenty-eight separate functions were identified for these disordered regions, with numerous disordered regions implicated in molecular recognition via binding to other proteins, or to nucleic acids (69). Others believe that functional disorder fits better into at least five broad classes based on their mode of action (4, 73). These broad classes include entropic chains, effectors, scavengers, assemblers and display sites. Recent research added chaperones to this list (74). Obviously,

for these proteins, the predominant structure-function paradigm is insufficient, suggesting a more comprehensive view of the protein structure/function relationships is needed. In fact, a new paradigm has been recently proposed (5, 60, 63, 71) to elaborate the sequence-to-structure-to-function scheme in a way that includes the novel functions of disordered proteins.

Thus, intrinsically disordered proteins exist as dynamic structural ensembles without a fixed tertiary structure. There is evidence that many of these flexible proteins or regions undergo disorder-to-order transitions upon binding (64). A large decrease in conformation entropy accompanies disorder-to-order transition, which uncouples specificity from binding strength. This phenomenon has the effect of making highly specific interactions easily reversible, which is beneficial for cells, especially in the inducible responses typically involved in signaling and regulation.

Overall, intrinsic protein disorder is a widespread phenomenon and intrinsically disordered proteins (also known as natively unfolded or intrinsically unstructured proteins) are involved in a number of important biological functions. These proteins form a realm of structurally diverse conformations which includes native molten globules, native pre-molten globule, and native coils.

Hydration and Stability of the Newly Defined Partially Folded States

The typical molten globule state is more open than the native state, but still represents a compact structure (1). The increased flexibility of the side chains and the backbone leads to an influx of water, so that the molten globule state is rather highly hydrated (24). This water does not represent an increase in bound water, but rather a type of protein influenced or "trapped but exchangeable" water such as that studied by NMR relaxation techniques (75). In addition, the loosely packed side chains may emphasize the importance of solvent-separated hydrophobic interactions in the molten globule state, whereby a water molecule separating two hydrophobic residues lends a small degree of stabilization to the protein structure. IUPs, including NU_{PMG} and NU_{coil} are more open than the molten globule state and therefore have an even greater propensity for water hydration. In fact, this conclusion has been recently supported using solid-state NMR relaxation measurements, where by freezing nonhydrate (bulk) water out it has been shown that IUPs bind a significantly larger amount of water than globular proteins (76).

Three Dimensional Structures and Molecular Modeling Studies

To explore the range of possible states of denaturation available for the milk protein, α -LA, a series of rapid molecular dynamics (MD) simulations in

vacuo has been conducted. These simulations mimic the action that heat or shear would have on the folded polypeptide chain. In essence, by adding energy to the model, we shift the molecular energy profile from bottom to top. We used the bovine α -LA protein data base code 1HFZ, which contains bound Ca^{2+} (holoprotein), and compared it to the same structure with the Ca^{2+} removed (apoprotein). The MD simulations were conducted at 5° and 298°K for the apo and holo forms. The 5°K simulation for the holoprotein in vacuo rapidly came to equilibrium (overnight) as judged by the change of the radius of gyration (R_g) with time. Similar curves were obtained for the other simulations. This equilibrium position implies that a partially folded intermediate might represent a stable trap somewhere near the middle of the energy landscape representing the protein folding. Comparisons of two of the models generated for the apoprotein form of α -LA by the MD simulations with α -LA are shown in Figure 5. Here it can be seen that removal of Ca^{2+} followed by MD results in two different unfolded states at two different temperatures. The analyses of these models are presented in Table I, where they are compared with experimental small-angle X-ray (SAXS) data for bovine α -LA. The R_g at 5°K increased from 14.3 to 18.4 Å, which is comparable to the overall change found for MD simulations of human α -LA carried out for days by including water molecules in the calculation (explicit water) (19). However, it must be noted that secondary structure was rapidly lost in our simulations, whereas in the human α -LA in water, secondary structure was reasonably constant.



Figure 5. Rapid MD simulations of the apoprotein form of α -LA in vacuo, showing the native holo state (left) and the effect of simulations at 5°K and 298°K (center and right respectively) of the apoform.

As noted above, a number of quantitative measures for the classification of protein states were presented (7). One such measure is the relationship of protein hydrodynamic volume to sequence length. In essence a folded globular protein such as α -LA will have a much smaller hydrated volume than it would in the denatured state. Interestingly, the molecular mass dependencies for the

hydrodynamic volumes of MGs and PMGs were shown to be described by separate equations (5). Using the R_g values given in Table I along with Uversky's regression analyses, it is possible to classify that the states produced by the molecular dynamics simulations as N, MG, PMG, and U, as shown in Table I. As expected the experimentally derived states agree well with the calculations (N, MG, and U). The rapid simulation of the holoprotein at 5K produced a molecule only slightly larger than the MG state, and at 298K formed a PMG state. The apoprotein, however, at 5K passed through the MG state to the PMG state and then to the U state at 298K. Using these techniques it is possible to rapidly examine new surfaces created by partial denaturation in each state. Note that removal of the Ca^{2+} ion leads to greater destabilization of the molecule. This is in accord with experimental data which show in DSC, a much

Table I. Comparison of Molecular Dynamics Simulated R_g Values with Experimental Data and Uversky's Classifications^a

α -LA form	R_g (Å)	Uversky classification ^a
Experimental ^b		
Native	15.7	N
Molten globule	17.2	MG
Urea unfolded	30.0	U
Molecular Dynamics		
Holo-protein	14.3	N
3.5 ps 5°K	18.4	MG
40 ps 298°K	21.9	PMG
Apo-protein	14.3	N
1.5 ps 5°K	21.4	PMG
20 ps 298°K	31.6	U

^aUversky (5). N = native state, MG = molten globule state, U = urea denatured, PMG = pre-molten globule.

^bKataoka (23) by SAXS.

lowered temperature of denaturation for the apoprotein (Figure 3). These simulations also demonstrate the outer limits for denaturation of the protein with and without Ca^{2+} and in the absence of disulfide rupture. In addition, they also suggest that the bovine α -LA would have more new surface aromaticity for protein-protein interactions upon partial denaturation even without disulfide rupture. These new hydrophobic contacts could lead to new potential protein

products from whey isolates. Such products could have nutraceutical or nanotechnological applications.

Partial Denaturation and Aggregation vs. Functional Self-Association

From the perspective of protein folding, association represents a natural process whereby multimeric complexes (*i.e.*, functional ultrastructures) are formed from the structured monomers. Thus, protein-protein interactions which lead to biologically competent structures exemplify the functional self-association (6). In contrast, protein-protein interactions involving MG or other conformations of globular proteins, as well as different categories of IUPs and IDPs may lead to non-competent structures. This phenomenon is known as aggregation as defined by Jaenicke and Lilie (6). Many amyloid or conformational disorders such as Alzheimer's, Parkinson's, and Huntington's disease, numerous neurodegenerative disorders, systemic amyloidosis and many others may arise, in part, from such aggregation of structurally altered proteins (77). At first glance, these folding variants could be viewed as detrimental to the assembly of biological structures for IUPs and ID proteins. However it has been pointed out that the innate pliability of these proteins or protein regions does often play a significant role in protein function and might be responsible for "on-line" biological assemblages (5, 59, 61, 62, 65, 69, 78). IUPs and IDPs appear to have rather diverse functionalities (see above); they may engage in co-folding with other proteins, bind to a membrane surface, interact with other macromolecules, bind metal ions or metabolites, and react with DNA or RNA.

The results of MD simulations described above suggest that many new contact areas for protein-protein interactions may be available in a partially denatured state such as MGs or upon further denaturation as demonstrated in Figure 6 for α -LA. In fact Goers *et al.* (79) have reported that α -LA formed amyloid fibrils from its MG state and reduced S-carboxymethylated (RCM) α -LA has an even greater propensity for fibril formation. In addition, research on human α -LA has demonstrated that structurally altered forms of the protein may bind oleic acid, refold and serve as anti-tumor and anti-bacterial agents (80, 81). These experiments demonstrate clearly that partial denaturation of α -LA with and without Ca^{2+} could lead to new and potentially interesting food ingredients, nutraceuticals or nanostructures capable of binding metal ions.

Conclusion

In conclusion, as the field of structural biology evolves, we will learn more about the basic structures of the milk proteins. Perhaps 2D X-ray

crystallography or EM reconstruction may yield higher resolution models of globular proteins in these new intermediate states, possibly even at the atomic level. However, as the field progresses, we need to be aware of the opportunities these advances present for enhancement of dairy products or for adaptation of milk proteins as food ingredients. For example:

1. Increased hydration which does not represent an increase in bound water, but rather a type of protein influenced or "trapped but exchangeable" water could lead to new ingredients for intermediate moisture foods.
2. New hydrophobic contacts as seen in Figure 6, could lead to new potential protein products from whey isolates for applications in snack foods.
3. Goers *et al.* (79) have reported that α -LA and its RCM form can form amyloid fibrils from its MG state it may be possible to produce nanofibrils from these proteins which upon binding metal ions yield novel products for nanotechnology.
4. Research on human α -LA has demonstrated that structurally altered forms of the protein may bind oleic acid, refold and serve as anti-tumor and anti-bacterial agents (80, 81).

To more fully take advantage of the unique properties of the milk proteins, we will need new alternative and cost effective means of fractionation. In addition, new insights into present processing methodologies will be required to yield innovative processes needed for future applications. So we are at the beginning of an exciting era in protein chemistry and hopefully food technology. The question now arises, how can this "new view" be applied to casein structure? This will be addressed in the following chapter.

References

1. Ptitsyn, O. B. *Adv. Protein Chem.* **1995**, *47*, 83-229.
2. Arai, M.; Kuwajima, K. *Adv. Protein Chem.* **2000**, *53*, 209-282.
3. Dyson, H. J.; Wright, P. E. *Adv. Protein Chem.* **2002**, *62*, 311-340.
4. Tompa, P. *Trends Biochem. Sci.* **2002**, *27*, 527-533.
5. Uversky, V. N. *Protein Sci.* **2002**, *11*, 739-756.
6. Jaenicke, R.; Lilie, H. *Adv. Protein Chem.* **2000**, *53*, 329-401.
7. Uversky, V. N. *Cell. Mol. Life Sci.* **2003**, *60*, 1852-1871.
8. Anfinsen, C. B. *Science* **1973**, *181*, 223-230.
9. Tanford, C. *Adv. Protein Chem.* **1968**, *23*, 121-282.
10. Kuwajima, K.; Nitta, K.; Yoneyama, M.; Sugai, S. *J. Mol. Biol.* **1976**, *106*, 359-373.
11. Dolgikh, D. A.; Gilmanishin, R. I.; Brazhnikov, E. V.; Bychkova, V. E.; Semisotnov, G. V.; Venyaminov, S. Y.; Ptitsyn, O. B. *FEBS Lett.* **1981**, *136*, 311-314.

12. Dolgikh, D. A.; Abaturon, L. V.; Bolotina, I. A.; Brazhnikov, E. V.; Bychkova, V. E.; Gilmanshin, R. I.; Lebdev, Y. O.; Semisotnov, G. V.; Tiktopulo, E. I.; Ptitsyn, O. B. *Eur. Biophys. J.* **1985**, *13*, 109-121.
13. Xie, D.; Bhakuni, V.; Freire, E. *Biochemistry* **1991**, *30*, 10673-10678.
14. Bychkova, V. E.; Ptitsyn, O. B. *Biofizika* **1993**, *38*, 58-66.
15. Uverskii, U. N. *Biofizika* **1998**, *43*, 416-421.
16. Uversky, V. N.; Ptitsyn, O. B. *Biochemistry* **1994**, *33*, 2782-2791.
17. Uversky, V. N.; Ptitsyn, O. B. *J. Mol. Biol.* **1996**, *255*, 215-228.
18. Kuznetsova, I. M.; Stepanenko, O. V.; Turoverov, K. K.; Zhu, L.; Zhou, J. M.; Fink, A. L.; Uversky, V. N. *Biochim. Biophys. Acta* **2002**, *1596*, 138-155.
19. Georlette, D.; Blaise, V.; Bouillenne, F.; Damien, B.; Thorbjarnardottir, S. H.; Depiereux, E.; Gerday, C.; Uversky, V. N.; Feller, G. *Biophys. J.* **2004**, *86*, 1089-1104.
20. Uversky, V. N.; Karnoup, A. S.; Segel, D. J.; Seshadri, S.; Doniach, S.; Fink, A. L. *J. Mol. Biol.* **1998**, *278*, 879-894.
21. Tcherkasskaya, O.; Uversky, V. N. *Proteins* **2001**, *44*, 244-254.
22. Semisotnov, G. V.; Kihara, H.; Kotova, N. V.; Kimura, K.; Amemiya, Y.; Wakabayashi, K.; Serdyuk, I. N.; Timchenko, A. A.; Chiba, K.; Nikaido, K.; Ikura, T.; Kuwajima, K. *J. Mol. Biol.* **1996**, *262*, 559-574.
23. Kataoka, M.; Kuwajima, K.; Tokunaga, F.; Goto, Y. *Protein Sci.* **1997**, *6*, 422-430.
24. Kharakoz, D. P.; Bychkova, V. E. *Biochemistry* **1997**, *36*, 1882-1890.
25. Eliezer, D.; Chiba, K.; Tsuruta, H.; Doniach, S.; Hodgson, K. O.; Kihara, H. *Biophys. J.* **1993**, *65*, 912-917.
26. Baum, J.; Dobson, C. M.; Evans, P. A.; Hanley, C. *Biochemistry* **1989**, *28*, 7-13.
27. Bushnell, G. W.; Louie, G. V.; Brayer, G. D. *J. Mol. Biol.* **1990**, *214*, 585-595.
28. Chyan, C. L.; Wormald, C.; Dobson, C. M.; Evans, P. A.; Baum, J. *Biochemistry* **1993**, *32*, 568-591.
29. Jeng, M. F.; Englander, S. W.; Elove, G. A.; Wand, A. J.; Roder, H. *Biochemistry* **1990**, *29*, 10433-10437.
30. Wu, L. C.; Laub, P. B.; Elove, G. A.; Carey, J.; Roder, H. *Biochemistry* **1993**, *32*, 10271-10276.
31. Eliezer, D.; Yao, J.; Dyson, H. J.; Wright, P. E. *Nat. Struct. Biol.* **1998**, *5*, 148-155.
32. Bose, H. S.; Whittal, R. M.; Baldwin, M. A.; Miller, W. L. *Proc. Natl. Acad. Sci. USA* **1999**, *96*, 7250-7255.
33. Bracken, C. *J. Mol. Graph. Model.* **2001**, *19*, 3-12.
34. Fontana, A.; Polverino de Laureto, P.; De Filippis, V.; Scaramella, E.; Zambonin, M. *Fold. Des.* **1997**, *2*, R17-26.

35. Polverino de Laureto, P.; De Filippis, V.; Di Bello, M.; Zambonin, M.; Fontana, A. *Biochemistry* **1995**, *34*, 12596-12604.
36. Semisotnov, G. V.; Rodionova, N. A.; Razgulyaev, O. I.; Uversky, V. N.; Gripas, A. F.; Gilmanshin, R. I. *Biopolymers* **1991**, *31*, 119-128.
37. Uversky, V. N.; Winter, S.; Lober, G. *Biophys. Chem.* **1996**, *60*, 79-88.
38. Uversky, V. N. *Biochemistry* **1993**, *32*, 13288-13298.
39. Uversky, V. N. *Protein Pept. Lett.* **1997**, *4*, 355-367.
40. Tcherkasskaya, O.; Uversky, V. N. *Protein Pept. Lett.* **2003**, *10*, 239-245.
41. Tcherkasskaya, O.; Davidson, E. A.; Uversky, V. N. *J. Proteome Res.* **2003**, *2*, 37-42.
42. Bychkova, V. E.; Pain, R. H.; Ptitsyn, O. B. *FEBS Lett.* **1988**, *238*, 231-234.
43. Uversky, V. N.; Narizhneva, N. V. *Biochemistry (Mosc)* **1998**, *63*, 420-433.
44. Bychkova, V. E.; Berni, R.; Rossi, G. L.; Kutysenko, V. P.; Ptitsyn, O. B. *Biochemistry* **1992**, *31*, 7566-7571.
45. Narizhneva, N. V.; Uversky, V. N. *Protein Pept. Lett.* **1997**, *4*, 243-249.
46. Uversky, V. N.; Narizhneva, N. V.; Ivanova, T. V.; Tomashevski, A. Y. *Biochemistry* **1997**, *36*, 13638-13645.
47. Baldwin, R. L. *Trends Biochem. Sci.* **1986**, *11*, 6-9.
48. Finkelstein, A. V.; Galzitskaya, O. V.; Badretdinov, A. Y. *Prog. Biophys. Mol. Biol.* **1996**, *65*, A412.
49. Shortle, D. *Curr. Opin. Struct. Biol.* **1996**, *6*, 24-30.
50. Dill, K. A.; Shortle, D. *Annu. Rev. Biochem.* **1991**, *60*, 795-825.
51. Pappu, R. V.; Srinivasan, R.; Rose, G. D. *Proc. Natl. Acad. Sci. U S A* **2000**, *97*, 12565-12570.
52. Baldwin, R. L.; Zimm, B. H. *Proc. Natl. Acad. Sci. U S A* **2000**, *97*, 12391-12392.
53. Plaxco, K. W.; Gross, M. *Nat. Struct. Biol.* **2001**, *8*, 659-660.
54. Hammarstrom, P.; Carlsson, U. *Biochem. Biophys. Res. Commun.* **2000**, *276*, 393-398.
55. Shortle, D. *Adv. Protein Chem.* **2002**, *62*, 1-23.
56. Smith, L. J.; Fiebig, K.M., Schwalbe, H., Dobson, C.M. *Fold. Des.* **1996**, *1*, R95-106.
57. Ramachandran, G. N.; Sasisekharan, V. *Adv. Protein Chem.* **1968**, *23*, 283-438.
58. Shimizu, S.; Chan, H. S. *Proteins* **2002**, *49*, 560-566.
59. Uversky, V. N.; Oldfield, C. J.; Dunker, A. K. *J. Mol. Recognit.* **2005**, *18*, 343-384.
60. Dunker, A. K.; Lawson, J. D.; Brown, C. J.; Williams, R. M.; Romero, P.; Oh, J. S.; Oldfield, C. J.; Campen, A. M.; Ratliff, C. M.; Hipps, K. W.; Ausio, J.; Nissen, M. S.; Reeves, R.; Kang, C.; Kissinger, C. R.; Bailey, R.

- W.; Griswold, M. D.; Chiu, W.; Garner, E. C.; Obradovic, Z. *J. Mol. Graph. Model.* **2001**, *19*, 26-59.
61. Wright, P. E.; Dyson, H. J. *J. Mol. Biol.* **1999**, *293*, 321-331.
 62. Uversky, V. N.; Gillespie, J. R.; Fink, A. L. *Proteins* **2000**, *41*, 415-427.
 63. Uversky, V. N. *Eur. J. Biochem.* **2002**, *269*, 2-12.
 64. Dyson, H. J.; Wright, P. E. *Curr. Opin. Struct. Biol.* **2002**, *12*, 54-60.
 65. Dyson, H. J.; Wright, P. E. *Nat. Rev. Mol. Cell. Biol.* **2005**, *6*, 197-208.
 66. Oldfield, C. J.; Cheng, Y.; Cortese, M. S.; Brown, C. J.; Uversky, V. N.; Dunker, A. K. *Biochemistry* **2005**, *44*, 1989-2000.
 67. Dunker, A. K.; Obradovic, Z.; Romero, P.; Garner, E. C.; Brown, C. J. *Genome Inform. Ser. Workshop Genome Inform.* **2000**, *11*, 161-171.
 68. Iakoucheva, L. M.; Brown, C. J.; Lawson, J. D.; Obradovic, Z.; Dunker, A. K. *J. Mol. Biol.* **2002**, *323*, 573-584.
 69. Dunker, A. K.; Brown, C. J.; Lawson, J. D.; Iakoucheva, L. M.; Obradovic, Z. *Biochemistry* **2002**, *41*, 6573-6582.
 70. Fink, A. L. *Curr. Opin. Struct. Biol.* **2005**, *15*, 35-41.
 71. Dunker, A. K.; Obradovic, Z. *Nat. Biotechnol.* **2001**, *19*, 805-806.
 72. Dunker, A. K.; Brown, C. J.; Obradovic, Z. *Adv. Protein Chem.* **2002**, *62*, 25-49.
 73. Tompa, P. *Bioessays* **2003**, *25*, 847-855.
 74. Tompa, P.; Csermely, P. *FASEB J.* **2004**, *18*, 1169-1175.
 75. Mora-Gutierrez, A.; Kumosinski, T. F.; Farrell, H. M., Jr. *J. Agric. Food Chem.* **1997**, *45*, 4545-4553.
 76. Bokor, M.; Csizmok, V.; Kovacs, D.; Banki, P.; Friedrich, P.; Tompa, P.; Tompa, K. *Biophys. J.* **2005**, *88*, 2030-2037.
 77. Uversky, V. N.; Fink, A. L. *Biochim. Biophys. Acta* **2004**, *1698*, 131-153.
 78. Oldfield, C. J.; Cheng, Y.; Cortese, M. S.; Romero, P.; Uversky, V. N.; Dunker, A. K. *Biochemistry* **2005**, *44*, 12454-12470.
 79. Goers, J.; Permyakov, S. E.; Permyakov, E. A.; Uversky, V. N.; Fink, A. L. *Biochemistry* **2002**, *41*, 12546-12551.
 80. Hakansson, A.; Svensson, M.; Mossberg, A. K.; Sabharwal, H.; Linse, S.; Lazou, I.; Lonnerdal, B.; Svanborg, C. *Mol. Microbiol.* **2000**, *35*, 589-600.
 81. Svensson, M.; Fast, J.; Mossberg, A. K.; C., D.; Gustafsson, L.; Hallgren, O.; Brooks, C. L.; Berliner, L.; Linse, S.; Svanborg, C. *Protein Sci.* **2003**, *12*, 2794-2804.

Chapter 2

Polysaccharides: Molecules, Clusters, Networks, and Interactions

Gillian Eggleston¹ and Jonathan P. Doyle²

¹Commodity Utilization Unit, Southern Regional Research Center,
Agricultural Research Service, U.S. Department of Agriculture,
New Orleans, LA 70124

²Department of Food and Nutritional Sciences, University College Cork,
Cork, Ireland

This paper reviews the structural organization of polysaccharides with respect to molecules, clusters (aggregates), networks and interactions. As for proteins, different levels of structural organization exist for polysaccharides. The primary structure describes the covalent sequence of monosaccharide residues in the polymer chain; the secondary “ordered” structure defines any geometrically regular arrangement in space that this sequence may adopt; the tertiary structure defines the way these arrangements pack together and higher quaternary structures mostly define polysaccharide-polysaccharide interactions. Up-to-date experimental techniques to characterize secondary and higher structural organization are described. Polysaccharide clusters and gel networks are illustrated with carrageenan, alginate, pectin, and gellan. Higher levels of structural organization (polysaccharide—polysaccharide interactions), are discussed for the synergistic interactions of galactomannans or konjac glucomannan with helix-forming algal polysaccharides or xanthan. Finally the future outlook for the fast growing area of the three-dimensional structure of polysaccharides at the molecular level is discussed.

Introduction

Polysaccharide chains are built up from monosaccharide units (often known simply as "sugars"). These have ring structures. The most common type of sugar ring, and the only one considered in this review, is the 6-membered "pyranose aldohexose" structure shown in Figure 1. Linkage into carbohydrate chains involves formation of glycosidic bonds between adjacent residues (Figure 2). The glycosidic bond joins C-1 of one residue to the oxygen atom on C-2, C-3, C-4, or C-6 of the next residue, and can have either the α or β configuration (Figure 1). Polysaccharides are composed of > 10 monosaccharides, and can be classified as homopolysaccharides, in which all the monosaccharides are the same, and heteropolysaccharides, which contain at least two different types of monosaccharide. Both can be either linear or branched. Branches can be single monosaccharides, chains of two or more monosaccharides of uniform number, or chains containing a variable number of monosaccharides.

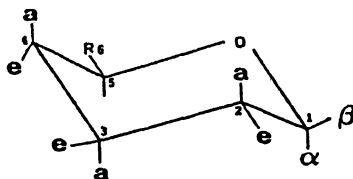


Figure 1. The carbohydrate pyranose ring structure, in the most stable (4C_1) chair conformation. Hydroxyl groups on carbons 2, 3 and 4 of different monosaccharides may be either axial (a) or equatorial (e) as illustrated. Axial linkage at carbon 1 is denoted as α and equatorial as β . Monosaccharides in the L series are the exact mirror image of the D-conformation illustrated.

The familiar classification of different levels of structural organisation in proteins into primary, secondary, tertiary and quaternary can be extended (1) to polysaccharides, but with some characteristic differences. Unlike proteins, polysaccharides normally have primary structures (sequence of covalently-linked residues) based on a simple repeating pattern. The secondary structure of both proteins and polysaccharides defines the shape (conformation) of the polymer chains, particularly geometrically-regular arrangements. However, with the possible exception of molecular organisation within starch granules (2), there is

no polysaccharide equivalent of the tertiary structure of globular proteins, and tertiary structure of polysaccharides normally refers to homotypic intermolecular assemblies such as double helices. There are also no polysaccharides with sub-unit structures, and the term "quaternary structure" is used to describe heterotypic assemblies of different polysaccharides.

The large differences in the functional properties of polysaccharides, such as water solubility, viscosity, aggregation and crystallization, gelation, digestibility, and biological recognition, are due to their great variation in primary structures which, in turn, determine the secondary and tertiary structures adopted in both aqueous solution and the solid state. The dominant factor is the way in which the monosaccharide units are linked. For example, cellulose, curdlan, pullulan, amylose, amylopectin and dextran have widely different properties, but are all polymers of D-glucose (i.e., glucans) linked in different ways. Conversely, different monosaccharides linked in the same way often give polysaccharides with very similar properties (3).

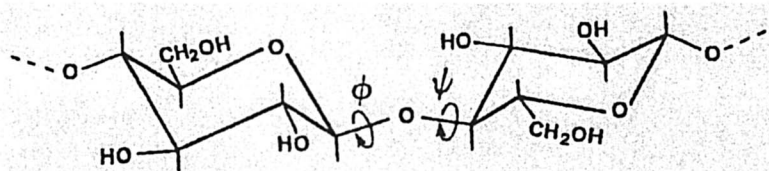


Figure 2. Glycosidic bond between adjacent residues in carbohydrate chains, illustrated for the (1 → 4)-β-D-glucan structure of cellulose. Chain geometry is determined by the torsional angles ϕ and ψ .

Polysaccharide Molecules: Primary and Secondary Structures

The nature of secondary "ordered" structures of polysaccharides depends on the geometric arrangement of the covalent linkages to and from each residue in the primary structure. The primary structures of most polysaccharides of industrial significance are based on six-membered (pyranose) rings, which are essentially locked in a single chair-like geometry. Linkages between adjacent residues can be either through equatorial or axial bonds, as shown in Figure 1. For glycosidic bonds where the linkage is through an oxygen atom attached to a ring carbon, the relative orientations of the participating monosaccharides are defined by the two torsional angles ϕ and ψ (Figure 2). When the connecting linkage is between C-1 of one monosaccharide and C-6 of the other, there is an extra covalent bond and torsion angle (ω), giving freedom to adopt a much wider range of orientations (4).

Four main classes of linkage geometry, leading to different secondary structures of polysaccharides, were identified in computer-modelling studies by Rees and Scott (5). (1) Polysaccharides linked di-equatorially at C-1 and C-4 of the pyranose ring, which adopt flat, extended ribbon-like ordered structures (e.g., cellulose, a (1→4)-β-D-glucan). (2) Polysaccharides linked axially at carbon positions 1 and 4, which adopt a highly buckled ribbon-like ordered structure (e.g., (1→4)-α-L-gulonate sequences in alginate). (3) Polysaccharides where the linkages to and from the ring are no longer parallel, (e.g., (1→4)-axial-equatorial; (1→3)-di-equatorial) which adopt spiral (hollow helix) ordered structures (e.g., amylose, which is based on (1→4)-α-D-glucan, and curdlan which is based on (1→3)-β-D-glucan). (4) Polysaccharides where the linkage is to C-6 rather than to one of the carbons on the ring, which tend not to adopt ordered structures in solution and are very flexible (e.g., dextran, a (1→6)-α-D-glucan). X-ray and electron-diffraction studies of various homoglycans have demonstrated that the chain conformations of these polysaccharides in crystals are reasonably consistent with the predictions of Rees and Scott (5).

Analysis of the Different Higher Structures of Polysaccharides

The analysis of polysaccharide chains involves two approaches: (1) the characterization of the single-chain conformation free from interchain interactions, and (2) the analysis of the higher structures that include interchain interactions. The single-chain conformation is determined mostly by the primary structure. It is not the aim of this chapter to discuss the analysis of the primary structure of polysaccharides and we refer the reader to the review of Harris *et al.* (6). Instead the present focus is on the analyses of polysaccharide secondary, tertiary, and quaternary structures.

The basic objectives in the application of various physical techniques to analyse polysaccharide higher structures are to i) characterize chain geometry, ii) identify conformational order under hydrated conditions, and iii) monitor order-disorder transition behavior (7). Thermally-induced order-disorder transitions provide direct evidence of conformational order and, if hysteresis behavior is present, the occurrence of aggregation, and intermolecular networks. They may be monitored by discontinuities in the temperature course of physical properties such as optical activity, gel rigidity (storage modulus, G'), NMR, and by thermal transitions in DSC.

X-ray fiber diffraction is the only method for examining ordered structures at atomic resolution. To analyze the crystal and molecular structure of polysaccharides with high resolution, a fiber diagram of high quality is necessary. For that a sample must be well oriented and highly crystalline.

The preparation of fibers requires that the concentrated polysaccharide solutions or gels be stretched and at least partially dehydrated. Using computer modeling programs (e.g., Linked-Atom Least Squares program, LALS), possible crystal models are constructed and each is assessed against the stereochemical restraints and the X-ray diffraction data at individual steps of the analysis (8). As the structure determination proceeds, inferior models are eliminated, and the most probable one is selected to represent the true structure. It is important to note, however, that adoption of an ordered structure in the solid state does not necessarily imply that the same, or any, ordered structure survives under hydrated conditions. Model geometries from crystal structures of small molecules have also been extrapolated to give model polysaccharide chains (9).

The chiroptical techniques of optical rotatory dispersion (ORD) and circular dichroism (CD) are well established as being sensitive and valuable probes of the three-dimensional geometry and, therefore, molecular structure and conformation of polysaccharide molecules (10). Polysaccharide chains are obvious candidates for these techniques because they are all optically active, although one of the major limitations in CD is the need for a suitable chromophore. Both ORD and CD techniques examine the differences in the interaction of left and right handed circularly polarised light with the electrons of asymmetric molecules; ORD is a measure of the different rates of propagation, while CD arises mainly from differential absorption, although it can also be caused by differential scattering.

Rheological analyses of polysaccharide solutions or gels can provide information on the macroscopic properties of higher structures of polysaccharides, e.g., overall molecular shape, aggregation, and intermolecular networks. Polysaccharide solutions, gels, and biological assemblies demonstrate properties intermediate (11) between the two idealized extremes of rheological behavior, i.e., both solid-like and liquid-like (viscoelastic) responses. Quantitatively, these two modes of response can be resolved (12) by small-deformation oscillatory rheometry (also known as mechanical spectroscopy). A sinusoidal oscillatory strain at a fixed amplitude and frequency is applied to a sample. If the resultant stress wave is exactly in-phase the material is perfectly solid, whereas, for purely viscous (liquid) systems, the resultant stress wave will be exactly 90° out-of-phase. Therefore, the resolution of induced stress into in-phase and out-of-phase components gives a measure of the degree of the solid- and liquid-like nature of a viscoelastic polysaccharide, which are characterized by the rigidity (storage) modulus G' and viscosity (loss) modulus G'' , respectively.

In dilute solutions, where the polymer chains are isolated, liquid-like response predominates: $G'' \gg G'$, with G'' increasing in proportion to frequency. At higher concentrations, where the individual chains interpenetrate one another to form an entangled network ("semi-dilute" regime), liquid-like character

predominates at low frequencies, where there is sufficient time for entanglements to come apart within the period of oscillation, but as the frequency is increased the response of the entangled network becomes progressively more like that of a solid, with G' rising above G'' . Permanent networks (true gels) show properties approaching those of elastic solids, with $G' \gg G''$ and both moduli showing little dependence on frequency. Intrinsic viscosity, which is determined by direct comparison of solution viscosity with that of the solvent over a range of low concentrations, and then extrapolating to infinite dilution, provides an index of random coil dimensions and, therefore, chain conformation (13).

Differential scanning calorimetry (DSC) is another powerful method used to probe the conformational behavior of polysaccharides. It is precise, can be used for turbid systems, does not impose any mechanical perturbation on the system, and can quantify any thermally-induced changes in conformation and packing of polysaccharides, which gives direct access to the enthalpy change of the process (ΔH) and the transition temperature.

Nuclear magnetic resonance (NMR) spectroscopy is also applied widely in structural and conformational studies of polysaccharides, and often complements other methods, including X-ray diffraction, light scattering, and small-angle X-ray (or neutron) scattering. Although conventional high-resolution NMR is used mainly for analysis of primary structure, reduction in molecular mobility on adoption of ordered conformations leads to loss of detectable high-resolution signal due to extreme line-broadening, and the reduction in peak area can be used to monitor disorder–order transitions. Molecular mobility can also be characterized more directly by measurements of relaxation times, correlation times, and self-diffusion coefficients. For more information on the NMR analysis of polysaccharides we refer the reader to the excellent review of Kajiwaru and Miyamoto (14). NMR combined with computer molecular modeling allows for better interpretation of structural information contained in, for example, coupling constants to evaluate the magnitude of the torsion angles across the glycosidic bonds and nuclear Overhauser effects to estimate distances between protons located in rather close proximity. It is even being used to model polysaccharide–polysaccharide interactions (15).

Electron microscopy has also played an important role in imaging the ultrastructure of polysaccharides, including pectins (16) and κ -carrageenan gels (17). In Atomic Force Microscopy (AFM), the microscope generates images by 'feeling' the detail of the surface of the specimen. Early studies by Kirby *et al.* (18) showed considerable promise, and more recently AFM has been used to visualize the internal structure of starch (19) and the nanostructure of native pectin sugar acid gels (20).

Polysaccharide Clusters (Aggregates) and Networks

The term “cluster” is not as commonly used for polysaccharide higher structures as it is for proteins, but has been used as a synonym for polysaccharide aggregates. In gels, polysaccharide molecules aggregate into one continuous three-dimensional network that “fills” the liquid. The gel network consists of polysaccharide molecules joined in junction zones by non-covalent bonds. The nature of the ordered junction zones varies between different gelling systems. This section is intended to summarise the current understanding of the aggregation and network behavior of four, illustrative gel-forming polysaccharides.

Carrageenans

Carrageenans are the main structural polysaccharides in numerous species of marine red algae (*Rhodophyceae*), and are located in the intracellular matrix of the plant tissue. The carrageenans of greatest practical importance are iota and kappa, which form gels, and lambda, which is non-gelling and used as a thickener (21). Gelation occurs on cooling, and involves the adoption of a double helix structure which melts again on heating (7). All carrageenans are biosynthesized as soluble polymers that have a linear, alternating sequence of β -(1 \rightarrow 3)- and α -(1 \rightarrow 4)-linked D-galactose residues with varying degrees of sulfation. The gelling forms are produced by a subsequent enzymatic process in which (1 \rightarrow 4)-linked residues are converted to 3,6-anhydride. Insertion of the anhydride bridge changes the ring geometry from the normal 4C_1 chair form (Figure 1) to the mirror-image 1C_4 , ring form, and converts the bonds at C-1 and C-4 from axial to equatorial. Only the diequatorial arrangement is compatible with adoption of the double helix structure required for gel formation. In λ -carrageenan there is no conversion to the anhydride form and, therefore, no gelation. It is generally accepted that κ -carrageenan gels are cross-linked by ordered aggregates of double helices (tertiary structures), and that the formation of a three-dimensional network is promoted by helix-incompatible “kink” units (lacking the 3,6-anhydride bridge), which limit the length of the individual helices and thus allow chains to participate in several different junction zones (7). The helix forming repeating sequence of κ -carrageenan has one negative charge per disaccharide and ι -carrageenan has two negative charges per repeat. Association of chains into double helices is, therefore, inhibited by intermolecular electrostatic repulsion. Counterions enhance the thermal stability of the carrageenan double helix and promote network formation by helix-helix aggregation. Due to the high charge density of ι -carrageenan, binding is probably limited to non-specific ‘atmospheric’

attraction, with divalent ions being particularly effective in promoting gelation (22). Gelation of κ -carrageenan, unlike that of iota, is greatly enhanced by specific monovalent ions (K^+ , Rb^+ , Cs^+), which suppress electrostatic repulsion by binding directly to the helices (23), and therefore promote helix-helix aggregation.

Alginate

Alginates occur naturally as structural polysaccharides in marine brown algae (*Phaeophyceae*) and as extracellular polysaccharides secreted by certain species of bacteria. Alginate is a (1 \rightarrow 4)-linked block co-polymer of β -D-mannuronate and α -L-guluronate, with residues grouped in long, homopolymeric sequences of both types and in heteropolymeric sequences with both sugars present in roughly equal amounts (21). Sodium alginate solutions gel upon the addition of Ca^{2+} ions, which fill the cavities formed between polyguluronate sequences on different chains. This is referred to as the "egg-box" model, which was proposed by Grant and co-workers (24), based on circular dichroism and conformational studies (Figure 3).

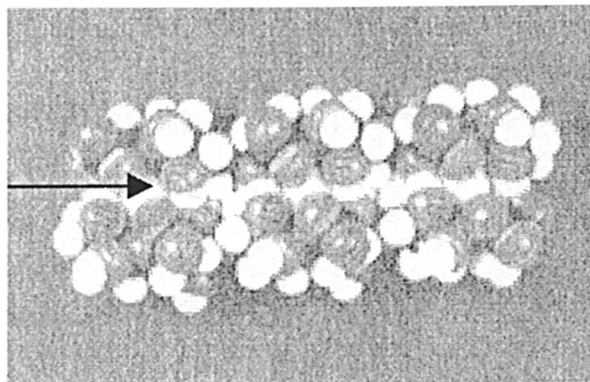


Figure 3. "Egg-box" model for the gelation of alginates and LM pectin. Arrow indicates position of bound calcium ions.

From experimental evidence that the proportion of Ca^{2+} ions tightly bound within the gel network is equivalent to half the total stoichiometric requirement of polyguluronate, Morris *et al.* (25) proposed the preferential formation of a dimeric structure in which only the inner faces of each participating chain are involved in binding of Ca^{2+} . Unlike polyguluronate, polymannuronate does not bind Ca^{2+} ions. This is because the inter-residue linkages, which are diequatorial, give rise to a flat, ribbon-like structure. Therefore, the strength of the gel

network depends on the guluronate content in the alginate used, and the concentration of Ca^{2+} ions.

Pectins

Pectin is a heterogeneous polysaccharide located in the cell walls of many plants. The primary structure consists predominantly of homopolymeric sequences of (1→4)-linked α -D-galacturonate residues, but also contains "rhamnogalacturonan" sequences in which galacturonate residues alternate with (1→2)-linked α -L-rhamnose (26). In native pectin, the rhamnogalacturonan regions are linked covalently to long sidechains of neutral sugars, which attach the pectin to other components of the plant cell wall. However, these sidechains are almost completely removed in extraction of commercial pectins. It is generally believed that polygalacturonate and rhamnogalacturonan occur together in linear chains, although there has been a recent speculative proposal (27) that the polygalacturonate sequences are attached as sidechains to a rhamnogalacturonan backbone. A proportion of the galacturonate residues occur as the methyl ester; the methyl ester content can be decreased by hydrolysis in mild alkali (converting COOCH_3 to COO^-). The percentage of galacturonate residues in the methyl ester form is known as the "degree of esterification" (DE); pectins with $\text{DE} > 50$ are classified as "high-methoxy" (HM); those with $\text{DE} < 50$ are classified as "low-methoxy" (LM).

HM pectin is normally gelled by lowering the pH and adding high concentrations (typically 60-65%) of sucrose or other sugars. Reduction in pH promotes gelation by partial conversion of COO^- to COOH , thus reducing the electrostatic repulsion between the chains. Co-solutes promote gelation by replacing large amounts of water, making less water available to maintain the polymer chains in solution. It is generally accepted that gel junctions involve the three-fold helix structure visualised by X-ray fiber diffraction (28). At low temperature, the helices appear to be joined together by hydrogen bonds (29); as the temperature is raised, these bonds dissociate, but are progressively replaced by hydrophobic associations between methyl ester groups, which may explain why HM pectin gels do not melt on heating. LM pectins form gels with Ca^{2+} in the same way as alginate, with the poly-D-galacturonate sequences in an ordered, two-fold conformation, stabilised by chelation of divalent cations between the polysaccharide chains. With swamping levels of monovalent counterions, interchain association in hydrated systems is limited to the formation of dimers, but at higher concentrations of Ca^{2+} , where it is the sole or principal counterion, larger assemblies can be formed (30). As the esterified galacturonate residues in LM pectin cannot contribute to the electrostatic binding of Ca^{2+} , the "egg-box" junctions are less stable than in calcium alginate gels.

Current understanding of pectin networks has come largely from studies of commercial extracts. However, investigations using electron microscopy to visualise microgel fragments released on progressive disaggregation of plant tissue (31) have shown subunits composed of aggregated rods and segmented rods, consistent with the above description of branched networks held together by non-covalent association of chain sequences into aggregated junctions.

Gellan

Gellan gum is an extracellular polysaccharide produced by the bacterium *Sphingomonas elodea*. The primary structure of gellan has the complex tetrasaccharide repeating sequence of β -D-glucose, β -D-glucuronic acid, β -D-glucose and α -L-rhamnose (32). Three out of four linkages in every repeat unit in the backbone are (1 \rightarrow 4)-diequatorial (as in cellulose), but the fourth linkage is at C-3, introducing a systematic "twist" which promotes a helical conformation. The native polysaccharide, as biosynthesised, is partially esterified with L-glycerate at O-2 of the first glucose and O-acetate at O-6 of the same residue (33). In commercial production, alkali pre-treatment of the fermentation broth prior to alcohol precipitation removes both of these acyl substituents almost completely, giving "low acyl" gellan ("gellan gum"). Without exposure to alkali, "high acyl" gellan is produced.

Based on X-ray diffraction patterns, gellan has been shown to exist in the solid state as a co-axial double helix with three-fold symmetry, similar to carrageenan (34). Divalent cations promote gelation much more strongly than monovalent cations by site-binding between pairs of carboxyl groups on neighbouring helices, similar to the alginate/pectin "egg-box" structure proposed by Grant and co-workers (24). In comparison, monovalent cations neutralise charge by specific site-binding to the individual helices, thus reducing the electrostatic barrier to aggregation (35). Recent studies by Doyle *et al.* (36) suggest similar behavior in the gelation of κ -carrageenan in the presence of K^+ and Ca^{2+} cations, indicating the same underlying mechanism of gel formation for both polysaccharides. The effect of aggregation is to stabilise the associated helices to temperatures above those at which individual helices will form on cooling, causing thermal hysteresis (37), and to provide an additional mechanism of interchain association, giving rise to a continuous gel network.

"High acyl" gellan has the same overall double helix structure as the low acyl form but the ordered structure is inherently more stable than that of the deacylated material because of the formation of additional hydrogen bonds by the glyceryl groups; consequently gelation occurs at a much higher temperature (35). The presence of the glyceryl groups, however, disrupts the binding site required for cation-mediated aggregation; consequently, the concentration of

“high acyl” gellan required for gelation is much higher than for the “low acyl” form, and the resulting gels are much weaker and less rigid (38).

Polysaccharide Interactions

Although the adoption of ordered tertiary structures, such as carrageenan double helices and alginate “egg box” dimers, underlies many of the biological and technological properties of polysaccharides, higher “quarternary” levels of structural organization can also occur, notably in the “synergistic” interactions of galactomannans and konjac glucomannan with certain other polysaccharides. Current views on the mechanisms of gelation in these mixtures are summarized in this section.

Synergistic interactions of carrageenans and agars with galactomannans and glucomannans

Galactomannans are storage polysaccharides from the seed endosperm of plants in the *Leguminosea* family. They have a (1→4)-diequatorially-linked linear backbone of β -D-mannose residues, some of which carry single-sugar sidechains of (1→6)-linked α -D-galactose. The presence of these sidechains confers solubility on the polymer and their content is normally characterised by the molar ratio of mannose to galactose (M/G). Konjac glucomannan is obtained from the tubers of *Amorphophallus konjac* and has a linear backbone of (1→4)-linked β -D-mannose and β -D-glucose, in the ratio 1.6:1. Solubility is conferred by the presence of acetyl groups (approximately 1 acetyl group per 17 residues) at the C-6 position, and short oligosaccharide sidechains at the C-3 position of the mannoses. When these non-gelling plant polysaccharides are mixed with gel-forming algal polysaccharides such as agarose, furcellaran or κ -carrageenan, there is a “synergistic” enhancement in network properties, such as greater gel strength, greater elasticity and less syneresis, as well as a reduction in the minimum gelling concentration of the algal polysaccharide. Within the galactomannan series the extent of synergistic interaction increases as the galactose substitution decreases. This led to the proposal (39) that interaction occurs by attachment of the unsubstituted regions of the mannan backbone to the algal polysaccharide helix, with more heavily substituted regions acting as interconnecting sequences in the hydrated network (Figure 4). Efficient binding, however, requires some helix–helix aggregation of the algal polysaccharide, a possibility which was also noted by Dea *et al.* (39), and which is supported by the absence of detectable synergism for iota carrageenan (40).

Morris (41) concluded that: “despite all the debate about the exact mechanism of interaction, this model [Dea *et al.* (39)] still appears to offer the most direct explanation of all available experimental evidence.”

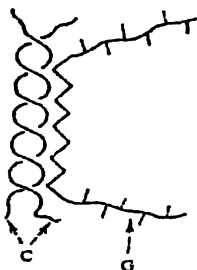


Figure 4. Schematic model proposed for binding of galactomannan (G) to κ -carrageenan (C) in its ordered conformation. Similar models have also been proposed for the interaction of galactomannans and konjac glucomannan with agarose and furcellaran. (Reproduced from 39).

Gelation of xanthan with galactomannans and glucomannans

Xanthan is the extracellular polysaccharide from the bacterium *Xanthomonas campestris*. It has a (1 \rightarrow 4)-linked linear backbone of β -D-glucose, as in cellulose, and is solubilised by charged trisaccharide sidechains attached at O-3 of alternate glucose residues to give a pentasaccharide repeating sequence (42). On cooling and/or addition of salt, it undergoes a co-operative conformational transition (43) from a disordered coil to a rigid ordered structure (5-fold helix). Solutions of xanthan in its ordered conformation show tenuous “weak gel” properties, which appear to arise from weak association between the helical sequences, and are sensitive to ionic environment. Xanthan alone, however, does not give “true” (self-supporting) gels, but will form strong and cohesive gels when mixed with plant galactomannans and konjac glucomannan.

Synergistic interactions between xanthan and galactomannans were first reported more than 30 years ago by Rocks (44). Raising the M/G ratio favors gelation (i.e., interaction increases with decreasing galactose content): locust bean gum (M/G ratio \sim 3.5) gives strong cohesive gels; tara gum (M/G ratio \sim 2.8) forms only a weak gel, and guar gum (M/G ratio \sim 1.6) only produces an enhancement of viscosity at low temperature (43, 45-46). This led to the suggestion (43) that synergistic gelation occurs by intermolecular binding

between the surface of the xanthan 5-fold helix and unsubstituted regions of the mannan backbone. Later, however, Cairns *et al.* (47) concluded that the interaction involves formation of heterotypic junction zones between the mannan backbone of the galactomannan and the cellulosic backbone of the xanthan, with (1→4)-diequatorial linkage geometry in both polymers providing a complementary fit, and can occur only when the xanthan is disordered. This proposal was based on two main lines of evidence: (i) X-ray diffraction of fibers prepared from orientated xanthan–galactomannan mixtures prepared at low temperatures where the xanthan helix is already present, but after heating to a temperature above the gel–sol transition and re-cooling, a cohesive gel was formed. The latter, however, may be explained in terms of the mixing process which prevents the formation of a cohesive network; this is the basis behind the formation of “fluid gels” which convert to a continuous network after heating and re-cooling (48). Subsequently, Goycoolea *et al.* (49) showed that by varying ionic condition, xanthan could be either ordered or disordered when gelation occurred. More recently, Cronin and co-workers (50) found that treating non-gelling mixtures of ordered xanthan and guar gum with α -galactosidase to generate unsubstituted regions of the mannan backbone, gave gels that were much stronger than those obtained by cooling the same concentrations of xanthan and locust bean gum. This experiment was performed under quiescent conditions (no mixing), and clearly demonstrates that there is no need for the xanthan chains to be disordered when forming junctions with galactomannans.

Studying the effects of variations of the xanthan chemical structure also tested the effects of helix stability on mixed gel formation. The strength of the mixed gels was determined to be heavily dependant on the level of acetyl substitution, which led to the conclusion that the presence of acetate groups on the xanthan backbone does inhibit xanthan–galactomannan interaction (51).

Similar mechanisms of gelation have also been proposed for the interaction of xanthan and konjac glucomannan. In xanthan–glucomannan systems, however, there is much stronger interaction between the two polysaccharides. The formation of recognizable gels was found at total polysaccharide levels of only 0.02%, which is the lowest gelling concentration observed for a carbohydrate system (3).

Future Outlook

The requirement for information regarding the three-dimensional structure of polysaccharides at the molecular level is fast growing (52) and is expected to grow further in the next decade. This is for a number of reasons. (1) Polysaccharides are increasingly being regarded as biodegradable polymer materials, compared to the usual synthetic polymers. (2) Thanks

to the emerging technology of bio-based processing, petroleum is being replaced by polysaccharides as the biomass feedstocks for the new biorefineries.

(3) Polysaccharides are the most abundant organic materials in nature.

(4) A great variety of polysaccharides composed of various monosaccharide residues and linkages has been found.

References

1. Rees, D. A.; Welsh E. J. *Angew. Chem. Int. Ed. Eng.*, **1977**, 1, 16, 214-224.
2. Hizukuri, S. *Carbohydrate Res*, **1986**, 147, 342-347.
3. Dea, I.C.M. In *Industrial Gums*, Whistler, R.L.; BeMiller, J. N. Eds.; 3rd Edition, Academic Press: London, **1993**, pp. 21-52.
4. Rees, D. A.; Morris, E. R.; Thom, D.; Madden, J. K. In: *Polysaccharides*, Vol. 1, Aspinall G. O., Ed., Academic Press: New York, **1982**; Chapter 5, pp. 195-290.
5. Rees, D.A.; Scott, W.E. *J. Chem. Soc.* **1971**, B, 469.
6. Harris, P.; Morrison, A.; Dacombe, C. In *Food Science and Technology Series: Polysaccharides and their Applications*, Stephan, A.M., Ed., Marcel Dekker: New York. **1995**, pp. 577-606.
7. Morris, E. R. *Food Chem.* **1980**, 6, 15-39.
8. Smith, P.J.C.; Arnott, S. *Acta Crystallogr.* **1978**, A34, 3.
9. French, A.D.; Johnson, G. P. *Cellulose* **2004**, 11, 5-22.
10. Morris, E. R. In *Physical Techniques for the Study of Food Biopolymers*, Ross-Murphy, S.B. Ed.; Chapman and Hall: London, **1994**, pp. 15-64.
11. Morris, E. R.; Ross-Murphy, S.B. In *Techniques in Carbohydrate Metabolism*, Northcote, D.H., Ed., Elsevier: Amsterdam. **1981**, B310
12. Ferry, J.D. In *Viscoelastic Properties of Polymers*, Wiley: New York, **1980**, 3rd edition.
13. Morris, E.R.; Cutler, A.N.; Ross-Murphy, S.B.; Rees, D.A.; Price, J. *Carbohydr. Polym.* **1981**, 1, 5-21.
14. Kajiwara, K.; Miyamoto, T. In *Polysaccharides Structural Diversity and Functional Versatility*. Dumitriu, S. Ed., Marcell Dekker: New York, **1998**, pp. 1-55.
15. Tvarosky, I.; Taravel, F. R. In *Polysaccharides Structural Diversity and Functional Versatility*. Dumitriu, S. Ed., Marcell Dekker: New York, **1998**, pp. 173-210.
16. Fishman, M.L.; Cooke, P. H.; Hotchkiss, A.; Damert, W. *Carbohdyr. Res.* **1993**, 248, 303-316.
17. Hermansson, A.M.; Eriksson, E.; Jordansson, E. *Carbohydr. Polym.* **1991**, 16, 297-320.

18. Kirby, A.R.; Gunning, A.P.; Morris, V.J. *Trends in Food Sci. and Tech.* **1995**, *6*, 359-365.
19. Ridout, M.J.; Gunning, A.P.; Wilson, R.H.; Parker, M.L.; Morris, V.J. *Carbohydr Polym.* **2001**, *50*, 123-132.
20. Fishman, M.L.; Cooke, P.H.; Coffin, D.R. *Biomacromolecules* **2004**, *5*, 334-341.
21. Stanley, N.F. In *Food Gels*, P.Harris, P., Ed.; Elsevier: London, **1990**, pp. 79-119.
22. Morris, E.R. In *Gums and Stabilisers for the Food Industry 5*, Phillips, G.O.; Wedlock, D.J.; Williams, P.A.; Eds.; IRL Press: Oxford, **1990**, pp. 483-496.
23. Picullel, L. In *Food Polysaccharides and their Applications*, A.M. Stephen, Ed.; Marcel Dekker: New York, **1995**, pp. 205-238.
24. Grant, G.T.; Morris, E.R.; Rees, D.A.; Smith, P.J.C.; Thom, D. *FEBS Lett.* **1973**, *32*, 195-198.
25. Morris, E.R.; Rees, D.A.; Thom, D.; Boyd, J. *Carbohydr. Res.* **1978**, *66*, 145-154.
26. De Vries, J.A.; Rombouts, F.M.; Voragen, A.G.J.; Pilnik, W. *Carbohydr. Polym.* **1982**, *2*, 25-33.
27. Walkinshaw, M.D.; Arnott, S. *J. Mol. Biol.* **1981**, *153*, 1075-1085.
28. Vinken, J.-P.; Schols, H.A.; Oomen, R.J.F.J.; McCann, M.C.; Ulvskov, P.; Voragen, A.G.J.; Visser, G.F. *Plant Physiol.* **2003**, *132*, 1781-1789.
29. Evageliou, V.; Richardson, R.K.; Morris, E.R. *Carbohydr. Polym.* **2000**, *42*, 245-259.
30. Morris, E.R.; Powell, D.A.; Gidley, M.J.; Rees, D.A. *J. Mol. Biol.* **1982**, *155*, 507-516.
31. Fishman, M.L.; Cooke, P.C.; Levaj, B.; Gillespie, D.T.; Sondey, S.M.; Scorza, R. *Archiv. Biochem. Biophys.* **1992**, *294*, 253-260.
32. O'Neill, M.A.; Selvendran, R.R.; Morris, V.J. *Carbohydr. Res.* **1983**, *124*, 123-133.
33. Kuo, M.-S.; Mort, A.J.; Dell, A. *Carbohydr. Res.* **1986**, *156*, 173-187.
34. Chandrasekaran, R.; Millane, R.P.; Arnott, S.; Atkins, E.D.T. *Carbohydr. Polym.* **1988**, *175*, 1-15.
35. Morris, E.R.; Gothard, M.G.E.; Hember, M.W.N.; Manning, C.E.; Robinson, G. *Carbohydr. Polym.* **1996**, *30*, 165-175.
36. Doyle, J.P.; Giannouli, P.; Philp, K.; Morris, E.R. In *Gums and Stabilisers for the Food Industry 11*, Phillips, G.O.; Williams, P.A.; Eds.; Royal Society of Chemistry: Cambridge, **2002**, pp. 158-164.
37. Morris, E. R.; Norton, I. T. In *Aggregation Processes in Solution*. Wyn-Jones, E.; Gormally, J., Eds., Elsevier: Amsterdam, **1983**, pp. 549-593.

38. Baird, J.K.; Talaskek, T.A.; Chang, H. In *Gums and Stabilisers for the Food Industry 6*, Phillips, G.O.; Wedlock, D.J.; Williams, P.A.; Eds.; IRL Press: Oxford, 1992, pp. 479-487.
39. Dea, I.C.M.; McKinnon, A.A.; Rees, D.A. *J. Mol. Biol.* 1972, 68, 153-172.
40. Moriano, A.L. In *Food Colloids*, Graham, H.D., Ed., AVI:Westport, 1977, pp. 347-381.
41. Morris, E. R. In *Biopolymer Mixtures*, Harding, S.E.; Hill, S.E.; Mitchell, J.R. Eds.; Nottingham University Press: Nottingham, 1996, pp. 247-287.
42. Melton, L.D.; Mindt, L.; Rees, D.A.; Sanderson, G.R. *Carbohydr. Res.* 1976, 46, 245.
43. Morris, E.R.; Rees, D.A.; Young, G.; Walkinshaw, M.D.; Darke, A. *J. Mol. Biol.* 1977, 110, 1-16.
44. Rocks, J.K. *Food Technology* 1971, 25, 476-483.
45. McCleary, B.V.; Dea, I.C.M.; Windust, J.; Cooke, D. *Carbohydr. Polym.* 1984, 4, 253-270.
46. Lopes, L.; Andrade, C.T.; Milas, M.; Rinaudo, M. *Carbohydr. Polym.* 1992, 17, 121-126.
47. Goycoolea, F.M.; Foster, T.J.; Richardson, R.K.; Morris, E.R.; Gidley, M.J. In *Gums and Stabilisers for the Food Industry 7*, Phillips, G.O.; Wedlock, D.J.; Williams, P.A.; Eds.; IRL Press: Oxford, 1994, pp. 333-344.
48. Cairns, P.; Miles, M.J.; Morris, V.J.; Brownsey G.J. (1987). *Carbohydr. Polym.* 1987, 6, 257-268.
49. Norton, I.T.; Jarvis, D.A.; Foster, T.J. *Int. J. Biol. Macromol.* 1999, 26, 255-261.
50. Cronin, C.E.; Giannouli, P.; McCleary, B.V.; Brooks, M.; Morris, E.R. In *Gums and Stabilisers for the Food Industry 11*, Phillips, G.O.; Williams, P.A.; Eds.; Royal Society of Chemistry: Cambridge, 2002, pp. 289-296.
51. Shatwell, K.P.; Sutherland, I.W.; Ross-Murphy, S.B.; Dea, I.C.M. *Carbohydr. Polym.* 1991, 14, 131-147.
52. Ogawa, K; Yui, T. In *Polysaccharides Structural Diversity and Functional Versatility*. Dumitriu, S., Ed., Dekker: New York, 1998, pp. 101-129.

Chapter 3

Collagen Networks: Nature and Beyond

Eleanor M. Brown

**Eastern Regional Research Center, Agricultural Research Service,
U.S. Department of Agriculture, 600 East Mermaid Lane,
Wyndmoor, PA 19038**

The major fibrous collagens (types I, II, and III) perform a variety of structural functions in the skin, tendons, bones and cornea of animals. The basic structure of these molecules is the collagen triple helix, consisting of three chains with multiple repeats of the Gly-Xxx-Yyy tripeptide. In nature, these helices further associate into fibers, the length and supramolecular aggregate forms of which vary with the functional requirements. Enzyme-catalyzed crosslinks involving the short, nonhelical telopeptides at the N- and C-termini of the triple helix contribute to fiber stability. As a basis for manufactured goods including biomedical devices and leather, the collagen network is further stabilized by the addition of synthetic crosslinks formed by the action of transglutaminase, dialdehydes, tannins or mineral tannages. These crosslinks contribute to high hydrothermal stability and resistance to microbial attack for collagen-based materials. Nature's network, with a little additional stabilization, finds many commercial applications.

Discussions of renewable biopolymers generally focus on carbohydrates, particularly, cellulose, lignin, starch and pectin. When attention is turned to proteins, it is usually plant proteins such as soy and zein that are replenished by annual harvests. Nonetheless, animal proteins, mainly keratin and collagen are major byproducts of the meat industry and thus clearly renewable resources. Keratins, the primary proteins of wool, feathers and hair are used, as is, in a variety of products or modified for additional functionality.

Collagen Structure

Collagen, a family of structural proteins located in the extracellular matrix of connective tissue, provides a structural basis for the mechanical and biochemical properties of tissues and organs (1). The more than 20 distinct types of collagen account for about one third of the total protein of vertebrate animals. Based on structure and supramolecular organization, collagens are grouped as fibril-forming (types I, II, III, V, XI), fibril-associated (types IX, XII, XIV), membrane (types IV, VII, VIII, X) or other specific function (2). The signature characteristic of collagen is the triple helix comprised of three separate polypeptide chains. Fibrillar collagens are triple-helical over essentially their entire length, and all collagens are triple-helical in some part of their structure. In addition to biological function, the fibril-forming collagens find technological uses as molecular frameworks in the food, medical and leather industries (3).

Collagens are noted for their high glycine (Gly), proline (Pro) and hydroxyproline (Hpr) content. The primary structure of the helical domain is the repeating tripeptide (Gly-Xxx-Yyy)_n. About 25% of the tripeptide repeats are Gly-Pro-Y or Gly-X-Hpr, and other amino acids (not tryptophan, tyrosine, or cysteine) are found in the X and Y positions. The individual peptide chains that form the triple helix are designated as α chains. Type I collagen, found mainly in skin, bone, and tendon is comprised of two identical $\alpha 1(I)$ chains and one similar $\alpha 2(I)$ chain. Type II collagen, found in cartilage, and type III, found in fetal skin and together with type I collagen in mature skin, are homotrimers comprised of three identical $\alpha 1(II)$ and $\alpha 1(III)$ chains, respectively.

The helical domain of bovine type I collagen is 1014 residues long. Each chain forms a left-handed polyproline helix, having three residues per turn with a pitch of 0.94 nm. The Gly residue at every third position allows these helices to pack together in the formation of a right-handed triple helix. The three chains are staggered by one residue, with the Gly residues forming a shallow helix in the center and the X and Y sidechains directed outward to form a helical ridge (2, 4). The triple helical collagen molecule, sometimes called tropocollagen, is stabilized by peptide and hydrogen bonds as well as steric interactions. The Gly residues permit close packing, rigid Pro rings prevent rotation about the peptide bond, and the hydroxyl groups of Hpr provide sites for water bridges and sidechain interactions.

Supramolecular structures are formed by self-association of individual triple helices. Although microfibrils of fiber-forming collagens have not been isolated, several structures based on four to six helices as the primary unit (5) have been proposed to account for patterns observed by microscopy. Higher order structures include the fibril and fiber bundle composed of multiple microfibrils and fibrils, respectively. Electron micrographs of intact organs exhibit a periodic banding pattern (Figure 1) characteristic of the collagen fiber. The origin of this pattern is the quarter-stagger arrangement of individual molecules, resulting in gap and overlap regions. Short telopeptide sequences, not Gly-X-Y, located in the gap region at the amino and carboxyl ends of the triple helix are important in fibril formation and stabilization (4). The repeating unit of the banding pattern is called a D space, a molecule is 4.4 D space long with 0.6 D gap; the assembly is a flexible rod about 1.5 nm by 300 nm (4).

Collagen as a Raw Material

Leather, produced by soaking and stretching dried hides in animal fat or brain tissue, a treatment that helped to soften the hide while giving it a coating that protected against microbial and water damage, was perhaps humankind's first manufactured product. Vegetable tanning, in which stacks of hides in pits were soaked with tree bark, was well established by the Middle Ages. Early vegetable tanning took many months because bark tannins are weak and diffusion through a stack of hides was slow. The advent of mixed tannin and spray-dried extracts, synthetic polyphenols, and the use of drums instead of pits have shortened the process to a few days for production of specialty leathers for saddles, harnesses, belts, shoe soles and a variety of crafts (6). Historically, leathers were heavy, utilizing the entire thickness of the hide. By the early 20th century, mineral (Cr, Al, Fe, Ti, Zr), organic (aldehyde, acrylate, polyphenol) and combination tannages had come into use for the manufacture of lighter, thinner, and softer leathers. The most valuable of these use the grain layer, which is split from the dermal layer. When a tanned hide is split, the dermal layer may be processed as suede. If the hide is split prior to tanning, the collagen-rich dermal layer becomes raw material for a variety of biomaterials.

Tanning processes developed empirically and remain more art form than science. From a practical perspective, tanning is a multistep process that stabilizes the collagen matrix of the hide, giving it strength and resistance to organisms that would otherwise attack and destroy it. During the 20th century, chromium (Cr III) came to be the most widely used and studied tanning agent. Although Cr(III) is a very efficient tanning agent for the production of high

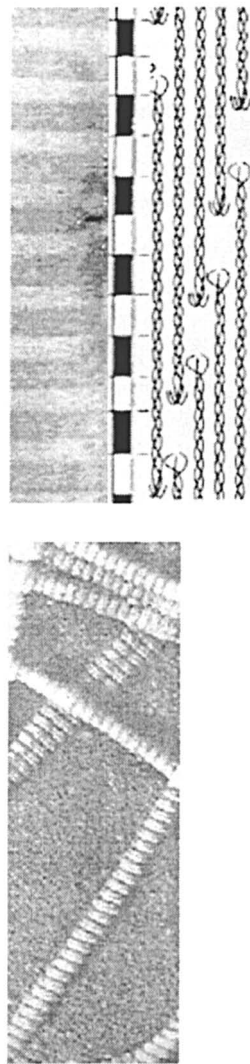


Figure 1. Micrographs of skin (left) and a fibril (top right), schematics of gap and overlap (middle right), and microfibril assembly (bottom right).

quality leather, the nature of the chromium-collagen interaction is poorly understood. Until recently, most attempts at describing the chemistry of chrome tanning focused on the crosslinking of collagen fibrils. The primary chrome-tanning agent, "basic chrome sulfate," is a mixture of Cr(III) complexes, where two or more chromium atoms connected by oxygen and/or hydroxyl bridges have varying numbers of associated sulfate ions (7). One role of chromium, in the tanning of leather, is to crosslink the collagen fibrils by forming complexes with the carboxyl groups of glutamic and aspartic acid side chains on collagen (8, 9). Other mineral tannages have generally been assumed to follow the chromium model. Vegetable tannins were thought to react with collagen by means of electrostatic, hydrophobic, and coordinate forces (8) and to crosslink or cluster between basic sidechains. Glutaraldehyde was considered to interact with collagen through lysine-to-lysine crosslinks via either the monomer or a condensed polymer as the tanning agent (10). Acrylamide was shown to bind to lysine residues and derivatives such as N,N'-methylenebisacrylamide and higher homologues could form crosslinks between lysine sidechains (11).

While different tannages produce leathers that are distinguishable, all are recognizable as leather. Many of the steps in tanning are common to most tannages. Recent studies (12 – 14) suggest that tanning may better be described in terms of protein modification, than as simply crosslinking. For industrial and biomedical applications, collagen is usually isolated from the skin, tendon or bone and then modified or crosslinked to form a stable matrix not unlike that of leather. In the search for mechanistic details of collagen modifications that result in a stabilized matrix, whether as leather or some other application, the roles of several types of interactions must be considered. Covalent crosslinks, electrostatic interactions (salt bridges), hydrophobic interactions, hydrogen bonds, and control of water activity are among the contributing factors in a stabilization mechanism.

One goal of this research is to contribute to an understanding at the molecular level of the mechanisms of tanning. A second is to understand the effects of processing conditions on the supramolecular structure of collagen. Leather-related studies utilize model tanning systems based on soluble collagen and conditions that mimic tanning processes, to explore the interactions of tanning agents (15) with monomeric collagen in mildly acidic solution and the effects of added salts (16) on the stability of the collagen triple helix. The effects of processing conditions and crosslinking on the molecular structure of collagen from the dermal layer of the hide, a coproduct of leather production, are studied for biomaterial uses.

Experimental Tanning Model

Circular dichroism (CD) spectroscopy, a commonly used technique for monitoring protein conformation as conditions are changed, requires a protein in

an optically clear solution. Pepsin-solubilized type I collagen from bovine skin (Cohesion, Palo Alto, CA) purchased as a sterile solution in 0.012 M HCl at a concentration of 3 mg/mL was dialyzed in 10,000 MW cutoff dialysis cassettes (Pierce, Rockford, IL) against 50 mM HAc overnight at 4 °C, with one change of dialysate, and then centrifuged at 165,000g in a Beckman L8-70 (Beckman Coulter, Fullerton, CA) preparative ultracentrifuge at 25 °C for one hour. The supernatant contained the soluble collagen used in further experiments (15). Other chemicals were reagent grade. A four-step process modified from the data of Taylor et al. (17) was used to simulate a model-tanning system. In the first step, collagen solubilized in 50 mM HAc was considered to be a model for hide collagen (pH ~ 4) at the start of tanning. In the second step, the collagen solution was acidified to pH 2 to simulate a pickling step. A tanning agent or neutral salt was then added to the acidified collagen. Finally, in a simulated fixative step, the collagen mixture was slowly neutralized to pH 4 with 0.4 M NaHCO₃.

Thermal stability

The amount of triple helical structure and its thermal stability were determined from UV and CD spectra at each stage of the simulated tanning process. Degassed samples, 300 μL in volume, were placed in 1 mm pathlength stoppered cuvettes. The concentration of collagen in solution was estimated from the UV absorbance at 218 nm ($\epsilon = 883,129 \text{ cm}^{-1}\text{-L-mole}^{-1}$) (18). The stoppered cuvette containing the sample was then refrigerated at 4° C for at least 12 hours to maximize the formation of triple helical structure, and then scanned from 250 nm to 200 nm at 10 °C on an AVIV Model 215 Circular Dichroism Spectrometer (AVIV Biomedical, Lakewood, NJ). Melting curves were obtained by recording the CD signal at 223 nm every 0.5 deg between 10 °C and 50 °C with a time constant of 10 sec and a heating rate of 3 deg per hour. A final scan of the sample at 50 °C was recorded. The CD signal in mdeg was converted to molar ellipticity on a mean residue basis:

$$[\theta]_{\lambda} = \theta_{\lambda} / ncd \text{ deg cm}^2 \text{ dmol}^{-1}$$

n is the number of amino acid residues in the protein chain, c is the molar concentration, and d is the pathlength in millimeters.

Figures 2a and 2b show the absorbance spectrum at ambient temperature and the CD spectra at 10 °C and at 50 °C of soluble collagen at pH 4.3 in 50 mM HAc. The absence of tryptophan residues and the low levels of tyrosine give the near-UV region of the absorbance spectrum a flat appearance. A small positive band near 223 nm, and a larger negative band at 198 nm are characteristics of the collagen triple helix. As the temperature of a monomeric solution of collagen is increased, the helical conformation is lost and above

45 °C the CD spectrum becomes relatively featureless. The mean residue ellipticity for type I collagen in dilute (1 - 2mg/mL) and slightly acidic solutions (pH 3 - 5) at 10 °C was remarkably constant at $[\Theta]_{223\text{nm}} = 6000 \pm 400$ (14 measurements) on different collagen preparations, and with neutral salt concentrations up to 0.2 M.

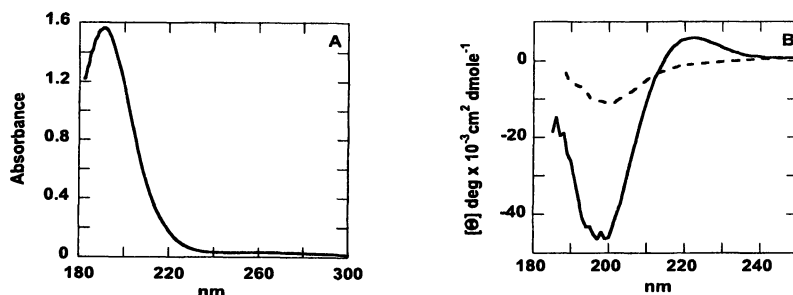


Figure 2. A. Absorbance spectrum of acid-soluble bovine type I collagen. B. Corresponding CD spectra, solid line at 10 °C and dashed line at 50 °C.

The relative flatness of the melting profile (Figure 3Aa) at temperatures below 25 °C and above 45 °C suggests that collagen in dilute, slightly acidic solutions (pH 3 - 5) denatures in the 25 °C to 45 °C temperature range by a two-step process characterized by a pre-denaturation transition (Tp) followed by complete denaturation (Td). Values for Tp and Td were obtained from the derivative of the melting profile (Figure 3B). When the acidity of the collagen solution was increased to pH 1 - 2, Td approached Tp, and a single transition was seen (Figure 3Ab). Addition of a tanning agent, Cr(III) or Al, at low pH had little effect on the melting profile (Figure 3Ac), but neutralization of the reaction mixture back to pH 4 had a significant effect on the melting profile (Figure 3Ad). The initial helical content was reduced by about 50%, suggesting that the action of the tanning agent during the neutralization step may 'fix' some of the collagen in an orientation that cancels a portion of the CD activity. No solid residue was observed, but crosslinking within or between collagen monomers could contribute to the appearance of less helical structure. In mineral tanning, a maximum of about five crosslinks per collagen triple helix are predicted (20); the melting behavior (Figure 3Ad) suggests that mineral crosslinks may form primarily in regions where the helical structure has been destabilized by the acidic conditions. Thus the crosslinks may stabilize a partially denatured conformation of collagen that still retains some helical structure.

Similar values of Tp and Td for acid-soluble collagen in dilute solution have been reported from both calorimetric (20) and CD studies (16). The temperatures associated with Tp (25 - 35 °C) and Td (30 - 40 °C) depend on heating rate, pH, concentration of collagen, and other components of the solution. At a heating rate of 3 °C per hour, values of Tp = 33.3 °C \pm 1.6 °C and

$T_d = 39.7 \text{ }^\circ\text{C} \pm 1.0 \text{ }^\circ\text{C}$ were obtained from the derivatives of the melting curves for seven separate experiments with collagen samples at pH 4 without added salt. At pH 2, a single transition at $33.3 \text{ }^\circ\text{C} \pm 0.3 \text{ }^\circ\text{C}$ was observed. When neutral salts (NaCl, KCl) were added to the collagen solution at pH 4, both T_p and T_d decreased as the concentration of salt was increased. At salt concentrations above 0.3 M NaCl or 0.4 M KCl collagen samples became gelatinous.

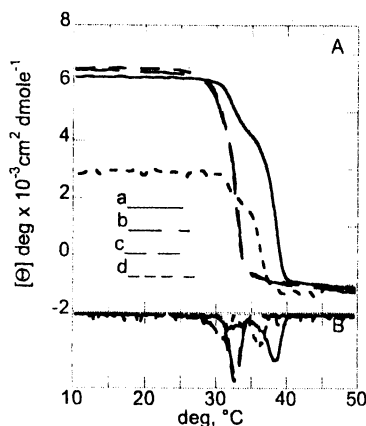


Figure 3. *A: Melting profiles for soluble collagen under conditions of simulated tanning. (a) in 50mM HAc (pH4.3); (b) after acidification with H_2SO_4 (pH 2); (c) after addition of $\text{Al}_2(\text{SO}_4)_3$; and (d) after neutralization with NaHCO_3 (pH4). B: Derivative plots of the melting profiles.*

The thermal behavior of fibrillar collagens is complex and not thoroughly understood despite numerous studies over at least the past thirty years (21 – 23). Multiple thermal transitions at temperatures between 50 °C and 110 °C have been reported for intact fibrillar collagens. The mechanisms responsible for those transitions may be related to the thermal stability or shrinkage temperature that is a primary characteristic of the conversion of hide to leather. In the context of tanning, the shrinkage temperature of a raw hide is between 50 °C and 60 °C, while that of a suitably tanned leather is in the vicinity of 100 °C. The destabilization of the triple helix by the addition of neutral salts suggests that at least part of the structural stability of collagen may be due to electrostatic interactions. It is well known that ionizable and hydrophobic side chains tend to be grouped in patches along a collagen triple helix (24, 25). At high salt concentrations there is the possibility of stabilizing effects from electrostatic and hydrophobic interactions (26) as well as from hydrogen bonds and the electron withdrawing character of Hpr (27).

Biomaterial model

The Collagen Research Group at Widener University prepared macromolecular collagen suspensions. A dilute aqueous suspension of crude collagen, from the lower split of a bovine hide (not tanned) was ball-milled for seven days to produce a loose collection of separated fibrils that is the starting material for several environmental and biotechnology applications (28). To gain an understanding of the effects of this treatment on the collagen molecule, crude and milled collagen were studied at the fiber, fibril and molecular level.

Effects of milling on collagen structure

Scanning electron microscopy (SEM) was used to follow the effect of milling on the surface area of collagen fibers. Active surface area, defined as the surface area able to interact with the liquid in which the collagen is blended, was calculated from the diameters of fiber bundles as determined from digital image analysis of micrographs as described previously (29). SEM micrographs at 10000x magnification of crude, four day and seven day milled collagen are shown from left to right in Figure 4.

To evaluate the integrity of collagen molecules during the milling process, sodium dodecyl sulfate polyacrylamide gel electrophoresis (SDS-PAGE) (30) was performed on a Phast-Gel System (Pharmacia Biotech Inc., Piscataway, NJ) with modifications as described previously (31). Gels were imaged using Personal Densitometer SI (Molecular Dynamics, Sunnyvale, CA) and ImageQuant software (Molecular Dynamics). Crude collagen, day 1, day 4, and day 7 milled collagen all had similar band patterns (Figure 5A) with major bands at 220000 Da, 140000 Da, and 130000 Da. The dark band above the separating gel represents a portion of the sample that remained in the stacking gel and is >200000 Da. Gel electrophoresis indicates that the unraveling process is a purely physical process since the protein band pattern is consistent throughout the ball-milling. Milling increases the active surface area of the collagen without chemically altering or denaturing the collagen.

Crosslinking studies

Seven day ball-milled collagen fibrils and water were blended into a dilute organic acid dispersion (28), frozen and milled under liquid nitrogen in a model 6800 CertiPrep freezer mill (Spex, Metuchen, NJ) and lyophilized. This insoluble collagen powder was used for crosslinking studies. The effects of glutaraldehyde (GA), microbial transglutaminase (mTgase), and dehydrothermal (DHT) treatments on insoluble collagen powder were evaluated (32). In a typical GA crosslinking procedure, 20 mg of collagen was reacted with 5 ml of 0.625% (w/w) GA in phosphate buffered saline (PBS), pH 7.4 for 4 hours at 4 °C. For DHT crosslinking (33) the powdered collagen was equilibrated for one hour at a

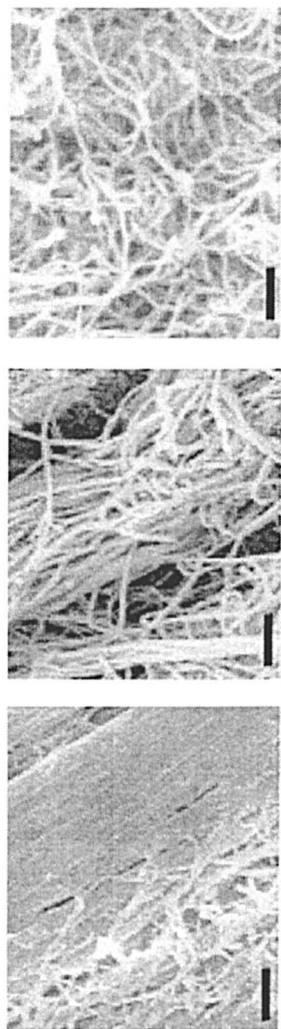


Figure 4. SEM at 10,000x of crude, four and seven day milled collagen. Bars on the micrographs are 1.4 μm in length.

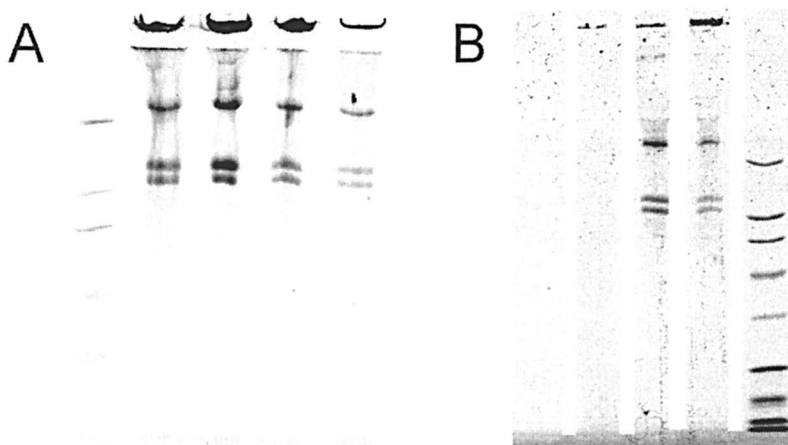


Figure 5. SDS-PAGE: left to right of (A) high MW standards (200,000 – 45000 Da), crude collagen, 1, 4, and 7-day milled collagen on a 7.5% gel and (B) collagen treated for crosslinking with GA, DHT, mTgase, a 7-day milled control, and broad MW standards (210,000 – 7100 Da) on a 4 – 15% gel

pressure less than 100 mTorr in a vacuum oven at ambient temperature. The temperature was then raised to 110 °C for 24 hours and allowed to cool to below 50 °C before the vacuum was released. Enzymatic crosslinking was accomplished by incubating 25 mg collagen with 1.25 U mTgase in PBS for 24 hours in a shaker water bath at 30 °C (32). After crosslinking, GA and mTgase products were washed three times for twenty minutes with PBS, washed overnight in water, and lyophilized.

The effectiveness of crosslinking was evaluated from the molecular weight profile, free amine content and resistance to collagenase of the product. Molecular weight analysis of crosslinked samples was by SDS-PAGE (30). The gel pattern (Figure 5B) for collagen powder is typical of bovine skin collagens, with bands characteristic of single chains of type I or type III collagen and a higher molecular weight band representing natively crosslinked chains. The pattern for mTgase treated collagen contains additional bands near the interface between the stacking and separating gels, representing crosslinked material that was separated by the conditions of the SDS-PAGE experiment. DHT crosslinked collagen produces a band of high molecular weight material in the stacking gel, and a faint streak of low molecular weight material in the separating gel, indicative of partial hydrolysis. GA crosslinked collagen was not disassociated by SDS-PAGE preparation procedures and did not enter the gel, a result that is consistent with the formation of large covalently crosslinked complexes.

Because lysine side chains are participants in many crosslinking schemes, the change in the number of free lysines is an indication of the number of crosslinks formed. The number of free lysyl-amines present per 1000 amino acids was determined spectrophotometrically by measuring the trinitrophenyllysine produced by reaction with 2,4,6-trinitrobenzenesulfonic acid (TNBS) (34). The lysine plus hydroxylysine content of type I bovine collagen, calculated from the amino acid sequence, is 30.6 residues per 1000 residues. The number of hydroxylysines is variable, and their participation in naturally occurring crosslinks is responsible for some variability in the free amine analysis. Based on the average of nine determinations on the collagen powder the free lysine content of this sample was 27.7 ± 1.7 per 1000 residues. Treated samples were analyzed in triplicate. The free amine contents as a function of crosslinking scheme were GA (9.0 ± 0.7), DHT (28.7 ± 0.5), and mTgase (22.0 ± 4.7). In light of the different crosslinking mechanisms, the results are reasonable. GA treatment of collagen results in the formation of large stable aggregates, individual links are between amine groups, if two lysine residues are involved in each crosslink, there may be as many as 9 GA crosslinks per 1000 residues. With DHT, a physical 'crosslinking' method, the primary interactions are hydrophobic, and despite the potential for lysinoalanine formation (35), lysine does not appear to be involved. The formation of ϵ -(γ -glutamyl)lysine links between the γ -carboxamide group of a glutamine residue and a primary amino group is catalyzed by mTgase (36). The consumption of 5 – 6 lysine sidechains per 1000 residues by the mTgase reaction thus represents that number of crosslinks.

Collagenase resistance was assayed with bacterial collagenase (Worthington, NJ) using the Worthington procedure as detailed previously (33). GA treatment provided the greatest resistance to collagenase (Figure 6) in good agreement with reports from other laboratories (34, 37).

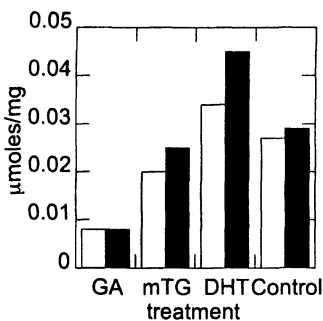


Figure 6. Collagenase resistance as a function of crosslinking treatment. Black columns represent twice the concentration of collagenase as white columns.

DHT treatment, reported to partially denature collagen fibrils (38), produced a product that was less collagenase-resistant than untreated collagen. Treatment of collagen with mTgase produces a limited number of crosslinks and increases the collagenase resistance about 20% over that of control collagen.

Discussion

The collagens are a biologically diverse family of proteins based on the deceptively simple sequence of amino acids (Gly-X-Y)₁₀₀₋₄₀₀, a pattern that gives the entire family of collagens a very high level of homology. The presence of Pro or Hyp at the X or Y position in about 25% of the tripeptide repeats imposes a rigid elongated coil type structure on the individual chains. The content of hydroxylysine (Hly) and the naturally occurring crosslinks between the nonhelical telopeptides and Hly residues increase as the animal ages. Intuitively, one might expect these changes to increase the thermal stability of the triple helical conformation. However, the work of Notbohm et al. (39) showed that higher than typical levels of hydroxylysine residues resulted in slightly less stable helices.

The unique characteristics of the fiber forming collagens make them useful ingredients for the manufacture of biomaterials. The dimensional stability of collagen is closely related to its organized molecular structure, and results from the interplay of electrostatic, hydrophobic, and van der Waals interactions in addition to hydrogen and covalent bonds. The hydrothermal stability of a manufactured biomaterial such as leather will reflect the stability of collagen structures at the molecular level as well as at several levels of supramolecular structure. Although the transition temperatures characteristic of hydrothermal stability of collagen in solution or in a fibrous matrix will vary with the level of supramolecular structure in the substrate, ultimately the characteristics of the particular collagen will determine the properties of the product. Thus hydrothermal stability is an important factor in the evaluation of collagen-based materials. Calfskin is a common source of fibrous collagen prepared in research laboratories (20, 40). Commercially available collagens are often prepared from the skin or tendons, of mature animals and thus may be better models for the study of biomaterials.

Conclusions

A very simplified model was used to simulate several molecular aspects of mineral tanning. With this model, measurable effects on the conformation and conformational stability of soluble collagen under the conditions of tanning could be seen and provided confirmation of their requirement in tanning. When a dilute suspension of collagen fiber bundles is milled, the fibers are separated

into fibrils, with a 200-fold increase in active surface area, without harming the monomer collagen structure. Insoluble collagen fibrils were modified by glutaraldehyde, dehydrothermal treatment and microbial transglutaminase. Each modifying treatment produced a different degree of apparent crosslinking, collagenase resistance, and aggregate size. These and other treatments of collagen and its partially hydrolyzed form (gelatin) make them suitable materials for a range of industrial applications.

Acknowledgements

The author thanks M. M Taylor (ERRC, ARS) for guidance on tanning processes and use of mTgase, M. A. Seltzer and A. Lastowka (Widener U.), whose thesis research at ERRC formed the basis for the biomaterials section, and A. Elsetinow and R. Wildermuth for their technical contributions.

Reference to a brand or firm name does not constitute endorsement by the U. S. Department of Agriculture over others of a similar nature not mentioned.

References

1. Gelse, K.; Poschl, E.; Aigner, T., Collagens - structure, function, and biosynthesis. *Adv. Drug Delivery Rev.* **2003**, *55*, 1531-1546.
2. Van der Rest, M; Garrone, R., Collagen family of proteins. *FASEB Journal* **1991**, *5*, 2814-2823.
3. Bailey, A. J., Collagen--Nature's framework in the medical, food and leather industries. *J Soc. Leather Tech. Chem.* **1992**, *76*, 111-128.
4. Kadler, K., The structure of collagens. *Protein Profiles* **1994**, *1*, 535-560.
5. Miller, A.; Piez, D. A. D., Structure and packing of microfibrils in collagen. *J. Mol. Biol.* **1973**, *75*, 441-447.
6. Anonymous, A Survey of Modern Vegetable Tannage., *Tanning Extract Producers Federation Limited* **1974**, Chapter 1.
7. Takenouchi, K.; Kondo, K.; Nakamura, F., Changes in the chromium complex composition of masked chrome solutions during tannage and affinity of various chromium complexes for collagen. *J. Soc. Leather Techn. Chem.* **1981**, *75*, 190-196.
8. Gustavson, K. H., Some protein-chemical aspects of tanning processes. *Adv. Protein Chem.* **1949**, *5*, 354-412.
9. Harlan, J. W.; Fearheller, S. H., Chemistry of the crosslinking of collagen during tanning. In: *Protein Crosslinking: Biochemical and Molecular Aspects*, M. Friedman (ed) *Advances in Experimental Medicine and Biology*, **1977**, *86A*, 425-440.
10. Fearheller, S. H., The chemistry of glutaraldehyde tanning and the properties of glutaraldehyde tanned leather. A review after 20 years

- practice. *Proceedings of the 16th Congress Internat. Union Leather Techn. Chem. Soc Versailles, France, 1979*, pp. 79-87.
11. Fearheller, S. H.; Scholnick, F.; and Li, Y., Crosslinking of collagen with acrylamide derivatives II: N,N'-methylenebisacrylamide and higher homologs. *J. Am. Leather Chemists Assoc.* **1991**, *86*, 171-178.
 12. Covington, A. D.; Song, L., Crosslinking - what crosslinking? Studies on the general mechanism of tanning. *Proceedings 27th Congress Internat. Union Leather Techn. Chem. Soc. Cancun, Mexico, 2003*, pp.148-152.
 13. Ramasami, T., Approach towards a unified theory for tanning: Wilson's dream. *J. Am. Leather Chem. Assoc.* **2001**, *96*, 290-304.
 14. Brown, E. M.; Taylor, M. M., Essential chromium? *J. Am. Leather Chem. Assoc.* **2003**, *98*, 408-414.
 15. Brown, E. M.; Dudley, R. L.; Elsetinow, A. R., A conformational study of collagen as affected by tanning procedures. *J. Am. Leather Chem. Assoc.* **1997**, *92*, 225-233.
 16. Brown, E. M.; Farrell, H. M., Jr.; Wildermuth, R. J., Influence of neutral salts on the hydrothermal stability of acid-soluble collagen. *J. Prot. Chem.* **2000**, *19*, 85-92.
 17. Taylor, M. M.; Diefendorf, E. J.; Hannigan, M. V.; Artymyshyn, B.; Phillips, J. G.; Fearheller, S. H.; Bailey, D. G., Wet process technology III. Development of a standard process. *J. Am. Leather Chem. Assoc.* **1986**, *81*, 43-61.
 18. Na, G.C., UV Spectroscopic characterization of type I collagen. *Collagen Rel. Res.* **1988**, *8*, 315-330.
 19. Covington A. D., Modern tanning chemistry. *Chemical Society Reviews* **1997**, 111-126.
 20. Komsa-Penkova, R.; Koynova, R.; Kostov, G.; and Tenchov, B. G., Thermal stability of calf skin collagen type I in salt solutions. *Biochim. Biophys. Acta* **1996**, *1297*, 171-181.
 21. Wallace, D. G.; Condell, R. A.; Donovan, J. W.; Paivinen, A.; Rhee, W. M.; Wade, S. B., Multiple denaturational transitions in fibrillar collagen. *Biopolymers* **1986**, *25*, 1875-1893.
 22. McClain, P. E.; Wiley, E. R., Differential scanning calorimeter studies of the thermal transitions of collagen: Implications on structure and stability. *J. Biol. Chem.* **1972**, *247*, 692-697.
 23. Finch, A.; Ledward, D. A., Shrinkage of collagen fibres: A differential scanning calorimetric study. *Biochim. Biophys. Acta* **1972**, *278*, 433-439.
 24. Hulmes, D. J. S.; Miller, A.; Parry, D. A. D.; Piez, K. A.; Woodhead-Galloway, J., Analysis of the primary structure of collagen for the origins of molecular packing. *J. Mol. Biol.* **1973**, *79*, 137-148.
 25. King, G.; Brown, E. M.; Chen, J. M., Computer model of a bovine type I collagen microfibril. *Protein Engineering* **1996**, *9*, 43-49.
 26. Gekko, K.; Shozo, K., Increased thermal stability of collagen in the presence of sugars and polyols. *J. Biochem.* **1983**, *94*, 199-205.

27. Holmgren, S. K.; Taylor, K. M.; Bretscher, L. E.; Raines, R. T., Code for collagen's stability deciphered. *Nature* **1998**, 392, 666-667.
28. Maffia G. J., Collagen-based dispersions and macroporous structures. U. S. Patent 6,660,829. December 9, **2003**.
29. Maffia, G. J.; Seltzer, M. A.; Cooke, P. H.; Brown, E.M., Collagen Processing. *J. Am. Leather Chem. Assoc.* **2004**, 99, 164-169.
30. Laemmli, U. K., Cleavage of structural proteins during the assembly of the head of bacteriophage T4. *Nature* **1970**, 227, 680-685.
31. Brown, E. M.; Thompson, C. J.; Taylor, M. M., Molecular size and conformation of protein recovered from chrome shavings. *J. Am. Leather Chem. Assoc.* **1994**, 89, 215-220.
32. Lastowka, A.; Maffia, G.; Brown, E. M., A comparison of chemical, physical and enzymatic crosslinking of bovine type I collagen. *J. Am. Leather Chem. Assoc.* **2005**, 100, 196-202.
33. Weadock, K. S.; Miller, E. J.; Keuffel, E. L.; Dunn, M. G., Effect of physical crosslinking methods on collagen-fiber durability in proteolytic solutions. *J. Biomed. Mater. Res.* **1996**, 32, 221-226.
34. Olde Damink, L. H. H.; Dijkstra, P. J.; Van Luyn, M. J. A.; Van Wachem, P. B.; Nieuwenhuis, P.; Feijen, J., Glutaraldehyde as a crosslinking agent for collagen-based biomaterials. *J. Mat. Sci: Mat. Med.* **1995**, 6, 460-472.
35. Friedman, M., Chemistry, Biochemistry, Nutrition, and Microbiology of Lysinoalanine, Lanthionine, and Histidinoalanine in Food and Other Proteins. *J. Agric. Food Chem.* **1999**, 47, 1295-1319.
36. Folk, J. E.; Finlayson, J. S., The ϵ -(γ -glutamyl)lysine crosslink and the catalytic role of transglutaminase. *Adv. Protein Chemistry* **1977**, 31, 2-133.
37. Jorge-Herrero, E.; Fernandez, P.; Turnay, J.; Olmo, N.; Calero, P.; Garcia, R.; Freile, I.; Castillo-Olivares, J., Influence of different chemical cross-linking treatments on the properties of bovine pericardium and collagen. *Biomaterials* **1999**, 20, 539-45.
38. Gorham, S. D.; Light, N. D.; Diamond, A. M.; Willins, M. J.; Bailey, A. J.; Wess, T. J.; Leslie, N.J., Effect of chemical modifications on the susceptibility of collagen to proteolysis. II. Dehydrothermal crosslinking. *Int. J. Biol. Macromol.* **1992**, 14, 129-138.
39. Notbohm, H.; Mosler, S.; Bodo, M.; Yang, C.; Lehmann, H.; Batge, B.; Muller, P.K., Comparative study on the thermostability of collagen-I of skin and bone - Influence of posttranslational hydroxylation of prolyl and lysyl residues. *J. Protein Chem.* **1992**, 11, 635-643.
40. Na, G.C., Monomer and oligomer of type I collagen: Molecular properties and fibril assembly. *Biochemistry* **1989**, 28, 7161-7167.

Chapter 4

New Views of Protein Structure: Applications to the Caseins: Protein Structure and Functionality

H. M. Farrell, Jr.^{1,*}, P. X. Qi¹, and V. N. Uversky²⁻⁴

¹Eastern Regional Research Center, Agricultural Research Service,
U.S. Department of Agriculture, 600 East Mermaid Lane,
Wyndmoor, PA 19038

²Department of Biochemistry and Molecular Biology, School of Medicine,
Indiana University, Indianapolis, IN 46202

³Institute for Biological Instrumentation, Russian Academy of Sciences,
142292 Pushchino, Moscow Region, Russia

⁴Molecular Kinetics, 6201 La Pas Trail, Suite 160, Indianapolis, IN 46268

Advances in the field of protein chemistry have enhanced our understanding of the possible intermediates which may occur during protein folding and unfolding. An enormous amount of information has been generated on folding pathways of globular proteins leading to the discovery of the molten globule state as a specific folding intermediate. Other partially folded conformations including pre-molten globule have been found that are intermediate between the random coils and compact globular conformations. Furthermore, many proteins appear as natively unfolded, intrinsically unstructured, or intrinsically disordered under physiological conditions. Purified caseins are not truly random coils, but appear to share many of the properties of these newly described intermediate states. Since casein structure is still being debated, clarifying how the caseins fit with these newly described protein states would be beneficial. In this review quantitative measures

based upon known physical and chemical properties of the caseins are used for their classification. By taking advantage of this "new view" of protein folding, and applying these concepts to casein fractions it may be possible to generate new potential food products from casein or casein fractions. Such products could also have nutraceutical or nanotechnological applications.

Historic Views of Casein Structure

From all of the concepts regarding casein (CN) structure-function which have been set forth over the years, two fundamental functions of CN can be envisioned: the effective transport of calcium and the self-associations which lead to the colloidal state (1). Although the four major bovine CNs have been studied for many years (2), the molecular structural basis for their function in self-association reactions in milk has been elusive. Historically, optical rotatory dispersion data from our laboratory demonstrated a lack of α -helix in the CNs, and since that was all that could be measured at the time, CNs were considered to be the model for random coil proteins (1). This would represent the "old view" of CN structure. However, as sequences became available, and circular dichroism (CD) was employed as tool for protein analysis (3) the possibility of some ordered structure in CNs was considered. In 1982, Swaisgood (1) was perhaps the first to suggest that the CNs were neither rigid globular nor random coil proteins and that they could be composed of rather distinct functional domains. The next important step on the road to the understanding of CN structure may be the concept of Holt and Sawyer (4) which suggests that CNs are rheomorphic in nature. In this instance, the "formed under flow" hypothesis suggest that CN structure is completely dynamic. In its extreme, this hypothesis may be considered as the "spaghetti plate" analogy, in that no regular structures occur until aggregates are formed. Supporting this hypothesis was the observation of Paulsson and Dejmek (5) that pure CNs, when studied by differential scanning calorimetry (DSC), showed flat endotherms on heating. These flat DSC scans are quite reminiscent of those found for α -lactalbumin either in the acid state or in dilute solutions of guanidine as shown by Xie *et al.* (6). It has thus been tempting to suggest that the native form of CNs is a type of molten globule (MG) state with a significant amount of open, but defined structure. The question remains whether or not this defined structure is localized to selective areas and persists during association reactions. Paulsson and Dejmek

(5) had indeed suggested this alternative view, that CNs exhibit no DSC peak, because they contain heat stable structures.

The idea that CNs have little or no fixed structure, however, remained as the prevalent view. In contrast, data, which we collected in collaboration with Heino Susi, appeared to be at odds with this concept (7). We applied Susi's Raman methodologies, which he had developed for globular proteins, to the CNs. Analysis of the data revealed that all of the CNs had intricate Amide I profiles, similar to those obtained for some globular proteins, with a moderate distribution of various secondary structure elements. The patterns of all purified CNs and their mixtures showed bands characteristic of reasonable amounts of β -turns and sheet and a modest amount of α -helix. The importance of the polyproline II (PPII) in protein structure has only recently been recognized (8, 9). We had demonstrated its presence in β -CN (10) and in the N-terminal portion of α_{s1} -CN (11) by CD and FTIR experiments. Concurrently Syme *et al.* (12) had shown the presence of PPII in CNs by Raman optical activity. CNs appear then to contain significant amounts of defined secondary structure. It has, therefore, been somewhat difficult to reconcile the general view that structure gives rise to function with the random chain or rheomorphic hypothesis where function gives rise to structure.

Starting about 1990, we began to conduct a series of 3D molecular modeling experiments on CN. In these studies, we attempted to derive CN structures from the basic Anfinsen hypothesis. The amount of conformational space sampled by the protein was constrained in the computer experiments to predicted secondary structure-derived from primary sequence data. We further constrained the global structure by requiring that it conform to Raman and FTIR limits. Finally, the number of turns were increased from algorithm predictions to correlate the spectroscopic data with the abundance of proline in the CNs, which being structure-breaking residues for helix and sheet can be instrumental in the formation of turns (13). Using these principles in conjunction with force field calculations, we arrived at refined energy minimized working models for β -, κ -, and α_{s1} -CN (14). These models are given in Figure 1 (15). They not only aid in visualizing the properties of the CNs but also may aid in their classification according to the new intermediate state nomenclature.

Implications of the "New View" for Protein Structure

The idea that a protein may unfold through a multi-step process has in turn led to the "new view" of protein folding as opposed to one simple intermediate as shown in eq 1.



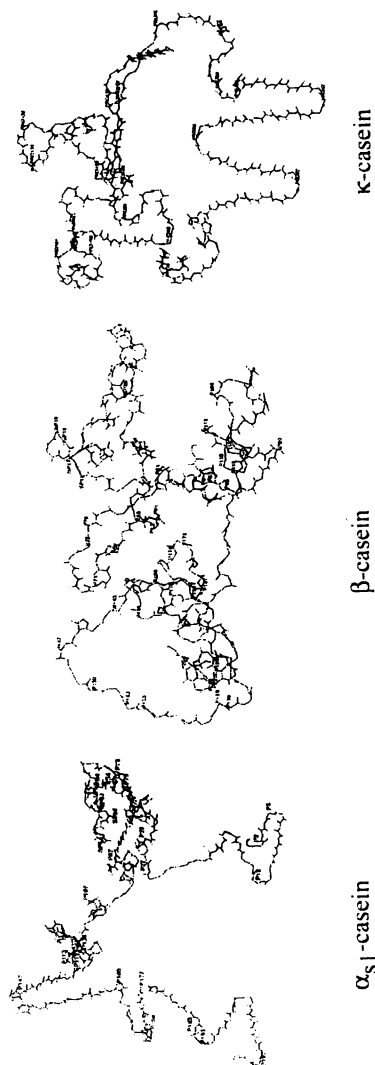


Figure 1. Energy minimized 3D structures of α_s1 -, β - and κ -CN's left, right, bottom respectively. The peptide backbones have the proline residues (P) labeled from Kumosinski et al. (15).

During folding, a protein chain may "sample" a significant amount of conformational space before settling into a selective energy minimum. Indeed, several false minima may lay quite close or even somewhat remotely removed from the true global minimum (16). Such an intermediate area has been postulated to be the molten globule state as shown in Figure 2 for the theoretical energy landscape of a "minimally frustrated" heteropolymer, as folding is viewed from top to bottom. The parameter Q is the global order parameter and represents a value of 1.0 for all interactions in the native state, and 0.0 for the completely unfolded protein. Reflection of the interactions between Q , E , and S result in a three dimensional funnel. In the "new view" then the intermediate state of eq 1 is now defined as a multiplicity of states which includes not only the molten globule as defined in Figure 2, but also a number of conformationally defined states which reside above the molten globule (MG) region (16). These new states, working upward from the molten globule state of Figure 2, have been previously defined as pre-molten globule (PMG) and natively unfolded (NU) based upon their physical and chemical properties, for a review see reference 16. A different classification by means of biological function has also been attempted (17) and under the general heading of intrinsically unstructured protein (IUP) five functional definitions of these new states have been elucidated.

The following statements summarize some of the salient features of the new view and the new protein species (MG, PMG, U) as previously described (16) for globular proteins in general; and some specific attributes of NU and IUP:

1. During folding, the search of the possible protein energy landscape may be limited somewhat by primary structure, but the landscape certainly is much wider with many more possible intermediates than previously thought.

2. Most likely many proteins can, under denaturing conditions, fall into a molten globule state (MG). This compact partially folded state is globular, contains much native secondary structure, possibly some tertiary elements, but does not have rigid tertiary structure. In addition there is a freer rotation of aromatic side chains.

3. Similarly, many globular proteins may adopt a more extended partially folded conformation, the pre-molten globule state (PMG). This conformation is characterized by significant reduction in secondary structure, loss of compactness and absence of globular core.

4. A polypeptide chain in the unfolded state (U) never adopts true random coil conformation and significant amount of residual structure is present even at extremely harsh denaturing conditions.

5. For α -lactalbumin and some other ligand binding proteins, removal of bound cations can lead to destabilization of structure, and perhaps lead to alternative intermediate states.

6. Internal hydration can lend some stability to the new intermediate states, whose open and more flexible structures allow more surface for water interactions and possible binding of lipids or other macromolecules.

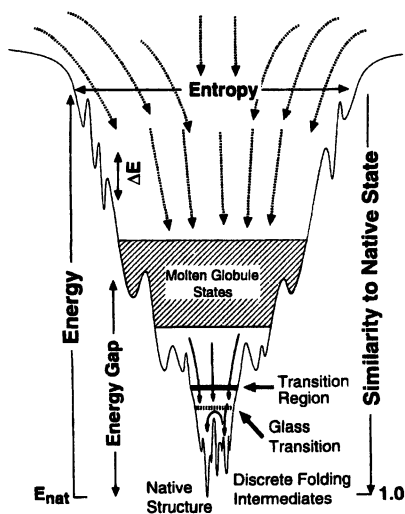


Figure 2. A schematic representation for the energy landscape for a minimally frustrated heteropolymer during protein folding. E_{nat} is the minimum potential energy for the native state. From Onuchic et al.(18); reprinted courtesy of Academic Press, San Diego, CA.

7. Misfolding, and new surfaces for interactions can cause altered protein-protein interactions (aggregation) to issue forth from all of these newly described states.

8. Many proteins were shown to be intrinsically disordered (ID), intrinsically unstructured (IU) or natively unfolded (NU); i.e., being functional, they were characterized by the lack of rigid tertiary structure under the physiologic conditions. For these proteins, function may originate from different partially folded conformations and from structural transitions between them.

The question now arises, how can this "new view" be applied to CN structure?

Classification of CNs Among the New Intermediate States

The major hallmark of the ID or NU proteins is that they do not fold and remain trapped in conformational energy states above that of the MG state depicted in Figure 2, whereas native molten globules (which represent a subset of intrinsically disordered proteins) are trapped in the MG-like conformational energy states (see Figure 2). This results from three properties of these proteins: first they contain high contents of proline and glutamine leading to segments of PPII which produce extended structures, second a high net charge which prevents close approach of segments of the protein molecules (18), and finally a low hydrophobicity which does not allow for hydrophobic collapse into a highly folded structure. More detailed statistical analysis revealed that amino acid sequences encoding for the intrinsically disordered proteins or regions are significantly different from those characteristic for the ordered proteins on the basis of local amino acid composition, flexibility, hydrophobicity, charge, coordination number and several other factors (19, 20, 21). A signature of a probable intrinsically disordered region is the presence of low sequence complexity coupled with amino-acid compositional bias, characterized by a low content of so-called order-promoting residues such as Cys and bulky hydrophobic amino acids (Val, Leu, Ile, Met, Phe, Tyr and Trp), which would normally form the core of a folded globular protein, and a high proportion of particular polar and charged amino acids (Gln, Ser, Pro, Glu, Lys and, on occasion, Gly and Ala), known as disorder-promoting residues (22).

Figure 3 illustrates composition profiling of α_{S1} -, α_{S2} -, β - and κ -CNs as compared to that of set of ordered proteins. This compositional profiling is based on the approach developed for intrinsically disordered proteins (19). In Figure 3, the bar for a given amino acid represents the fractional difference in composition between a given CN and a set of ordered proteins. Thus, data presented in this figure can be used to better understand the physical reasons for the unusual conformational behavior of CNs. Figure 3 shows that in comparison with the averaged ordered protein, CNs display reductions in such strong structure-promoting amino acids residues (those on the left) as Trp and Cys and significant enrichments in some of the disorder-promoting amino acids (those on the right; e.g. Pro, Ser, Glu and Gln). On the other hand, the compositional

profiles in Figure 3 are quite different from those observed for typical intrinsically disordered proteins and some CNs are enriched in some order-promoting residues, including Ile (α_{S2} -, β -, and κ -CN), Tyr (α_{S2} -, β -, and κ -CN), Val (α_{S2} -, β -, and κ -CN), and Leu (α_{S1} - and β -CN), being depleted in some disorder-promoting residues, including Arg, Gly, and Asp. This determines relatively high hydrophobicity of CNs (1, 2). It has been pointed out that arginine residues more prone to enhance protein thermostability than lysine

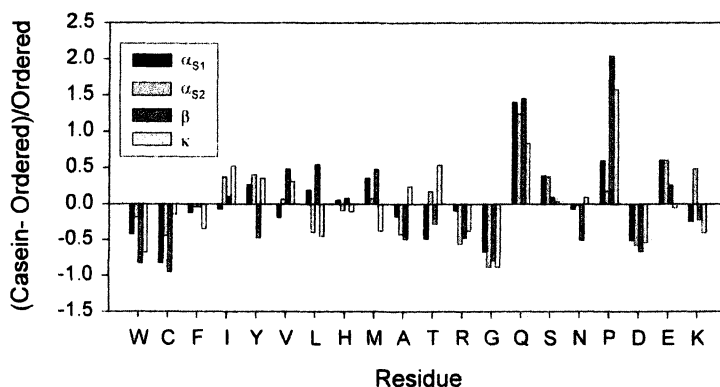


Figure 3. Composition profiling of α_{S1} -, α_{S2} -, β - and κ -CNs. The bar for a given amino acid represents the fractional difference in composition between a given subclass of CNs and a set of ordered proteins. The fractional difference is calculated as $(C_{CN} - C_{ordered})/C_{ordered}$, where C_{CN} is the composition of a given amino acid in a given CN subclass, and $C_{ordered}$ is the corresponding composition in a set of ordered proteins. The residues are ordered by Vihinen's flexibility scale (23). Negative values indicate that the given CN subclass has less than order, positive indicates more than order.

residues by facilitating more ionic (2 salt-bridges and 5 H-bond) interactions through their guanidino group (24-26). In a comparative genomics study that used genome sequences of *Archaea*, protein models generated from cold-adapted archaea were found to have fewer arginines (27). Thus, the reduction in Arg content might contribute to the increased flexibility of CNs.

To gain further information on abundance of intrinsic disorder in CNs, we analyzed their sequences using two binary predictors of intrinsic disorder, charge-hydrophathy-plot (CH-plot) (28) and cumulative distribution function (CDF) analysis (29). Both of these methods perform binary classification of whole proteins as either mostly disordered or mostly ordered, where mostly ordered indicates proteins that contain more ordered residues than disordered residues and mostly disordered indicates proteins that contain more disordered residues than ordered residues (30).

Ordered and disordered proteins plotted in CH space can be separated to a significant degree by a linear boundary, with proteins located above this boundary line being disordered and with proteins below the boundary line being ordered (28). CDF analysis summarizes the per-residue disorder predictions by plotting PONDR[®] scores against their cumulative frequency, which allows ordered and disordered proteins to be distinguished based on the distribution of prediction scores. Here, order-disorder classification is based on whether a CDF curve is above or below a majority of boundary points (30). Results of these analyses for the 11 α_{S1} -CNs, 9 α_{S2} -CNs, 13 β -CNs and 20 κ -CNs with known sequences are shown in Figure 4.

Figure 4A shows that the majority of points corresponding to the individual α_{S1} - and α_{S2} -CNs as well as to the “averaged” α_{S1} - and α_{S2} -CNs are located above the boundary separating natively unfolded and compact molecules. This means that α_{S1} - and α_{S2} -CNs are predicted to be natively unfolded. On the other hand, points corresponding to the individual and “averaged” β - and κ -CNs fall below the boundary, suggesting that these proteins might be more compact. On the other hand, according to CDF analysis (Figure 4B), the vast majority of individual CNs (48 of 53) and all four “averaged” CNs are predicted to be disordered, as their corresponding CDF curves are located below a majority of boundary points. The apparent discrepancy in the results retrieved by these two predictors is due to the different principles used in their development.

In fact, the CH-plot is a linear classifier that takes into account only two parameters—charge and hydrophobicity of the particular sequence (28), whereas CDF analysis is dependent upon the output of the PONDR[®] VL-XT predictor, a nonlinear neural network classifier, which was trained to distinguish order and disorder based on a significantly larger feature space that explicitly includes net charge and hydropathy (22, 31). Thus, CH space represents a subset of PONDR[®] VL-XT feature space (30). By default, CH-plot analysis is predisposed to discriminate proteins with substantial amounts of extended disorder (random coils and PMGs) from proteins with globular conformations (MG-like and rigid well-structured proteins). On the other hand, PONDR-based CDF analysis may discriminate all disordered conformations including MGs from rigid well-folded proteins. In application to CNs this means that α_{S1} - and α_{S2} -CNs are predicted to be natively unfolded proteins with extended coil-like or PMG-like conformations, whereas β - and κ -CNs should possess MG-like properties. This hypothesis was confirmed by the analysis of structural properties of several representative CNs.

The propensity of ID and NU proteins to remain in an extended state causes these proteins to exhibit abnormally high Stokes radii relative to those found for folded proteins of the same sequence length. The 3D models generated for the CNs can be used to generate a hydrated volume (V_H) as was previously done above for the α -lactalbumin models (16). Next the calculated V_H can then be

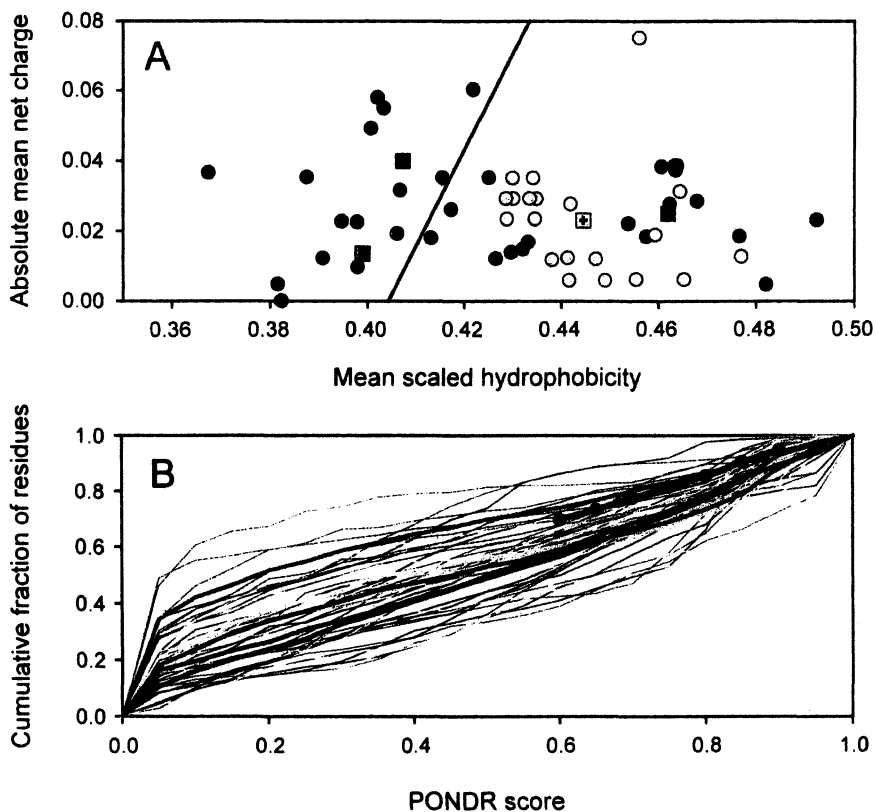


*Figure 4. Disorder predictions on 11 α_{S1} -CNs (red symbols and lines), 9 α_{S2} -CNs (green symbols and lines), 13 β -CNs (blue symbols and lines), and 20 κ -CNs (yellow symbols and lines). **A.** CH-plot (28). The black line represents the order-disorder boundary calculated according to Oldfield et al. (30). Crossed squares correspond to the “averaged” α_{S1} -, α_{S2} -, β - and κ -CNs, for which charge and hydrophobicity values were averaged over corresponding CN subclasses. **B.** CDF analysis (29). The order-disorder boundary is plotted as black line with circles. Bold lines correspond to the “averaged” α_{S1} -, α_{S2} -, β - and κ -CNs, for which cumulative fractions of residues were averaged over corresponding CN subclasses. These calculations were performed POND^R CDF and CH algorithms. Access to POND^R is provided by Molecular Kinetics (www.molecularkinetics.com). (See page 1 of color inserts.)*

compared with both the Uversky plots (32) and with experimental values to help classify the individual CNs. Note that Uversky (32) also pointed out that a significant number of NU proteins do display residual structure and suggested two distinct classifications for them, coil-like (NU_{coil}) and PMG-like (NU_{PMG}). To simplify the calculations the average sequence length for the three larger CNs (α_{s1} -, α_{s2} - and β -CN) was taken to be 205 and a V_{H} calculated for each state. Table I shows the results of these calculations. The V_{H} calculated from the 3D models for the two α -CNs are in agreement with the predictions of Figure 4 in that the proteins are not folded, and place the two molecules in the NU_{coil} state. The α -CN models may be overextended in that the actual gel permeation chromatography (GPC) radii (33) argue for the NU_{PMG} state for these two proteins. In contrast the calculations for the β - and κ -CN models place these two molecules in the more compact MG state. It will be recalled that the hydrophathy plots for the latter two also suggested a more folded state. The experimental gel-permeation chromatography (GPC) values argue for the NU_{PMG} state for β -CN and the NU_{coil} state for the somewhat smaller κ -CN. Overall all of these data suggest that the CNs do represent a somewhat diverse group of NU or IDP molecules and are neither compact globular proteins nor random coils.

Table I. Hydrated Volumes for the CNs from Models and Experiments: Uversky (32) Classifications^a. Values in \AA^3 Derived from Molecular Models and Experiment as Compared to Theory for Intermediate Sates

Casein	Model Value ^b	GPC Monomer ^c	Monomer in Polymer
α_{s1} -	260,000 (NU_{coil})	180,000 (NU_{PMG})	
α_{s2} - ^d	240,000 (NU_{coil})	180,000 (NU_{PMG})	
β -	65,500 (MG)	180,000 (NU_{PMG})	77,600 (MG)
κ -	66,000 (MG)	180,000 (NU_{coil})	59,700 (MG)

^aLetters in parentheses represent the following classifications for the three larger CNs: N = 47,000; MG = 66,000; PMG = 132,000; NU_{PMG} = 150,000; NU_{coil} = 288,000; and U in urea = 350,000. Values for the smaller κ -CN are 15% lower.

^bKumosinski *et al.* (15, 34), for α_{s1} -, β - and κ -CN.

^cPepper and Farrell (33).

^dHoagland *et al.* (35) for α_{s2} -CN.

CNs then, based upon model building, may represent "native" IDs with both persistent secondary structures (which maybe incapable of tertiary folds) and highly flexible elements as well. For CNs, these persistent secondary structure elements such as the sheet-turn-sheet motifs may lead to self-association, but no hydrophobic compression occurs and the proteins remain expanded and highly

hydrated. In essence, they may move from secondary to quaternary structure without forming complex tertiary folded intermediates, which are characterized by DSC profiles for globular proteins like α -lactalbumin (16).

Environmental Effects on CN Monomer Size and Classification

For purified κ -CN, using the weight average R_H from dynamic light scattering (DLS), and the weight average molecular weight from sedimentation equilibrium studies, the apparent volume of the κ -CN monomer occupied within the polymer can be estimated. The value obtained from this calculation as shown in Table II is 59,700 \AA^3 and it is quite close to that of the Uversky prediction of 54,000 \AA^3 for the MG state of κ -CN and to the model monomer volume (Table I). However, the monomer within the polymer is about 1/3 of the GPC volume for the monomer alone (Table I). In the purified κ -CN polymer, the individual monomer may therefore be more compact than the monomer alone as judged by GPC. Thus, the 3D model may appropriately represent the structure of the monomer within the κ -CN polymer and suggests that the κ -CN monomer is in an MG-like state within the polymer. As noted above, Ca^{2+} plays a significant role in the stabilization of α -lactalbumin. Metal ions play a similar role for purified κ -CN.

By electron microscopy (EM), purified κ -CN particles are somewhat

Table II. Changes in Calculated Hydrated Volumes V_H with Environmental Changes for Polymers of κ - and β -CNs. Values in \AA^3 for Comparison to Uversky (33) Intermediate States

Casein	R_H	Weight average MW	V_H Monomer in Polymer ^a
κ -CN	96 ^b	1.18×10^6 ^c	59,700 (MG)
+ EDTA	196 ^b	0.89×10^6 ^c	600,000 (>U)
β -CN 30°	103 ^d	1.42×10^6 ^d	77,600 (MG)
20°	110 ^e	1.20×10^6 ^f	112,000 (PMG)
5°	83 ^d	0.43×10^6 ^d	133,000 (PMG)

^aLetters in parentheses represent state as defined in Table I.

^bDynamic light scattering Farrell *et al.* (36).

^cSedimentation equilibrium Farrell *et al.* (36, 37, 38).

^dSAXS Kajiwaru *et al.* (39).

^eSAXS Andrews *et al.* (40).

^fSedimentation equilibrium Takase *et al.* (41).

spherical and have average radii of 9.0 nm. Treatment of κ -CN with EDTA removes bound metal ions and leads to a broader size distribution (or radii) estimated by dynamic light scattering, and an expanded shape as viewed by EM (36, 37), which results in an extremely large volume for the EDTA treated protein as seen in Table II. This indicates that the polymer is comprised of largely disordered monomers (probably in the U state) but the overall polymerization degree is maintained by disulfide bonds. Thus, κ -CN may be in an extended state upon reduction and dilution to monomer (NU_{coil}), compressed to MG in its normal polymer, and then “denatured” by EDTA treatment to a state $> \text{U}$ in urea.

β -CN forms large polymers that are highly temperature dependent. The association can be described by a model based upon “micelle” formation above a critical protein concentration (1, 2). As the temperature is increased, a limiting plateau is reached in size but the molecular weight increases (10, 42). Following the calculations outlined above for κ -CN, an apparent volume per monomer within the polymer ($77,600 \text{ \AA}^3$) can be calculated for β -CN at 30°C (Table II). This value is close to the Uversky prediction of $66,000 \text{ \AA}^3$ for the MG state and to the value generated from the 3D model (Table III). As the temperature is decreased to 20°C , the molecular weight falls but not the polymer size. Thus, the monomer is more flexible and becomes intermediate between the MG and the PMG states and at 5°C it is nearly identical to the PMG state. In all cases, the V_{H} values estimated for the β -CN monomer within its polymer are considerably less than those found by GPC at low concentrations for the monomeric β -CN ($180,000 \text{ \AA}^3$). Thus, the degree of compression is either related to the available size of the polymer, or alternatively conformational changes in the monomer allow for more efficient packing within the polymer (19, 42). As was the case with κ -CN, the 3D model of β -CN is more representative of the compressed component monomer within the polymer at temperatures approaching physiological. This fact, however points to the potential uses of isolated fractions of CN as proteins with multipotential functionalities.

Casein Hydration

One of the proposed features of the MG, PMG and U states of globular proteins and an important aspect of IUPs and IDPs is the increased internal hydration due to the more open structure. For example, in Table I, for a native globular protein, about 20,000 of its total volume of $47,000 \text{ \AA}^3$ (V_{H}) would be due to cavities and layers of water, or about $0.5\text{g H}_2\text{O/g}$ protein (as the van der Waals molecular volume of a 205 residue protein is about $25,000 \text{ \AA}^3$). For the CNs, the openness of their structures and the 3D models (Figure 1) suggest that these proteins can readily accommodate extremely high water content in their interior space. The water content of micelles and submicelles varies from 1 to 8

g H₂O/g protein (4, 43, 44). In a series of studies on CN water interactions, Mora Gutierrez *et al.* (45) have used ¹⁷O NMR to probe and enumerate sources of bound, trapped and preferentially absorbed water molecules. These cavities and voids have been correlated with the 3D model of sodium caseinate (33, 43). For CNs in the MG state the excess hydration would double to 1g H₂O/g protein and rise to 4g H₂O/g protein in the GPC monomer. Thus some of the physical and chemical properties of CNs are in accord with their occurrence in NU and PMG states.

Amyloid Formation and Casein Secretion

Amyloid bodies (corpor amylacae) have been reported to occur in secretory mammary tissues of various species. These amyloid bodies were isolated from bovine mammary gland by Niewold *et al.* (46). The major amyloid protein was identified as 32 to 45 residue fragments of α_{s2} -CN. These fragments all begin at residue 81 and can be due to the limited trypsinolysis of α_{s2} -CN. This segment of the molecule has been predicted to be α -helical (residues 77 to 91) followed by turn and then β -sheet (95-113 region) (34). It is possible that this segment may undergo a transition to β -sheet after cleavage and seed amyloid formation, which is typical behavior for amylogenic proteins (47, 48). Alternatively the complete molecule could be involved in the fibrillation process. This property could be used to produce nanofibrils for new technical applications.

Purified κ -CN occurs as a characteristic ladder group of disulfide bonded monomers as revealed by SDS gel electrophoresis. These polymers range from trimers to octamers and higher oligomers as shown by Groves *et al.* (49). To study the role of disulfide bonding in κ -CN, the protein was reduced and carboxymethylated (RCM) as described (49). There was little change in the estimated amounts of secondary structure by FTIR or CD from that reported either for native or EDTA treated κ -CN (35, 36). However this modification affected dramatically the propensity of κ -CN to aggregate. Negatively stained EM images of the κ -CN at 25°C showed particles much like those seen for the parent protein. The RCM protein, when heated to 37°C polymerized into long rod-like (amyloid) structures as seen in Figure 5. The sample also contains the spherical particles seen at 25°C for the native κ -CN (35, 36). On the basis of near-UV CD and docking of the 3D model, it is possible to conclude that there may exist a tyrosine rich sheet-turn sheet motif in κ -CN (residues 15 to 65) which may allow for the formation of these amyloid-like fibrils (38). Interestingly there is a 72 % homology between residues 81 to 121 of α_{s2} -Cn and residues 24 to 64 in κ -CN, and both of these segments of the molecules have been now implicated in amyloid formation. In the case of κ -CN, no proteolysis has occurred so the whole molecule produces the amyloid-like structures seen in Figure 5. It is our contention that this potential for alternate forms of aggregation

arises from the MG or NU_{PMG} state of κ -CN and α_{s2} -CN. We further propose that these proteins may possess the potential to produce a bio-fibrils for application to nanotechnology. This may be particularly true for κ -CN which not only produces fibrils but also binds metal ions (36).

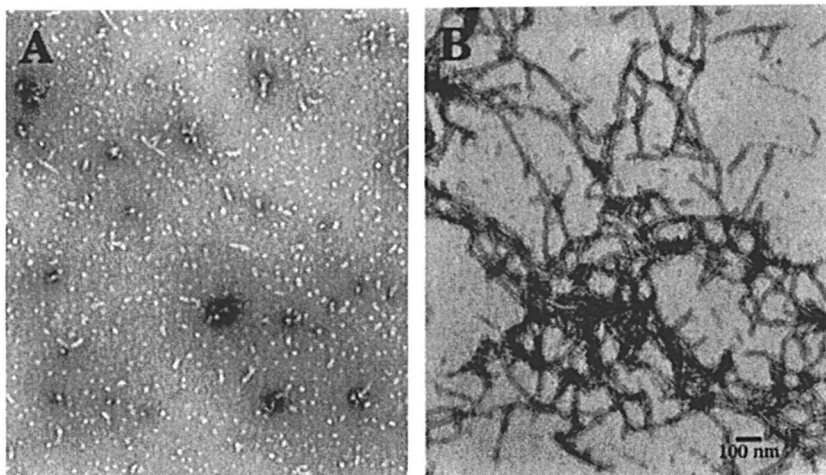


Figure 5. Transmission electron micrograph of a general field of negatively stained (uranyl acetate 2%) κ -CN (A) and reduced carboxymethylated κ -CN both heated for 1 hr at 37°C (B); the bar indicates 100 nm, and the magnification is 45,000 \times (38).

During the synthesis and secretion of CN by mammary gland, CN, calcium and phosphate accumulate in the *Golgi* vesicles of the secretory cells as shown in Figure 6. In the early stages of CN micelle formation, small particles of protein and perhaps some amyloid-like fibrils are seen. As secretion progresses, these fibrils and particles condense into the fully formed colloidal CN micelles (50, 51). It has been shown *in vitro* that α_{s1} -CN blocks the RCM- κ -CN's ability to form fibrils (38). It can be speculated then that these protein-protein interactions prevent accumulation of amyloid aggregates, which cannot be successfully secreted. Preliminary analysis (52) has also revealed that partially phosphorylated human β -CN will also form complexes with RCM-bovine κ -CN and inhibit fibril formation. Then in the presence of calcium these interaction products form particles similar to human milk micelles. It is interesting to note that for the most part β - and κ -CNs predominate in human milk, which is very poor in α_{s1} - and α_{s2} -CNs.

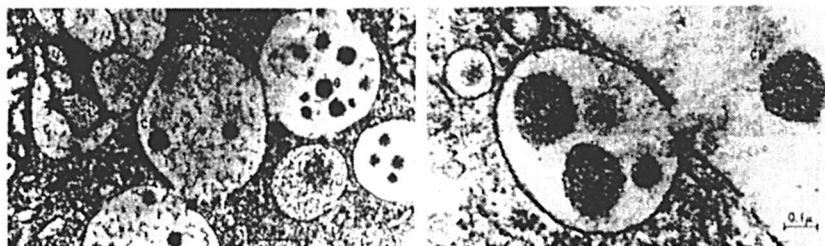


Figure 6. Formation of colloidal CN micelles (CMs) within the Golgi vacuoles of mammary gland alveoli. Top shows the aggregation of submicellar particles into micelles and fibril-like structures. Bottom shows a vacuole about to discharge its contents into the alveolar lumen; a CM is already present in the lumen (Reproduced from reference 50).

The overriding biological function of CN is to bind and carry calcium to the neonate. Tompa (18) has placed the CNs in a subcategory of IUPs termed scavengers because multivalent binding of calcium phosphate is necessary for their function. To serve this function a number of on-line protein-protein associations must occur and aggregations leading to amyloid or other non-productive complexes must be avoided. Clearly protein-protein associations begin in the lumen of the endoplasmic reticulum and progress into the Golgi vesicles where phosphorylation of the CNs begins and calcium accretion occurs (51). There are perhaps a number of possible association patterns, which may be predicted for the CNs, yet the system must be somewhat pliable as many species of mammals exhibit a variety of themes of CN composition. It must be noted that all CNs so far discovered are variations of the four major bovine CNs. Apparently a good deal of redundancy occurs in these on-line interactions as all species competently produce CN micelles, but at the heart of the interactions are most likely conserved protein sequences which lead to competent CN colloids for the transport of calcium and phosphate in a highly bioassimilable state.

Conclusion

In conclusion, as the field of structural biology evolves, we will learn more about the basic structures of the CNs. Perhaps 2D X-ray crystallography or EM reconstruction may yield higher resolution models of the CNs, possibly even at the atomic level. However, as the field progresses, we need to be aware of the opportunities these advances present for enhancement of dairy products or for adaptation of milk proteins as food ingredients. To more fully take advantage of the unique properties of the CNs, we will need new alternative and cost effective

means of fractionation. In addition, new insights into present processing methodologies will be required to yield the innovative processes needed for future applications. So we are at the beginning of an exciting era in protein chemistry and hopefully food technology.

References

1. Swaisgood, H. E. In *Advanced dairy chemistry: proteins*; Fox, P. F.; McSweeney, P. L. H., Eds.; Kluwer Academic / Plenum Publishers: New York, NY, 2003; Vol. 1, pp. 139-201.
2. Farrell, H. M., Jr.; Jimenez-Flores, R.; Bleck, G. T.; Brown, E. M.; Butler, J. E.; Creamer, L. K.; Hicks, C. L.; Hollar, C. M.; Ng-Kwai-Hang, K. F.; Swaisgood, H. E. *J. Dairy Sci.* **2004**, *87*, 1641-1674.
3. Creamer, L. K.; Richardson, T.; Parry, D. A. *Arch. Biochem. Biophys.* **1981**, *211*, 689-696.
4. Holt, C.; Sawyer, L. *J. Chem. Soc. Faraday Trans.* **1993**, *89*, 2683-2692.
5. Paulsson, M.; Dejmek, P. *J. Dairy Sci.* **1990**, *73*, 590-600.
6. Xie, D.; Bhakuni, V.; Freire, E. *Biochemistry* **1991**, *30*, 10673-10678.
7. Byler, D. M.; Farrell, H. M., Jr.; Susi, H. *J. Dairy Sci.* **1988**, *71*, 2622-2629.
8. Shi, Z.; Woody, R. W.; Kallenbach, N. R. *Adv. Protein Chem.* **2002**, *62*, 163-240.
9. Creamer, T. P.; Campbell, M. N. *Adv. Protein Chem.* **2002**, *62*, 263-282.
10. Farrell, H. M., Jr.; Wickham, E. D.; Unruh, J. J.; Qi, P. X.; Hoagland, P. D. *Food Hydrocolloids* **2001**, *15*, 341-354.
11. Malin, E. L.; Alaimo, M. H.; Brown, E. M.; Aramini, J. M.; Germann, M. W.; Farrell, H. M., Jr.; McSweeney, P. L.; Fox, P. F. *J. Protein Chem.* **2001**, *20*, 391-404.
12. Syme, C. D.; Blanch, E. W.; Holt, C.; Jakes, R.; Goedert, M.; Hecht, L.; Barron, L. D. *Eur. J. Biochem.* **2002**, *269*, 148-156.
13. Kumosinski, T. F.; Brown, E. M.; Farrell, H. M., Jr. *J. Dairy Sci.* **1993**, *76*, 2507-2520.
14. Farrell, H. M., Jr.; Brown, E. M.; Hoagland, P. D.; Malin, E. L. In *Advanced Dairy Chemistry - 1: Proteins, 3rd edition*; Fox, P. F.; McSweeney, P. L. H., Eds.; Kluwer Academic/Plenum Publishers: New York, 2003; Vol. 1 Part A, pp. 203-231.
15. Kumosinski, T. F.; King, G.; Farrell, H. M., Jr. *J. Protein Chem.* **1994**, *13*, 701-714.
16. Farrell, H. M., Jr.; Qi, P. X.; Uversky, V. N. Proceeding chapter. In *Advances in Biopolymers: Molecules, clusters, networks and interactions*; Fishman, M.; Qi, P. X. Eds.; American Chemical Society Publishers: Washington, DC.

17. Tompa, P. *Trends Biochem. Sci.* **2002**, *27*, 527-533.
18. Onuchic, J. N.; Nymeyer, H.; Garcia, A. E.; Chahine, J.; Socci, N. D. *Adv. Protein Chem.* **2000**, *53*, 87-152.
19. Dunker, A. K.; Lawson, J. D.; Brown, C. J.; Williams, R. M.; Romero, P.; Oh, J. S.; Oldfield, C. J.; Campen, A. M.; Ratliff, C. M.; Hipps, K. W.; Ausio, J.; Nissen, M. S.; Reeves, R.; Kang, C.; Kissinger, C. R.; Bailey, R. W.; Griswold, M. D.; Chiu, W.; Garner, E. C.; Obradovic, Z. *J. Mol. Graph. Model.* **2001**, *19*, 26-59.
20. Romero, P.; Obradovic, Z.; Dunker, A. K. *Genome Bioinformatics* **1997**, *8*, 110-124.
21. Dunker, A. K.; Garner, E.; Guillot, S.; Romero, P.; Albrecht, K.; Hart, J.; Obradovic, Z.; Kissinger, C.; Villafranca, J. E. *Pac. Symp. Biocomput.* **1998**, 473-484.
22. Romero, P.; Obradovic, Z.; Li, X.; Garner, E. C.; Brown, C. J.; Dunker, A. K. *Proteins* **2001**, *42*, 38-48.
23. Vihinen, M. *Protein Eng.* **1987**, *1*, 477-480.
24. Cupo, P.; El-Deiry, W.; Whitney, P. L.; Awad, W. M., Jr. *J. Biol. Chem.* **1980**, *255*, 10828-10833.
25. Mrabet, N. T.; Van den Broeck, A.; Van den brande, I.; Stanssens, P.; Laroche, Y.; Lambeir, A. M.; Matthijssens, G.; Jenkins, J.; Chiadmi, M.; van Tilbeurgh, H.; Rey, F.; Janin, J.; Quax, W. J.; Lasters, I.; De Maeyer, M.; Wodak, S. J. *Biochemistry* **1992**, *31*, 2239-2253.
26. D'Amico, S.; Gerday, C.; Feller, G. *J. Biol. Chem.* **2001**, *276*, 25791-25796.
27. Saunders, N. F.; Thomas, T.; Curmi, P. M.; Mattick, J. S.; Kuczek, E.; Slade, R.; Davis, J.; Franzmann, P. D.; Boone, D.; Rusterholtz, K.; Feldman, R.; Gates, C.; Bench, S.; Sowers, K.; Kadner, K.; Aerts, A.; Dehal, P.; Detter, C.; Glavina, T.; Lucas, S.; Richardson, P.; Larimer, F.; Hauser, L.; Land, M.; Cavicchioli, R. *Genome Res.* **2003**, *13*, 1580-1588.
28. Uversky, V. N.; Gillespie, J. R.; Fink, A. L. *Proteins* **2000**, *41*, 415-427.
29. Dunker, A. K.; Obradovic, Z.; Romero, P.; Garner, E. C.; Brown, C. J. *Genome Inform. Ser. Workshop Genome Inform.* **2000**, *11*, 161-171.
30. Oldfield, C. J.; Cheng, Y.; Cortese, M. S.; Brown, C. J.; Uversky, V. N.; Dunker, A. K. *Biochemistry* **2005**, *44*, 1989-2000.
31. Li, X.; Romero, P.; Rani, M.; Dunker, A. K.; Obradovic, Z. *Genome Inform. Ser. Workshop Genome Inform.* **1999**, *10*, 30-40.
32. Uversky, V. N. *Protein Sci.* **2002**, *11*, 739-756.
33. Pepper, L.; Farrell, H. M., Jr. *J. Dairy Sci.* **1982**, *65*, 2259-2266.
34. Kumosinski, T. F.; King, G.; Farrell, H. M., Jr. *J. Protein Chem.* **1994**, *13*, 681-700.
35. Hoagland, P. D.; Unruh, J. J.; Wickham, E. D.; Farrell, H. M., Jr. *J. Dairy Sci.* **2001**, *84*, 1944-1949.

36. Farrell, H. M., Jr.; Kumosinski, T. F.; Cooke, P. H.; King, G.; Hoagland, P. D.; Wickham, E. D.; Dower, H. J.; Groves, M. L. *J. Protein Chem.* **1996**, *15*, 435-445.
37. Farrell, H. M., Jr.; Kumosinski, T. F.; Cooke, P. H.; Hoagland, P. D.; Wickham, E. D.; Unruh, J. J.; Groves, M. L. *Int. Dairy J.* **1999**, *9*, 193-199.
38. Farrell, H. M.; Cooke, P. H.; Wickham, E. D.; Piotrowski, E. G.; Hoagland, P. D. *J. Protein Chem.* **2003**, *22*, 259-273.
39. Kajiwara, K.; Niki, R.; Urakawa, H.; Hiragi, Y.; Donkai, N.; Nagura, M. *Biochim. Biophys. Acta* **1988**, *955*, 128-134.
40. Andrews, A. L.; Atkinson, D.; Evans, M. T. A.; Finer, E. G.; Green, J. P.; Phillips, M. C.; Robertson, N. *Biopolymers* **1979**, *18*, 1105-1121.
41. Takase, K.; Niki, R.; Arima, S. *Biochim. Biophys. Acta* **1980**, *622*, 1-8.
42. Qi, P. X.; Wickham, E. D.; Farrell, H. M., Jr. *Protein J.* **2004**, *23*, 389-402.
43. Farrell, H. M., Jr.; Qi, P. X.; Brown, E. M.; Cooke, P. H.; Tunick, M. H.; Wickham, E. D.; Unruh, J. J. *J. Dairy Sci.* **2002**, *85*, 459-471.
44. Farrell, H. M., Jr.; Kumosinski, T. F.; Malin, E. L.; Brown, E. M. In *Methods Mol Biol., Vol. 172: Calcium-binding Protein Protocols, Vol. 1: Reviews and Case Studies.*; Vogel, H. J., Ed.; Humana Press, Inc.: Totwa, NJ, 2002; Vol. 1, pp. 97-140.
45. Mora-Gutierrez, A.; Kumosinski, T. F.; Farrell, H. M., Jr. *J. Agric. Food Chem.* **1997**, *45*, 4545-4553
46. Niewold, T. A.; Murphy, C. L.; Hulskamp-Koch, C. A.; Tooten, P. C.; Gruys, E. *Amyloid* **1999**, *6*, 244-249.
47. Goers, J.; Permyakov, S. E.; Permyakov, E. A.; Uversky, V. N.; Fink, A. L. *Biochemistry* **2002**, *41*, 12546-12551.
48. Chiti, F.; Calamai, M.; Taddei, N.; Stefani, M.; Ramponi, G.; Dobson, C. M. *Proc. Natl. Acad. Sci. U S A* **2002**, *99*, 16419-16426.
49. Groves, M. L.; Dower, H. J.; Farrell, H. M., Jr. *J. Protein Chem.* **1992**, *11*, 21-28.
50. Farrell, H. M., Jr.; Thompson, M. P. *J. Dairy Sci.* **1971**, *54*, 1219-1228.
51. Farrell, H. M., Jr. In *Encyclopedia of Reproduction*; Knobil, E.; Neill, J. D., Eds.; Academic Press, Inc.: San Diego, CA, 1999; Vol. 3, pp. 256-263.
52. Sood, S. M.; Lekic, T.; Farrell, H. M., Jr.; Slattery, C. W. *FASEB J.* **2005**, *4*, A818.

Chapter 5

Importance of C-Terminal Region of Bovine β -Casein

Phoebe X. Qi*

Eastern Regional Research Center, Agricultural Research Service,
U.S. Department of Agriculture, 600 East Mermaid Lane,
Wyndmoor, PA 19038

Bovine β -casein (β -CN) with the C-terminal truncated by chymosin digestion, 1-192 fragment (β -CN-(f 1-192)), was examined using circular dichroism (CD) under various temperature and solvent conditions. The effect of C-terminal deletion on the structure and stability of the parent protein, β -casein (β -CN), is analyzed and discussed. Analytical ultracentrifugation results showed reduced degree of self-association in β -CN-(f 1-192) compared to whole β -casein. CONTIN/LL analysis of the CD data revealed clear changes in the overall secondary structural content in β -CN-(f 1-192) in the temperature range studied (5 to 70°C). Results obtained in this work suggest significant secondary structure disruption of β -casein upon its C-terminal deletion. It has been shown that 80% trifluoroethanol (TFE) at low temperatures ($\leq 25^\circ\text{C}$) can effectively induce α -helical content in β -CN-(f 1-192), to the same level as that of β -CN. In addition, sodium dodecyl sulfate (SDS) at greater than micellar concentration is capable of refolding β -CN-(f 1-192). Temperature dependence of these induced structures was also studied. Furthermore, binding experiments with the common hydrophobic probe-8-Anilino-1-naphthalene sulfonate (ANS) illustrated that β -CN-(f 1-192) is nearly incapable of binding to ANS. These results clearly demonstrated that the tail peptide, β -CN-(f 193-209) is important in maintaining the hydrophobic core of β -CN.

Introduction

It has been well established (1-3) that native bovine β -casein undergoes an endothermic self-association that reaches a limiting size depending on the ionic strength. The critical micelle model (4, 5) has been applied to describe this highly concentration and temperature dependent process. Largely because of this self-association behavior, it has been difficult to obtain detailed information on its three-dimensional structure by either X-ray crystallography or NMR spectroscopy, two of the most common and definitive techniques for determining protein structures.

In earlier studies (6, 7), β -casein was believed to have a conformation approximating a complete random coil with little or no regular secondary structure under physiological conditions, *i.e.* aqueous solution, neutral pH and low ionic strength. The "rheomorphic" hypothesis proposed by Holt and Sawyer (8) in the 90's suggested that all structures in caseins are completely flexible and form in response to flow. The latest development in understanding structure-function relationship of proteins, however, has classified caseins as a member of the growing family of natively unfolded (9) or intrinsically unstructured proteins (10). These proteins have been shown to exhibit little or no ordered secondary structure, almost complete lack of globularity, low compactness, and high intramolecular flexibility under physiological conditions *in vitro*. The functional role of these proteins is particularly an evolving area of much research (11). Our work (12, 13) on thermal and alkaline denaturation of native β -CN suggested that caseins would fall between the "pre-molten globule" and the "natively unfolded pre-molten globule" states based on descriptions by Uversky (14).

Early work by Thompson *et al.* (15) using sedimentation velocity ultracentrifugation suggested that removal of the last three hydrophobic C-terminal amino acids of β -casein greatly diminished its ability to self-associate. The critical role of C-terminal region in the self-association process of bovine β -casein was suggested by Berry and Creamer (16) for chymosin cleaved fragment 1-189 by zonal column chromatography. Bu *et al.* (17), however, recently found chymosin treatment of recombinant non-phosphorylated human β -casein did not completely abolish self-association and that colloidal calcium complexes were still present. In addition, Visser and Slangen (18) suggested that Leu(192)-Tyr(193) was a more susceptible chymosin cleavage site.

To investigate the effect of C-terminal deletion on the structure and stability of β -casein, we used electrospray ionization mass spectrometry (ESI-MS) to quantitatively establish the cleavage site by chymosin. We examined and

characterized the secondary structure of the fragment from chymosin digestion at various temperature and solvent conditions in comparison to that of its parent protein, β -casein. In this paper, we report apparent differences in the self-association as well as the structures of the two proteins.

Materials and Methods

Materials

Anilino-8-naphthalenesulfonic acid (ANS) of high purity was purchased from Molecular Probes (Eugene, OR). All other reagents used were of analytical grade or 'ACS certified' from Sigma (St. Louis, MO). Isolation and purification of β -casein were performed as described previously (19).

β -CN-(f1-192) was prepared following initial pilot studies by HPLC using reverse phase C-18 column to optimize the digestion reaction of the parent protein (β -CN). Digestion reaction conditions were as follows: 300 mg β -casein was dissolved in 300 ml 0.01 M NH_4Ac . The pH of the solution was adjusted to 6.55 with acetic acid. The solution was placed into a 5°C water bath, and the solution temperature was monitored closely until it was equilibrated. 600 μl of 2.44 mg/ml chymosin (rennin) solution was then added, mixed and digested for exactly one hour. 15ml ethanol was added immediately to the solution, which was then transferred to a lyophilizing flask and freeze-dried. The freezing terminated the reaction and was done immediately after the sample was removed from the 5°C bath. The added ethanol makes the final product less electrostatic and easier to work with. The genetic variant used in this work was β -casein A¹ and the larger fragment of chymosin cleaved products was β -CN-(f1-192) as determined by electrospray ionization mass spectrometry (ESI-MS). The SDS-gel electrophoresis (Figure 1) shows purity of greater than 90%. Protein concentrations used in Figure 1 are as follows: lane A and B are at 1.0 mg/ml; lane C, D and E are at 0.2 mg/ml.

Circular dichroism (CD) spectroscopy

Far-UV CD experiments were carried out with 0.17 ± 0.02 mg/ml (7.67 μM) β -CN-(f1-192) in a 2 mM PIPES (piperazine-N,N'-bis(2-ethanesulfonic

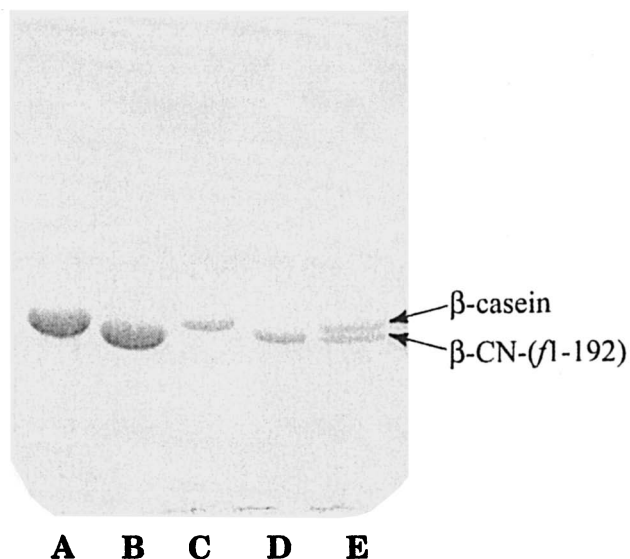


Figure 1. SDS-PAGE gel electrophoresis of chymosin cleaved products of bovine β -casein. Lanes A & C represent native β -casein, lanes B & D represent purified fragment β -CN-(f1-192), and lane E is the digestion mixture.

acid)), 4 mM KCl buffer at pH 6.75 ($I=7.5$ mM) or a 33 mM potassium phosphate buffer at pH 6.75 ($I=50$ mM). Successive measurements in the far UV region (190-250 nm) were made with overlapping samples at the following temperature points: 4°, 10°, 15°, 20°, 25°, 37°, 50°, 60° and 70°C. All solvents for CD measurements were first filtered through a Millipore 0.22 μm pore filter. Dissolved protein and peptide samples were filtered through a 0.45 μm pore regenerated cellulose filter. Extinction coefficient of β -CN-(f1-192) was calculated to be $\epsilon_{280}=0.43$ l g⁻¹ cm⁻¹ based on Wetlaufer (20) from absorbance spectra obtained on a Beckman DU-7 UV-Vis spectrophotometer (Palo Alto, CA), using an extinction coefficient of $\epsilon_{280}=0.45$ l g⁻¹ cm⁻¹ for native β -casein. Circular dichroism spectra were recorded on an Aviv model 60DS spectrophotometer (Aviv Associates, Lakewood, NJ) using cells of appropriate path lengths and a scan time of 4.0 s/nm. The jacketed cells were attached to a circulating constant temperature bath; the equilibration time of the sample was calculated to be 30 min for a 30° change in the bath temperature. All spectra are

corrected for solvent contributions and are expressed in units of mean residue ellipticity (far-UV) degrees $\text{cm}^2 \text{dmole}^{-1}$ relative to wavelength. Analysis of protein secondary structure from CD spectra was accomplished using the CONTIN/LL procedure of CDPro software package (21, 22) with 48 proteins in the reference set.

Non-linear regression analysis

We have previously (13) used a series of equations derived from the theory of thermodynamic linkage (23) to qualitatively describe the concentration, temperature dependent self-association behavior of β -CN. β -CN-(f1-192) was subjected to similar studies and the results will be reported elsewhere (24). The following equation (eq 1) has been used (13) to quantitatively describe and compare temperature induced self-association and conformational changes in the two proteins:

$$\varphi_{\text{app}} = \frac{\varphi_0}{1 + k_1^n T^n} + \frac{\varphi_1 k_1^n T^n}{1 + k_1^n T^n} + \frac{(\varphi_2 - \varphi_1) k_2^m T^m}{1 + k_2^m T^m} \quad (1)$$

It should be noted that the above expression is valid for sequential reduction only, *i.e.* assuming $k_1^n \gg k_2^m$ and $k_1^n \gg 1$.

Fluorescence spectroscopy

Fluorescence spectra were recorded with a Florolog-3 spectrofluorometer (Jobin Yvon, Inc., Edison, NJ) equipped with a Peltier sample cooler. A 1 cm path-length quartz cell at room temperature (20°C-24°C) was used in this work. ANS binding studies were carried out by titrating increasing ANS concentration into a fixed protein concentration (5.0 μM) in PIPES buffer, I=50 mM, pH 6.75. An excitation wavelength (λ_{ex}) of 380 nm was used, and fluorescence emission was recorded from 400 to 600 nm. All the spectra were corrected for solvent and protein contributions to ANS fluorescence.

Analytical ultracentrifugation

For analytical ultracentrifugation, the protein samples were dissolved in 25 mM PIPES (and 8 mM KCl, I=50 mM) buffer, pH 6.75 at concentrations ranging from 1.0 to 3.0 mg/ml. Samples and solvents were filtered with a Waters (Milford, MA) HVLV 0.45 μm membrane filter. Phast gel electrophoresis in SDS showed a nearly identical pattern of protein components before and after filtration; less than 1% of the material was retained on the filter as ascertained by UV spectroscopy. Sedimentation equilibrium experiments were performed using a Beckman Optima XL-A (Palo Alto, CA) analytical ultracentrifuge at speeds ranging from 6,000 to 12,000 rpm at various temperatures. A 12 mm charcoal-epon 6 channel centerpiece was used with quartz windows in a wide aperture window holder. The solvent density used in these experiments was 1.0044 at 25°C. This value was calculated from the data as previously described using 0.564 cc/g as the partial specific volume of PIPES. The partial specific volumes of β -CN and β -CN-(f1-192) were taken as 0.728 and 0.739 respectively (25). Data were collected at 280 nm using the standard XL-A procedure. The plots of absorption relative to radius were analyzed directly for weight average molecular weight using the program IDEAL1; a part of the Optima XL-A data analysis software. As the absorbance offsets were not allowed to float in these analyses, weight average molecular weights can be obtained. Increased molecular weight with increased ionic strength was anticipated by the data of Schmidt (26) who clearly demonstrated self-association for native β -casein. Schmidt and coworkers used the following model to analyze their data:



Where $i\beta$ refers to the unbound protein, and $i \gg 1$ ranging from 20 to 50. Other models such as the formation of polymer through a critical micelle concentration have also been used by others (3). Analysis of the current data was accomplished using ASSOC4 which is for a system of up to four species. This model represents a parallel association scheme where monomer is simultaneously in equilibrium with dimer, trimer and tetramer when n_2 , n_3 and n_4 are integers 2, 3 and 4 in eq 2. In our experiments with β -CN and β -CN-(f1-192) the best fits were obtained by fixing the sequence molecular weight at 24,600 Da and 22,600 Da for the respective monomers and floating K values at the increasing integer values of n noted above; only one constant was required to fit the data. Analysis of all the data was accomplished using the following equation:

$$A_r = \text{EXP}[\ln(A_0) + H \times M \times (X^2 - X_0^2)]$$

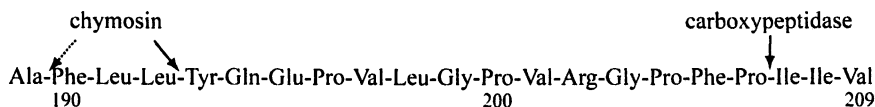
$$\begin{aligned}
 &+ \text{EXP}[n_2 \times \ln(A_0) + \ln(K_{a2}) + n_2 \times H \times M \times (X^2 - X_0^2)] \\
 &+ \text{EXP}[n_3 \times \ln(A_0) + \ln(K_{a3}) + n_3 \times H \times M \times (X^2 - X_0^2)] \\
 &+ \text{EXP}[n_4 \times \ln(A_0) + \ln(K_{a4}) + n_4 \times H \times M \times (X^2 - X_0^2)] \\
 &+ E
 \end{aligned} \tag{2}$$

Where A_r is total absorbance of all species at radius X ; EXP is exponent; ln is natural log; A_0 is absorbance of the monomer species at reference radius X_0 ; H is constant $[(1-\bar{v}\rho)\omega^2]/2RT$; M is apparent monomer molecular weight; X_0 is reference radius; n_i is stoichiometry for species I (number of monomers); K_{ai} is association constant for the monomer-mer equilibrium of species I ; and E is baseline offset.

Results and Discussion

Characterization of the protein fragment, β -CN-(f1-192)

A brief report (15) on the treatment of β -casein by carboxypeptidase at pH 7.0 indicated that the removal of the last three residues greatly decreased the self-association process. Creamer *et al.* (27) studied the action of milk-clotting enzyme chymosin (rennin) on β -casein by zonal column chromatography at neutral pH. They found that chymosin preferably splits off a C-terminal fragment from β -casein with a molecular weight of approximately 2000 Da. They further determined that the chymosin cleavage site was at Ala(189)-Phe(190) (see below) in their subsequent studies and suggested that the C-terminus is solely responsible for the self-association behavior of β -casein. It, however, was argued that zonal column chromatography could only qualitatively describe an associated system. Visser and Slangen (18) reexamined the specificity of chymosin on β -casein at 13°C and pH 5.4, and reported that Leu(192)-Tyr(193) is a much more susceptible site for chymosin cleavage. The following scheme summarizes the cleavage sites by chymosin and carboxypeptidase in the C-terminal region of β -casein.



In our experiments, the purified larger fragment from the reaction mixture was subjected to carboxypeptidase A analysis, and showed a rapid liberation of

Leu followed by Phe and Ala. The final molecular ratios were 1.0:0.9:1.9 for Ala:Phe:Leu, which is indicative of the sequence of Ala-Phe-Leu-Leu. Further quantitative characterization of the larger fragment was achieved by electrospray ionization mass spectrometry (ESI-MS). The obtained experimental value unambiguously identified that the larger fragment was β -CN-(f1-192) and the parent protein was genetic variant A¹ as shown in Table I.

Table I. ESI-MS analysis of molecular mass

	Expected MW (Da) ^a	Experimental Value (Da)
β -casein A ¹	24023	24019 ± 1
β -casein A ²	23983	
β -casein A ³	23974	
β -CN-(f1-192) A ¹	22160	22156 ± 1
β -CN-(f1-189) A ¹	21786	

^aCalculated based on molecular formula (28).

Reduction of self-association in β -CN-(f1-192)

The critical micelle model (3, 5, 29) has long been used to describe the dominant temperature and/or concentration mediated self-association of β -casein. It has also been shown that the association process is highly salt-dependent (1). The shape of the monomer, and the contributions of conformational change in the early stages of the association, however, remained controversial. Thurn *et al.* (29) found a molecular weight of 420,000 and an R_H of 13.2 nm for β -casein at 10°C; and the values increased to 1,400,000 and 16.3 nm at 25°C by static and dynamic light scattering. Monomers of β -casein have been reported to range from spherical particles of 10-20 nm diameter as viewed by electron microscopy (30) to long threads with an axial ratio of 12:1 as calculated from viscosity by Payens and van Markwijk (31). The classical calculations of Waugh *et al.* (4) clearly showed that on the average the β -casein monomer, within the polymer, must hold a lower volume than most proposed monomer models. Thus, a conformational change to a more compact structure prior to or during the association process seems necessary. Perhaps one reason for the controversy over the nature of the β -casein monomer is that much of the physical-chemical data has been collected at high protein concentrations (1 to 3% w/v, *i.e.* 416 μ m-1.25 mM) or high ionic strengths (0.2 to 0.4 M) which generally favor the self-association. In contrast, spectroscopic data are often collected on more dilute samples. Accordingly, we have reexamined the β -CN-(f1-

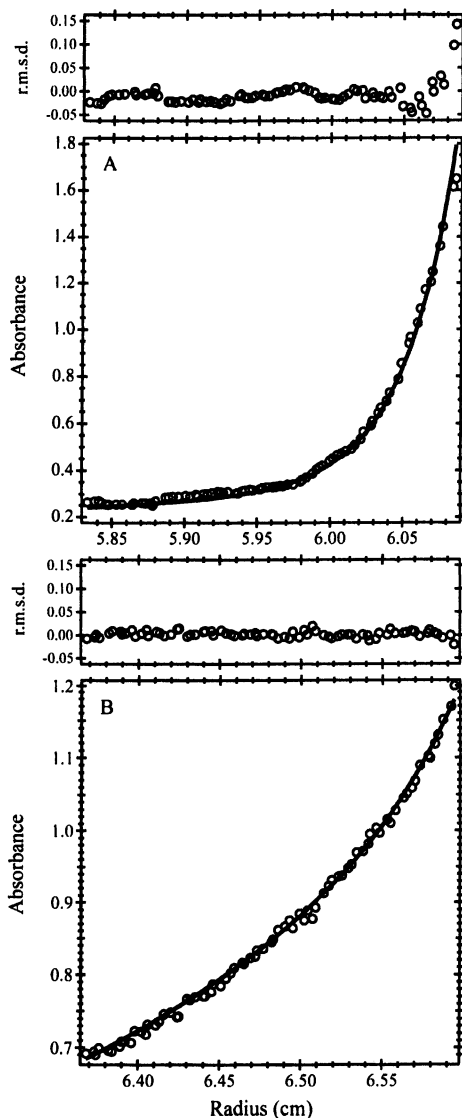


Figure 2. Analytical ultracentrifugation analysis of native β -casein (A) and β -CN-(f1-192) (B) at 25°C in PIPES buffer, at $I=50\text{mM}$ and pH 6.75. The fits to the absorbance vs. radius plot for eq 2 at 10,000 rpm for β -CN-(f1-192) and 9,000 rpm for β -casein, and the residual for the fits are also shown. Protein concentration was $83.3\ \mu\text{M}$ and $108.3\ \mu\text{M}$ for β -CN and β -CN-(f1-192) respectively.

192) self-association process and compared it to that of its parent protein, β -casein, at much reduced concentrations (1 to 2 mg/ml) and lower ionic strength (0.05 M) at neutral pH (6.75). Sedimentation equilibrium analysis was carried out from 25°C at various rotor speeds, as described in the experimental section. A considerable degree of self-association is clearly present as evidenced by the upward curvature of the data for β -casein; shown in Figure 2A. In contrast, self-association is greatly reduced for β -CN-(f1-192) in Figure 2B. Both curves were fitted with an assumed multi-species system. The fits to the absorbance vs. radius plot for eq 2 at 10,000 rpm for β -CN-(f1-192) and 9,000 rpm for β -casein, and the residual for the fits were also shown. The apparent “monomer” molecular weights near the meniscus were 22,500 Da and 24,600 for β -CN-(f1-192) and β -casein respectively.

Our observation that β -CN-(f1-192) exhibits apparently reduced but not completely abolished degree of self-association is in clear contradiction with the studies of Berry and Creamer on β -CN-(f1-189) by zonal column chromatography (16), which suggested that removal of a 20 amino acid peptide (β -CN-(f190-209)) completely destroyed β -CN's ability to self-associate. Our studies (24) of temperature dependent self-association behavior of β -CN-(f1-192) quantitatively established that although the C-terminal region of β -CN is important in the self-association process, other parts of the molecule may contribute significantly in maintaining the intermolecular interactions. Results by Bu *et al.* (17) on recombinant non-phosphorylated human β -casein appeared to be in close agreement with this assumption.

Secondary structure comparison between β -CN-(f1-192) and β -CN

The CONTIN/LL, a variant of the CONTIN procedure developed by Provencher and Glöckner (32) has been used by many to analyze the CD data and estimate secondary structure content of proteins and peptides. The database of 48 proteins (21) was chosen in this work because it contains both denatured proteins as well as left handed polyproline II (PPII) structural elements even though the output of the program does not explicitly index the content of PPII. In addition, the calculated spectra seemed to be generally in good agreement with our experimental data. Analysis of far-UV CD spectra of β -casein at room temperature (25°C), low ionic strength ($I=0.05$ M) and pH 6.75 indicates approximately 17% α -helix, 2% β -strand, 16% turns, and nearly 65% unordered, and these elements became 5%, 2%, 7%, and 87% for β -CN-(f1-192) under identical experimental conditions. Although residues 1 to 6 of β -CN were strongly predicted (33) to adopt α -helical conformation in the secondary

structure prediction, the lack of α -helix in the N-terminal portion of β -CN was clearly demonstrated in the NMR studies of the 1-25 peptide (34) as well as 1-42 peptide (35). Our work (36) on native β -casein (1-25) peptide and its dephosphorylated form revealed possible existence of polyproline II and turns in this region.

Figure 3 compares the CD spectra of β -CN-(f1-192) at various temperatures. It is apparent that there is a stronger similarity between the CD spectra of β -CN-(f1-192) and β -CN-(f1-25) than that between β -CN-(f1-192) and β -CN. The strong negative CD band in the region of 190-200 nm signifying unordered structural element in proteins (37) not only blue shifted for ~ 5 nm for β -CN-(f1-192) relative to β -CN, an increase of $\sim 2,500$ (degree $\text{cm}^2 \text{dmol}^{-1}$) in intensity at 25°C was also observed. This could likely be resulted from the increase of $\sim 22\%$ in unordered structure and a simultaneous reduction in both α -helical and turn contents compared to β -CN as indicated by the CONTIN/LL analysis. Overall, the CD spectra of β -CN-(f1-192) and β -CN-(f1-25) resemble to that of systemin which was found (38) to contain poly(L-proline) II type helix in many respects. This perhaps is not unanticipated because of the high number of proline residues, 34, which constitutes over 11% of the total residues in β -CN A¹. Consequently, β -CN may possess strong tendency to form left handed

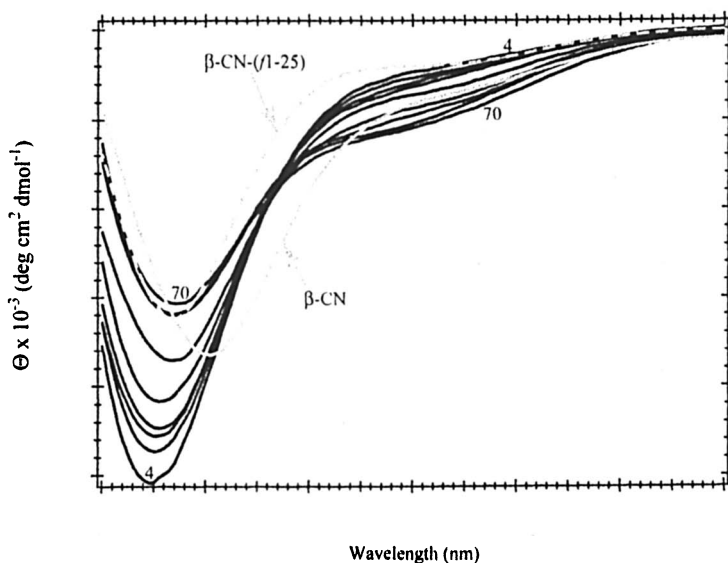


Figure 3. CD spectra of β -CN-(f1-192) at pH 6.75 and various temperatures (dark solid lines). Numbers labeled on the lines represent temperatures. The CD spectra of native β -CN (solid gray line) and β -CN-(f1-25) (dashed gray line) at 25°C was also plotted as a comparison. Protein concentration was $7.67 \mu\text{M}$.

poly(L-proline) II, which has been increasingly recognized as an important structural elements in unfolded proteins (39, 40).

Effect of temperature on the secondary structure of β -CN-(f1-192)

The temperature dependence of CD spectra of β -CN-(f1-192) (see Figure 3) appears to follow that of β -CN closely. The movement of polyproline II model peptide from aqueous to a more apolar (hydrophobic) environment (41) seems to mirror the changes seen for both β -CN and β -CN-(f1-192). Similar results (data not shown for reasons of clarity) were also obtained in analyzing the temperature dependence of CD spectra of a polyglutamate (MW750-1500) peptide at neutral pH which has been regarded as containing polyproline II conformations. Systemin that has been demonstrated (38) to contain PPII elements whose CD spectra were also found to display a similar temperature dependence behavior.

Unlike β -casein where the only meaningful change is an apparent increase in α -helical content ongoing from 2° to 70°C at pH 6.75 (12, 13), the amount of α -helix in β -CN-(f1-192) does not show noticeable temperature dependence based on the analysis from CONTIN/LL, indicating the calculated values for these elements are perhaps significantly lower (2%-5%), they are thus difficult to detect. One other explanation could be that there is little thermal unfolding in this class structure (however low it may be) as the protein is heated at pH 6.75. The amount of β -strand was found to follow a similar trend. The amount of turns, however, experienced noticeable reduction, to 7% at 25°C, and then returned to the value at 4° (14%) as temperature continues to increase. It is interesting to note that the amount of turns in its parent protein, β -CN, is also about 14% at higher temperature. The difference in self-association behavior between the two proteins could be attributable to the observed difference at elevated temperature even at low concentration. The extended (unordered) structure remains relatively unchanged as a function of temperature. A similar conservation of extended turns at high temperature had been previously observed for intact β -casein (A¹ variant) by Farrell *et al.* (12) and Graham *et al.* (42).

The temperature dependence of the CD spectra of β -CN-(f1-192) was quantitated and compared to that of β -casein in Figure 4. When fitted with eq 1, the predicted maximum change at temperatures greater than 70°C, the maximum ellipticity value ($\Delta\Theta_{\max}$) at 0°C and the mid-points of transitions in $T_{\theta_{224}}$ and $T_{\theta_{\max}}$ can be obtained for both β -CN-(f1-192) and β -casein. Table II compares changes in ellipticity at 224nm (Θ_{224} , Figure 4A), the maximum ellipticity (Θ_{\max} , Figure 4B), and the wavelength change at the maximum ellipticity (λ_{\max} , Figure 4C).

It appears that temperature has a comparable effect on the ellipticity at 224 nm for both β -casein and β -CN-(f1-192), indicated by a similar maximum

Table II. Analysis of change in Θ_{224} , Θ_{\max} and λ_{\max} based on eq 1.

	β -CN	β -CN-(f1-192)
$T_{\Theta_{224}}$ ($^{\circ}\text{C}$)	33	37
$\Delta\Theta_{224}$ ($\text{deg}\cdot\text{cm}^2\cdot\text{dmole}^{-1}$)	-3740	-3447
n	2	2
$T_{\Theta_{\max}}$ ($^{\circ}\text{C}$)	78	34
$\Delta\Theta_{\max}$ ($\text{deg}\cdot\text{cm}^2\cdot\text{dmole}^{-1}$)	21,500	10,010
n	1	2
$T_{\lambda_{\max}}$ ($^{\circ}\text{C}$)	10, 41	12, 36
$\Delta\lambda_{\max}$ (nm)	3.4	2.0
n	20	24
m	3	32

ellipticity change ($\Delta\Theta_{224}$) and a slightly higher midpoint transition temperature ($T_{\Theta_{224}}$) for β -CN-(f1-192) than β -casein. A hint of cooperativity existed in both cases, *i. e.* $n=2$. The maximum changes in the maximum ellipticity ($\Delta\Theta_{\max}$) were estimated to be $\sim 10,010$ and $\sim 21,500$ degrees $\cdot \text{cm}^2/\text{dmole}$ for β -CN-(f1-192) and β -casein respectively. A much higher midpoint transition temperature (78°C) was found for β -CN than for β -CN-(f1-192) (34°C). Moreover, cooperativity of the transition is apparently less prominent for β -casein ($n=1$) than for β -CN-(f1-192) ($n=2$). It is important to note that both transitions observed in Figure 4A and B are highly reversible and showed little or no hysteresis.

Graham *et al.* (42) have calculated that the far-UV CD spectrum of β -casein at ~ 200 nm arises from larger Cotton effects in its ORD curves in the near vacuum UV area. If this hypothesis holds true, the red shift in λ_{\max} observed here (Figure 4C) could suggest meaningful structural changes in the backbone. A close examination of λ_{\max} found that two distinctive transitions, $T_{\lambda_1}=10^{\circ}\text{C}$ and $T_{\lambda_2}=41^{\circ}\text{C}$ could be fitted with eq 1 for β -casein, and $T_{\lambda_1}=12^{\circ}\text{C}$ and $T_{\lambda_2}=36^{\circ}\text{C}$ for β -CN-(f1-192). It is apparent that the transition points are comparable for each protein respectively. A much diffused transition behavior ($m=3$) was implicated for β -casein contrary to a sharp two-state transition for β -CN-(f1-192) in the higher temperature range ($> 30^{\circ}\text{C}$). This apparent distinction in the two proteins is most likely related to the difference in the self-association properties as temperature increases. The λ_{\max} temperature dependence behavior of λ_{\max} for β -CN-(f1-192) shown in Figure 4C grossly parallels a "typical" protein denaturation curve with a two-state transition. CONTIN/LL analysis of the CD spectra for the two proteins suggested a slight but visible loss of α -helical content and perhaps a comparable amount increase in unordered

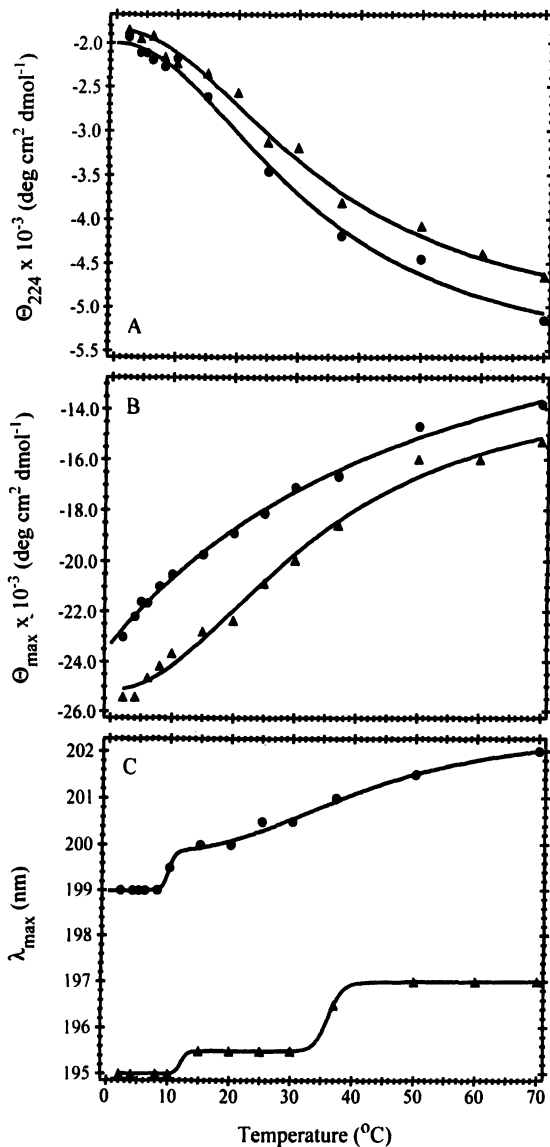


Figure 4. Temperature dependence of CD spectra of β -CN-(f1-192) (triangles) in comparison with that of β -CN (circles) at pH 6.75 and $I=50$ mM. A) ellipticity at 224 nm, B) maximum ellipticity (θ_{max}) in the far-UV region, and C) Maximum (λ_{max}) were plotted as a function of temperature. Protein concentration was 7.67 μ M.

structures. Using eq 1, a detailed analysis of Garnier's ORD data of β -casein (43) showed a transition at 5 to 10°C for change in A_{436} as a function of temperature. This, in all likelihood, approximates that of both β -casein and β -CN-(f1-192) in the low temperature range found in this work. The ORD data would, however, represent about 40% monomer for β -CN at the experimental concentration using our association constants (12).

Because β -casein is known to associate even at room temperature, the initial explanation for the mid-ranged (33°C) transition in β -casein might be cooperative self-association into the more hydrophobic environment of the polymer, *i.e.* the rheomorphic hypothesis (8). Analytical ultracentrifugation studies revealed (13, 24), however, the monomer content remains greater than 98% for β -casein and nearly 100% for β -CN-(f1-192) at the concentrations (0.17 ± 0.02 mg/ml) used in the CD experiments even at 37°C. The extrapolation of the analytical ultracentrifugation data to 50° and 70°C showed 71% and 46% monomer in β -casein at these respective temperatures for the same range of concentrations and nearly 100% monomer in β -CN-(f1-192) throughout. It is reasonable to assume that the transitions presented in Figure 4 and Table II reflect somewhat "true" changes in the structures of the β -casein and β -CN-(f1-192) monomers, not structural accommodation to the self-associated state. If the changes in the CD spectra indeed reflect movement to a more hydrophobic environment, then the monomer may be becoming more compact with increasing temperature. This model appears to reconcile with what was described as apparent thread-like structures at 2 to 4°C that become more compact monomers in the presence of polymer at 8.5°C in β -casein (31). As temperature increases, both β -CN-(f1-192) and β -casein monomers undergo subsequent conformational changes at ~34°C. The reduced degree of self-association in β -CN-(f1-192) can arguably be attributed to the missing of the apparent mid-point transition in the higher temperature range (78°C) found in β -casein. Based on these observations, we hypothesized that β -CN-(f1-192) monomer may possess less regular secondary structure (α -helix) at room temperature compare to its parent protein, β -casein monomer, but it may contain more thermal stable structural elements, such as extended structure.

Effect of bulk solvent environment on the secondary structure of β -CN-(f1-192)

The CD spectra of β -casein and β -CN-(f1-192) in organic solvents including methanol (MeOH) and 2,2,2-trifluoroethanol (TFE) are presented Figure 5 and Figure 6. It is evident that transferring to MeOH and TFE simultaneously

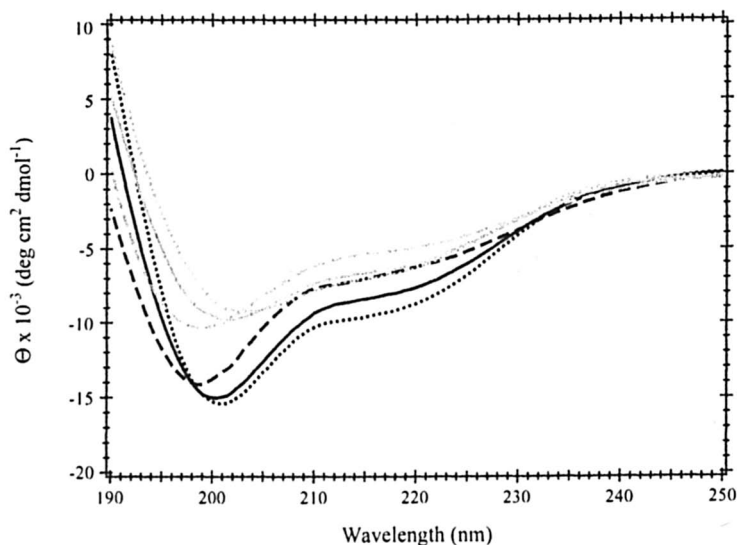


Figure 5. CD spectra of β -CN-(f1-192) and β -CN in 60% MeOH and pH 6.75 at various temperatures. Dark lines are for β -CN-(f1-192) and gray lines are for β -CN. Dotted lines are for 5°C, solid lines are for 25°C and dashed lines are for 70°C.

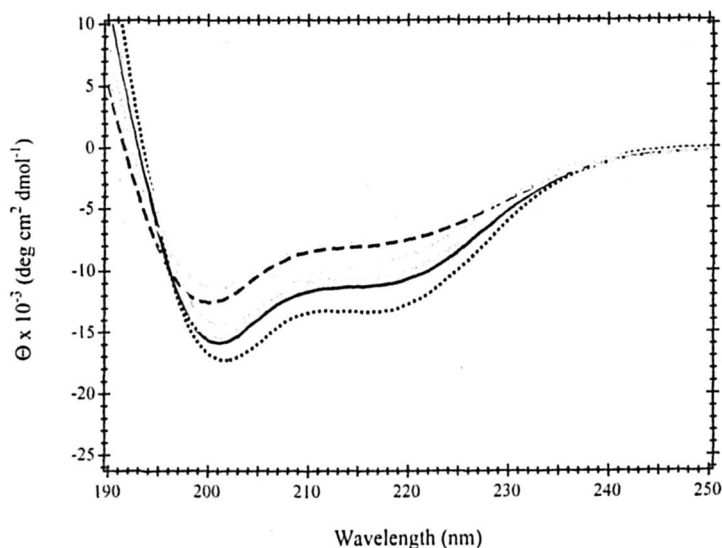


Figure 6. CD spectra of β -CN-(f1-192) and β -CN in 80% TFE and pH 6.75 at various temperatures. Dark lines are for β -CN-(f1-192) and gray lines are for β -CN. Dotted lines are for 5°C, solid lines are for 25°C and dashed lines are for 70°C.

Table III Secondary structure analysis for the CD spectra of β -CN-(f1-192) and β -CN in various solutions and temperatures

Solvent	T (°C)	α -Helix (%)	β -strand (%)	Turn (%)	Unordered (%)
β-CN					
PIPES buffer, pH 6.75	5	6.1	2.4	27.8	63.7
	25	17.2	2.5	15.8	64.6
	70	35.8	5.0	13.6	45.6
60% MeOH	5	6.1	12.7	18	63.2
	25	20.0	4.1	9.1	66.9
	70	0.0	2.7	4.9	92.4
80% TFE	5	19.1	14.1	15.0	51.7
	25	16.5	4.3	10.2	69.0
	70	4.6	3.2	32.5	40.7
18 mM SDS	5	21.5	1.3	7.6	69.7
	25	24.3	1.7	7.3	66.8
	70	23.8	1.6	6.0	68.7
β-CN-(f1-192)					
PIPES buffer, pH 6.75	5	5.3	3.2	13.8	77.7
	25	4.6	2.1	6.8	86.6
	70	2.4	1.6	15.5	80.4
60% MeOH	5	6.4	0.9	14.9	77.7
	25	2.4	3.1	11.2	83.2
	70	2.6	2.8	8.3	86.4
80% TFE	5	19.7	9.1	18.0	53.1
	25	14.7	4.3	10.0	71.1
	70	4.8	1.5	7.9	85.8
18 mM SDS	5	53.3	0.1	24.5	22.1
	25	42.6	3.1	13.1	41.1
	70	41.3	2.0	22.5	34.3

increases the band intensity at 220-230 nm that signifies α -helical structure and greatly reduces the intensity of the far-UV region (195-202 nm) band in addition to a red shift of over 5 nm. CONTIN/LL calculations suggested that TFE is more effective in inducing α -helical structures than MeOH at the three

temperatures (5°, 25°, and 70°C) examined, especially for β -CN-(f1-192). The findings for α -chymotrypsinogen A by Khan *et al.* (44) were reminiscent in many aspects. It also indicated that the amount of induced α -helical reached a "maximum" of 20% (in 80% TFE at 5° and 25°C) for both proteins, which is close to that of β -casein at 25°C (17%). Furthermore, Figure 5 and Figure 6 showed that temperature (70°C) might have a greater disrupting effect on the induced α -helical structures than on the "intrinsic" α -helical element in β -casein and β -CN-(f1-192), as discussed above. The fact that both MeOH and TFE can act as denaturants for proteins, particularly at higher temperatures, may also be substantially accountable for the loss of the induced α -helix, see Table III. The experimental data in TFE appeared to concur remarkably well with this assumption. The induced α -helical structure content dropped to less than 5% for both proteins at 70°C (from 20%).

Although there have been conflicting reports (45, 46) on whether alcohol enhances or induces α -helix and whether helix propensity is a prerequisite, the ability of TFE to induce more α -helical structure in β -casein and β -CN-(f1-192) seems to support the idea that both proteins retain unique and relatively stable secondary structures (very low level in the case of β -CN-(f1-192)) in aqueous solution. Our results confirmed that β -casein indeed contains low α -helical propensity.

The effect of temperature on the CD spectra for β -CN-(f1-192) and β -casein at micellar concentration of SDS (18 mM) was shown in Figure 8. It should be noted that low-level non-micellar concentrations of SDS were not used in this work because of the tendency of β -casein to polymerize under low SDS concentration (47). The CD spectra of β -CN-(f1-192) and β -casein bear strong similarity with each other in many respects. The principle negative bands red shifted for both proteins relative to that in aqueous solution though it is more striking for β -CN-(f1-192) than for β -CN, from 195 nm to 203 nm for β -CN-(f1-192), and from 200 nm to 202 nm for β -CN. Concurrently, this band undergoes reduction in intensity by nearly a half (-11,000 degree cm² dmol⁻¹) for β -CN-(f1-192) compared with that in PIPES buffer (-22,000 degree cm² dmol⁻¹, Figure 4 at 25°C). This reduction is only about 8,000 degree cm² dmol⁻¹ for native β -CN. The 220-230 nm band becomes much more prominent for both proteins, suggesting formation of α -helical structures. Little temperature dependence was observed throughout the range employed in this work for both proteins in micellar SDS. This is all but surprising, and is consistent with what was found for a poly-L-proline peptide (48). CONTIN/LL analysis (Table III) yielded a nearly two times higher level of α -helical content, 41-53%, for β -CN-(f1-192) than that (22-24%) for β -CN at all temperatures. The unordered structure fractions for β -CN-(f1-192) dropped accordingly as well, indicating more ordered structures were formed within the SDS micelles. These structures are quite resistant to temperature perturbation.

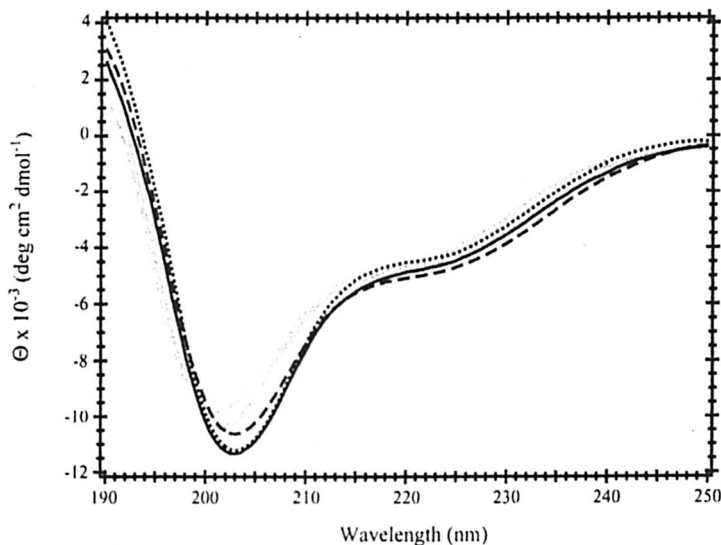


Figure 7. CD spectra of β -CN-(f1-192) and β -CN in SDS (18 mM) micelles at pH 6.75 and various temperatures. Dark lines are for β -CN-(f1-192) and gray lines are for β -CN. Dotted lines are for 5°C, solid lines are for 25°C and dashed lines are for 70°C.

It has been shown (49) that SDS can alter the helicity of many proteins. Those with low helicity often become more ordered and those having more helix less ordered. Recent work on acid-denatured cytochrome c (50) suggested occurrence of refolding and induction of “molten globule” states in SDS. Our results are clearly in agreement with the assumption that unfolded protein, β -CN-(f1-192), could regain orders and become refolded in micellar SDS. We further speculate that its great flexibility could make this process far more efficient than its parent protein, β -CN.

ANS binding

ANS fluorescence has been widely used to as a diagnostic indicator of exposed hydrophobic sites in proteins, especially in the detection of “molten globule” states (51). Although ANS binds to proteins mainly through electrostatic interactions, the fluorescence of ANS is enhanced by the presence of hydrophobic regions. There was a 2.5 fold enhancement of ANS fluorescence

in the presence of β -CN at 480 nm, which is also blue-shifted relative to ANS alone. In contrast, fluorescence of ANS was almost unaffected by β -CN-(f1-192) (Figure 8). The K_a of the binding complex between ANS and β -CN-(f1-192) can not be determined accurately because of the ineffective binding while the K_a of β -casein-ANS complex was determined to be $\sim 5.26 \times 10^4 \text{ M}^{-1}$ as reported previously (13). The near elimination of binding of β -CN to ANS brought about by the C-terminal truncation, consistent with the findings for β -CN-(f1-189) (16), suggests that C-terminal peptide, β -CN-(f189-209), plays an important role in the formation and stabilization of the complex between β -casein and ANS. Taken together the results obtained from the far-UV CD studies, we would like to propose that β -CN-(f1-192) resembles a “fully” unfolded globular protein in many respects.

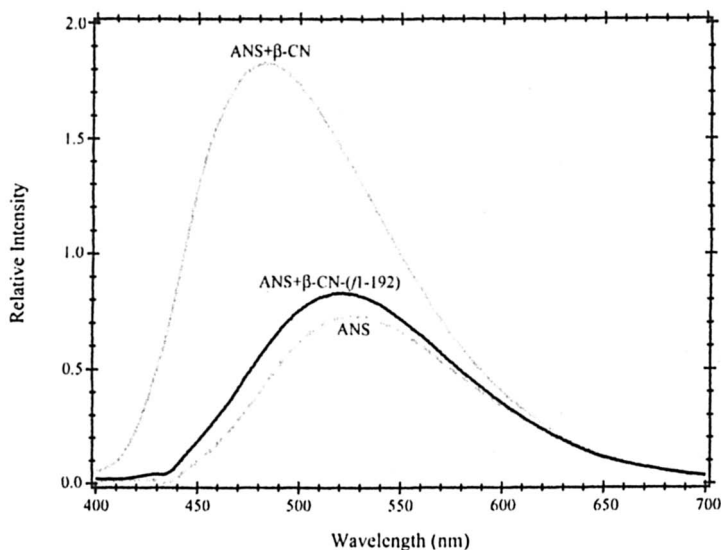


Figure 8. Fluorescence emission spectra of ANS only, in the presence of native β -CN and β -CN-(f1-192).

Conclusion

It has been shown that C-terminal deletion of bovine β -casein by chymosin cleavage can significantly affect the structure and stability of β -casein in the monomeric state. The degree of self-association has greatly been decreased, but not completely abolished. It was further suggested that the C-terminal 17 amino acid peptide plays a less critical (than previously believed) role in the formation and stabilization of self-association of β -CN. The secondary structure of β -

casein, α -helix in particular, has been considerably disrupted due to the truncation in the C-terminal region. Organic solvents, such as TFE and SDS, are effective in inducing α -helical structures, especially for β -CN-(f1-192). ANS fluorescence experiments indicated that the C-terminal peptide is important in maintaining the hydrophobic interaction between ANS and β -casein.

References

- Schmidt, D. G.; Payens, T. A. J. In *Surface and Colloid Science*; Matijevic, E., Ed.; John Wiley: New York, NY, 1976; Vol. 9, pp. 165-199.
- Andrews, A. L.; Atkinson, D.; Evans, M. T. A.; Finer, E. G.; Green, J. P.; Phillips, M. C.; Robertson, N. *Biopolymers* **1979**, *18*, 1105-1121.
- Tai, M.; Kegeles, G. *Biophys. Chem.* **1984**, *20*, 81-87.
- Waugh, D. F.; Creamer, L. K.; Slattery, C. W.; Dresdner, G. W. *Biochemistry* **1970**, *9*, 786-795.
- Takase, K.; Niki, R.; Arima, S. *Biochim. Biophys. Acta* **1980**, *622*, 1-8.
- Herskovits, T. T. *Biochemistry* **1966**, *5*, 1018-1026.
- Noelken, M.; Reibstein, M. *Arch. Biochem. Biophys.* **1968**, *123*, 397-402.
- Holt, C.; Sawyer, L. *J. Chem. Soc. Faraday Trans.* **1993**, *89*, 2683-2692.
- Uversky, V. N. *Eur. J. Biochem.* **2002**, *269*, 2-12.
- Tompa, P. *Trends Biochem. Sci.* **2002**, *27*, 527-533.
- Dyson, H. J.; Wright, P. E. *Nat. Rev. Mol. Cell. Biol.* **2005**, *6*, 197-208.
- Farrell, H. M., Jr.; Wickham, E. D.; Unruh, J. J.; Qi, P. X.; Hoagland, P. D. *Food Hydrocolloids* **2001**, *15*, 341-354.
- Qi, P. X.; Wickham, E. D.; Farrell, H. M., Jr. *Protein J.* **2004**, *23*, 389-402.
- Uversky, V. N. *Protein Sci.* **2002**, *11*, 739-756.
- Thompson, M. P.; Kalan, E. B.; Greenberg, R. *J. Dairy Sci.* **1967**, *50*, 767-769.
- Berry, G. P.; Creamer, L. K. *Biochemistry* **1975**, *14*, 3542-3545.
- Bu, H.; Sood, S. M.; Slattery, C. W. *Protein J.* **2004**, *23*, 509-517.
- Visser, S.; Slangen, K. *J. Neth. Milk Dairy J.* **1977**, *31*, 16-30.
- Thompson, M. P. *J. Dairy Sci.* **1966**, *49*, 792-795.
- Wetlaufer, D. B. *Adv. Protein Chem.* **1962**, *17*, 303-391.
- Sreerama, N.; Woody, R. W. *Anal. Biochem.* **2000**, *287*, 252-260.
- Sreerama, N.; Venyaminov, S. Y.; Woody, R. W. *Anal. Biochem.* **2000**, *287*, 243-251.
- Wyman, J., Jr. *Adv. Protein Chem.* **1964**, *19*, 223-286.
- Qi, P. X.; Wickham, E. D.; Piotrowski, E. G.; Fagerquist, C. K.; Farrell, H. M., Jr. *Protein J.*, Accepted.
- Eigel, W. N.; Butler, J. E.; Ernstrom, C. A.; Farrell, H. M., Jr.; Harwalkar, V. R.; Jenness, R.; Whitney, R. M. *J. Dairy Sci.* **1984**, *67*, 1599-1631.

26. Schmidt, D. G. *J. Dairy Res.* **1979**, *46*, 351-355.
27. Creamer, L. K.; Mills, O. E.; Richards, E. L. *J. Dairy Res.* **1971**, *38*, 269-280.
28. Farrell, H. M., Jr.; Jimenez-Flores, R.; Bleck, G. T.; Brown, E. M.; Butler, J. E.; Creamer, L. K.; Hicks, C. L.; Hollar, C. M.; Ng-Kwai-Hang, K. F.; Swaisgood, H. E. *J. Dairy Sci.* **2004**, *87*, 1641-1674.
29. Thurn, A.; Burchard, W.; Niki, R. *Polymer Sci.* **1987**, *265*, 653-666.
30. Arima, S.; Niki, R.; Takase, K. *J. Dairy Res.* **1979**, *46*, 281-282.
31. Payens, T. A. J.; van Markwijk, B. W. *Biochim. Biophys. Acta* **1963**, *71*, 517-530.
32. Provencher, S. W.; Glockner, J. *Biochemistry* **1981**, *20*, 33-37.
33. Chou, P. Y.; Fasman, G. D. *Annu. Rev. Biochem.* **1978**, *47*, 251-276.
34. Wahlgren, N. M.; Leonil, J.; Dejmek, P.; Drakenberg, T. *Biochim. Biophys. Acta* **1993**, *1202*, 121-128.
35. Wahlgren, N. M.; Dejmek, P.; Drakenberg, T. *J. Dairy Res.* **1994**, *61*, 495-506.
36. Farrell, H. M., Jr.; Qi, P. X.; Wickham, E. D.; Unruh, J. J. *J. Protein Chem.* **2002**, *21*, 307-321.
37. Saxena, V. P.; Wetlaufer, D. B. *Proc. Natl. Acad. Sci. U S A* **1971**, *68*, 969-972.
38. Toumadje, A.; Johnson, W. C., Jr. *J. Am. Chem. Soc.* **1995**, *117*, 7023-7024.
39. Shi, Z.; Woody, R. W.; Kallenbach, N. R. *Adv. Protein Chem.* **2002**, *62*, 163-240.
40. Rucker, A. L.; Creamer, T. P. *Protein Sci.* **2002**, *11*, 980-985.
41. Tiffany, M. L.; Krimm, S. *Biopolymers* **1968**, *6*, 1379-1382.
42. Graham, E. R. B.; Malcolm, G. N.; McKenzie, H. A. *Int. J. Biol. Macromol.* **1984**, *6*, 155-161.
43. Garnier, J. J. *Mol. Biol.* **1966**, *19*, 586-590.
44. Khan, F.; Khan, R. H.; Muzammil, S. *Biochim. Biophys. Acta* **2000**, *1481*, 229-236.
45. Sonnichsen, F. D.; Van Eyk, J. E.; Hodges, R. S.; Sykes, B. D. *Biochemistry* **1992**, *31*, 8790-8798.
46. Waterhous, D. V.; Johnson, W. C., Jr. *Biochemistry* **1994**, *33*, 2121-2128.
47. Creamer, L. K. *Arch. Biochem. Biophys.* **1980**, *199*, 172-178.
48. Ladokhin, A. S.; Selsted, M. E.; White, S. H. *Biochemistry* **1999**, *38*, 12313-12319.
49. Wu, C. S.; Ikeda, K.; Yang, J. T. *Biochemistry* **1981**, *20*, 566-570.
50. Xu, Q.; Keiderling, T. A. *Protein Sci.* **2004**, *13*, 2949-2959.
51. Semisotnov, G. V.; Rodionova, N. A.; Razgulyaev, O. I.; Uversky, V. N.; Gripas, A. F.; Gilmanshin, R. I. *Biopolymers* **1991**, *31*, 119-128.

Chapter 6

κ -Carrageenan Interaction with Bovine and Caprine Caseins as Shown by Sedimentation and NMR Spectroscopic Techniques

Implication of Surface Charge by a Homologous Three-Dimensional Model for α_{S2} -Casein: κ -Carrageenan–Casein Interaction

Harold M. Farrell, Jr.¹ and Adela Mora-Gutierrez²

¹Eastern Regional Research Center, Agricultural Research Service,
U.S. Department of Agriculture, 600 East Mermaid Lane,
Wyndmoor, PA 19038

²Cooperative Agricultural Research Center, Prairie View A&M University,
Prairie View, TX 77446

The solubility and hydration characteristics of κ -carrageenan-casein systems from bovine and caprine milk with incorporated salt (NaCl) were determined by means of sedimentation and ^{17}O nuclear magnetic resonance (NMR) experiments. Relative salt interaction parameters both for caseins alone and in mixtures with κ -carrageenan were assessed by nonlinear regression analysis from the characteristics of solubilization of the systems. The κ -carrageenan-casein interactions appear to depend largely on the ratios of κ - to α_{S1} -casein and possibly α_{S2} -casein. Second virial coefficients (B_0 values) and hydration products derived from ^{17}O NMR data suggest that while soluble at high salt, the caprine casein mixtures exhibit strong interactions, whereas the bovine counterparts do not. At lower salt concentrations

the solubility data and the ^{17}O NMR data are in agreement. Thus, a structural dependence upon protein components in salt containing κ -carrageenan-casein solutions from bovine and caprine milk has been demonstrated. The evidence suggested a role for α_{s2} -casein in the interactions observed. A homologous three dimensional model for α_{s2} -casein was developed to test this hypothesis. The model was produced by the use of a template model derived from a crystal structure of a human chloride intracellular channel (CLIC)-1 and demonstrates a large positively charged surface potential for interactions with the negatively charged the negatively charged κ -carrageenan.

Key Words: solubility; NMR, ^{17}O ; salt binding; water binding; κ -carrageenan; bovine casein; caprine casein; caprine α_{s1} -casein; bovine α_{s2} -casein; molecular modeling.

Abbreviation Key: NMR = Nuclear magnetic resonance

One of the most important properties of polysaccharide hydrocolloids in food systems (e.g., carrageenans, dextrans, starches) is their ability to complex protein to form modified food structures. In model systems complex formation has been observed, and although both polymers carry a net negative charge the interaction has been generally recognized to be electrostatic in nature (1-3). In milk systems κ -carrageenan is an important determiner of sensory texture, rheological properties and functional properties (4, 5). Salt cations and/or anions may not only affect protein-hydrocolloid electrostatic interactions, but may also alter water binding in carrageenan systems (6). Snoeren et al. (7) demonstrated that, at the pH and ionic strength prevailing in milk, it is mainly the casein micelles (and perhaps κ -casein in particular) that are involved in κ -carrageenan-protein interactions. The amino acid sequence of the κ -casein molecule suggests that in addition to the highly negatively charged macropeptide it has also areas of 'net' positive charge, which have been speculated to be on the surface of the casein micelle (8). Such an accumulation of positive charges is thought to be lacking in α_{s1} - and β -casein, where positive and negative amino acid side chains appear to be evenly distributed along the polypeptide chain (9, 10). Of all the protein fractions in milk, κ -casein is the most reactive through normal food processing (11).

Caprine caseins, in contrast to bovine caseins vary considerably in the types of casein present, some are poor in α_{s1} -casein and some are richer in α_{s2} -casein (12). The α_{s2} -casein has a primary structure quite different than the α_{s1} - and β -caseins. In a linear array the α_{s2} -casein displays a cluster of 'net' positive

charge for residues 170 through 207 at the C-terminal end (13). Physical chemical studies of α_{s2} -casein by Snoeren et al. (14) suggested a model in which this positively charged tail participates in the isodesmic self-association of the protein, this argues for a surface position for the positively charged cluster. Thus, caprine caseins rich in α_{s2} -casein may offer enhanced sites for interactions with κ -carrageenan, provided that this positive cluster is on the surface in associated whole casein.

Moreover, sodium caseinates from bovine and caprine milks containing varying casein components have not been characterized comparatively relative to their interaction with κ -carrageenan. This is especially true with regard to the elevated α_{s2} -casein content of some caprine milks. Therefore, the objective of this work is to examine the effect of NaCl on solubility and the hydration behavior of bovine casein and two caprine caseins of known casein distribution following complex formation with κ -carrageenan in the absence of calcium ions by use of sedimentation and ^{17}O nuclear magnetic resonance (NMR) techniques.

Materials and Methods

Materials

All reagents used were of analytical grade or 'ACS certified' from Aldrich, Baker, Sigma (St. Louis, MO). κ -carrageenan was obtained from Sigma Chemical Co. 99.8% deuterium oxide (D_2O) was obtained from Sigma (St. Louis, MO).

κ -carrageenan was exhaustively dialyzed against deionized water, which had been adjusted to pH 7.0 with 0.5 M sodium hydroxide, and then lyophilized

Preparation of Bovine and Caprine Caseins

Bovine casein was obtained from the milk of a Jersey cow. The caprine caseins characterized by high and low content of the α_{s1} -casein component were obtained from the milk of an Anglo-Nubian and a French-Alpine goat, respectively as previously described as previously described (15). The integrity of the samples was confirmed by polyacrylamide gel electrophoresis in sodium dodecyl sulfate (SDS), and densitometry was used to assess the relative concentrations of casein components (16). The compositions of the bovine and caprine caseins used in this study are given in Table I.

Table I. Comparison of the Percentage of Casein Distribution of Bovine and Caprine Caseins by Densitometry

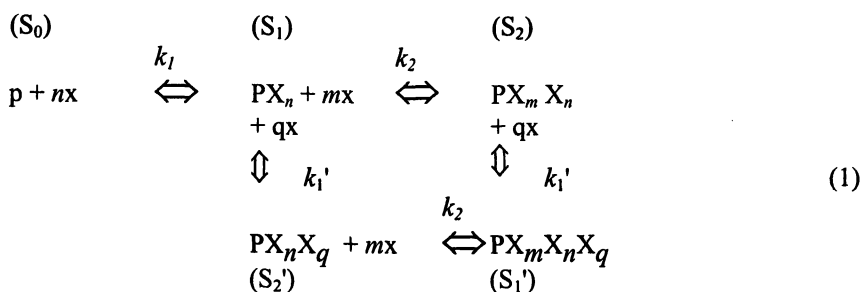
Casein type	Bovine	Caprine casein high in α_{s1} -casein	Caprine casein low in α_{s1} -casein
α_{s2} -casein	12.1	9.2	29.2
α_{s1} -casein	39.5	25.1	5.9
β -casein	37.2	51.6	50.5
κ -casein	11.2	13.8	14.4
α_{s2}/α_{s1} -ratio	0.3	0.4	5.0

Solubility Measurements

Solubility of pure caseins and κ -carrageenan-casein mixtures at 21°C, was determined as previously described (17-23).

Solubility Theory and Data Analysis

Wyman's concept for linked functions (18) was useful for the treatment of the sequential precipitation (salting-out) and resolubilization (salting-in) of individual bovine and caprine casein components as a function of added calcium (19-23). Here, we have extended that theory to assume that the triphasic sequential changes in solubility (e.g., Fig. 1 bottom) which occur with increasing NaCl concentration are also thermodynamically linked to salt concentrations. The mechanism of precipitation could be salt-binding followed by charge neutralization (20) or bulk salt-solvent surface tension incremental effects i.e., change in solvent-solute interactions by added cosolute namely salt (24, 25). Therefore, the application of linked functions as developed by Wyman (18) can be used to treat these processes if the following equilibria are assumed:



where p is the unbound protein, x is the free salt, n, m, and q are the apparent number of moles of X bound to species PX_n , $PX_n X_m$, and $PX_n X_m X_q$; S_0 , S_1 , S_1' , and S_2' are the solubilities of the species indicated. The mathematical

relationship representing this stoichiometry has been previously derived (19-23) and the model equation used in analysis of the data is:

$$S_{app} = \frac{S_0}{1+k_1^n x^n} + \frac{S_1 k_1^n x^n}{1+k_1^n x^n} + \frac{(S_2 - S_1) k_2^m x^m}{1+k_2^m x^m + k_1^q x^q + k_2^m k_1^q x^m x^q} + \frac{S_1' k_2^m x^m k_1^q x^q}{(1+k_2^m x^m)(1+k_1^q x^q)} \quad (2)$$

Eq. 2 represents sequential binding (i.e., $k_1 > k_2 > k_1'$ and where n sites saturate prior to the binding of m sites on the protein). Also, for n , m , or $q > 1$, k_1 , k_2 and k_1' represent an average value for each of the n , m or q binding sites. In reality, n , m or q moles of salt will bind with only one equilibrium constant (k_i) (i.e., $k_1 = k_1^n$; $k_2 = k_2^m$; and $k_1' = k_1^q$). Finally, protein- κ -carrageenan complexes have very high molecular weight, so that the molar concentrations of salt (up to 0.9 M) far exceed the molarity of the complexes. Therefore, total salt may be used rather than "free" salt when binding is implied. This is analogous with enzyme kinetics where substrate concentration $[S] \gg$ enzyme concentration $[E]$.

The model in Eq. 2 was applied in the present study to the Na^+ -induced solubility profiles of bovine and caprine whole caseins in the absence and in the presence of κ -carrageenan. The statistical analysis of this model has been previously given (19-23).

Preparation of Samples for NMR Measurements

A set of bovine and caprine casein solutions was mixed with 0.0078 % (w/v) κ -carrageenan. A second set of samples was prepared by adding incremental amounts of casein from 0 to 6% (w/v) to a constant ratio of κ -carrageenan and salt to water. After mixing, the solutions were heated to 80°C for 5 min to prevent local aggregation, subsequently cooled to room temperature, and then allowed to equilibrate at 4°C in ice, prior to the ^{17}O NMR measurements. The pD was 7.2 for all the samples. pD was calculated from the equation $\text{pD} = \text{pH} + 0.4$ (26).

About 4 mL of well-dispersed and thoroughly mixed pure casein and κ -carrageenan-casein in D_2O solutions were transferred to 10-mm high-resolution NMR tubes (Wilmad, Buena, NJ). In all experiments two independent series of NMR measurements were conducted at 21 ± 1 °C.

^{17}O NMR Transverse Relaxation Rate Measurements

A XL-200 multinuclear spectrometer (Varian Associates, Palo Alto, CA) was used for the ^{17}O NMR R_2 relaxation measurements. Natural abundance ^{17}O

(3.7×10^{-2} %) measurements were made in D₂O. Single pulse experiments were done at $21 \pm 1^\circ\text{C}$, at a resonance frequency of 27.1 MHz. The samples were spun at 12 ± 1 Hz. Other conditions were as follows: 90° , pulse width of 19 μs , acquisition time of 0.50 s and a spectral width of 5 KHz. The number of scans for adequate signal-to-noise ($> 100:1$) was about 1000. Fourier transforms were carried out on line with a Varian 4000 series data system computer with Pascal software (v. 6.3). Spectra were stored in an 8K point array, which provided adequate resolution. The line width (ν_{obs}) at half-height of each spectrum was obtained by using the computer line fit routine available on the XL-200 Varian computer software (Varian Associates). The ^{17}O NMR transverse relaxation rate (R_2 , s^{-1}) was then calculated from the line width by (27) and the net or differential transverse relaxation rate ΔR_2 (s^{-1}) was calculated as follows:

$$\Delta R_2 (\text{s}^{-1}) = \pi (\Delta \nu_{\text{obs}} - \Delta \nu_{\text{free}}) \quad (3)$$

where $\Delta \nu_{\text{free}}$ is the line width at half-height for D₂O without added protein.

NMR Hydration Theory and Data Analysis

Interpretation of NMR relaxation data is highly model-dependent (28) and the application of different models to the same data may lead to somewhat conflicting concepts. The isotropic two-state model for water-macromolecule interactions, has been applied to several polymer systems (29-34) and has been described in detail (35-40). For proteins this description includes substitution of the activity coefficient, γ and the virial expansion of osmotic pressure as a function of protein concentration. The application of virial coefficients to the nonideality of macromolecules in solution is discussed by (41-49).

By applying the protein activity concept, as discussed in a previous report (12), in conjunction with the two-site model with fast exchange model one obtains:

$$R_{2\text{obs}} - R_{2\text{F}} = n_{\text{H}}(R_{2\text{B}} - R_{2\text{F}})C_{\text{p}} \exp[2B_0C_{\text{p}} + 2B_{0.5}C_{\text{p}}^{0.5} + 0.667B_{1.5}C_{\text{p}}^{1.5} + 1.5B_2C_{\text{p}}^2 + \dots] \quad (4)$$

where $R_{2\text{obs}}$ is the measured transverse relaxation rate corrected for inhomogeneity broadening; the subscripts "B" and "F" stand for "bound" and "free" water; n_{H} is the hydration number (i.e., the average number of water molecules "bound" per molecule of dry protein); C_{p} is the varying protein concentration, B_i are the virial coefficients. The virial coefficients are a measure of the various intermolecular interactions (41, 39). The B_0 virial coefficient reflects the repulsive or attractive forces arising from the net protein charge Z , the protein excluded volume, and a preferential interaction term (47-49, 12).

Our ^{17}O NMR data was analyzed with a quasi-Newton nonlinear regression program as described in a previous paper (12). Root mean square (RMS) values were normalized to be within at least 5% error of the fit for all the data.

Molecular Modeling of Bovine α_{s2} -Casein

One route to an approximate three dimensional (3D) model is to find a protein with a strong homology and a known 3D structure (50). Such structures for the caseins are not readily available in conventional database searches. The CLIC (chloride intracellular channel) molecules, while not closely related to α_{s2} -casein did show sufficient homology to proceed with the work. The initial homologies were established using the T-coffee program of Notredame et al. (51) found on the ExpASy web site (expasy.org). The model was generated from the human CLIC-4 model found at the same site (Q9Y696). This latter model in turn is based on the X-ray template of a soluble fragment of human CLIC-1 (PDB file 1KOM). Initial alignments and set up parameters for the model were accomplished using the program Deep View/ Swiss PDB Viewer 3.7 obtained from the ExpASy site. After initial manipulations by the author, the model was then submitted as a project to the ExpASy modeling group; such modeling is computer based and produced without human intervention. Therefore the model for α_{s2} -casein provides some basis for caution in that it is based on a secondary homology and produced with only set rules. Interpretation of the model must be carefully considered in that it has the characteristics of an X-ray structure but lacks the certitude of direct crystallographic data. After viewing the original model it was apparent that the putative site for casein-casein interactions (52) was partially blocked (this could also represent the membrane interaction site in the CLIC proteins). Several manipulations of the bond angles at the base of the proposed site were attempted and the easiest change to accentuate the movement of the interaction site finally proved to be a minor adjustment of the Phi/Psi angles of Ala 116 from $-60/-60$ to $-60/0$. The pseudo-charge representation of the Ala adjusted molecule used the electrostatic surface calculation of the Deep View program with the dielectric constant of the solvent set at 150 and that of the protein at 10; the red potential is -1.8 , the white is 0, and the blue is $+1.8$.

Results and Discussion

Solubility Characteristics

Neutral salts have a profound effect on the solubility of proteins, on the structure of hydrocolloids and on protein-hydrocolloid electrostatic interactions.

Therefore, the solubility of bovine casein and two caprine caseins with high and low levels of α_{s1} -casein were determined at 90000 g in order to test the effect of NaCl treatment on their solubility and on their interactions with κ -carrageenan.

In these experiments no gels were formed because of the low concentration of κ -carrageenan and the high concentration of casein (53). Figure 1 shows the solubility of whole bovine casein as a function of NaCl concentration. It is interesting to note that a dip occurs in the profile at about 0.5 M NaCl. For the individual bovine caseins, κ - and β -caseins are quite soluble in this region, but α_{s1} -casein is not (54, 55). Thus the salting out of α_{s1} -casein, above 0.6 M can be prevented by its complexation with either κ - or β -casein (54).

For caprine casein high in α_{s1} -casein a similar profile is obtained (Figure 1), but the caprine casein low in α_{s1} -casein gives a different profile. It should be noted that this latter caseinate although low in α_{s1} -casein is relatively high in α_{s2} -casein (Table I). Curiously, the degree of aggregation of bovine α_{s2} -casein increases on going from 0.02 to 0.2 M NaCl; it then decreases back to a dimer above 0.6 M NaCl (14). So α_{s2} -casein shows no insolubility over this range of salt concentration. The reason for the behavior of the caprine casein low α_{s1} -casein must somehow lie in casein-casein interactions peculiar to this caprine mixture. Table II summarizes quantitative differences in relevant parameters of pure caseins derived from the solubility data (Figure 1) by nonlinear regression analysis using Eq. 2. The salting-out constant, k_1 , for the caprine casein low in α_{s1} -casein is significantly higher than those of bovine and caprine casein high in α_{s1} -casein (Table II). This suggests that the solubility of low caprine casein is much more sensitive to Na^+ ions. Nevertheless, the predicted maximal solubilities of casein salted out (S_1) are all within the experimental error (86.1 % \pm 3.4 average and sd for for all three).

The salting out of caprine casein low in α_{s1} - occurs at salt concentrations far too low for surface increment effects on hydrophobicity (24, 25) to be operative. Taken with the fact that micelles of caprine casein low in α_{s1} -casein are destabilized by lower concentrations of added Ca^{2+} (22), this type of casein may contain fairly selective cation binding sites which lead to destabilization (precipitation).

As incipient precipitation occurs, then salt binding to lower affinity sites may in turn lead to resolubilization of these milk proteins at higher salt concentrations ($1/k_2$ average = 0.77 M). The value for the salting-in constants for all caseins are nearly equivalent an indication that a common mechanism, perhaps salt binding to the proteins, is at work.

The n and m values are the same; i.e., $n = 2$ and $m = 6$ for the bovine and the caprine caseins in the absence of κ -carrageenan, but the values of n or m represent a class of protein binding sites rather than a single binding site linked to the solubility change of the protein (56).

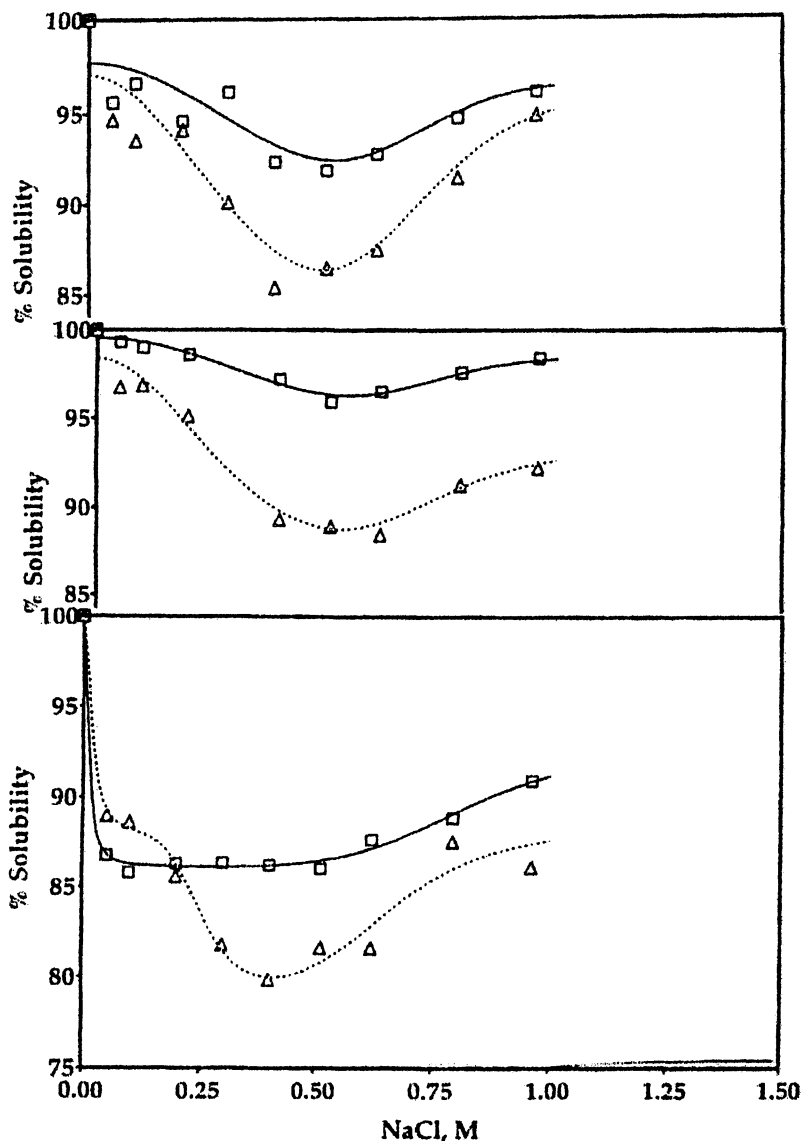


Figure 1. Solubility at 21 °C of casein and κ -carrageenan-casein with NaCl at pH 7.0, 0.005 M EDTA.: (Top) caprine casein high in α_{s1} -casein; (Middle) bovine casein; (Bottom) caprine casein low in α_{s1} -casein. Triplicate determinations and fitted by Eq. 2. Results are given in Table II. (Reproduced from *J. Ag. Food Chem.* 1998; 46, 4987–4996. Copyright 1998 American Chemical Society.)

Table II. Salt-Induced Insolubility and Solubility of Bovine and Caprine Caseins (2%) and κ -Carrageenan (0.028%) Mixtures at 21°C and at 90000g^{a,b}

<i>Casein type</i>	k_1 , L/mol	S_1 , %	k_1' L/mol	S_2' , %	k_2 , L/mol	S_2 , %
Casein alone						
Bovine	1.5±1.3	89.4±12.7	-	-	1.3±0.1	96.4±5.8
Caprine high in α_{s1} -casein	1.7±1.3	82.6±18.4	-	-	1.4±0.3	94.0±9.3
Low in α_{s1} -casein	83.7±29.0	86.1±0.2	-	-	1.2±0.1	92.7±1.2
With κ-carrageenan						
Bovine	2.9±1.4	82.9±7.0	-	-	1.4±0.3	92.2±4.7
Caprine high in α_{s1} -casein	2.4±1.9	75.8±19.3	-	-	1.4±0.3	94.3±11.9
Low in α_{s1} -casein	54.3±18.2	87.9±2.1	3.9±0.8	79.0±2.1	1.5±0.3	88.3±2.8 ^c

^aSolutions buffered at pH 7.0, 0.005 M EDTA.

^b $n = 2$ and $m = 6$ for all calculations; $q = 6$.

^c S_1' of Eq. 1.

For κ -carrageenan alone, Snoeren (55) demonstrated that the molecule is 35 to 40% salted out under the conditions used here. In studying the isolated bovine caseins only κ -casein and not β - or α_{s1} -casein could reverse this precipitation (55). As it is evident from Figure 1, the addition of κ -carrageenan decreased solubility of all of the caseins, apparently due to the formation of κ -carrageenan-casein aggregates. Equilibrium dialysis studies (57, 58) have shown that NaCl can alter both n and K_a in isolated α_{s1} -casein while light scattering and optical rotation studies have revealed that in the presence of NaCl κ -carrageenan undergoes a conformational change (55). The implication of this work is that these interactions described for the κ -carrageenan molecule (59, 60) and the individual casein components (58) may carry over to the κ -carrageenan-casein complex. A comparison of the solubility curves of the κ -carrageenan-casein mixtures shows that the extent of the aggregates formed is much greater in the caprine caseins than in the bovine casein, particularly the caprine casein low in α_{s1} -casein. The reason for such differences is probably associated with either their higher β -casein content or increased % of α_{s2} -casein, in the case of the low α_{s1} -casein (Table I). It is well established that κ -carrageenan specifically interacts with κ -casein (55, 57), but α_{s2} -casein has not been studied in this regard and its positively charged C-terminal tail (14) may facilitate this interaction.

Hydration Characteristics

From the point of view of concentration, proteins are often the most important and most reactive ingredients that can be added to a structured/textured carrageenan food system. However, the exact physical state of the majority of water within the carrageenan-protein complex is not well understood, as the water may be partially immobilized or trapped. ^{17}O NMR water relaxation experiments may be used to report upon the water in such systems (38, 48, 49). Since salt also influences water-macromolecule interactions, the hydration characteristics of κ -carrageenan-casein complexes of bovine and caprine caseins were determined in the absence and in the presence of NaCl. The ^{17}O NMR relaxation (R_2) results are given in Figure 2 for bovine casein with κ -carrageenan.

As seen in Figure 2A, the ^{17}O NMR transverse relaxation rates increased nonlinearly with milk protein concentration. Under ideal conditions this relationship is linear as exemplified by the bovine casein with κ -carrageenan at 0.9 M NaCl (Figure 2B). None of the caprine caseins reverted to linear behavior in this study. The marked deviations from linearity at higher protein concentrations have been postulated to be due to protein-protein interactions (39). The results obtained from the nonlinear regression analysis of the ^{17}O NMR relaxation data according to Eq. 4 are presented in Table III. In the investigated protein concentration range (0-7% w/v), the use of virial coefficients other than B_0 was not necessary. The positive sign of the second order virial coefficient B_0 indicates that charge-charge repulsive interactions are present and increase in all the κ -carrageenan-casein systems, as the protein concentration increases at constant concentration of κ -carrageenan (0.0078%).

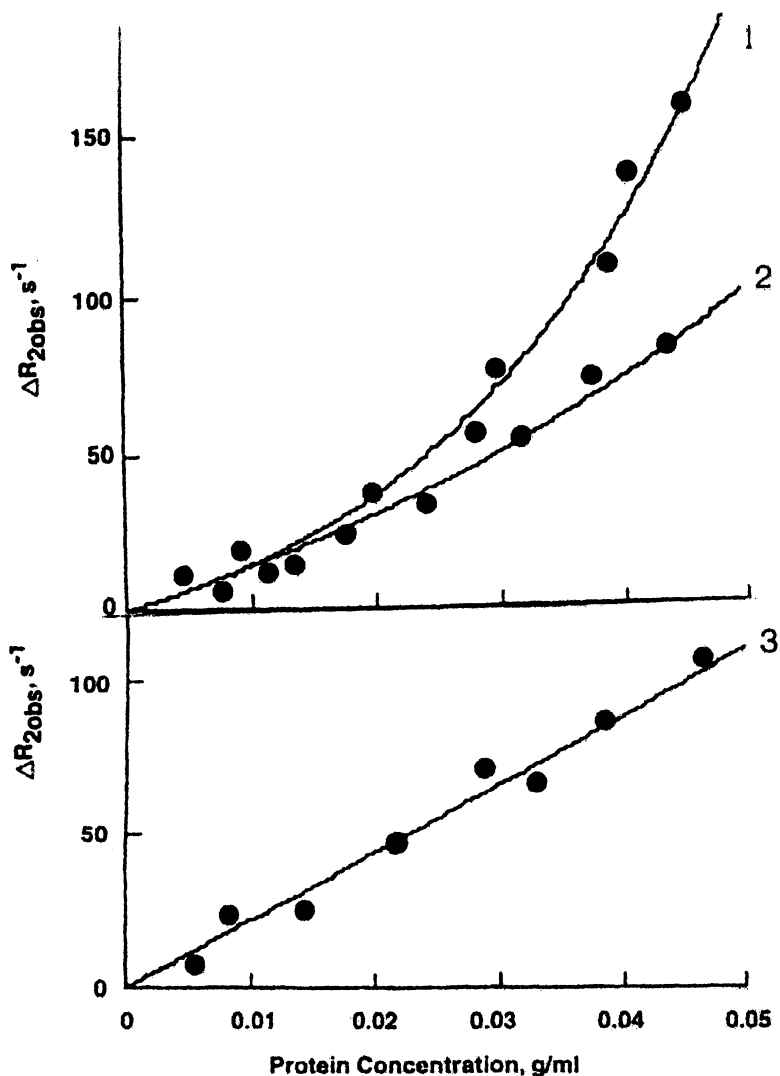


Figure 2. Dependence of the O^{17} NMR transverse relaxation rates, ΔR_2 (s^{-1}), on bovine casein concentration (g/mL) with 0.0078% κ -carrageenan at pD 7.2 and at 21 ± 1 °C. (Top) 0.2 M NaCl (1); 0.5 M NaCl (2). (Bottom) 0.9 M NaCl (3). Data were fitted by Eq. 4. Results are in Table III.

(Reproduced from *J. Ag. Food Chem.* **1998**; 46, 4987–4996. Copyright 1998 American Chemical Society.)

These elevated B_0 values argue for complex formation. As the macromolecules aggregate, the repulsion of their net negative charges is sensed by the B_0 parameter: the greater the complexation, the greater the B_0 value. For bovine casein with κ -carrageenan at 0.9M NaCl, complexation is inhibited and B_0 falls to near zero. The B_0 values of Table III clearly indicate that at pH 7.2 and in the

Table III. Calculated Hydration Products $n_H\Delta R^a$ and Virial Coefficients B_0^c from Nonlinear Regression Analysis of Oxygen-17 NMR Transverse Relaxation Data for Bovine and Caprine Casein Solutions in the Presence of 0.0078% κ -Carrageenan at $21 \pm 1^\circ\text{C}$ and pD 7.2 using Eq. 9. Values in the Absence of κ -Carrageenan, Represented by Superscripts b and d.

<i>NaCl</i> (M)	$n_H\Delta R$	$n_H\Delta R^b$	B_0^c	B_0^d
bovine casein				
0.0	1786 ± 49.9	2595	8.2 ± 0.7	3.6
0.2	1037 ± 25.3	2487	13.6 ± 0.7	4.3
0.5	1207 ± 33.2		5.1 ± 0.6	
0.9	2179 ± 12.7		0.3 ± 0.1	
caprine casein high in α_{s1} -casein				
0.0	1100 ± 38.9	3358	5.2 ± 0.9	0.8
0.2	190 ± 8.3	3069	23.9 ± 0.9	1.5
0.5	378 ± 19.4		12.7 ± 1.0	
0.9	525 ± 22.3		11.1 ± 0.8	
caprine casein low in α_{s1} -casein				
0.0	1339 ± 38.9	1806	5.9 ± 0.3	4.8
0.2	291 ± 11.7	1828	26.5 ± 1.0	3.8
0.5	358 ± 14.5		18.5 ± 0.9	
0.9	679 ± 28.6		14.1 ± 1.1	

presence or absence of NaCl, all of the κ -carrageenan-casein complexes (except bovine casein at 0.9 M) exhibit larger deviations from ideal behavior than do the caseins alone, an indication of complexation. In aqueous solutions at 1.0% concentration κ -carrageenan molecules undergo a sol/gel transition with an accompanying coil/helix transition. In the experiments conducted here the sol/gel transition is inhibited by the lowered concentration of κ -carrageenan and the presence of casein (53). As predicted by Drohan et al. (53) casein- κ -carrageenan interactions should predominate in our experiments. However, the salt dependent conformational change in the κ -carrageenan may not initially occur as electron micrographs of α -casein- κ -carrageenan complexes, at 0.07 M NaCl, reflect the thickened (coiled) state for κ -carrageenan (55). Thus at low ionic strength the coiled hydrocolloid and casein would be predicted to have minimum degree of interaction. The B_0 values of Table III however show an interaction even with no added NaCl. Thus the NMR relaxation experiments are detecting strong protein-hydrocolloid interactions under these conditions. The

relaxation of the κ -carrageenan alone is reflected in the ordinant values of Figures 2A and B, and is minimal.

It is shown that under the experimental conditions the κ -carrageenan-casein complex of bovine casein is more "hydrated" ($n_H\Delta R = 1786 \text{ mL g}^{-1} \text{ s}^{-1}$) than the κ -carrageenan-casein complex of caprine caseins characterized by high and low content of the α_{s1} -casein component ($n_H\Delta R = 1100$ and $1339 \text{ g}^{-1} \text{ s}^{-1}$, respectively), but again without the polysaccharide these values are much higher for all caseins alone. As this parameter measures both size and hydration, either the particles are dehydrated or complexation between the caseins and the κ -carrageenan is occurring.

A decrease in the hydration product $n_H\Delta R$ (Table III) is seen for all the κ -carrageenan-casein systems of bovine and caprine caseins relative to the casein only system. Table III also shows the effect of ionic strength on the hydration product $n_H\Delta R$ of bovine and caprine caseins. The hydration product of the three caseins decreased with NaCl concentrations of 0.2 M, but showed somewhat higher values at 0.9 M. As described above, if the interaction of the carrageenan-protein complex with NaCl is due to changes in the electrostatic interactions with increased ionic strength, the hydration product $n_H\Delta R$ should at first decrease with increased interactions and then return to normal values as interactions are abolished at high salt. While this occurred for bovine casein, this tendency was not observed for caprine caseins (Table III). Thus, the importance of interactions was suggested in the NMR hydration characteristics of caprine caseins and their κ -carrageenan-casein mixtures, whereas Table II reports no significant differences in S_2 . Thus, solubility studies suggest limited interactions in solution at high salt but the NMR studies point to extensive interactions for the caprine caseins, but lesser for the bovine casein. Once again the compositional differences between the caprine and bovine caseins may play a role here. The overall higher percentage of β -casein (50 vs. 37%) yields a lower net charge for both caprine caseins. Next both caprine have elevated α_{s2} - to α_{s1} -ratios (Table I), thus potentially displaying positively charged patches from α_{s2} -casein on the surfaces of the whole casein complexes.

A Homologous Molecular Model for α_{s2} -Casein

Tables II and III show the significant differences in this study, in that the caprine casein low in α_{s1} - (high in α_{s2} -) casein shows a strong interaction with κ -carrageenan even at elevated salt concentrations. The speculation that α_{s2} -casein might be involved in the binding of a highly negatively charged species such as κ -carrageenan is supported by the fact that its C-terminal 47 residues carry a net charge of +9 (61-63). Because of the net hydrophobicity of the latter segment, it is uncertain whether or not this segment would be surface accessible for interaction with the highly negatively charged κ -carrageenan. Hoagland et al. (64) have assessed possible structural arrangements that are in

accord with currently available spectral data and one could speculate from this analysis that the positively charged section might be surface accessible. This latter argument is supported by the physical chemical data of Snoeren et al. (14). Although three-dimensional (3D) molecular models have been presented for the other three major caseins (52), no 3D models have been published for α_{s2} -casein. One reason for this is the segmental domain nature of the molecule as noted by Swaisgood (63). The α_{s2} - molecule can be represented by four domains: an N-terminal anionic, a central hydrophobic domain, another anionic domain, and finally the C-terminal domain, which is both hydrophobic and cationic. In contrast the other caseins are more linear amphiphiles with only two domains one hydrophilic and one hydrophobic. One route to an approximate 3D model would be to find a protein with a strong homology and a known 3D structure (50). Such structures do not appear to be available in database searches.

The CLIC (chloride intracellular channel) molecules form a novel class of recently discovered proteins (65, 66). These proteins are often found free in the cytosol of cells, but have the ability to alter their conformation and insert themselves into membranes within the cell, hence the name intracellular, and in model systems they allow chloride movement through membranes. CLIC proteins interact with a variety of intracellular membranes such as mitochondrial, nuclear, Golgi, and sarcoplasmic (67-70). It is not known if these proteins bind directly to the membranes or to receptors on the membranes, nor which portions of the molecules are inserted into the membranes (71). Within this family there are five members termed CLIC proteins 1 to 5, which share strong structural homologies with each other. Known defects in these proteins can cause several molecular disease states (72). Recently it has been shown that the loss of *exe-4*, a CLIC protein of *C. elegans*, prevents opening of excretory vesicles. The interaction of the CLIC proteins by insertion into model bilayers appeared reminiscent of the interactions of β -casein with model membranes as detailed by Casanova and Dickinson (73). Comparisons of the amino acid sequences of the human CLIC proteins with bovine β -casein, using the T-coffee program of Notredame et al. (51), showed only marginal homology. CLIC-3 and CLIC-4 however showed better homology with α_{s2} -casein as seen in Table IV. While the degree of homology between the CLIC proteins and α_{s2} -casein is only about 58% there was sufficient similarity to proceed with the production of a working 3D model by threading the α_{s2} -casein structure onto a model of CLIC-4. It must be noted that the CLIC-4 model found in the Swiss Model Repository of the ExPASy web site, is itself a working model produced from the crystal structure of a soluble monomeric fragment of human CLIC-1. The homologous model produced for α_{s2} -casein is shown as a C- α trace in Figure 3A.

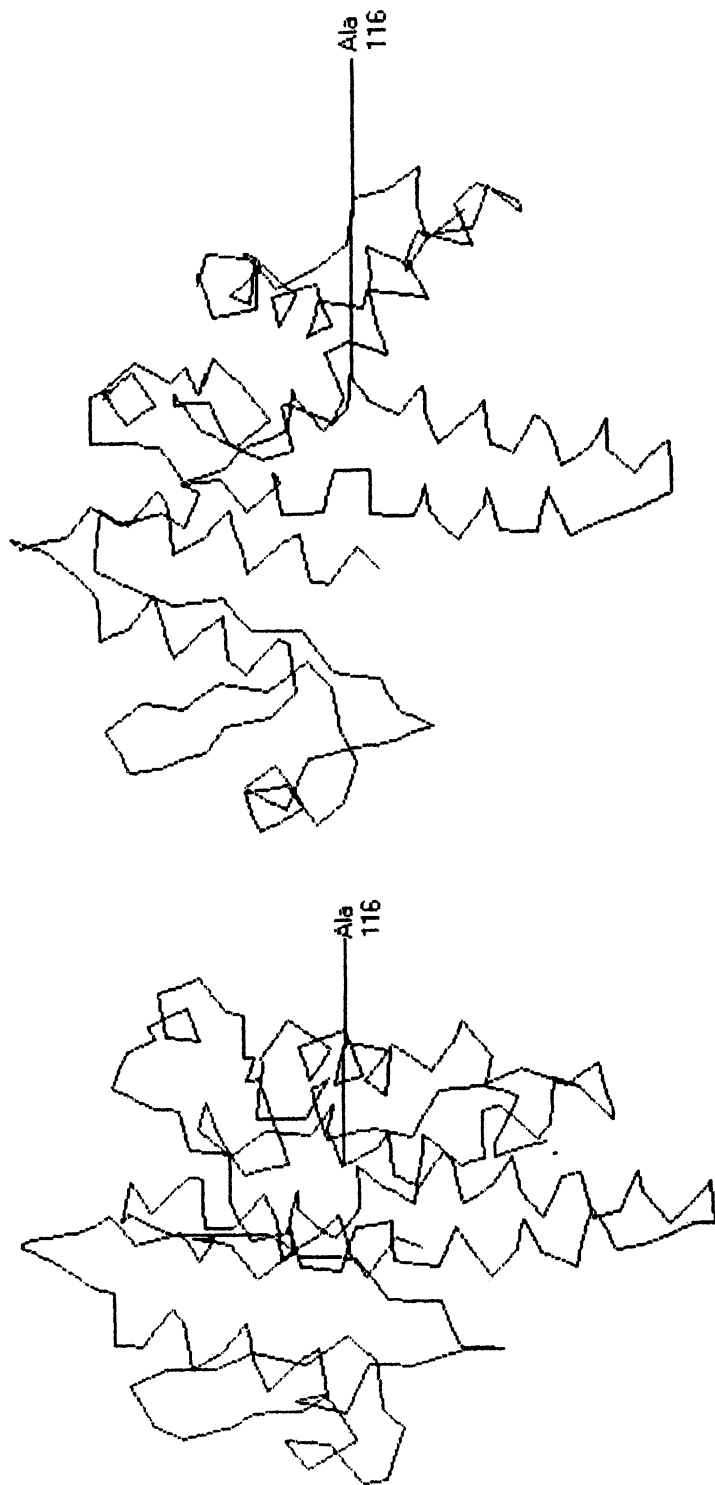


Figure 3. (Left) The Ca trace of the backbone structure of α_s2 -casein derived by homologous modeling. The amino acid sequence of α_s2 -casein was threaded unto the model of CLIC-4. (Right) Manipulation of Ala 116 to produce an accessible hydrophobic central core (52).

Table IV. T-Coffee^a Scores for Comparison of Bovine α_{s2} -Casein with Human CLIC-Proteins

	β -casein	α_{s2} -casein	CLIC-proteins
CLIC-1	39	40	
CLIC-2	30	45	
CLIC-3	35	57	98 ^b
CLIC-4	34	58	
CLIC-5	37	35	
α_{s2} -casein	33		

^aNotredame et al. (51).

^bAll human CLIC-proteins average a score of 98 in pair wise comparisons.

In previous models for κ -casein, portions of a hydrophobic section of the molecule (residues 17 to 65) were used as docking sites for other caseins (52). This section of κ -casein is also somewhat homologous with the central hydrophobic portion of α_{s2} -casein (residues 77 to 119) and to segments of the CLIC proteins, and could represent a protein-protein or protein-lipid interaction site. The homologous model showed this segment in α_{s2} -casein to be partially exposed for such interactions. The manipulation of only one residue (Ala 116) caused this hydrophobic section to further protrude into space to provide a good site for potential interactions with other caseins (Figure 3B). This manipulation may also shed some light on the CLIC proteins as the literature suggests the necessity of C- and N-terminal portions in membrane insertion (65). Here a central hydrophobic section is implicated. When the α_{s2} -working model was fitted with a surface and a pseudo-electrostatic charge calculated, a trefoil like representation shown in Figure 4 in color was produced. Note at that at six o'clock the hydrophobic central core extends downward and on the upper surface, the separation of charges produces both a highly negatively charged domain (red) as well as a unique positive surface (blue) for the potential attachment of κ -carrageenan. With the exception of small portions of κ -casein and α_{s1} -casein this represents the most definitive representation of positive charge on the caseins. Thus this working model supports the above NMR data suggestive of a possible role for α_{s2} -casein in the interaction of casein and κ -carrageenan.

Conclusions

The solubility and hydration properties of the salt containing κ -carrageenan-casein system from bovine and caprine milk reflected milk protein composition,

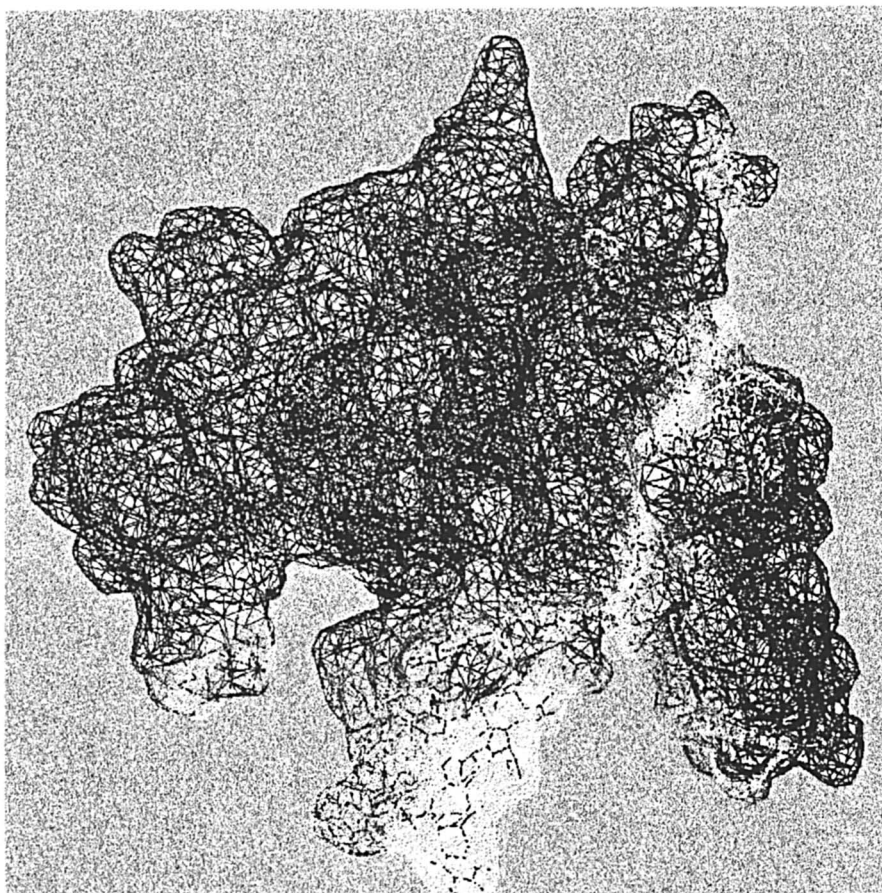


Figure 4. Pseudo-charge surface representation of the model of Figure 3 B. The negative charges on the top left (red) are due to the two anionic sections of the molecule. The positively charged C-terminal is on the top right (blue); this surface region would serve as a site for reaction with poly anions such as κ -carrageenan. The region of the molecule extending from the center to 6 o'clock represents the central hydrophobic core region; it is lightly colored and could react with other caseins as suggested for κ -casein (52). (See page 2 of color inserts.)

in particular κ -, α_{s2} - and α_{s1} -casein. The results reported here indicate that caprine caseins may undergo significant interactions with κ -carrageenan and with NaCl. Although the amount of κ -carrageenan used in this study (0.0078% w/v), does not generate enough three-dimensional structure to form gels, the increased interactions with caprine caseins particularly that low in α_{s1} -casein (high in α_{s2} -casein) suggest that a positive tail proposed by Snoeren et al. (14) for α_{s2} -casein could enhance κ -carrageenan binding and electrostatic complex formation for this protein system. The homologous model produced for α_{s2} -casein shows a strongly positively charged area, which may be surface accessible for interaction with the polysulfated κ -carrageenan. Finally, ^{17}O NMR spectroscopy offers a sensitive means for probing the interactions of κ -carrageenan with caseins by sensing the motion and hydration of complex formation not available from simple solubility studies that result from variations in ionic strength (NaCl) and from molecular and ionic interactions.

References

1. Sasaki, S.; Noguchi, H. Interaction of fibrinogen with dextran sulfate. *J. Gen. Physiol.* **1959**, *43*, 1-12.
2. Mathews, M. B. *Biochem. J.* **1965**, *96*, 710-716.
3. Brink, B.; Wasteson, A. *Biochem. J.* **1971**, *121*, 227-233.
4. Andersen, G. *Milchwissenschaft* **1962**, *17*, 75-79.
5. Payens, T. A. J. *J. Dairy Sci.* **1972**, *55*, 141-150.
6. Rey, D. K.; Labuza, T. P. *J. Food Sci.* **1981**, *46*, 786-789.
7. Snoeren, T. H. M.; Payens, T. A. J.; Jeunink, J.; Both, P. *Milchwissenschaft* **1975**, *30*, 393-396.
8. Mercier, J. C.; Brignon, G.; Ribadeu-Dumas, B. *Eur. J. Biochem.* **1973**, *35*, 222-235.
9. Mercier, J. C.; Grosclaude, F.; Ribadeu-Dumas, B. *Eur. J. Biochem.* **1971**, *23*, 41-51.
10. Ribadeu-Dumas, B.; Brignon, G.; Grosclaude, F.; Mercier, J. C. *Eur. J. Biochem.* **1972**, *25*, 505-514.
11. Morr, C. V. *J. Dairy Sci.* **1974**, *58*, 977-984.
12. Mora-Gutierrez, A.; Kumosinski, T. F.; Farrell, H. M., Jr. *J. Agric. Food Chem.* **1997**, *45*, 4545-4553.
13. Farrell, H. M., Jr. In *Fundamentals of Dairy Chemistry*. Wong, N., Ed.; Van Nostrand Reinhold: New York, 1988; Chapter 9, pp. 461-510.
14. Snoeren, T. H. M.; Markwijk, B. van.; Montfort, R. van. *Biochim. Biophys. Acta.* **1980**, *622*, 268-276.
15. Mora-Gutierrez, A.; Kumosinski, T. F.; Farrell, H. M., Jr. *J. Dairy Sci.* **1991**, *74*, 3303-3307.
16. Basch, J. J.; Farrell, H. M., Jr.; Walsh, R. A.; Konstance, R. P.; Kumosinski, T. F. *J. Dairy Sci.* **1989**, *72*, 591-603.

17. Pepper, L.; Farrell, Jr., H. M. *J. Dairy Sci.* **1982**, *65*, 2259-2266.
18. Wyman, J., Jr. Linked functions and reciprocal effects in hemoglobin: a second look. *Adv. Prot. Chem.* **1964**, *19*, 223-285.
19. Farrell, H. M. Jr.; Kumosinski, T. F. *J. Ind. Microbiol.* **1988**, *3*, 61-71.
20. Farrell, H. M., Jr.; Kumosinski, T. F.; Pulaski, P.; Thompson, M. P. *Arch. Biochem. Biophys.* **1988**, *265*, 146-158.
21. Mora-Gutierrez, A.; Farrell, H. M., Jr.; Kumosinski, T. F. *J. Agric. Food Chem.* **1993a**, *41*, 372-379.
22. Mora-Gutierrez, A.; Farrell, H. M., Jr.; Kumosinski, T. F. *J. Dairy Sci.* **1993b**, *76*, 3690-3697.
23. Mora-Gutierrez, A.; Farrell, H. M., Jr.; Kumosinski, T. F. *J. Dairy Sci.* **1993c**, *76*, 3698-3710.
24. Melander, W.; Horvath, C. *Arch. Biochem. Biophys.* **1977a**, *183*, 200-215.
25. Melander, W.; Horvath, C. *J. Solid-Phase Biochem.* **1977b**, *2*, 141-161.
26. Covington, A. K.; Raabo, M.; Robinson, R. A.; Bates R. G. *Anal. Chem.* **1968**, *40*, 700-706.
27. Dwek, R. A. In *Nuclear Magnetic Resonance (NMR) in Biochemistry*; Clarendon Press: Oxford, U.K., 1973; pp. 11-47.
28. Finney, J. L.; Goodfellow, J. M.; Poole, P. L. In *Structural Molecular Biology*; Davies, D. B.; Saenger, W.; Danyluk, S. S., Eds.; Plenum Press: New York, 1982; pp. 387-426.
29. Child, T. F.; Pryce, N. G. *Biopolymers* **1972**, *11*, 409-429.
30. Cooke, R.; Wien, R. *Ann. NY Acad. Sci.* **1973**, *204*, 197-203.
31. Oakes, J. J. *Chem. Soc. Faraday Trans.* **1976**, *72*, 216-227.
32. Hansen, J. R. *J. Agric. Food Chem.* **1978**, *26*, 301-304.
33. Derbyshire, W. In *Water: A Comprehensive Treatise*; Franks, F., Ed.; Plenum Press; New York, 1982; Vol. 7, pp. 339-469.
34. Mora-Gutierrez, A.; Baianu, I. C. *J. Food Sci.* **1990**, *55*, 462-465.
35. Cooke, R.; Kuntz, I. D. *Ann. Rev. Biophys. Bioeng.* Mullings, L. J. (ed). **9035**: 95. 1974.
36. Zimmerman, J. R.; Brittin, W. E. *J. Phys. Chem.* **1957**, *61*, 1328-1333.
37. Halle, B.; Andersson, T.; Forsén, S.; Lindman, B. *J. Am. Chem. Soc.* **1981**, *103*, 500-508.
38. Kumosinski, T. F.; Pessen, H. *Arch. Biochem. Biophys.* **1982**, *218*, 286-302.
39. Pessen, H.; Kumosinski, T. F. *Methods Enzymol.* **1985**, *117*, 219-255.
40. Kirkwood, J. G.; Shumaker, J. B. *Proc. Natl. Acad. Sci. U.S.A.* **1952**, *38*, 863-871.
41. Tanford, C. In *Physical Chemistry of Macromolecules*, Wiley: New York, 1963; Chapter 4, pp. 293-294.
42. Richards, E. G. In *An Introduction to the Physical Properties of Large Molecules in Solution*, Cambridge University Press: Cambridge, 1980; Chapter 2, pp. 15-35.

43. Bates, R. G. The activity concept in analytical chemistry. In *Ions and Molecules in Solution*; Tanaka, N.; Ohtaki, H.; Tanamushi, R., Eds.; Elsevier Science Publishers: Amsterdam, 1982; pp. 237-250.
44. Kumosinski, T. F.; Pessen, H.; Prestrelski, S. J.; Farrell, H. M., Jr. *Arch. Biochem. Biophys.* **1987**, *257*, 259-268.
45. Myers-Betts, P. A.; Baianu, I. C. *J. Agric. Food Chem.* **1990**, *38*, 477-483.
46. Kakalis, L. T.; Baianu, I. C.; Kumosinski, T. F. *J. Agric. Food Chem.* **1990**, *38*, 639-647.
47. Mora-Gutierrez, A.; Farrell, H. M., Jr.; Kumosinski, T. F. *J. Agric. Food Chem.* **1995**, *43*, 2574-2579.
48. Mora-Gutierrez, A.; Farrell, H. M., Jr.; Kumosinski, T. F. *J. Agric. Food Chem.* **1996a**, *44*, 48-53.
49. Mora-Gutierrez, A.; Farrell, H. M., Jr.; Kumosinski, T. F. *J. Agric. Food Chem.* **1996b**, *44*, 796-803.
50. Sawyer, L.; Barlow, P. N.; Boland, M. J.; Creamer, L. K.; Denton, H.; Edwards, P. J. B.; Holt, C.; Jameson, G. B.; Kontopidis, G.; Norris, G. E.; Uhrinova, S.; Wu, S.-Y. *Int. Dairy J.* **2002**, *12*, 299-310.
51. Notredame, C.; Higgins, D.; Heringa, J. *J. Mol. Biol.* **2000**, *302*, 203-217.
52. Kumosinski, T. F.; King, G.; Farrell, H. M., Jr. *J. Prot. Chem.* **1994**, *13*, 681-700.
53. Drohan, D. D.; Tziboula, A.; McNulty, D.; Horne, D. S. *Food Hydrocolloids* **1997**, *11*, 101-107.
54. Waugh, D. F.; Creamer, L. K.; Slattery, C. W.; Dresdner, G. W. *Biochemistry* **1970**, *9*, 786-795.
55. Snoeren, T. H. M. In *Kappa-carrageenan. A study on its physico-chemical properties, sol-gel transition and interaction with milk proteins*. Veenman, H., Zonen, B. V., Eds.; Nizon-Verslagen: Wageningen, 1976; pp. 37-56.
56. Tanford, C. In *Physical Chemistry of Macromolecules*, Wiley: New York, 1961; Chapter 5, pp. 624-625.
57. Grindrod, J.; Nickerson, T. A. *J. Dairy Sci.* **1968**, *51*, 834-841.
58. Parker, T. G.; Dalglish, D. G. *J. Dairy Res.* **1981**, *48*, 71-76.
59. Rees, D. A. *Adv. Carbohydr. Chem. and Biochem.* **1969**, *24*, 267-332.
60. Rees, D. A.; Morris, E. R.; John, D.; Madden, J. K. In *The Polysaccharides*. Aspinall, G. O., Ed.; Academic Press: New York, 1982; Vol. 1, Chapter 5, pp 276-281.
61. Schmidt, D. G. In *Developments in Dairy Chemistry*; Fox, P. F., Ed.; Applied Science Publishers: Essex, England, 1982; pp 61-93.
62. Farrell, H. M., Jr.; Jimenez-Flores, R.; Bleck, G. T.; Brown, E. M.; Butler, J. E.; Creamer, L. K.; Hicks, C. L.; Hollar, C. M.; Ng-Kwai-Hang, K. F.; Swaisgood H. E. *J. Dairy Sci.* **2004**, *87*, 1641-1674.
63. Swaisgood, H. E. In *Advanced Dairy Chemistry-1*; Editor, P. F. Fox; Elsevier Applied Science: New York, NY, 1992; pp 63-110.
64. Hoagland, P. D.; Unruh, J. J.; Wickham, E. D.; Farrell, H. M., Jr. *J. Dairy Sci.* **2001**, *84*, 1944-1949.

65. Paul, S. M.; Beitel, G. J. *Science* **2003**, *302*, 2077-2078.
66. Ashley, R. H. *Mol. Membr. Biol.* **2003**, *20*, 1-11.
67. Fernandez-Salas, E.; Sagar, M.; Cheng, C.; Yuspa, S. H.; Weinberg, W. C. *J. Biol. Chem.* **1999**, *274*, 36488-36497.
68. Suh, K. S.; Mutoh, M.; Nagashima, K.; Fernandez-Salas, E.; Edwards, L. E.; Hayes, D. D.; Crutchley, J. M.; Marin, K. G.; Dumont, R. A.; Levy, J. M.; Cheng, C.; Garfield, S.; Yuspa, S. H. *J. Biol. Chem.* **2004**, *279*, 4632-4641.
69. Shanks, R. A.; Larocca, M. C.; Berryman, M.; Edwards, J. C.; Urshdinani, T.; Navarre, J.; Goldenring, J. H. *J. Biol. Chem.* **2002**, *277*, 40973-40908.
70. Board, P. G.; Coggan, M.; Watson, S.; Gage, P. W.; Dulhunty, A. F. *Int. J. Biochem. Cell Biol.* **2004**, *36*, 1599-1612.
71. Berryman, M.; Bruno, J.; Price, J.; Edwards, J. C. *J. Biol. Chem.* **2004**, *279*, 34794-34801.
72. Cromer, B. A.; Morton, C. J.; Board, P. G.; Parker, M. W. *Eur. Biophys. J.* **2002**, *31*, 356-364.
73. Casanova, H.; Dickinson, E. J. *Colloid Interface Sci.* **1998**, *207*, 82-89.

Footnote

Mention of trade names or commercial products in this publication is solely for the purpose of providing information and does not imply recommendation or endorsement by Prairie View A&M University or the U.S. Department of Agriculture.

Chapter 7

Pasteurization Affects Aggregation of Acidified Milk Dispersions and Pectin

Brian Barnes¹, Milena Corredig², and Louise Wicker^{3,*}

¹GoldKist, Inc., P.O. Box 2210, Atlanta, GA 30301

²Department of Food Science, University of Guelph, Guelph, Ontario N1G 2Q1, Canada

³Department of Food Science and Technology, University of Georgia, Athens, GA 30602

Commercial pectins were added at stabilizing levels to acidified milk dispersions and the effect of pectin type and pasteurization on the pectin-protein interaction was evaluated by gel permeation chromatography with in-line multi-angle light scattering, refractive index, and UV detectors. Commercial pectins had no apparent effect on the differences in molecular weight distributions of the soluble material in the dispersions. The weight average molecular weight (M_w) of individual pectins were 1.2 to over 4 million and were polydisperse with M_w/M_n ratios greater than 1.0. The M_w of soluble components in the mixed dispersions were 2-8 times higher than pectin alone and had greater polydispersity. Pasteurization had a greater effect on molecular weight distributions and polydispersity than pectin type. A second, high molecular weight aggregate was observed in all pasteurized samples. This aggregate was ≈ 10 times larger after pasteurization compared to non-pasteurized samples.

Pectin inhibits heat-induced aggregation, serum separation, sedimentation, and influences the rheological properties of acidified milk beverages. It is believed that electrostatic interactions play a strong role in the stabilization of acidified milk proteins with anionic polysaccharides such as pectin (1-3). Pectin adsorption and steric stabilization are important in pectin stabilized acidified milk beverages (4). The mechanism of destabilization depends on pectin concentration and varies from bridging flocculation to depletion flocculation from low to high concentration (5). In stable dispersions, less than 20% of the critical concentration of added pectin to prevent bridging flocculation is actually adsorbed to the protein surface (6).

Pectin is composed of α -1 \rightarrow 4-linked D-galacturonic acid, is partially esterified with methyl esters, is interrupted by 1 \rightarrow 2 linked L-rhamnose, and has blocks of neutral sugar side chains (7). Commercial pectins differ in levels of uronic acid, degree of esterification, molecular weight, neutral sugar content, and Ca^{2+} sensitivity. These factors potentially influence the stability and texture of acidified milk beverages. Multi-angle light scattering with in-line size exclusion chromatography is used to estimate molecular weight of de-esterified pectates (8), to assess process induced changes in pectin MW due to homogenization (9), charge modification of pectin (10), and aggregation of heated whey protein-pectin dispersions (11, 12). Molecular differences between commercial pectins influence the rheological properties of acidified milk dispersions and pasteurization of dispersions influence stability, particle size, and rheological properties of acidified milk systems (13). The objective of this study was to determine the effect of pectin type and pasteurization on the molecular weight distribution of the soluble fraction in acidified milk beverages at stabilizing levels of pectin. This information may assist in predicting the stability and rheological properties of acidified milk dispersions.

Materials and Methods

Sample Preparation

Low-heat skim milk powder (SPEC 6010, New Zealand Dairy Board, Wellington, NZ) was hydrated at room temperature using de-ionized water to contain 16% MSNF and 6.4% protein. The dispersions were acidified to pH 4.1 at 30° C for 16 hours with glucono- δ -lactone (3.4% w/w) (Sigma Chemical Co., St. Louis, MO). Commercial pectins (Danisco Grindsted AMD 780 (DAN) (New Century, Kansas), Genu-Pectin Type JMJ (JMJ) (Wilmington, Delaware, and Genu-Pectin Type X-6903 (6903) (Copenhagen, Denmark)] were used in

this study. Levels of uronic acid were determined using the colorimetric m-hydroxydiphenyl method (MHDP) (14). A stock 0.90% uronic acid pectin dispersion was made and stored at 4° C. After acidification, aliquots of acidified milk gel were mixed with pectin and water so that the final dispersions contained 3.2% protein, 8% MSNF, and 0.45% uronic acid. The pH of the solutions was adjusted to 4.1 using either 10% sodium hydroxide solution or a 6 N HCl solution. The samples were homogenized at 17.2 MPa at 4 passes using an Avestin Emulsiflex C-5 high-pressure homogenizer (Ottawa, ON). After homogenization, half the volume of the pectin-containing dispersions was pasteurized (75° C, 60 seconds). The dispersions were immediately cooled and stored at 4° C. The dispersions were then centrifuged at 3000 x g for 20 minutes. The soluble phase (supernatant) was frozen until analysis.

Analysis

The molecular weight was estimated using the HPLC and light scattering method described by Corredig et al. (15). The supernatants were diluted 1:5 in 0.5 M sodium acetate solution (pH 4.1), and insoluble material was removed from the re-suspended supernatants and by centrifugation using an Eppendorf centrifuge at maximum velocity (13,000 RPM) for 5 minutes in 0.45 μ m Durapore centrifugal filter tubes (Cat. No. UFC30HV00, Millipore, Bedford, MA). Pectin controls were prepared at 0.45 % (w/v) in 0.5 M sodium acetate, pH 4.1. Samples were injected with a 50 μ L loop in a Spectrasystem autosampler (AS 3000, Thermoseparation Products, San Jose, CA). The flow rate was set to 0.6 mL/min. A BioSep-SEC-S column (300 * 7.5 mm, Phenomenex, Torrance, CA) was employed for the separation. The three, in-line detectors included a multi-angle light scattering detector (LS), refractive index (RI) detector (Wyatt Technologies, Santa Barbara, CA), and a variable wavelength detector (280 nm) (Isco, V4 series, Lincoln, NE). The multi-angle, digital signal processing light scattering detector (DAWN DSP-F) was equipped with a F2 flow cell and a He-Ne laser-light source (L = 633 nm). The refractive index detector was the Optilab DSP interferometric refractometer (Wyatt Technologies, Santa Barbara, CA) operating at 633 nm and room temperature. The UV detector was operated at 280 nm at room temperature. Elution data was processed using the Astra/Easi SEC software, molecular weight as number average (M_n), weight average (M_w), z-average (M_z), and polydispersity (M_w/M_n) were calculated. Representative chromatograms are presented and the data reported is the average of 4 replications.

Results & Discussion

Each of the three detectors presented a different elution profile of milk protein-pectin dispersions (data not shown). The LS detector indicated a single, large molecular weight aggregate, which eluted between ≈ 4.0 and 6.5 mL. The RI detector indicated a small peak corresponding to the one detected by LS in addition to a second smaller molecular weight peak eluting between ≈ 8.5 and 10.0 mL. The UV detector indicated a peak coincident with the single LS peak and peaks present at the same elution points as the RI detector, indicating that protein was present. The results suggest that the material that eluted between 4.0 and 6.5 mL was very large but of limited quantity. The material that elutes between 8.5 and 10.0 mL is likely to consist of monomeric and oligomeric serum protein.

Based on the differences in the RI and UV signal, the smaller molecular weight peaks are likely to contain no pectin and is thus primarily composed of milk protein. When the pectin without protein was analyzed, the control pectin dispersions eluted between 6.5 and 8.5 mL. No difference in molecular weight of dispersions was observed between the three pectins.

The fraction of the soluble dispersion that passed through a $0.45 \mu\text{m}$ filter represented the fraction used for analysis. A high degree of insoluble material existed and was lost upon centrifugation and filtration. Hence, the samples were not necessarily representative of the total aggregate fraction, but of the soluble, filterable fraction at pH 4.1. Sequential filtration of pectate solutions through 0.8 , 0.45 , 0.2 , and $0.06 \mu\text{m}$ pore diameter membranes also resulted in selective loss of high molecular weight material (8).

In all cases, the average molecular weight of the protein-pectin dispersions was larger than pectin controls (Table 1). It is also worth noting that the molecular weight data of the pectin controls in the acetate buffer (pH 4.1) is in contrast to the values obtained earlier (15) when analyzed in 50mM NaNO_3 (pH 5.8), or 50mM NaNO_3 with 10mM sodium phosphate (pH 7). An average molecular weight of the pectins in sodium nitrate buffer was 2.67×10^5 , 4.30×10^5 , and 2.71×10^5 , for DAN, MJJ, 6903, respectively. In this study, an average molecular weight (Mw) of 0.45% pectin in sodium acetate buffer was $1.17 \times 10^6 \pm 8.84 \times 10^5$, $1.94 \times 10^6 \pm 4.91 \times 10^5$, $4.26 \times 10^6 \pm 1.48 \times 10^6$ for DAN, MJJ, and 6903, respectively. Separation of pectin-pectin interactions from pectin-protein interactions may be possible, but only by analysis of individual slices of the chromatogram, and probably not feasible due to the variability in pectin aggregation.

While no apparent difference in molecular weight distribution was observed between the samples stabilized with different pectins, a noticeable difference was found between the pasteurized and non-pasteurized samples (Table I).

Table I. Averages of particle size data of centrifuged (3000 x g, 20 minutes), homogenized acidified milk dispersions (pH 4.1), with varying pectin type & heat treatment (75° C, 60 seconds).

Sample	M_n	M_w^d	M_z	M_w/M_n
DAN	$5.67 \times 10^6 \pm 9.13 \times 10^5$	$8.08 \times 10^6 \pm 1.53 \times 10^6$	$1.66 \times 10^7 \pm 1.51 \times 10^6$	1.42 ± 0.08
DAN(Past.)	$1.11 \times 10^7 \pm 2.81 \times 10^6$	$3.88 \times 10^7 \pm 9.25 \times 10^6$	$1.69 \times 10^8 \pm 7.44 \times 10^7$	3.53 ± 0.26
JMJ	$4.44 \times 10^6 \pm 3.07 \times 10^6$	$5.99 \times 10^6 \pm 4.15 \times 10^6$	$1.00 \times 10^7 \pm 6.85 \times 10^6$	1.35 ± 0.04
JMJ(Past.)	$9.26 \times 10^6 \pm 3.72 \times 10^6$	$3.39 \times 10^7 \pm 8.28 \times 10^6$	$1.41 \times 10^8 \pm 5.86 \times 10^7$	3.85 ± 0.71
6903	$6.01 \times 10^6 \pm 4.16 \times 10^6$	$7.47 \times 10^6 \pm 5.14 \times 10^6$	$1.08 \times 10^7 \pm 7.06 \times 10^6$	1.25 ± 0.03
6903(Past.)	$1.35 \times 10^7 \pm 6.67 \times 10^6$	$3.92 \times 10^7 \pm 1.56 \times 10^7$	$1.07 \times 10^8 \pm 3.18 \times 10^7$	3.19 ± 0.81

^d M_w of DAN (0.45% w/v) = $1.17 \times 10^6 \pm 8.84 \times 10^5$, M_w of JMJ (0.45% w/v) = $1.94 \times 10^6 \pm 4.91 \times 10^5$, & M_w of 6903 (0.45% w/v) = $4.26 \times 10^6 \pm 1.48 \times 10^6$

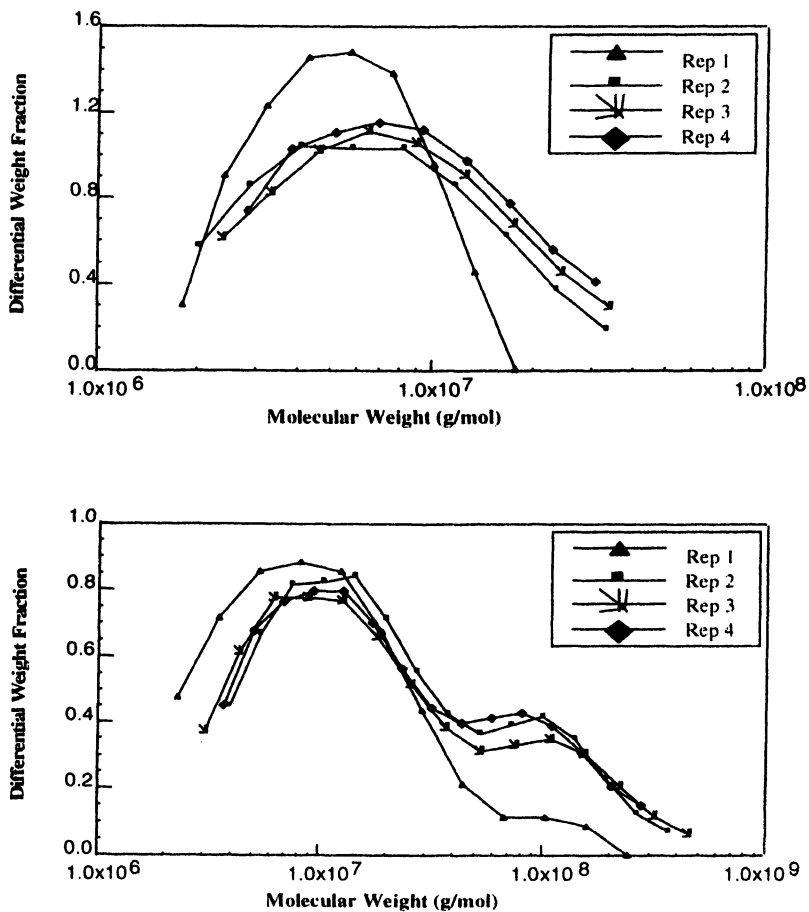


Figure 1a & b. Representative molecular weight distribution of supernatants obtained from centrifuged (3000 x g, 20 minutes), non-pasteurized (a) and pasteurized (b) acidified milk dispersions (pH 4.1) stabilized with pectin (injected volume 50 μ L; mobile phase: 0.5 M sodium acetate, pH 4.1).

Pasteurized samples demonstrated a bimodal peak whereas the non-pasteurized showed only a single peak. See Figures 1a and 1b for sample chromatograms. Consequentially, polydispersity as determined by M_w/M_n , was larger for the pasteurized samples (≈ 3.5) as compared to the non-pasteurized (≈ 1.5).

Because the UV signal of the largest molecular weight aggregate is low, it is probable that only a small percentage of the protein interact with pectin to form detectable aggregates. The nature of the interaction is unknown, but pectin may interact with protein as milk protein aggregates or as free proteins. Upon demineralization resulting from the acidification process, little dissociation of casein sub-units from the micelle occurs, particularly at typical fermentation temperatures (30°C) (16). However, freezing or filtering the samples before analysis may have increased the quantity of proteins. The pectin may be interacting with free calcium lost upon acid gelation and the proteins are entrapped in a calcium pectate network. Electrostatic interactions may be disrupted in 0.5 M sodium acetate, which would facilitate separation of aggregates and individual components by HPSEC that are stabilized by electrostatic interactions. The presence of aggregates in 0.5 M sodium acetate suggests that hydrophobic interactions may be responsible for stabilization of the high molecular weight aggregates.

The mechanism of the pasteurization effect on aggregate size cannot be deduced from this study. The high molecular weight aggregates in the pasteurized samples confirms that heat enhances the detection of larger aggregate sizes. Pasteurization may increase aggregate size but it is also possible that pasteurization solubilizes some large aggregates that were not measurable without pasteurization. Pasteurization may increase the solubility and filterability of some very large aggregates.

Conclusions

Differences existing between commercial pectins do not have an effect on the molecular weight of the protein-pectin aggregates found in this analysis. However, pasteurization increases the molecular weight and polydispersity of these systems. The source of the high molecular weight species cannot be positively identified. The limited solubility of the supernatants in the 0.5 M sodium acetate buffer and the apparent aggregation of the pectin solutions influences the measurement of the true molecular weight distribution of the samples. The high molecular weight and polydispersity of the samples obtained from the pasteurized dispersions may be related to differences in solubility, not interaction differences.

References

1. Parker, A.; Boulenguer, P.; Kravtchenko, T. P. In *Food Hydrocolloids: Structures, properties, and functions*; Nishinari, K.; Doi, E., Eds. Plenum Press: New York, 1993.
2. Pedersen, H. C. A.; Jorgensen, B. B. *Food Hydrocolloids* **1991**, *5*, 323-328.
3. Pereyra, R.; Schmidt, K. A.; Wicker, L. *J. Agric. Food Chem.* **1997**, *45*, 3448-3451.
4. Syrbe, A.; Bauer, W. J.; Klostermeyer, N. *Int. Dairy J.* **1998**, *8*, 179-193.
5. Maroziane, A.; de Kruif, C. G. *Food Hydrocolloids* **2000**, *14*, 391-394.
6. Tromp, R. H.; de Kruif, C. G.; van Eijk, M.; Rolin, C. *Food Hydrocolloids* **2004**, *18*, 565-572.
7. Voragen, A. G. J.; Pilnik, W.; Thibault, J. F.; Axelos, M. A. V.; Renard, C. M. G. C. In *Food Polysaccharides and Their Applications*; Stephen, A. M., Ed. Marcel Dekker, Inc: New York, 1995; Vol. 67, pp 287-339.
8. Malovikova, A.; Rinaudo, M.; Milas, M. *Carbohydr. Polym.* **1993**, *22*, 87-92.
9. Corredig, M.; Wicker, L. *Food Hydrocolloids* **2001**, *15*, 17-23.
10. Hunter, J. L.; Wicker, L. Univ Georgia, Dept Food Sci & Technol, Athens, GA; **2005**. Unpublished.
11. Beaulieu, M.; Corredig, M.; Turgeon, S. L.; Wicker, L.; Doublier, J. L. *Food Hydrocolloids* **2005**, *19*, 803-812.
12. Kazmierski, M.; Wicker, L.; Corredig, M. *J. Food Sci.* **2003**, *68*, 1673-1679.
13. Barnes, B.; Corredig, M.; Wicker, L., Univ Guelph, Dept Food Sci, Guelph, ON; Univ Georgia, Dept Food Sci & Technol, Athens, GA; Unpublished.
14. Blumenkrantz, N.; Asboe-Hansen, G. *Anal. Biochem.* **1973**, *54*, 484-489.
15. Corredig, M.; Kerr, W.; Wicker, L. *Food Hydrocolloids* **2000**, *14*, 41-47.
16. Law, A. J. R.; Leaver, J. *J. Agric. Food Chem.* **1998**, *46*, 5008-5016.

Chapter 8

Characterization of Intercultivar Variation on the Linear Viscoelastic Network Properties of Wheat Gluten II: Effects of Temperature and L-Cysteine

Hongquan Liang¹, Chia C. Lee¹, Patricia Rayas-Duarte², and Steven J. Mulvaney¹

¹Department of Food Science, Cornell University, Ithaca, NY 14853

²Food and Agricultural Products Center, Oklahoma State University, Stillwater, OK 74078

Both non-covalent and disulfide bonds are known to be important contributors to the unusual viscoelastic properties of wheat gluten, but it has been difficult to decouple their effects on such. In this work, the effects of added L-cysteine and an increase in temperature on the stress relaxation behavior of three glutens with different high molecular weight subunit composition were compared. An increase in temperature up to 40°C decreased the apparent network strength for all of the glutens, but the decrease in viscoelasticity varied between the glutens with different subunit composition. It was found that addition of 250 ppm L-cysteine at 25°C to these glutens eliminated most evidence of a network structure in their stress relaxation patterns, but the resulting extended power law stress relaxation curves did not superpose themselves at 25°C. These results suggest that use of the linear viscoelastic network strength of gluten shows promise as a new tool for assessing the intercultivar variations in gluten network structures.

Introduction

Wet gluten is obtained from mixed wheat flour dough by washing out the water-soluble albumin proteins, the salt-soluble globulin proteins and starch. The cohesive gluten that is recovered after washing of the dough shows very interesting material properties. It can be stretched, and if not stretched too far, will return to its original shape, i.e., the deformation is recoverable like an elastic rubber band. Gluten obtained from doughs of different wheat cultivars are more or less resistant to extension, a property generally referred to as gluten strength. Dough and gluten can also be stretched until they break, the deformation at break representing the property referred to as extensibility. Wheat cultivars used for production of high loaf volume pan bread must give mixed doughs that have a certain balance between extensibility and elasticity to ensure both good dough handling properties and the ability to expand and hold CO₂ gas during proofing and oven rise (1).

In more general polymer science terms, soft cohesive materials like gluten and natural rubber that are both extensible and elastic are classified as viscoelastic materials. It is clear that the viscoelasticity of wheat gluten and dough is the result of specific gluten proteins forming an elastic network in the presence of water and some mechanical energy input. But, relating differences in the viscoelasticity of dough or gluten obtained from different wheat cultivars to the cereal protein composition in grains or flour is complicated by the hierarchical structures that the cereal proteins adopt when hydrated. Shewry et al (2) remind us that the wheat gluten proteins are a highly complex mixture with at least 50 individual protein components being separated by two-dimensional isoelectric focusing/SDS-PAGE of reduced total fractions. Only some of these individual cereal proteins assemble themselves into an elastic network in gluten during mixing of wheat doughs.

Cereal chemistry and rheology: some background

The exact biochemical basis for why differences in gluten protein composition in flour, e.g., presence or absence of certain wheat proteins or their proportions of the total gluten protein, causes differences in the viscoelastic properties of glutes and doughs is still not known for certain. However, wheat doughs prepared from wheat lines that were devoid of a class of cereal proteins referred to as high molecular weight glutenin subunits (HMW-GS) were described as plastic, not elastic, and the gluten obtained from these doughs was

described as having the consistency of chewed gum (3). Thus, it seems certain that the HMW-GS are necessary in order to observe the property of recoverable deformation in wheat gluten and dough, but determining how exactly they interact with each other and the other cereal proteins to form an elastic network structure in gluten remains a challenge.

One major problem that arises in any attempt to relate HMW-GS composition to the viscoelasticity of hydrated cereal proteins is the fact that determination of the individual HMW-GS composition of a wheat cultivar requires reduction of disulfide bonds to liberate the individual subunits from the native crosslinked glutenin structures that are naturally present in wheat flour. Another problem is that only a portion of the glutenin proteins are soluble with the presently used methodology, even after reduction of disulfide bonds and alkylation, and limited information is known about the remaining insoluble proteins. Thus, explaining viscoelasticity of gluten in the hydrated state requires a hypothetical "reassembling" of all of the subunits back into crosslinked clusters, and ultimately into a connected glutenin network structure. Ewart (4) provides a review of the major hypotheses for glutenin network structures that have resulted primarily from extraction and fractionation studies of the wheat proteins from flour. Kasarda (5) reviews how molecular modeling has led to a better understanding of how the structures of individual glutenin subunits, in particular the number and locations of cysteine residues, might determine the properties of glutenin polymers. It is important to keep in mind here though that the term "glutenin polymers" in the context of cereal science refers to structures that result presumably mainly from the disulfide crosslinking of certain subunits into larger molecular weight clusters that exist in wheat flour, and not individual linear molecules as would usually be the case in synthetic polymer science. This is an important, and sometimes overlooked, conceptual difference when it comes to interpreting experimental viscoelastic data in terms of underlying network structures. This point will be emphasized further in the results and discussion section of this paper.

The HMW-GS and wheat quality

Despite some of the obvious difficulties in relating HMW-GS composition to viscoelasticity of gluten or dough, the basis of elucidating structure-function relationships in wheat has narrowed over the last 20 years or so to focus mainly on the HMW-GS (2). A numbering system (nomenclature) for cataloging the HMW-GS of wheat cultivars based on their electrophoretic patterns was

published by Payne and Lawrence (6) and remains in worldwide use today. In a widely cited study, Payne et al. (7) determined the HMW-GS in grain for about 185 varieties of wheat, and observed differences in the both the number (3 to 5) of HMW-GS and their mobility in SDS-PAGE analysis. In a nutshell, the HMW-GS are coded by three chromosomes (1A, 1B, and 1D), and allelic variation is observed at each locus.

A major finding of the early work with HMW-GS was that the 1D allelic subunit pair designated as "5+10" was strongly correlated with improved bread loaf volume relative to its allelic alternative 1D subunit pair 2+12 (8, 9). But, there were a large number of 2+12 cultivars in the sample set. Of the 92% of the 185 cultivars that had either the 5+10 or the 2+12 1D coded pair of subunits, 55% were 2+12. On the other hand, analysis of the HMW-GS subunits in 70 Canadian grown wheats showed that essentially all of the hard wheats had the "5+10" subunits (10), while 43 out of 44 hard red spring wheats grown in North Dakota also contained the 5+10 1D coded pair of subunits (11). Apparently, most of the wheat breeders in North America had been selecting for stronger gluten when the end use was yeasted bread, unknowing with a result of a gene pool in which 5+10 is common. Likewise, breeders had been selecting for weaker gluten when the end-use was baked products such as cookies, cakes and crackers, unknowing resulting in gene pools with an abundance of 2+12 cultivars. But, there are a number of exceptions found in which relatively strong gluten wheat cultivars also contain 2+12 subunits.

Given the above, it is not too surprising that tremendous efforts have been made to determine whether correlations between the intercultural variations in the composition of the HMW-GS alone are sufficient for prediction of wheat quality in breeding programs. Primard et al (12) tested this exact hypothesis with 286 experimental wheat lines, and followed up with an additional study involving 100 hard winter wheat lines of diverse origin (13). They found no significant differences in mean quality parameters (grain protein, dough mix time and dough tolerance to overmixing) in lines that contained the alternative 1A coded subunits 1 or 2*, or the 1B coded alternatives 7+8 versus 7+9, or 7+8 versus 13+16, and also observed a wide range of mixograph characteristics for a population of wheat lines all carrying 5+10 1D subunits. In a later study it was concluded that allelic variations did not always result in significant quality differences, nor did allelic variation result in changes in the complete spectrum of quality variables (13). Khan et al (11) noted that interactions between gliadin and glutenin protein fractions seemed to be the important factor in influencing breadmaking quality parameters.

Thus, it appears that knowing the HMW-GS subunit composition is only part of the "complete package" of information needed by breeders and cereal chemists for prediction of the functional traits in early generation experimental wheat lines. In the next section we describe how linear viscoelastic rheological

measurements on gluten can be used to obtain a direct measure of the network strength in gluten, which can be recovered from mixed doughs easily, and still retains the unique extensibility and elasticity of hydrated wheat proteins. The latter two being important functional aspects of total wheat quality.

Linear viscoelastic network strength of gluten as an index of wheat quality

It is clear that many different combinations of chemical and/or physical dough properties and/or loaf volume measurement have been traditionally used as indices of wheat quality. Overall, mixed results have been obtained when attempting to correlate these measures of wheat quality with various wheat protein fractions or subunit composition. However, none of these methods that have been traditionally used as indices of wheat quality actually provide a direct non-destructive measure of the intercultivar variation in the “strength” of the elastic network in whole gluten. Thus, determination of the native network strength of whole gluten itself has been largely left out of the wheat quality loop, although the amount of wet gluten recovered from wheat flour has been used.

Based on the above discussion, we think that development of an experimental rheological technique that allows for determination of the native network strength in gluten would be an important addition to the tools used for assessment of intercultivar variations in wheat quality. Linear viscoelastic measurements are very sensitive to small relative differences in network connectivity, which has been demonstrated by their ability to track very well changes in the extent of curing in chemical crosslinking reactions (14, 15). Characterizing the network strength of gluten in the fundamental (universal) units of polymer science will also allow for direct comparisons with a wide range of synthetic polymer networks with varied, but well characterized types of network structures and degrees of crosslinking. This should help us to better understand the basic nature of the interactions (entanglements, disulfide crosslinks, and/or non-covalent interactions) involved in the elastic gluten network structure, which in turn can be related to the chemistry of the cereal proteins.

This concept will be tested here by determining the viscoelastic properties of gluteins from “5+10” wheat cultivars differing only in their 1B HMW-GS compositions. The effects of temperature and addition of a reducing agent on the viscoelastic properties will also be determined. The former to test the hypothesis that differences in viscoelastic properties between these cultivars may diminish as the temperature is increased, and the latter to verify which portion of the viscoelastic spectrum corresponds to the disulfide crosslinked network in whole gluten.

Materials and Methods

Two single cultivar hard white spring wheat (HWS) flours, Golden 86 and Argent, were obtained from Cook Natural Products (Oakland, CA.). A Canadian Western Extra Strong (CWES) red wheat cultivar, Glenlea, was used as an example of a very strong wheat for comparison. L-cysteine was obtained from Sigma Chemical Co. (St. Louis, MO).

Table 1. Protein content of flours and the HMW-GS (1A, 1B, 1D) subunits for the three cultivars.

<i>Cultivars</i>	<i>Argent</i>	<i>Golden 86</i>	<i>Glenlea</i>
<i>Properties</i>			
Flour			
Protein (%)	13.5	13.17	12.9
HMW-GS subunits			
1A	2*	2*	2*
1B	7+9	7+8	7+8
1D	5+10	5+10	5+10

Thus, all three cultivars contain the full complement of five HMW-GS, and differ in only one HMW-GS subunit, 1By9 for Argent versus 1By8 for Glenlea and Golden 86.

Wet gluten was obtained from each flour according to AACC method 38-10 (AACC) with some modification as described in Lee and Mulvaney (16). Gluten samples (60% water content on total weight basis) were prepared for rheological studies as described previously (16). Briefly, the gluten powder was rehydrated and then pressed between two aluminum plates with a 2.5 mm gap for 1 hour to form a gluten sheet of uniform thickness. Shear stress relaxation experiments (1% strain) were done with a Bohlin VOR-M rheometer (Bohlin Instruments, Cranbury, NJ), using parallel plate geometry as described previously (16). The shear relaxation modulus ($G(t)$) was obtained for 10,000s for control glutes at 15, 25, 35, and 40 °C, but only at 15, 25 and 35 °C for L-cysteine containing samples due to limited quantities of flours. Minitab version 12.0 (Minitab Inc, State College, PA, USA) was used for statistical analysis of rheological parameters. Differences in results were considered statistically significant at $P < 0.05$.

Results

Parameterization of gluten stress relaxation curves

Figure 1 shows the stress relaxation curves ($G(t)$ versus time) for the three glutes used here, including identification of the four parameters used to compare results between glutes. This parameterization procedure was developed previously by Lee and Mulvaney (16), and was used to compare glutes and glutenins from a series of Canadian wheat cultivars representing different statutory wheat classes. $G(t)$ showed two distinct relaxation modes for

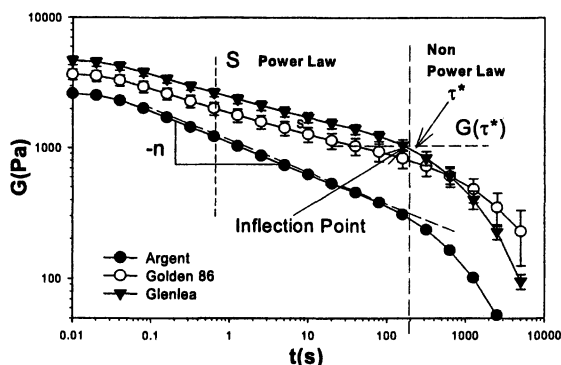


Figure 1. Illustration of parameterization of stress relaxation patterns for Argent, Golden 86 and Glenlea glutes. $G(\tau^)$ is considered the "base" network strength associated with τ^* , the longest relaxation time. S is the strength of the power law relaxation mode and n is the magnitude of the power law relaxation exponent (see equation 1). Temperature was 25 °C and strain was 1% for this example.*

times greater than about 0.1 s, an initial power law relaxation mode followed by a non power law relaxation mode. Bohlin and Carlson (17) were perhaps the first to observe these two distinct relaxation modes for gluten and dough in stress relaxation. However, neither their unique way of parameterizing the stress relaxation results nor their interpretation of the experimental data in terms of coordinated flow units has been carried forward in the cereal science literature. But, in fairness those researchers did not have the information that we have today related to glutenin subunits and the important role they play in the elasticity of gluten.

Any power law phenomenon is characterized by a slope on log-log coordinates, and not a single characteristic time. Therefore, the slope of the power law relaxation mode (n) and an intercept (S) were obtained via linear regression of equation (1), which was adapted from Mours and Winter (18). The original context of the use of eq. 1 by Mours and Winters was to describe the extended power law relaxation that was observed for a crosslinking polymer at the critical point of gelation, the critical degree of crosslinking denoting the transition from a viscoelastic liquid behavior to a viscoelastic solid-like behavior. We think this analogy is appropriate for gluten, since all indications are that only some of the gluten proteins are linked together by covalent disulfide bonds (19), the remainder presumably existing as clusters of different size or as monomeric (uncrosslinked) gliadin.

$$\log G(t) = -n \log(t) + \log(S) \quad (1)$$

The relaxation time corresponding to the long time inflection point of the $G(t)$ curve was denoted as τ^* . The corresponding value of $G(t)$ at τ^* was denoted as $G(\tau^*)$. We think that these parameters are indicative of the lifetime of the native crosslinked network structure in gluten and the linear viscoelastic network strength of that network, respectively.

Effect of temperature on n , S , τ^* and $G(\tau^*)$

As shown in Table 2, an increase in temperature had no significant effect ($P < 0.05$) on n for either the Argent, Golden 86 or Glenlea glutes. However, for a given temperature of 15, 25, 35 or 40 °C, the n values for Golden 86 (0.19, 0.17, 0.18 and 0.17) and Glenlea (0.17, 0.16, 0.16 and 0.18) glutes were significantly lower than those for Argent gluten (0.25, 0.24, 0.25 and 0.24). An increase in temperature had no significant effect on S for Argent gluten. Increasing the temperature to 35 °C for Golden 86 gluten caused S to decrease significantly from 2253 Pa sⁿ at 15 °C to 1006 Pa sⁿ at 35 °C, which was also similar to the value of S at 40 °C (1172 Pa sⁿ). S for Glenlea gluten also significantly decreased from 2505 Pa sⁿ at 25 °C to 1396 Pa sⁿ at 40 °C, but S for Glenlea gluten showed a higher S value (1935 Pa sⁿ) than Golden 86 (1006 Pa sⁿ) at 35 °C.

However, at 40 °C S for all three glutes became similar to each other. Thus, differences in S between these glutes that were so apparent at 15 °C decreased with increased temperature and disappeared at 40 °C. These results support the hypothesis presented earlier those differences in viscoelastic properties may diminish, and become more similar to each other, as the temperature is increased.

The decrease in S , which is a short time parameter, with increased temperature may actually result from a decrease in the base network strength,

Table 2. Effect of temperature on the stress relaxation parameters (n , S , τ^* and $G(\tau^*)$) for gluten obtained from three wheat cultivars (Argent, Golden 86 and Glenlea).

Temperature ($^{\circ}\text{C}$)	Argent			
	n	S (Pa s^n)	τ^* (s)	$G(\tau^*)$ (Pa)
15	0.25 \pm 0.004 ^a	1214 \pm 131 ^a	289 \pm 65 ^{a,b}	296 \pm 63 ^{a,b}
25	0.24 \pm 0.001 ^a	1094 \pm 42 ^a	189 \pm 11 ^b	289 \pm 1 ^a
35	0.25 \pm 0.001 ^a	956 \pm 112 ^a	67 \pm 4 ^a	322 \pm 35 ^{a,b}
40	0.24 \pm 0.006 ^a	1027 \pm 55 ^a	56 \pm 0 ^c	373 \pm 10 ^b
	Golden 86			
15	0.19 \pm 0.004 ^{a,b}	2253 \pm 13 ^a	1790 \pm 205 ^a	469 \pm 15 ^a
25	0.17 \pm 0.008 ^{a,b}	1894 \pm 218 ^{a,c}	1450 \pm 328 ^{a,b}	459 \pm 145 ^{a,b}
35	0.18 \pm 0.001 ^a	1006 \pm 26 ^b	409 \pm 93 ^b	291 \pm 28 ^b
40	0.17 \pm 0.002 ^b	1172 \pm 17 ^c	253 \pm 29 ^b	405 \pm 33 ^{a,b}
	Glenlea			
15	0.17 \pm 0.004 ^a	2391 \pm 277 ^a	800 \pm 92 ^a	689 \pm 77 ^a
25	0.16 \pm 0.004 ^a	2505 \pm 193 ^a	459 \pm 104 ^{a,b}	721 \pm 20 ^a
35	0.16 \pm 0.004 ^a	1935 \pm 21 ^{a,b}	189 \pm 11 ^b	684 \pm 11 ^a
40	0.18 \pm 0.002 ^a	1396 \pm 139 ^b	119 \pm 7 ^c	501 \pm 79 ^a

Values of the same cultivar bearing different superscript letters in the same column are significantly different ($P < 0.05$).

$G(\tau^*)$, at longer times. In other words, if the latter is weakened then the power law relaxation mode should also be shifted to lower values of $G(t)$. This will be discussed further below.

An increase in temperature had a significant effect ($P < 0.05$) on τ^* for all three glutes. τ^* of Argent gluten decreased from 189 s at 25 $^{\circ}\text{C}$ to 56 s at 40 $^{\circ}\text{C}$. τ^* for Golden 86 and Glenlea gluten, 1450 and 459 s at 25 $^{\circ}\text{C}$, respectively, was lowered to 253 and 119 s, respectively at 40 $^{\circ}\text{C}$. For a given temperature, (15, 35 or 40 $^{\circ}\text{C}$) τ^* for Golden 86 gluten was significantly greater than those for Glenlea and Argent glutes. Argent gluten had the smallest value of τ^* at every temperature. The higher was τ^* for glutes at 15 $^{\circ}\text{C}$, the greater was the decrease of τ^* at higher temperature. $G(\tau^*)$ also decreased with increased temperature for Golden 86 and Glenlea glutes, but was not significantly different for any of the glutes at 40 $^{\circ}\text{C}$.

These results indicate that "stronger" glutes (in the linear viscoelastic sense) maintained their values of τ^* and $G(\tau^*)$ at higher levels as the temperature was increased. But, at 40 $^{\circ}\text{C}$ these three glutes could not be distinguished based on significant differences in $G(\tau^*)$ (or S). τ^* was the only viscoelastic parameter that remained significantly different for all three glutes

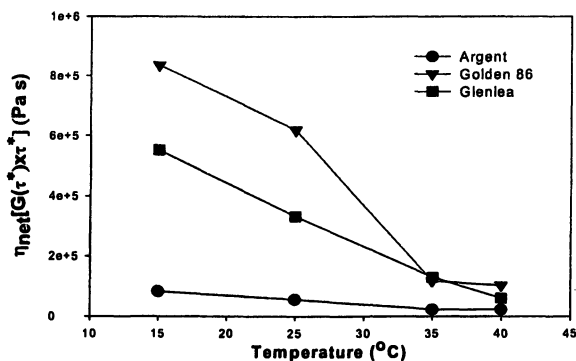


Figure 2. Effect of temperature on the linear viscoelastic viscosity (η_{net}) of gluten from different cultivars at 15, 25, 35 and 40 °C, and 1% strain.

at 40 °C. Lefebvre et al (20) demonstrated clearly that heating gluten to 40 °C and cooling did not result in any irreversible changes in the gluten viscoelastic properties. Thus, we assume that the decrease in the viscoelastic properties seen here is also reversible, but that assumption was not tested.

Contribution of the reversible network to the viscosity of gluten

The contribution due to the reversible (time dependent) network on the linear viscoelasticity of these glutes was estimated as $\eta_{net} = G(\tau^*) \cdot \tau^*$ as suggested by Rubinstein et al. (21) for reversible networks in general. η_{net} was found to distinguish very well between glutes obtained from Canadian wheats of different statutory class, and which showed clear differences in their tensile deformation forces at 25 °C (16). As shown in Figure 2, η_{net} for all three glutes decreased greatly as the temperature was increased to 40 °C, but the magnitude of that decrease was different for the glutes. η_{net} for Argent gluten decreased from 82,000 Pa·s at 15 °C to 21,000 Pa·s at 40 °C, compared with Golden 86 gluten which decreased from 836,000 Pa·s at 15 °C to 101,000 Pa·s at 40 °C. η_{net} for Glenlea gluten decreased from 552,000 Pa·s at 15 °C to 59,000 Pa·s at 40 °C.

The three glutes also showed differences between them for a given temperature. At 15 °C, η_{net} for Argent gluten (82,000 Pa·s) was much lower than that of Golden 86 and Glenlea gluten (836,000 and 552,000 Pa·s). At 35 °C, η_{net} for Argent was still the lowest (22,000 Pa·s), while η_{net} for Golden 86 and Glenlea glutes became more similar to each other (116,000 compared to 129,000 Pa·s, respectively). At 40 °C, η_{net} for Golden 86, Glenlea and Argent

were 101,000, 59,000 and 21,000 Pa•s, respectively. These values for η_{net} were 12%, 11% and 26% of the value for η_{net} at 15 °C for Golden 86, Glenlea and Argent, respectively. Thus, while the actual values were lower for Argent gluten, the weaker Argent gluten lost proportionately less of its initial network viscosity as the temperature was increased. Whether or not the obviously weaker viscoelasticity of Argent gluten is related to its difference in the 1B coded HMW-GS (1By9 versus 1By8 for Golden 86 and Glenlea) cannot be said for sure here. But it does suggest that further work along these lines using gluten from more cultivars with variations in their HMW-GS is warranted.

Effect of added L-cysteine

Addition of reducing agents during dough mixing is well known to result in weaker doughs and increased solubility of the glutenin proteins (19). Graveland et al. (22) reported that during dough mixing the SDS-insoluble gel protein is broken down to an SDS-soluble form as a consequence of the reduction of disulfide bonds. Gao et al (23), also showed that mixing doughs in the presence of an increasing amount of reducing agent led to progressive breakdown of the glutenin polymers extracted from the mixed dough. But, as far as we know, isolation of the effect of addition of a reducing agent on a direct measurement of the linear viscoelastic network strength of whole glutes of different strength has not been shown. Here, we assume that the power law relaxation mode of gluten is due primarily to the uncrosslinked fraction of gluten, while $G(\tau^*)$ represents the disulfide crosslinked portion of the glutenin in gluten. Thus, we would expect that addition of L-cysteine would act to convert the network portion of the glutenin in gluten to large uncrosslinked clusters. If this does happen, then we should expect to see a disappearance of the inflection in $G(t)$ (and the corresponding $G(\tau^*)$), and the extension of the power law relaxation mode to longer times. The extent of this transformation in the viscoelastic spectrum should reflect the extent to which the elastic network is converted to clusters, which are presumed to associate primarily via non-covalent interactions.

Figures 3a, b and c show the stress relaxation patterns for Argent and Golden 86 glutes with no added L-cysteine (Cys 0), 125 ppm (Cys 125) and 250 ppm (Cys 250) respectively at 25 °C. A striking result of addition of L-cysteine (250 ppm) at 25 °C was that the inflection in $G(t)$ apparent for all glutes at 25 °C (Cys0) essentially disappeared upon addition of L-cysteine, regardless of any other factor. Thus, regardless of any initial difference in linear viscoelastic parameters at 25 °C, each gluten gel was reduced (literally) to a limiting power law relaxation pattern (or nearly so) covering at least five decades of time. Additional work with higher doses of reducing agent and more samples of glutes from different cultivars is needed to verify that this is indeed a

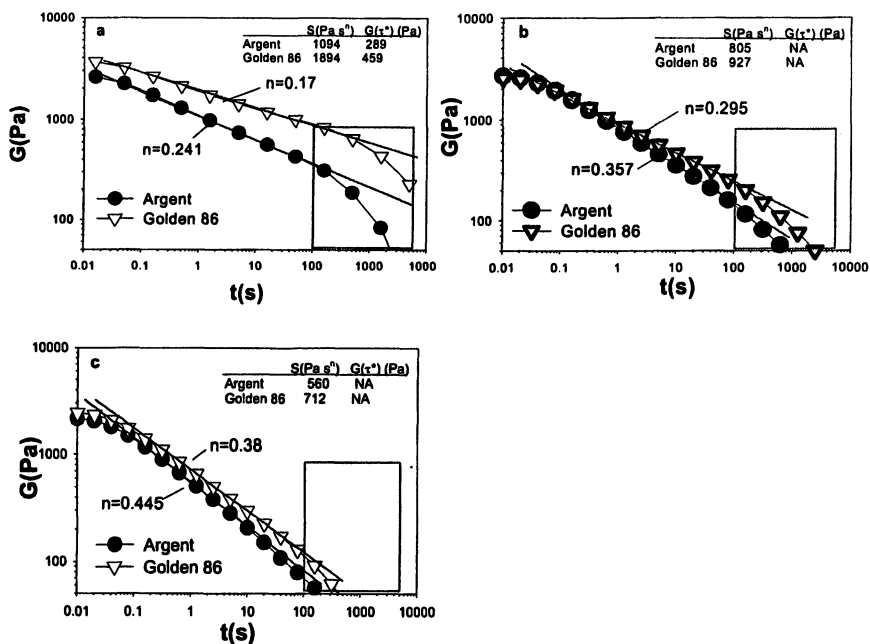


Figure 3. The stress relaxation patterns for Argent and Golden 86 glutes with different added levels of L-cysteine, 0 ppm (a), 125 ppm (b) and 250 ppm (c). Temperature was 25 °C and the strain was 1%. See text for definitions of S and $G(\tau^*)$.

universal limiting behavior of gluten gels.

This unusual power law relaxation pattern in the terminal zone of viscoelasticity has been attributed to the presence of a distribution of sizes of self-similar branched clusters at the gel point for crosslinking synthetic polymers (14, 15). For example, Plazek and Chay (15) showed clearly how a network structure evolved during curing of an epoxy resin by comparing the creep compliance curves for a series of mixtures with different amounts of crosslinking agent. At the gel point (or very near to it), the creep compliance and the retardation spectrum both showed extended power law behavior at long times for five decades. This interpretation of power law relaxation as representing a critical degree of crosslinking related to the first appearance of a network in chemical gelation seems consistent with the proposed structures of glutenin extracted from wheat flour, which involve crosslinking of HMW-GS and other cereal proteins via disulfide bonds. Apparently, we can observe this critical power law behavior in gluten by removing rheologically effective disulfide crosslinks by addition of a sufficient quantity of reducing agent.

Discussion

It is apparent that these “5+10” glutens from different cultivars showed a wide range of linear viscoelastic network strengths at lower temperatures, the differences decreasing as the temperature was increased. This suggests that differences in physical dough or gluten properties determined at 25 °C may not be as relevant to bread loaf volume as they are to dough handling properties at those lower temperatures. Results for the addition of L-cysteine to these glutens support the hypothesis that the viscoelastic parameters, τ^* and $G(\tau^*)$, are associated with the disulfide crosslinked portion of glutenin in gluten, but both are also influenced by an increase in temperature. This probably reflects the complexity of whole gluten, and the fact that virtually all the gluten proteins probably contribute in some way or another to the viscoelasticity of gluten. As suggested by Primard et al (12), it may not be practical to determine all of the biochemical characteristics of the cereal proteins needed to predict cereal quality via multiple regression correlation models. The experimental approach shown here involving direct determination of relative differences in the native linear viscoelastic network strength in glutens from different wheat cultivars may be a useful alternative to that type of multiple regression modeling of quality, even if some ambiguity remains about the exact relationships between underlying chemistry and rheology.

Conclusions

The interpretation presented here that addition of L-cysteine to gluten results in a “network to cluster” transition, is consistent with both the critical power law relaxation of synthetic polymer gels at the gel point, and with the extensive cereal chemistry literature showing indirectly that only a portion of the glutenin proteins are likely crosslinked into a network structure via disulfide bonds in whole gluten. Additional work is underway applying this rheological technique, as well as creep and recovery testing, to a wider range of 5+10 bread wheat cultivars with allelic variation at the 1A and 1B locus. That work is intended to provide additional evidence as to the potential practical usefulness of linear viscoelastic measurements in assessment of wheat quality.

Acknowledgement

We gratefully acknowledge our collaborators, Dr. J.E. Dexter and N.M. Edwards, of the Canadian Grain Laboratory (Canadian Grain Commission,

Winnipeg, MB) for providing us with Glenlea flour used here, and Cook Natural Products (Oakland, CA.) for the donation of flour samples of Golden 86 and Argent and providing their physical properties.

References

1. Dexter, J. E. *Grains and oilseeds: handling, marketing and processing*; Canadian International Grains Institute: Winnipeg, MB, 1993; pp 697-722.
2. Shewry, R. P.; Halford, G. N.; Belton, S. P.; Tatham, S. A. *Phil. Trans. R. Soc. Lond. B* **2002**, *357*, 133-142.
3. Gao, L.; Bushuk, W. *Cereal Chem.* **1993**, *70*, 475-480.
4. Ewart, D. A. J.; *Food Chem.* **1990**, *38*, 159-169.
5. Kasarda, D.D.; *Cereal Food World*, **1999**,*44*, 566-571.
6. Payne, I. P.; Lawrence, J. G. *Cereal Res. Commun.* **1983**, *11*, 29-33.
7. Payne, I. P.; Holt, M. L.; Law, N.C. *Theor. Appl. Genet.* **1981**, *60*, 229-236.
8. Payne, I. P.; Corfield, G. K.; Holt, M. L.; Blackman, A. J. *J. Sci. Food Agric.* **1981**,*32*,51-60.
9. Moonen, E. H. J.; Scheepstra, A.; Graveland, A.; *Euphytica*, **1982**, *31*, 677-690.
10. Lukow, M. O.; Payne, I. P.; Tkachuk, R. *J. Sci. Food Agric.* **1989**, *46*, 451-460.
11. Khan, K. ; Tamminga, G. ; Lukow, O. *Cereal Chem.* **1989**, *66*, 391-396
12. Primard, S.; Graybosch, R.; Peterson, J. C.; Lee, J. *Cereal Chem.* **1991**, *68*, 305-312.
13. Graybosch, A. R.; Peterson, J. C.; Lee, J.; Shelton, R. D. *Crop Sci.* **1994**, *34*, 628-635.
14. Winter, H. H. *MRS Bull.* **1991**, *16*, 24-26.
15. Plazek, J.D.; Chay, I. *J. Polym. Sci.: Part B: Polym. Phys.* **1991**, *29*,17-29
16. Lee, C.C.; Mulvaney, S.J. *J. Agric. Food Chem.* **2003**, *51*, 2317-2327.
17. Bohlin, L.; Carlson, T. L.-G. *Colloids Surf.* **1981**, *2*, 59-69.
18. Mours, M.; Winter, H.H. *Macromolecules* **1996**, *29*, 7221-7229.
19. Shewry, R. P.; Tatham, S. A. *J. Cereal Sci.* **1997**, *25*, 207-227.
20. Lefebvre, J.; Popineau, Y. ; Deshayes, G. ; Lavenant, L. *Cereal Chem.* **2000**, *77*, 193-201.
21. Rubinstein, M.; Semenov, A.N. *Macromolecules*, **1998**, *31*, 1386-1397
22. Graveland, A.; Bosveld, P.; Lichtendonk, J. W.; Moonen, E. H. H.; Scheepstra, A. *J. Sci. Food Agric.* **1982**, *33*, 1117-1128.
23. Gao, L.; NG, W.K.P.; Bushuk, W. *Cereal Chem.* **1992**, *69*, 452-455.

Chapter 9

Cyclobutylthymidine Dimer Repair by DNA Photolyase in Real Time

Robert J. Stanley

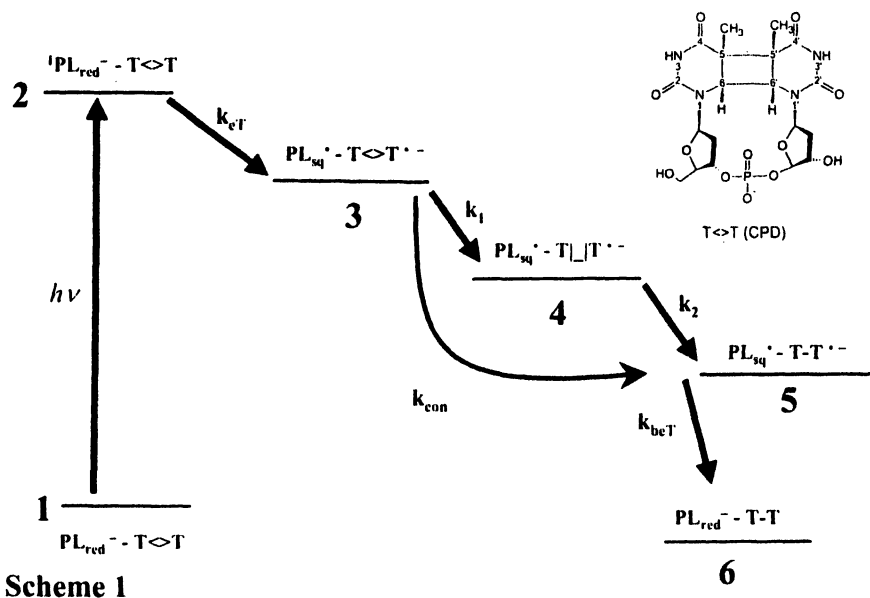
Department of Chemistry, 201 Beury Hall, Temple University,
Philadelphia, PA 19122

DNA photolyase (PL) is a monomeric flavoprotein that binds cyclobutylpyrimidine dimers (CPDs) and repairs them *via* photoinduced electron transfer from a reduced flavin adenine dinucleotide cofactor (FADH⁻) to the CPD. In spite of significant effort, the repair mechanism remains poorly understood. We have used femtosecond transient absorption spectroscopy to explore the electron transfer and repair kinetics of *A. nidulans* DNA photolyase with oligothymidine substrates in real time. Dimeric substrates show a concentration-dependent mixture of kinetics representing bound and unbound substrate. A longer pentameric substrate shows faster electron transfer than previously observed. Repair of the carbon-carbon double bonds (C=C) in the CPD appears to be complete by 1,500 ps. Target analysis of the kinetics is unable to distinguish between sequential and concerted models for the repair reaction, although the data are suggestive of the former.

DNA photolyase is a monomeric flavoprotein that binds and repairs cyclobutylpyrimidine dimers (CPDs) in DNA by a unique light-driven electron transfer mechanism.¹⁶ These CPDs are known to cause cell death and mutations and consequently photolyase is found widely distributed in all three kingdoms, including crop plants such as rice. Given the importance of these crops to human welfare, a thorough knowledge of the CPD repair mechanism is warranted.

Previous experiments have shown that repair of CPDs by photolyase is extremely fast and efficient. Repair is completed within about 2 nanoseconds after the absorption of blue light by the fully reduced anionic flavin adenine dinucleotide cofactor (FADH⁻).⁸ However, in spite of significant efforts, the details of the repair mechanism remain elusive.

The structures of *E. coli*¹⁴ and *A. nidulans*¹⁹ DNA photolyase have been solved in the absence of substrate. Recently, the photolyase-product complex structure has become available.¹³ The CPD appears to be within 4 Å of the FAD at the bottom of the cavity, confirming the hypothesis that the CPD must flip out of the DNA double helix into a cavity in the protein.^{14,2,3}



This static picture provides a framework against which the dynamics of the reaction must be reconciled. The 1st step in the putative repair mechanism (see Scheme 1) involves the formation of a CPD radical anion ($T \langle \rangle T^{\bullet -}$) by electron transfer from ${}^1\text{PL}_{\text{red}}^- + T \langle \rangle T \rightarrow \text{PL}_{\text{sq}}^* + T \langle \rangle T^{\bullet -}$ with rate constant k_{eT} , leaving the FAD cofactor in its semiquinone state, PL_{sq}^* . The thymidine dimer radical subsequently undergoes reorganization spontaneously at room temperature to form the monomer base and base anion radical ($T-T^{\bullet -}$).¹⁰ Bond scission is

thought to compete with recombination of the electron from $T \langle \rangle T^{\bullet -} + PL_{sq}^{\bullet} \rightarrow T \langle \rangle T + PL_{red}^-$ but this rate (k_{rec}) must be much slower than the (initial) bond scission rate, since the quantum yield for repair is nearly unity. Bond breaking may involve a sequential mechanism where the C5-C5' bond breaks with rate k_1 followed by scission of the C6-C6' bond (k_2) (or *vice versa*), or that bond scission is concerted (k_{con}). It is generally accepted that the electron from $T-T^{\bullet -}$ is transferred back to $FADH^{\bullet}$ to re-reduce the flavin to $FADH^-$ (k_{beT}) although when this back electron transfer step occurs has not been firmly established. Dissociation of the protein-substrate complex is thought to occur at a much slower rate. While this mechanism is reasonable, there is a paucity of experimental data to test its validity. This Proceedings offers experimental evidence to flesh out this mechanism.

Results and Discussion

We probed the temporal evolution of the ultraviolet spectral region with femtosecond resolution following absorption of blue light by photolyase because the repair of the CPD involves breaking the cyclobutane ring with concomitant reformation of the 5-5' and 6-6' C=C bonds of the adjacent thymidines. These bonds absorb strongly at 265 nm ($\epsilon = 9,500 \text{ M}^{-1} \text{ cm}^{-1}$).⁵ A minimal substrate length of 5 thymidines was used to obtain tight binding between the protein and substrate.^{9,11}

The kinetics probed at 265 nm after excitation at 396 nm were measured for $FADH^-$, PL_{red}^- , $PL_{red}^-:d(T \langle \rangle T)_2$, and $PL_{red}^-:d(T \langle \rangle T)_5$ with ~ 850 fs resolution. Transient absorption decays of PL_{red}^- and the $PL_{red}^-:d(T \langle \rangle T)_n$ complex ($n = 2, 5$) are shown in Figure 1. The lifetimes for the exponential model fits have been compiled in a previous publication.¹²

As a control, the decay of $^1FADH^-$ in pH 8.2 phosphate buffer was monitored at $\lambda_{probe} = 265$ nm (data not shown). $FADH^-$ was generated from FAD_{ox} by photoreduction in the presence of oxalate as described by Heelis *et al.*⁷ A negative-going transient was obtained which was assigned as a ground state bleach. The amplitude of the $^1FADH^-$ decay was linear with pump power above $5.2 \mu\text{J/pulse}$. The $^1FADH^-$ decay can not be fitted to a single exponential. A two-component exponential fit gives a $\tau_1 \sim 4$ ps component and a longer-lived component whose value depends on the length of the acquisition window used. The fast component agrees well with that obtained by Enescu *et al.*⁴

The signal for photolyase without substrate ($^1\text{PL}_{\text{red}}^-$) goes negative as well due to the ground state bleach of the FADH^- cofactor and then rises slowly and approaches $\Delta A = 0$ after about 3,000 ps (∇ , Figure 1). Two lifetimes were necessary to fit this decay, with most of the amplitude in the longer $\tau_2 \sim 851$ ps component, and a small amplitude component with a lifetime of $\tau_1 \sim 7$ ps. It

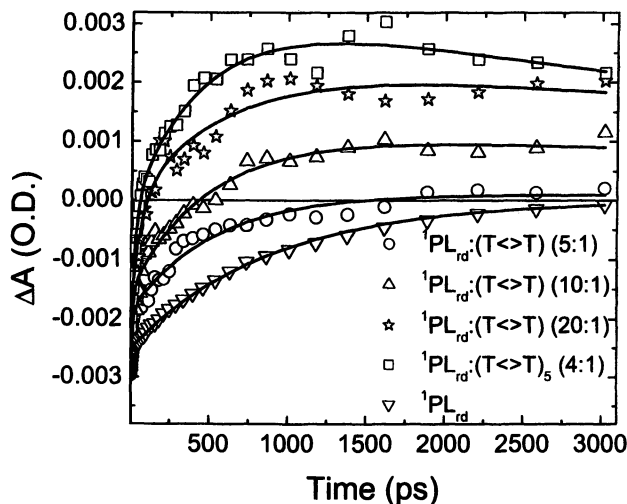


Figure 1: Transient absorption kinetics of photolyase:CPD complexes

should be noted that this is not really a proper control for the substrate studies as no electron transfer is expected in the absence of the CPD. Interestingly, a recent femtosecond fluorescence upconversion study of the $^1\text{FADH}^-$ cofactor in photolyase by Zhong and coworkers returned a single lifetime of 850 ps.¹⁸ The small difference between these measurements has yet to be reconciled.

The decay of the $\text{PL}_{\text{red}}^-:d(\text{T}\leftrightarrow\text{T})_2$ complex was obtained as a function of mole ratio of the protein to the substrate. This ratio was varied between 1:5, 1:10, and 1:20 (\square , \star , and \triangle respectively, figure 1). The solid lines represent a three-exponential function fit to the data. The decay of $^1\text{PL}_{\text{red}}^-:d(\text{T}\leftrightarrow\text{T})_2$ with a mole ratio of 1:5 shows a very fast component ($\tau_1 \sim 9$ ps) that is similar to the 7 ps component of $^1\text{PL}_{\text{red}}^-$. The fast components for the $d(\text{T}\leftrightarrow\text{T})_2$ 1:10 ($\tau_1 \sim 49$ ps) and 1:20 ($\tau_1 \sim 38$ ps) both trend towards shorter times with increasing

concentration of the substrate. The zero crossing changes from about 1,600 ps \rightarrow 400 ps \rightarrow 100 ps for the 1:5, 1:10, and 1:20 mole ratios respectively. The shift in the zero-crossing as a function of substrate suggests that the $^1\text{PL}_{\text{red}}^-:\text{d}(\text{T}\langle>\text{T})_2$ transients represent a sum of decays from protein:substrate complexes and free protein. This can be seen in Figure 2, where the transients for the dinucleotide substrate at different mole ratios to the protein are fitted using a linear combination of the $^1\text{PL}_{\text{red}}^-$ and the $^1\text{PL}_{\text{red}}^-:\text{d}(\text{T}\langle>\text{T})_5$ decays.

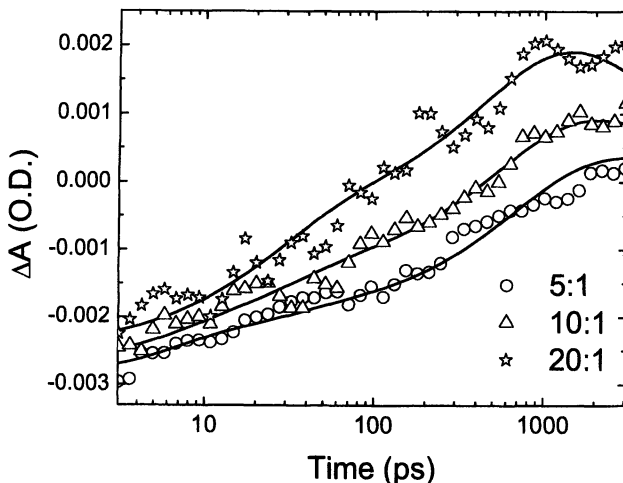


Figure 2: Fit (solid lines) of the dinucleotide kinetics to a linear combination of the pentameric protein:substrate and protein-only kinetics.

The initial rise time from the excitation pulse is particularly interesting because it contains information regarding the electron transfer lifetime from the photoexcited FADH^- to the initial acceptor in the protein:substrate complex. Both τ_1 and the zero-crossing are fastest for the $^1\text{PL}_{\text{red}}^-:\text{d}(\text{T}\langle>\text{T})_5$ complex with an average mole ratio of 1:4. The initial negative signal recovers promptly with a lifetime of $\tau_1 = 28 \pm 13$ ps. We assign this as the electron transfer lifetime, $\tau_1 = (k_{\text{eT}})^{-1}$, which is about four times shorter than previously thought.¹⁰ This in turn requires a re-thinking of the electronic coupling between the $^1\text{FADH}^-$ and the initial acceptor, suggesting that the initial acceptor may be a nearby molecule (e.g. adenine in FAD, a Trp residue) that the CPD is closer to the flavin than predicted.^{6,17,20} If the CPD is the initial acceptor then our results support the experimental work of Park *et al*¹⁴ and Berg and Sancar² and the theoretical treatment of Antony *et al*¹ (all of these studies used the *E. coli* protein).

To better explore the mechanism for repair, the first 100 ps kinetics for the protein:pentameric substrate is shown in figure 3. The zero crossing occurs around 60 ps for the repair of the pentameric substrate. If no repair took place then the signal should decay to $\Delta A \sim 0$. Instead, the absorbance change becomes positive and increases until a maximum is reached around 1,500 ps (see figure

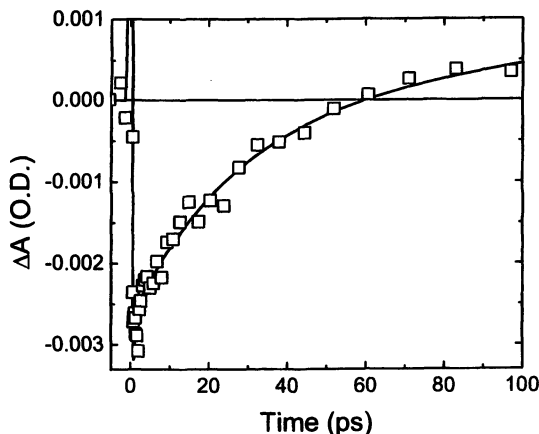


Figure 3: Initial rise of 265 nm transient for the $PL:(T \leftrightarrow T)_5$ complex.

1). These data suggest that there are two quite different time scales at play and that scission of the cyclobutane bond of the CPD takes place in two steps. The first step occurs directly after electron transfer to the CPD with little or no activation barrier. The second bond scission takes place at least an order of magnitude slower with a much larger activation barrier. This is at least consistent with the observations that an activation barrier exists for bond scission¹⁰ but *not* for electron transfer.¹⁵

A target analysis based on Scheme 1 was performed in an attempt to account for these observations. The differential equations implicit in Scheme 1 were integrated using reasonable estimates for the 265 nm extinction coefficients for the putative species. The transient absorption data were fitted to this model in a nonlinear least squares sense using k_1 and k_2 as adjustable parameters. The fits for three scenarios are shown in figure 4. Both a linear time base (top panel) and a logarithmic time base (bottom panel) are shown. Roughly equivalent fits are obtained for two different sequential models (250 ps/250 ps and 60 ps/600 ps), and the (quasi) concerted model (300 ps/6 ps). Clearly more experimental information is needed to distinguish between these different

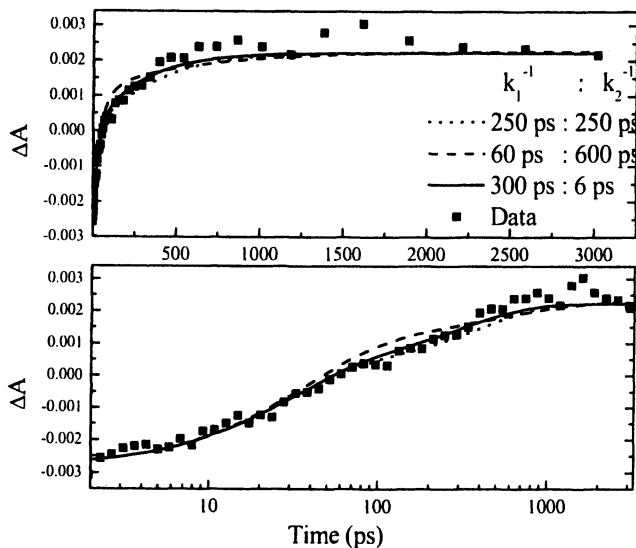


Figure 4: Fit of concerted and sequential models to transient absorption data.

mechanisms mechanism. We are currently engaged in visible light continuum probe studies to obtain this additional information.

Summary

In this Proceedings, we have used femtosecond transient absorption kinetics to understand the mechanism of *A. nidulans* DNA photolyase with oligothymidine substrates in real time. The two color experiments suggest that the repair mechanism may be sequential, although quantitative modeling of the transient absorption data do not lead to a definitive picture of the process. The concentration dependence of the minimal substrate suggests that a longer substrate should henceforth be considered "minimal". The use of a pentameric substrate appears to bind adequately to the protein. Thus, in spite of significant effort, including our own, a detailed understanding of the repair function of DNA photolyase is still in its infancy.

Acknowledgements

We gratefully acknowledge research support from NSF MCB-0347087.

References

- (1) Antony, J.; Medvedev, D. M.; Stuchebrukhov, A. A. *J. Am. Chem. Soc.* 2000, *122*, 1057-1065.
- (2) Berg, B. J. V.; Sancar, G. B. *J. Biol. Chem.* 1998, *273*, 20276-20284.
- (3) Christine, K. S.; MacFarlane IV, A. W.; Yang, K.; Stanley, R. J. *Journal of Biological Chemistry* 2002, *277*, 38339-38344.
- (4) Enescu, M.; Lindqvist, L.; Soep, B. *Photochem. Photobiol.* 1998, *68*, 150-156.
- (5) Fisher, G. J.; Johns, H. E. Pyrimidine Photodimers. In *Photochemistry and Photobiology of Nucleic Acids*; Wang, S. Y., Ed.; Academic Press: New York, 1976; Vol. 1; pp 226-294.
- (6) Hahn, J.; Michel-Beyerle, M.-E.; Rösch, N. *J. Mol. Model.* 1998, *4*, 73-82.
- (7) Heelis, P. F.; Hartman, R. F.; Rose, S. D. *Photochemistry and Photobiology* 1993, *57*, 1053-1055.
- (8) Heelis, P. F.; Kim, S. T.; Okamura, T.; Sancar, A. *J. Photochem. Photobiol., B* 1993, *17*, 219-28.
- (9) Jorns, M. S.; Wang, B.; Jordan, S. P.; Chanderkar, L. P. *Biochemistry* 1990, *29*, 552-61.
- (10) Langenbacher, T.; Zhao, X.; Bieser, G.; Heelis, P. F.; Sancar, A.; Michel-Beyerle, M. E. *J. Am. Chem. Soc.* 1997, *119*, 10532-10536.
- (11) MacFarlane IV, A. W.; Stanley, R. J. *Biochemistry* 2001, *40*, 15203-15214.
- (12) MacFarlane IV, A. W.; Stanley, R. J. *Biochemistry* 2003, *42*, 8558-8568.
- (13) Mees, A.; Klar, T.; Gnau, P.; Hennecke, U.; Eker, A. P. M.; Carell, T.; Essen, L.-O. *Science* 2004, *306*, 1789-1793.
- (14) Park, H.-W.; Kim, S.-T.; Sancar, A.; Deisenhofer, J. *Science* 1995, *268*, 1866-72.
- (15) Rustandi, R. R.; Jorns, M. S. *Biochemistry* 1995, *34*, 2284-8.
- (16) Sancar, A. *Chemical Reviews* 2003, *103*, 2203-2237.
- (17) Sanders, D. B.; Wiest, O. *J. Amer. Chem. Soc.* 1998, *121*, 5127-5134.
- (18) Saxena, C.; Sancar, A.; Zhong, D. *J. Phys. Chem. B* 2004, *108*, 18026.
- (19) Tamada, T.; Kitadokoro, K.; Higuchi, Y.; Inaka, K.; Yasui, A.; De Ruiter, P. E.; Eker, A. P. M.; Miki, K. *Nature Structural Biology* 1997, *4*, 887-891.
- (20) Weber, S.; Moebius, K.; Richter, G.; Kay, C. W. M. *J. Am. Chem. Soc.* 2001, *123*, 3790-3798.

Chapter 10

Effects of Amylopectin Structure on the Organization and Properties of Starch Granules

Jay-lin Jane, Napaporn Atichokudomchai, Jin-Hee Park,
and Dong-Soon Suh

Department of Food Science and Human Nutrition, Iowa State University,
Ames, IA 50011

Amylopectin of waxy starch has a larger molecular weight than that of the normal starch counterpart. Amylose is located side by side, interspersed and intertwined with amylopectin in the normal starch granule. The structures of amylopectin, Naegeli/Lintner dextrin, and starch granules indicate that the short branch-chains of amylopectin, which are located in the middle of the crystalline region of amylopectin, are responsible for the starch crystallization into the orthorhombic unit cell and display the A-type polymorphism. The A-type polymorphic starch also shows voids in the granule, which increase access of enzyme hydrolysis and chemical penetration into the granule. Recent advances in the understanding of the structure of amylopectin and Naegeli/Lintner dextrin are summarized in the chapter. The mechanisms of starch crystallization and the formation of voids in the A-type polymorphic starch are proposed and discussed.

Starch is produced in higher plants for energy storage and is synthesized in amyloplasts (1). Starch biosynthesis in plants has a cooperative mechanism involving mainly ADP-glucose pyrophosphorylase, granule-bound starch synthase (GBSS), soluble starch synthases, branching enzymes and debranching enzymes (1). Various isoforms of these enzymes are expressed in different plants, mutants, organs, and at different developmental stages. Thus, starches of different botanical sources and isolated from different organs, such as seeds, fruit flesh, leaves, display different structures, shapes, and properties.

Starch consists mainly of amylopectin and amylose, highly branched and primarily linear structure, respectively. Normal starches, such as corn and rice, consist of about 70-80% amylopectin and 20-30% amylose. Waxy mutants of plants, missing the waxy gene encoded for granule-bound starch synthase expressed in the endosperm, produce only amylopectin in the endosperm. The mutation, however, does not affect other organs, such as the pericarp (2). Thus, the starch produced in the pericarp consists of normal concentration of amylose. Biosynthesis of amylopectin is faster than that of amylose, which is attributed to the increasing number of non-reducing ends in amylopectin molecules when the molecule develops more branch chains. The branch chains provide accepters for chain elongation at the non-reducing ends. Because of this, waxy mutants do not show yield loss. High-amylose mutants, however, display 20-25% yield loss, resulting from slower biosynthesis of amylose in starch granules (3).

Structures of Amylopectin

Molecular Weight of Amylopectin

Molecular weight of amylopectin is, in general, about 100 times larger than that of amylose. Thus, amylose and amylopectin can be separated using gel-permeation or size-exclusion chromatography. The molecular weight of amylopectin is significantly larger than that of any natural or synthetic molecules reported in the literature (4). There are no suitable reference standards available for the determination of the molecular weights for amylopectin using gel-permeation chromatography. A combination of high-performance size-exclusion chromatography and a multi-angle laser-light scattering detector has been used to determine the absolute molecular weight of amylopectin isolated from different botanical sources (4, 5). The results show that the molecular weights of amylopectin molecules are in the range of 7.0×10^7 to 5.7×10^9 , and the gyration radii ranged between 191 and 782 nm, which are substantially larger than that of glycogen isolated from cyanobacteria, 2×10^7 and 55 nm, respectively (Table 1) (4). Among the starches analyzed, the molecular weight of waxy starch amylopectin is in general larger than that of the normal starch counterpart, which could be attributed to the carbon flux that goes exclusively to

Table I. Amylopectin Molecular Weights and Gyration Radii of Selected Starches^a

	$M_w (\times 10^6)^b$	$R_z (nm)^c$	$\rho (g/mol/nm^3)^d$
<u>A-type starches</u>			
normal maize	4.9 (0.8) ^e	312 (23)	16.1
waxy maize	8.3 (0.2)	372 (11)	16.1
<i>du wx</i> maize	4.9 (0.5)	312 (13)	16.1
normal rice	26.8 (2.9)	581 (41)	13.7
waxy rice	56.8 (9.3)	782 (36)	11.9
sweet rice	13.9 (1.0)	486 (5)	12.1
normal wheat	3.1 (0.3)	302 (3)	11.3
waxy wheat	5.2 (0.4)	328 (6)	14.7
barley	1.3 (0.1)	201 (8)	16.0
waxy barley	6.8 (0.1)	341 (3)	17.1
cattail millet	2.7 (0.2)	278 (6)	12.6
mung bean	3.8 (0.2)	312 (3)	12.5
chinese taro	12.6 (3.6)	560 (15)	7.2
Tapioca	0.7 (0.1)	191 (25)	10.0
<u>B-type starches</u>			
<i>ae wx</i> maize	3.2 (0.2)	306 (8)	11.2
amylomaize V	2.4 (0.0)	357 (24)	5.3
amylomaize VII	1.7 (0.0)	389 (57)	2.9
potato	1.7 (0.2)	356 (36)	3.8
waxy potato	2.0 (0.2)	344 (37)	4.9
green leaf canna	3.4 (2.2)	436 (85)	4.1
<u>C-type starches</u>			
lotus root	1.5 (0.4)	280 (57)	6.8
water chestnut	7.1 (1.5)	230 (25)	58.4
green banana	1.9 (0.8)	286 (29)	8.1
<u>Glycogen</u>			
cyanobacterial ^f	0.2 (0.0)	55 (4)	99.2

^a Data were averages of at least two injections. ^b weight-average molecular weight.

^c z-average radius of gyration. ^d Density (ρ) = M_w/R_z^3 ^e Standard deviation.

^f Glycogen was isolated from *Synechocystis* sp. PCC6803 in our laboratory.

SOURCE: Reproduced with permission from reference 4. Copyright 2002.

the biosynthesis of amylopectin in the waxy starch. In normal starch, the carbon flux partitions between amylopectin and amylose.

When the log gyration radius ($\log R_z$) of amylopectin is plotted against the log molecular weight ($\log M_w$), the starches of the A-type polymorphism display a linear relationship with a slope of 0.334 and a correlation coefficient of $r = 0.96$ ($P < 0.05$) (Figure 1). The slope of 0.334 indicates that the amylopectin of the A-type starch has a compact, spherical shape. The strong linear relationship reflects similar branching structures of amylopectins among the A-type starches. The ratios of $\log R_z / \log M_w$ for most waxy A-type amylopectins are slightly smaller than that of the normal A-type starch amylopectin, which is reflected by the data points of waxy starch being slightly below the line of correlation (Figure 1). This difference can be attributed to the lack of extra-long branch chains in the waxy starch amylopectin (6). The amylopectins of the B-type polymorphic starches display larger gyration radii than that of the A-type starches on the same molecular weight basis, which result from longer branch chain-length of the amylopectin of the B-type starches (7).

Branch Structures of Amylopectin

Nikuni (8, 9) and French (10) independently proposed the cluster model of the branch structure of amylopectin. Worm-like structures of Naegeli dextrans are observed using transmission electron microscopy (TEM) after the amorphous branch structure of waxy maize starch is exhaustively hydrolyzed by sulfuric acid (15.2%, v/v) (11). These TEM micrographs demonstrate that most of the α -1-6 branch linkages of amylopectin are clustered closely and are hydrolyzed and removed by acid. Hizukuri (12) reveals the relationship between the amylopectin branch chain length and the polymorphism of starch, and further defines the structure model as A-chains, those that do not carry other chains; B1, B2, B3 chains, those that carry other chains and extend through one, two, and three clusters, respectively; and the C chain carries the reducing end of the amylopectin molecule (13).

Branch Chain-Length Distribution

Branch chain-lengths of selected amylopectins isolated from starches displaying the A-, B-, and C-type polymorphism have been determined using high-performance anion-exchange chromatography equipped with an on-line enzyme reactor and a pulse amperometric detector (7). The results show that amylopectins of the A-type polymorphic starches have shorter average branch chain-length, with degree of polymerization (DP) 18.8 - 23.5; that of the B-type starches have average DP 28.9 - 30.7; and that of the C-type starches have

average DP 25.4 - 26.7. The amylopectin of the A-type starch consists of larger mass-proportions of short chains (DP 6-12), 15.6% to 27.4% and smaller mass-proportions of long branch-chains (DP \geq 37), 6.6 - 19.3%. The longest branch-chains detected are in the range of DP 66 - 80. In contrast, the mass-proportion of short and long amylopectin branch-chains of the B-type starches are 8.5 - 12.3% and 26.1 - 29.5%, respectively, and that of the C-type starches are 16.4 - 17.8% and 21.0 - 24.0%, respectively. The longest branch-chains detected for the B-type and C-type starches are DP 84 - 86 and DP 79 - 83, respectively (7). The averages of the chromatograms of the three types of starches are shown in Figure 2. The results show that the A-type starches consist of a larger proportion of short branch chains, the B-type starches consist of a larger proportion of long branch-chains, and the C-type starches consist of both very short and very long branch-chains.

Structures of Branch Linkages of the A- and the B-type Amylopectin

To reveal differences in the branch-linkage structures between the A- and the B-type polymorphic amylopectin, starch granules of the A-, B-, and C-type polymorphism are subjected to exhaustive hydrolysis using sulfuric acid or hydrochloric acid at room or slightly above room temperature to produce Naegeli or Lintnerized dextrin (14, 15, 16, 17). The results show that the A-type starch is more susceptible to the acid hydrolysis at room temperature and is hydrolyzed faster than the B-type starch, possibly because of easy penetration of the acid into the A-type starch granules (18). When the hydrolysis temperature increases to 38°C, the rate of hydrolysis of potato starch increases because of excessive swelling of the potato starch granules at the elevated temperature (14, 16).

The Naegeli dextrans produced from the A-type and the B-type starch show distinctively different structures, i.e., the A-type starch produces the Naegeli dextrin with a substantial proportion of singly branched molecules, whereas the B-type starch produces the Naegeli dextrin with mostly linear molecules. The C-type starch produces the Naegeli dextrin with a structure in between the A- and the B-type. Because the A-type starches consist of more short branch-chains (DP 6-12) than do the B-type starches, the difference in the structures of the Naegeli dextrans could be attributed to the presence of larger proportions of short branch-chains (mostly A-chains and B1-chains) in the A-type starch, which are connected by α -1-6 linkages, and the branch linkages are located in the tightly packed crystalline region. Therefore, the α -1-6 linkages are protected by the surrounding crystalline structures and are resistant to acid hydrolysis (Figure 3). This result agreed with that reported by Hood and Mercier (19). Hood and Mercier report that chemical modification of starch takes place mainly in the amorphous region of amylopectin (19). The authors find that the hydroxypropyl

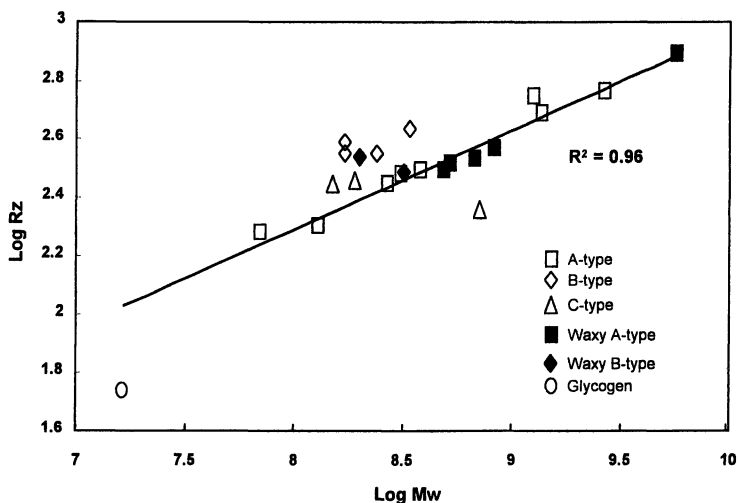


Figure 1. Relationships between the weight-average molecular weight (M_w) and z-average radius of gyration (R_z) of amylopectins. Data are plotted on Log-Log scale. The linear regression line on the graph comprises data of A-type amylopectin. (Reproduced with permission from reference 4. Copyright 2002.)

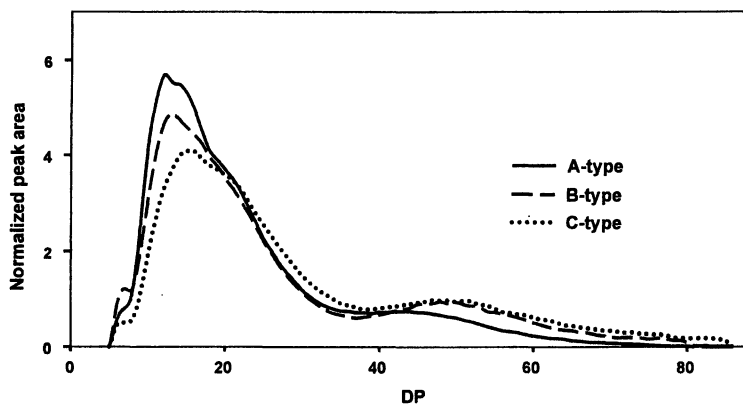


Figure 2. Average branch chain-length distributions of amylopectins isolated from the starches of the A-, B-, and the C-type polymorphism.

groups are concentrated around the region of α -1-6 branch linkages and a few hydroxypropyl groups located at the non-reducing ends of short branch chains. The authors also report that 50% of the DP15 (short) chains contain no modifying groups because they are located in the highly crystalline region.

The short branch A-chains and B1-chains form short double helices. The short double helices extend through only one cluster. Thus, these short double helices have more mobility to be rearranged and packed closely into an orthorhombic unit cell and develop the A-type polymorphism. Whereas, the large proportions of long branch-chains (B2-, B3-, and B4-chains) of the B-type polymorphic starch, which extend through two or more clusters, have more rigid structures and are less mobile. Thus, the starch retains the hexagonal unit cell packing. Because the hexagonal unit cell consists of an open channel and is not as tightly packed, it is plausible that this structure facilitates the acid hydrolysis of the α -1-6 glycosidic bonds located in the amorphous region and produce more linear chains. Models of amylopectin branch-chain structures of the A-type and the B-type polymorphic starches are shown in Figure 3.

Planchot, *et al.*, (20) report that Lintnerization of native granular wheat starch produces Lintner dextrin that displays the B-type polymorphism. This differs from the original A-type polymorphism of wheat starch. The Lintner dextrans of normal and waxy maize starch retain the A-type polymorphism. After α -amylolysis, the waxy maize Lintner dextrin is also converted to the B-type polymorphism. These results further suggest that the short branch chain-involved double helices might be hydrolyzed by acid (wheat starch) or sequentially hydrolyzed by acid and α -amylase (waxy maize starch) to generate an open channel in the packing unit and convert the A-type polymorphism to the B-type. Wheat amylopectin is known to have a very large proportion of short branch chains of DP6-DP17 (7).

Amylopectin Branch Chain-Length Variation Within the Starch Granule

Starch biosynthesis is known to initiate at the hilum, and the granule grows radially. To reveal if the branch chain-length of amylopectin is homogeneous through the granule, i.e., from the hilum to the periphery, starch granules are subjected to surface gelatinization using saturated neutral-salt solutions, such as lithium chloride or calcium chloride (21, 22). The saturated neutral salt solution consists of cations with large charge density, which interact with the -OH groups of starch molecules on the surface of the starch granule and release heat to gelatinize starch at the periphery of the granule. The saturated neutral salt solution also possesses large viscosity, which prevents the solution from penetrating into the inner part of the granule. Starch molecules on the surface of the granule can be gelatinized and separated from the ungelatinized remaining core starch (Figure 4). The extent of surface gelatinization can be controlled by

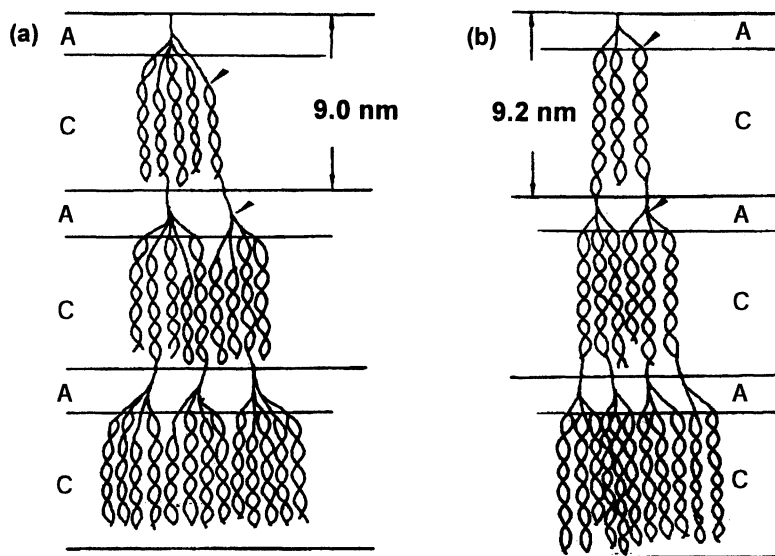
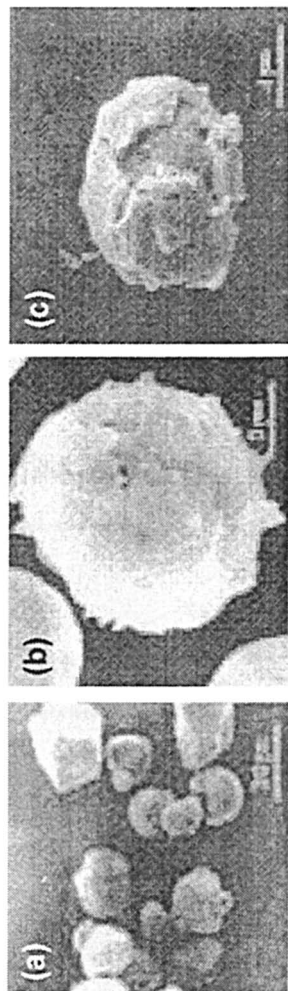


Figure 3. Proposed models for branching patterns of (a) waxy maize starch (A-type polymorphic) and (b) potato starch (B-type polymorphic). "A" and "C" stand for the amorphous and crystalline regions, respectively. 9.0 nm and 9.2 nm are the repeating distances of waxy maize and potato starches, respectively.

The arrows stand for the locations of branch linkages.

(Reproduced with permission from reference 14. Copyright 1997.)



*Figure 4. Scanning electron micrographs of normal maize starch granules and surface-gelatinized starch using a saturated LiCl solution. A. Normal maize starch granules with diameter > 5 μm ; B. 65% surface-gelatinized remaining granules; C. 84% surface-gelatinized remaining granules.
(Reproduced with permission from reference 22. Copyright 2000.)*

the time allowed for the salt solution treatment, and the gelatinized periphery starch separated from the inner core starch. The fractions are collected for structure analyses.

Results obtained from different levels of surface gelatinization show that amylopectin molecules at the core of the granule consist of more long branch-chains than those at the periphery (Table 2) (21). These results are consistent with the fact that small granules consist of more long branch-chains than large granules. In our recent studies on the development of maize starch granules, we observed the branch chain-length of endosperm amylopectin increased in the early development stage: average DP 23.6 on 10 days after pollination (DAP) up to DP 26.7 on 14 DAP. In the later development stage, the average branch chain-length decreased to DP 26.3 on 20 DAP and DP 25.4 on 30 DAP of matured seeds. All of these results indicate that the structures of starch granules are heterogeneous, and they are synthesized differently during the development of starch granules.

Table II. Branch chain length of amylopectin debranched with isoamylase^a

<i>Amylopectin</i>	<i>Branch chain length, dp^b</i>	
	<i>Long chain</i>	<i>Short chain</i>
Native potato starch	41.2 ± 1.3	13.2 ± 0.3
Potato starch (< 20 μm ^c)	44.7 ± 1.3	14.7 ± 0.7
Potato starch (30-52 μm ^c)	41.2 ± 1.8	13.2 ± 0.4
Potato starch (> 52 μm ^c)	34.0 ± 1.2	13.4 ± 0.2
Remaining granular starch after 80% chemical gelatinization	42.5 ± 1.8	13.1 ± 0.1
Chemically gelatinized starch (20% chemical gelatinization)	32.0 ± 0.8	13.1 ± 0.7

^a Data reported are the averages of duplicate sample and chemical analyses, except for the long chain of large granules (> 52 μm) (one sample and duplicate chemical analysis).

^b Determined with the three peak fractions; dp, degree of polymerization.

^c Diameter.

SOURCE: Reproduced with permission from reference 21. Copyright 1993.

Extra-Long Branch Chains of Amylopectin

Extra-long chains (ELC) of amylopectin have been reported in various normal starches, including wheat, maize, rice, sweet potato, and a small amount in potato (23). Comparing the amount of ELC present in normal (Centura and commercial wheat), semi-waxy (Kanto 107), and waxy wheat starch produced by wheat cultivars carrying three, two, and zero dosage of waxy gene,

respectively, Yoo and Jane (6) report that the content of ELC increases with the dosage of the waxy gene (encoding granular-bound starch synthase) in the plant (Figure 5). There is no ELC found in waxy wheat starch, but a smaller amount is found in the semi-waxy wheat (Kanto 107) starch produced by a mutant carrying two dosages waxy gene. These results confirm that ELC is elongated by granular-bound starch synthase.

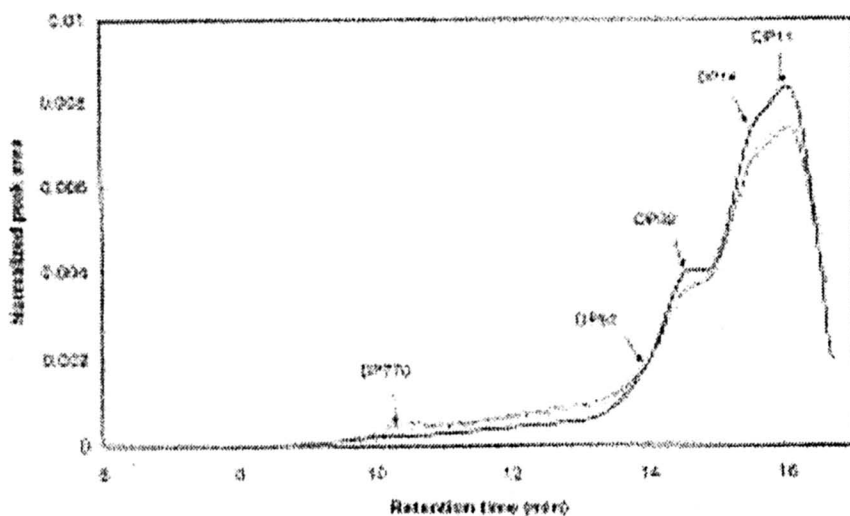


Figure 5. HPSEC chromatogram of isoamylase-debranched amylopectins. Peak areas of amylopectins of waxy (—), Kanto 107, a semi-waxy variety, (---), Centura, a normal variety, (- - -), and commercial wheat (· · · ·) were normalized. (Reproduced with permission from reference 6. Copyright 2002.)

The Organization and Properties of Starch Granules

It is well established that branch chain-lengths of amylopectin determine the polymorphism of native starch (7, 12) and starch gelatinization temperature (7, 24, 25, 26). The branch chain lengths also play an important role on the starch pasting properties (7). Many properties of starch granules are directly related to the structure of amylopectin. Examples are given as follows.

Enzyme Digestibility of Starch Granules

Starches of the B-type polymorphism are very resistant to enzyme hydrolysis, whereas that of the A-type are more digestible by enzymes (27, 28,

29, 30). The rates of enzyme hydrolysis of uncooked granular starch using porcine pancreatic α -amylase are shown in Figure 6. The relative rate of enzyme hydrolysis of the granular starch is affected by the following factors:

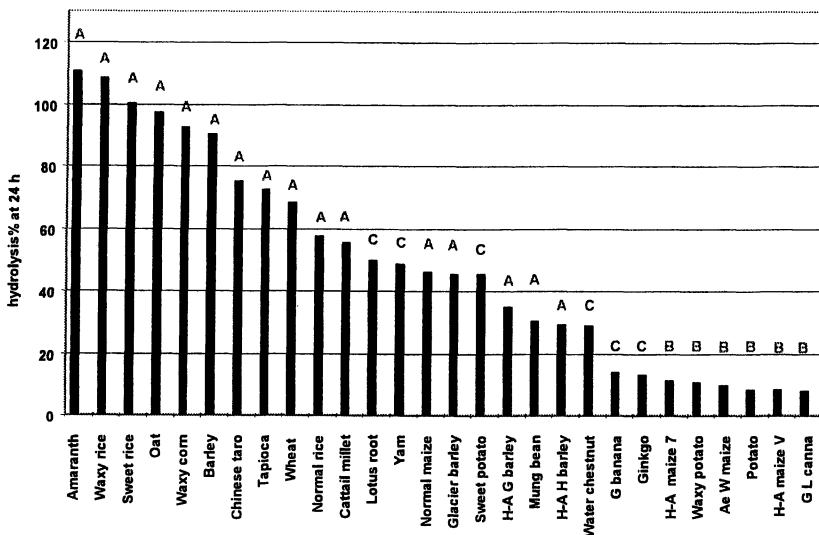


Figure 6. Relative enzyme digestibility of selected uncooked granular starches of different crystalline structures. A, B, and C stand for the types of crystallinity. (Reproduced with permission from reference 30. Copyright 2003.)

Polymorphism of the Starch

The enzyme hydrolysis rate of granular starch decreases with the starch polymorphisms, i.e., A-type > C-type > B-type (30). This can be attributed to the packing of the crystalline unit cell and its impact on the internal structure of starch granules. Because the starch polymorphism is directly related to the branch chain-length of amylopectin, the branch chain-length of amylopectin predominantly controls the enzyme hydrolysis of starch.

The Amylose Content of Starch

The amylose content of the starch also plays an important role on the enzyme digestibility of starch granules. This is demonstrated by the observation that almost all the waxy starches are more easily digested than the normal

starches and further more digestible than the high-amylose starch counterparts. These differences can be attributed to the fact that amylose in the starch granule is synthesized in parallel to the amylopectin, but remains at the amorphous form and does not form double helices with amylopectin (31). The amorphous amylose, however, intertwines with amylopectin (18, 31). The intertwining between the amylose and amylopectin restricts the swelling of the starch granule, resulting in the starch granule less susceptible to enzyme attack. Amylose and amylopectin molecules are oriented perpendicular to the surface of starch granules (10). The side-by-side arrangement of amylose to amylopectin, i.e., amylose extends through the crystalline and the amorphous region of amylopectin, reduces the contrast between the crystalline and the amorphous region determined by using the small angle x-ray scattering method (SAXS) (17). A schematic structure of cross-section of a normal maize starch granule is shown in Figure 7. Lineback proposed a similar scheme of starch granules with amylose located side by side with amylopectin (32). The scheme (Figure 7) shows that amylose is located side by side and is interspersed and intertwined with amylopectin. Amylose is more concentrated at the periphery, and amylopectin molecules located at the periphery consist of shorter branch chains.

Amylose present in normal and high-amylose starches, such as normal maize, normal barley, normal potato, high-amylose barley, and high-amylose maize starch, also slows down the rate of acid hydrolysis of these granular starches (14, 33, 34). The rate of acid hydrolysis of granular starch decreases with the increase in amylose content. Further more, normal and high-amylose cereal starches of barley (34) and maize (14) produce multiple-branched Naegeli dextrans as well as retrograded amylose after acid hydrolysis. Naegeli dextrans of potato, yam, sweet potato, tapioca, and banana starches do not show multiple-branched structures (14, 33). These results suggest that amylose-lipid complex developed in the cereal starch may hold the amylopectin lamella closely and further reduces the susceptibility of amylopectin branch structures to acid hydrolysis.

Internal Structures of Starch Granules With Different Polymorphisms

The difference in enzyme digestibility of starch granules and chemical penetration into starch granules (18) suggest that the internal structure of starch granules of the A- and the B-type polymorphisms must be different. It has been recognized for a long time that the A-type starch granule possesses weak points, which are susceptible to enzyme hydrolysis, and many A-type starches, such as sorghum and maize, display pinholes on the surface (35). Hellman and Melvin (36), using a gas absorption method, report that maize starch granules consist of more total surface area than the surface area of the granules, whereas the values for potato starch granules are about the same. BeMiller and co-workers reveal

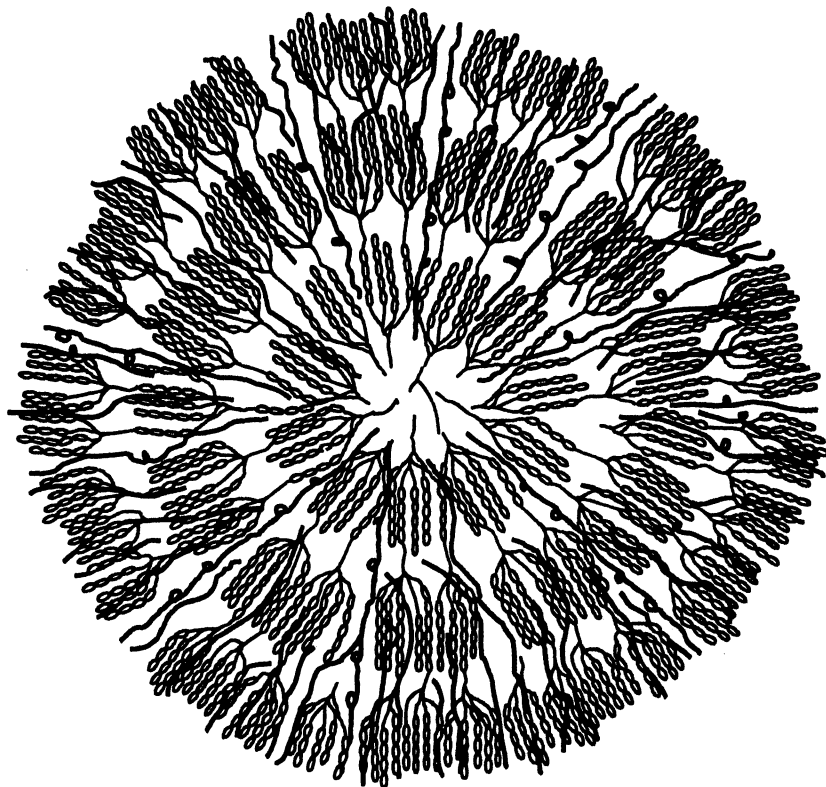
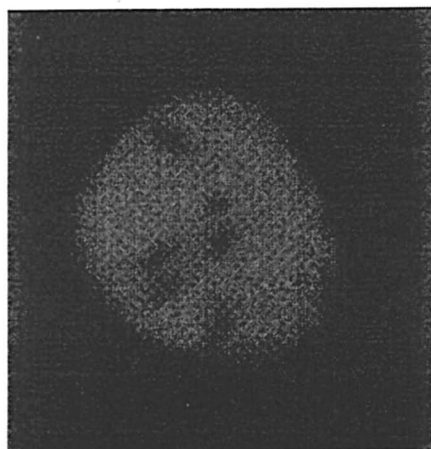


Figure 7. Schematic structure of cross section of a normal maize starch granule. Amylose, primarily linear molecule, is located side by side and is interspersed and intertwined with amylopectin. Amylose is more concentrated at the periphery of the granule. Amylopectin at the periphery consists of shorter branch chains. Amylose forms helical complex with lipids.

channels connecting the hilum and the pinholes on the surface of sorghum and maize starches using confocal laser scanning, scanning electron, and other types of microscopy (35, 37, 38). Starch is stained with methanolic merbromin (37) or derivatized with an ionic analog of propylene oxide and silver nitrate, then detecting the silver metal (38). Using rhodamine B-stained starch with unbound dye removed, Jane, *et al.*, report voids in the starch granules of the A-type polymorphism, including maize, waxy maize, sugary-2 maize, and wheat (39). The voids, however, are not found in the starch granules of the B- or C-type starch, including potato, high-amylose maize, and banana starch (Figure 8).

The voids reflect the heterogeneous structure of starch granules. It is plausible that during the biosynthesis of the A-type polymorphic starches, such



(b)



(a)

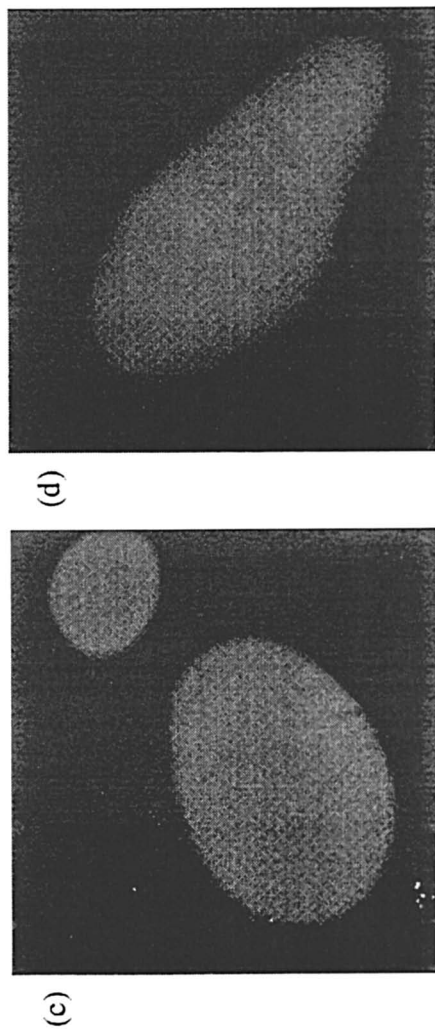


Figure 8. Confocal laser-light scanning micrographs of starch granules. Starch was stained with rhodamine B, and unbound dye was removed by rinsing with water and centrifuged immediately. (a) Waxy maize starch; (b) Normal maize starch; (c) Potato starch; and (d) Banana starch.

as maize and wheat, the abundance of short branch-chains facilitate the starch to crystallize to the orthorhombic unit cell, possibly transformed from the kinetically favored hexagonal packing unit, resulting in open space (voids) between crystal domains in the starch granule. For potato and other B- and some C-type starches, the starch consists of a large proportion of long B-chains (DP>36), which develop into stable hexagonal crystalline packing and do not go through the transformation. Thus, there are no voids present in these granules, and the starch granules are more resistant to enzyme hydrolysis and chemical penetration.

Summary

Amylopectin molecular weights range between 10^7 and 10^9 . Amylopectin of waxy starch is larger than that of the normal starch counterpart. Amylopectin molecules carrying more short chains facilitate orthorhombic unit packing and display the A-type polymorphism, whereas that carrying more long chains crystallize to a hexagonal unit and display the B-type polymorphism. After the short chains are removed by acid or by sequential acid and enzyme hydrolysis, the A-type polymorphism is converted to the B-type. Amylopectin molecules located in the inner part of granules consist of longer branch-chains than those located at the periphery. Extra-long branch chains are found in normal starch, lesser in semi-waxy mutant starch, but none in waxy starch, indicating they are elongated by granular-bound starch synthase. Starch granules of the A-type polymorphism display voids, which enhance susceptibility of the starch to enzyme hydrolysis and chemical penetration. The voids could result from the transformation of the B-type polymorphism, a kinetically favored conformation, to the A-type polymorphism, a thermodynamically favored conformation.

Acknowledgements

The authors thank Professor David Lineback for reviewing and his input to improve this manuscript.

References

1. Smith, A. M. *Biomacromolecules* **2001**, *2*, 335.
2. Nakamura, T.; Vrinten, P.; Hayakawa, K.; Ikeda, J. *Plant Physiol.* **1998**, *118*, 451.
3. Ferguson, V. High amylose and waxy corns. In: Specialty Corns. Ed. A. R.Hallauer. CRC Press, 2001, Boca Raton, pp 63-84.
4. Yoo, S. H.; Jane, J. *Carbohydr. Polym.* **2002**, *49*, 307.

5. Fishman, M. L.; Rodriguez, L.; Chau, H. K. *J. Ag. Food Chem.* **1996**, *44*, 3182.
6. Yoo, S. H.; Jane, J. *Carbohydr. Polymer.* **2002**, *49*, 297.
7. Jane, J.; Chen, Y.-Y.; Lee, L. F.; McPherson, A. E.; Wong, K.-S.; Radosavljevic, M.; Kasemsuwan, T. *Cereal Chem.* **1999**, *52*, 555.
8. Nikuni, Z. *Sci. of Cookery* **1969**, *2*, 6. (In Japanese)
9. Nikuni, Z. *Staerke/Starch* **1978**, *30*, 105.
10. French, D. *Denpun Kagaku* **1972**, *19*, 8.
11. Yamaguchi, M.; Kainuma, K.; French, D. *J. Ultrastruct. Res.* **1979**, *69*, 249.
12. Hizukuri, S. *Carbohydr. Res.* **1985**, *141*, 295.
13. Hizukuri, S. *Carbohydr. Res.* **1986**, *147*, 342.
14. Jane, J.; Wong, K. S.; McPherson, A. E. *Carbohydr. Res.* **1997**, *300*, 219.
15. Gerard, C.; Colonna, P.; Buleon, A.; Planchot, V. *Carbohydr. Polym.* **2002**, *48*, 131.
16. Nakazawa, Y.; Wang, Y. *J. Carbohydr. Res.* **2003**, *338*, 2871.
17. Vermeylen, R.; Goderis, B.; Reynaers, H.; and Delcour, J. A. *Biomacromolecules* **2004**, *5*, 1775.
18. Jane, J.; Xu, A.; Radosavljevic, M.; Seib, P. A. *Cereal Chem.* **1992**, *69*, 405.
19. Hood, L. F.; Mercier, C. *Carbohydr. Res.* **1978**, *61*, 53.
20. Planchot, V.; Colonna, P.; Buleon, A. *Carbohydr. Res.* **1997**, *298*, 319.
21. Jane, J.; Shen, J. *J. Carbohydr. Res.* **1993**, *247*, 279.
22. Pan, D. D.; Jane, J. *Biomacromolecules* **2000**, *1*, 126.
23. Hizukuri, S. Starch: Analytical aspects. In "Carbohydrates in Food." Eliasson, A. C., Ed.; Marcel Dekker, New York, NY, 1996, pp 347-429.
24. Shi, Y. C.; Seib, P. A., *Carbohydr. Res.* **1992**, *227*, 131.
25. Jane, J.; Shen, L.; Chen, J.; Lim, S.; Kasemsuwan, T.; Nip, W. K. *Cereal Chem.* **1992**, *69*, 528.
26. Yuan, R. C.; Thompson, D. B.; Boyer, C. D. *Cereal Chem.* **1993**, *70*, 81.
27. Fuwa, H.; Takaya, T.; Sugimoto, Y. Degradation of various starch granules by amylases. In: Mechanisms of saccharide of polymerization and depolymerization. Ed. J. J. Marshall. Academic Press, 1980. New York, NY, pp. 73-102.
28. Williamson, G.; Belshaw, N. J.; Self, D. J.; Noel, T. R.; Ring, S. G.; Cairns, P.; Morris, V. J.; Clark, S. A.; Parker, M. L. *Carbohydr. Polym.* **1992**, *18*, 179.
29. Kimura, A.; Robyt, J. F. *Carbohydr. Res.* **1995**, *277*, 87.
30. Jane, J.; Ao, Z.; Duvick, S. A.; Yoo, S. H.; Wong, K. S.; Gardner, C. *J. Appl. Glycosci.* **2003**, *50*, 167.
31. Kasemsuwan T.; Jane, J. *Cereal Chem.* **1994**, *71*, 282.
32. Lineback, D. R. *Bakers Digest* **1984**, 16.
33. McPherson, A. E.; Jane, J. *Carbohydr. Polym.* **1999**, *40*, 57.
34. Song, Y.; Jane, J. *Carbohydr. Polym.* **2000**, *41*, 365.
35. Fannon, J. E.; Hauber, R. J.; BeMiller, J. N. *Cereal Chem.* **1992**, *69*, 284.
36. Hellman, N. N.; Melvin, E. H. *J. Am. Chem. Soc.* **1950**, *72*, 5186.
37. Huber, K. C.; BeMiller, J. N. *Carbohydr. Polym.* **2000**, *41*, 269.

38. Gray, J. A., BeMiller, J. N. *Cereal Chem.* **2004**, *81*, 278.
39. Jane, J.; Atichokudomchai, N.; Suh, D. S. Internal Structures of Starch Granules Revealed by Confocal Laser-light Scanning Microscopy, in: *Starch: Progress in structural studies, modifications and applications*. P. Tomasik, V.P Yuryev, and E. Bertoft, Ed. Polish Society of Food Technologists, Cracow, 2004, pp 147-156.

Chapter 11

Derivatization of Starch Granules as Influenced by the Presence of Channels and Reaction Conditions

Jung-Ah Han,¹ Jonathan A. Gray^{1,2}, Kerry C. Huber^{1,3},
and James N. BeMiller^{1,*}

¹Whistler Center for Carbohydrate Research, Department of Food Science,
Purdue University, West Lafayette, IN 47907-2009

²Current address: Kraft Foods, Inc., Glenview, IL 60025

³Current address: Department of Food Science and Toxicology,
University of Idaho, Moscow, ID 83844

Research related to (a) effects of the presence of channels, (b) the natures of derivatizing reagents, and (c) the nature of the reaction medium and reaction conditions on the efficiency and location of derivatizing reactions in starch granules is reviewed. The presence of channels in starch granules influences the path of reagent solution penetration into granules. In granules in which channels are present, reagent solution largely passes through the channels to the interior cavity and then penetrates the granule matrix from the cavity outward, but granules are heterogeneous, both with respect to channelization and with respect to patterns of reagent solution penetration. Development of two methods to determine locations of reaction within granules is reviewed. Both methods revealed that phosphoryl chloride, a highly reactive reagent, reacts primarily on or near granule surfaces (the external surface of potato starch granules which have no channels, and all surfaces [predominately the surfaces of channels and the cavity, but also to a lesser extent the external surface] in corn starch granules). On the other hand, an analog of propylene oxide, a slowly reacting reagent, was able to diffuse throughout granules before reacting, resulting in more

uniform, but not completely homogeneous, derivatization. Factors effecting efficiency of the modification of waxy corn starch with propylene oxide and a derivative of it are reviewed. pH is the predominate variable. This data reinforced the previous conclusion that there is a correlation between swelling and reaction efficiency, with greater swelling resulting in greater efficiency. The research reviewed is practically important as one route to the production of improved modified starch products, especially modified food starches, within restrictions of types of reagents and degrees of modification that can be used.

Introduction

The research reviewed here is part of a broad research program that is based on two assumptions: (a) that starch products with improved properties and which impart needed functionalities will continue to be desired, and (b) that development of improved chemically modified starches, especially for, but not limited to, food use, is, and will continue to be, limited to currently allowed and used reagents and levels of add-on. There are several reasons why no new reagents or increased levels of derivatization will be allowed, viz., consumer safety, worker safety, environmental concerns, and economics.

Most starch products used industrially (whether in making paper products, in food formulations, or in other applications) have been chemically modified in one or more ways to improve their physicochemical properties in accordance with their intended functions. The modification(s) may be done to enhance positive attributes, minimize defects, or add new properties and functionalities.

Because it is unlikely that any new reagents or levels of their use will be allowed, even for nonfood applications, there are only four possibilities (other than physical modifications) for increasing the value of starch products: (a) control of reaction sites within starch granules, (b) control of reaction sites on starch polymer molecules, (c) biological modification of existing base starches (corn, potato, wheat, rice, tapioca/cassava, etc.), (d) use of new plant sources of starch (1). This review covers research related to the first named possibility. Other reviews of this research have already appeared (2, 3).

The research started with the knowledge that the structures of starch granules are not uniform throughout, i.e., that there are different micro- and ultrastructural regions within granules. Major differences occur in degrees of crystallinity (and in some cases types of crystallites present) and perhaps in the types of glassy amorphous structures present. The distribution of amylose and amylopectin, and perhaps supermolecular structures, varies from granule region

to granule region.³ From this understanding came the hypothesis that the patterns of chemical reactions, i.e., the location of reaction sites within granules, and the accessibility of individual starch polymer molecules to chemical reagents must be a function of granule architecture, i.e., granule macro-, micro-, and ultrastructures (4).

However, the structure of a starch granule is not only complex, it is incompletely understood. What makes it difficult to determine the structures of starch granules are the facts that, although starch granules from different plant sources have some structural similarities, they differ in the details of their macro-, micro-, and ultrastructures and the complex structures of granules varies not only between genotypes (both interspecies and intraspecies), but also between granules from a single plant source, i.e., it is likely that no two starch granules from a single seed or tuber are identical. Some support for the idea that structural differences between granules have the potential to affect patterns of chemical modifications has come from other laboratories (5).⁴ Compounding this complexity are the probabilities that responses of granules to different reaction conditions will vary and that a chemical modification itself will likely alter the structure of a granule so that the structure changes continuously over the course of a reaction (5).

Out of these realizations came the questions “Will starch granules from a single sources exhibit different reaction patterns under different conditions (different reagents, different reaction media, different temperatures)?” and “If so, do the changes in reaction sites within granules offer an avenue for preparation of different and/or improved products?” During the course of attempting to answer these questions, channels were discovered in certain starch granules.

Discovery of Starch Granule Channels

Hall and Sayre (6) reported finding surface pores on normal and waxy sorghum starch granules and concluded that they were artifacts. Fannon et al. (7) rediscovered pores on the surface of corn, sorghum, and millet (all in the *Panicoidae* subfamily of the *Graminae* family) starch granules and provided evidence that they were real anatomical features.⁵ It is important to note that

³ Reaction in amorphous vs. crystalline areas and derivatization of amylose vs. amylopectin, about both of which there is information, is not reviewed here.

⁴ The paper referenced should be consulted for the literature review within it.

⁵ Pores have also been observed within the equatorial groove of the A granules of wheat, barley, and rye starch granules (6, 7), but not on the surface of potato starch granules (7).

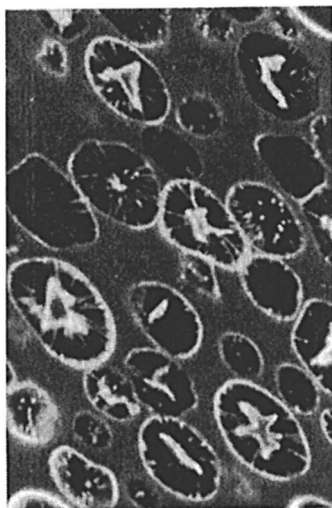


Figure 1. Photomicrograph of a section of hl sorghum starch granules whose cavities and channels were filled with a methanolic solution of merbromin viewed by fluorescence microscopy. Channels can be seen within the plane of the granule section and in cross-section. (Reprinted from Cereal Chemistry, Vol. 74, Kerry C. Huber and James N. BeMiller, Visualization of Channels and Cavities of Corn and Sorghum Starch Granules, p. 538, 1997, with permission from AACC International.)

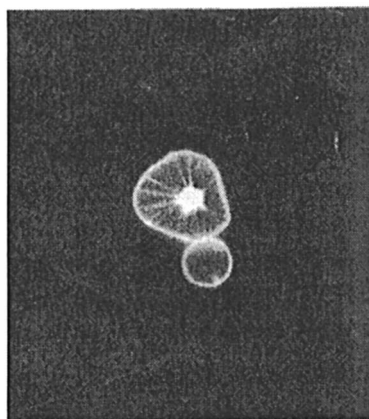


Figure 2. Photomicrograph (fluorescence microscopy) of whole normal corn starch granules after treatment with a methanolic solution of merbromin. (Reprinted from Cereal Chemistry, Vol. 74, Kerry C. Huber and James N. BeMiller, Visualization of Channels and Cavities of Corn and Sorghum Starch Granules, p. 540, 1997 with permission from AACC International.)

granule surface pores are large enough that they can be seen by scanning electron microscopy (SEM)⁶ and the channels that they are openings for can be viewed by light microscopy (fluorescence, CLSM, R-CLSM),⁶ so both are very large in molecular dimensions. The pores appeared to be somewhat clustered on the surfaces of granules, and the number per granule varied. Direct, but equivocal, evidence that there are, in the granule matrix, tube-like channels that open to the external surface, producing the observed pores was then presented (8). In searching the literature for other evidence of pores or channels, only indirect evidence was found, viz., that the total surface area of corn and sorghum starch granules available for gas absorption was greater than the external surface area, while with potato starch, on which no pores have been found (7), the two surface area values were about the same (9).

Conclusive evidence that, in corn and sorghum starch granules, channels connect the internal cavity and the outer surface (external environment) was then obtained (4, 10).⁷ The evidence was obtained by first soaking the granules in a non-swelling (methanolic) solution of merbromin, a fluorescent compound, then collecting them by filtration and washing them lightly to remove the excess dye. It was hypothesized that, under nonswelling conditions, solutions of the dye would fill channels and cavities without penetrating the granule matrix. Treated granules were then embedded, sectioned dry (without floating on water), and examined by fluorescence microscopy. Channels and a central cavity that were either filled or coated with the dye were clearly evident, providing the first unequivocal demonstration that, in some starch granules, there are channels connecting the granule exterior with the internal cavity (Fig. 1). Granules of all samples of sorghum, a mutant sorghum, normal corn, and waxy corn starch investigated in this way contained merbromin-filled or merbromin-stained channels and a cavity, but the number of channels per granule varied and the average number of channels per granule in a population of granules varied with the source of the granules. Channels could also be seen using fluorescence microscopy without embedding and sectioning (Fig. 2). Subsequently, confocal laser scanning microscopy (CLSM) was employed to view optical sections of granules treated with solutions of merbromin in methanol.

The same work produced additional evidence that starch granules contain an internal cavity at the point where the granule originated (the hilum) (10).

⁶ Abbreviations used: BSE - compositional backscattered electron imaging; CLSM - confocal laser scanning microscopy; DP - degree of polymerization; MS - molar substitution; R-CLSM - reflectance CLSM; SEM - scanning electron microscopy.

⁷ Most of the experimental evidence on which the published papers are based comes from photomicrographs. References 1, 2, 3, 4, 5, 6, 7, 8, 10, 12, 17, and 20 should be consulted for complete presentations of this evidence.

Central cavities (voids in mature starch granules where the hilum was originally) were first reported by Reichert in 1913 (11) and have since been observed many times (10).⁴ Huber and BeMiller (10) concluded that cavities are actual features of granules and not artifacts, although drying may enlarge them, and that external pores are openings to channels that, at least for the most part, connect the interior cavity to the external surface (4).⁴ They speculated that the process of polymer crystallization reduces the volume of the granule matrix, causing it to pull away from the hilum, the region surrounding the hilum being the least organized region of granules (12).⁴ Likewise, drying of the matrix would result in its shrinking. So both the interior cavity near the center of corn starch granules and the channels that connect them to the outer surface of the granule are anatomical features of granules that contain them.

At this point, it was hypothesized that pores, channels, and the internal cavity might influence reaction patterns within granules by (a) increasing the surface area available for reagent penetration into the granule matrix and/or (b) by providing a path that allows reagent solutions easy access to the less-organized region surrounding the cavity. (Discussions and references to access of amylolytic enzymes to the region surrounding the cavity can be found in references 2, 4, and 10. That enzymes have ready access to the region surrounding the cavity is evidence that molecules as large as protein molecules can pass through the channels.)

Effects of Channels on Granular Reactions

The first step in testing the above hypothesis was to investigate any relationship of granule channels to penetration of aqueous solutions of chemical reagents (4). Because we had found that aqueous solutions of merbromin penetrated the matrix of granules (as opposed to staying in channels and the cavity as did methanolic solutions of merbromin), we also hypothesized that, if penetration of a dye solution into the granule matrix could be followed, the path of reagent entry and the roles of channels and cavities in granular chemical reactions could be determined. Because the region surrounding the central cavity of the granule is believed to be the least organized (12),⁴ we further hypothesized that dye solution penetration would be most rapid through that region. To test these hypotheses, optical sections of corn starch granules which had been subjected to treatment with an aqueous solution of merbromin for 15, 30, and 60 sec were examined. The short-time treatment of corn starch granules produced intermediate rather than complete penetration and revealed that penetration of dye solution into the granule matrix occurred through both cavities (from the center outward) and the channels (laterally) (Fig. 3). Regardless of treatment length, the extent of dye solution penetration varied among granules (4). Because dye solution penetrated into the matrix laterally from channels, the channels no longer appeared as fine, distinct lines and became more indefinite as penetration progressed. Channels aided the

permeation process by delivering dye solution into the central cavity, which allowed entry into the granule matrix from the less-organized (12)⁴ region surrounding the cavity outward. Thus, pores and channels of normal corn starch granules increase the potential surface area available for reaction and facilitate dye and reagent solution penetration into the granule matrix. The possibility that in some granules some dye solution could have penetrated from the outside in could not be ruled out. The observed heterogeneity in dye solution penetration between granules indicated the potential for non-uniform substitution in a population of granules containing channels (corn starch, for example) during chemical modification.

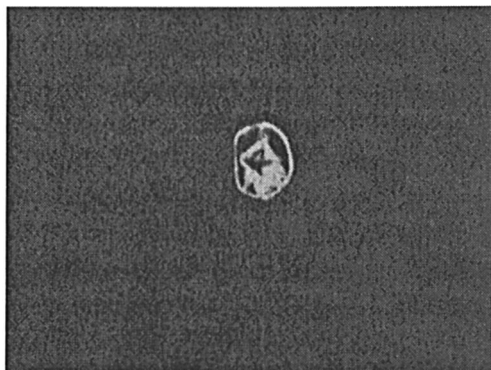


Figure 3. Optical section of a normal maize starch granule treated with an aqueous solution of merbromin for a short time viewed by CLSM depicting dye solution penetration into the granule matrix both from the cavity outward and laterally from channels. (Reprinted from Carbohydrate Polymers, Vol. 41, K.C. Huber and J.N. BeMiller, Channels of Maize and Sorghum Starch Granules, p. 274, 2000 with permission from Elsevier.)

Using a reactive dye for derivatization of waxy corn starch granules and non-swelling conditions, it was demonstrated that reactions could be confined to granule surfaces, which were largely the surfaces of channels and the cavity (5).

It was evident at this point that, because channels influenced the path of reagent solution penetration into granules, they were likely to influence where reactions took place within granules. Knowledge of where reactions took place required reliable methods to locate reaction sites (5). A review of the literature and attempted application of previously used methods led us to conclude that it was unlikely that any of the reported methods conclusively located derivatization sites within modified starch granules, so a program to develop better, more reliable methods of locating reaction sites within granules was undertaken.

Methods of Detecting Reaction Patterns Within Starch Granules

Our first developed method to observe actual granular reaction patterns within starch granules involved reactions of starches with reagents that would produce anionic derivatives. The anionic groups were then converted to thallium(I) salts and examined by SEM compositional backscattered electron imaging (SEM-BSE) (5). Observations of potato and sorghum starches reacted with phosphoryl chloride and waxy corn starch reacted with an anionic derivative of propylene oxide [sodium 3-chloro-2-hydroxy-1-propanesulfonate, for which there is evidence that, in alkaline solution, it is first converted into the epoxide before reacting with the starch (12)] revealed that granular patterns of reaction were influenced by both the type of starch and the type of reagent. Phosphoryl chloride, which is highly reactive so that it reacts before it can diffuse very far into a granule, reacted to a large extent at granule surfaces (Fig. 4). In contrast, the propylene oxide analog, which is less reactive so that its rate of diffusion into granules is greater than its rate of reaction, appeared to have reacted throughout the matrix of granules (Fig. 5).

We then developed a method that was both simpler and faster than the SEM-BSE method which requires exchange, washing, embedding, sectioning

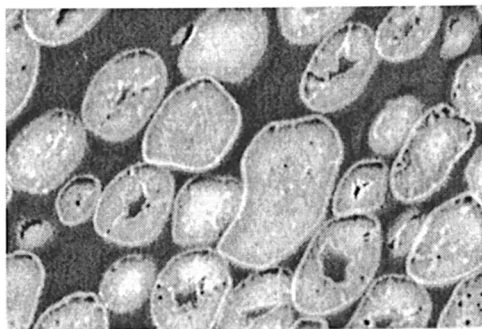


*Figure 4. Electron micrograph of sections of the thallium salt of POCl_3 -treated hl sorghum starch granules obtained via SEM-BSE. Reaction on the surfaces of channels can be seen as white lines or dots (cross-sections of channels). (Reproduced from *Cereal Chemistry*, Vol. 78, Kerry C. Huber and James N. BeMiller, *Location of Sites of Reaction Within Starch Granules*, p. 176, 2001 with permission from AACC International.)*

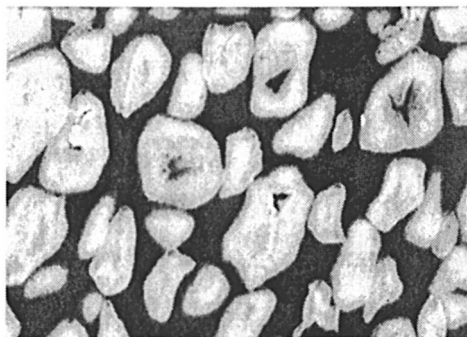
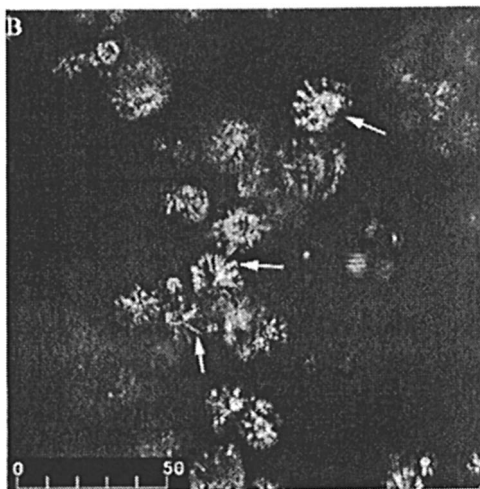


Figure 5. Electron micrograph of sections of the thallium salt of a partial 2-hydroxy-3-(thallium sulfonate)-propyl ether of waxy corn starch obtained via SEM-BSE. Rather uniform reaction throughout the granule matrix is indicated. (Reproduced from Cereal Chemistry, Vol. 78, Kerry C. Huber and James N. BeMiller, Location of Sites of Reaction Within Starch Granules, p. 177, 2001 with permission from AACC International.)

without floating sections on water, and examination by SEM-BSE. The new method utilized reflectance confocal laser scanning microscopy (R-CLSM) (12). The strategy was to produce anionic derivatives, followed by conversion of the derivatizing groups into silver salts, followed by reduction of the silver ions to silver atoms, and observation of the silver atoms by reflecting the CLSM laser beam off them.⁸ The method is less time consuming, primarily because embedding and sectioning is not required. It gives good sensitivity and resolution. To test the method, normal corn and potato starch granules were crosslinked to various degrees with phosphoryl chloride (POCl_3). Again, as found with the SEM-BSE method, at low levels of reagent addition, POCl_3 reactions appeared to be limited to granule surfaces, both the outside surface and the surfaces of channels and cavities, but especially the latter (Fig. 6). At higher levels of reagent addition, differences in intensities were more noticeable, i.e., the intensity of reflections was positively correlated with reagent concentration. Outer and inner surfaces (i.e., surfaces of channels and cavities) were highlighted. When still higher levels of reagent were used, evidence was obtained that POCl_3 was able to penetrate into and react in the starch matrix (5, 12). (A possible explanation for this phenomenon was presented (12).) When these higher concentrations of POCl_3 were used, some granules appeared to be substituted in both channels and the region surrounding the hilum. Still, reflections from channel and cavity surfaces were more intense than those from the matrix, indicating a non-uniform reaction with POCl_3 that occurs

⁸ The authors recognized that the method probably could not detect single silver atoms. Rather, perhaps, only clusters of silver atoms were detected.

preferentially at granule surfaces, both those at the granule periphery and those of interior features (channels and cavities). Control granules contained silver atoms in channels because of the protein and phosphoglyceride molecules lining them.



*Figure 6. Optical sections of the reduced silver salt form of POCl_3 -treated normal corn starch obtained via reflectance confocal laser scanning microscopy (R-CLSM). Arrows indicate possible channel and cavity surface reaction sites. (Reprinted from *Cereal Chemistry*, Vol. 81, Jonathan A. Gray and James N. BeMiller, *Development and Utilization of Reflectance Confocal Laser Scanning Microscopy to Locate Reaction Sites in Modified Starch Granules*, p. 281, 2004 with permission from AACC International.)*

Potato starch contains neither pores nor channels (as the terms are used in the context of this article and research). When potato starch was reacted with POCl_3 , it appeared that reaction was mainly limited to peripheral granule surfaces (Fig. 7). The reaction pattern differed from that of common corn starch, apparently only because the presence of channels in corn starch granules offer a path of entry into the interior, amorphous regions of the granule. Control granules (no POCl_3 treatment) contained silver atoms in concentric rings, due either to protein molecules or naturally occurring phosphate monoester groups (Fig. 8).

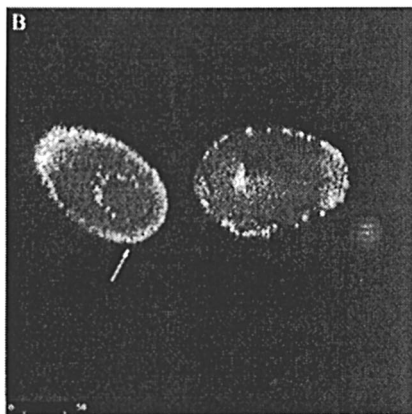


*Figure 7. A R-CLSM optical section of the reduced silver salt form of POCl_3 -treated potato starch obtained via R-CLSM. Arrow indicates peripheral surface to which reaction was mainly limited. (Reproduced from *Cereal Chemistry*, Vol. 81, Jonathan A. Gray and James N. BeMiller, *Development and Utilization of Reflectance Confocal Laser Scanning Microscopy to Locate Reaction Sites in Modified Starch Granules*, p. 282, 2004 with permission of AACC International.)*

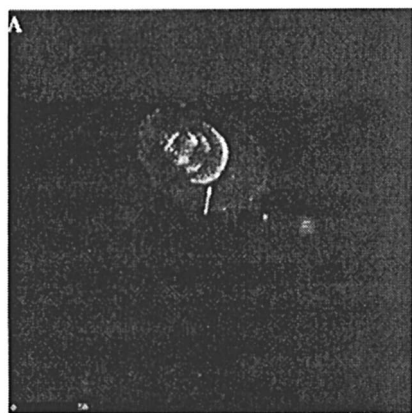


*Figure 8. A R-CLSM optical section of the reduced silver salt form of unreacted potato starch obtained via R-CLSM. Arrow indicates one of the internal rings where proteins and/or native phosphate monoesters might be located. (Reproduced from *Cereal Chemistry*, Vol. 81, Jonathan A. Gray and James N. BeMiller, *Development and Utilization of Reflectance Confocal Laser Scanning Microscopy to Locate Reaction Sites in Modified Starch Granules*, p. 282, 2004 with permission of AACC International.)*

Waxy corn starch granules were reacted with different amounts of the propylene oxide analog and then examined for comparison of the R-CLSM method to the SEM-BSE method used to locate hydroxypropylation reaction sites. Again, the intensity of reflections increased with increasing concentrations of reagent used. Little difference could be seen when comparing the control and the lowest level of modification using either method. Channels and cavities were evident in samples examined by either method. Some reacted granules appeared to be more modified in the regions surrounding the cavity when examined by the R-CLSM method. Channels were still noticeable, yet they were less distinct. When a higher level of reagent was used, reflection was intense and came from all regions of granules, including surfaces, the region around the cavity, and various regions of the matrix. In all cases, reaction had occurred throughout the entire granule, indicating a much more homogeneous reaction as compared to the reaction with POCl_3 (Fig. 9). However, some granules were not reacted throughout. Rather, a noticeable, apparently unreacted region was found just under the outer surface, where perhaps outer starch layers were less-penetrable due to the presence of highly organized/crystalline structures. Alternatively, derivatized amylose and/or amylopectin molecules could have leached from this region. The most highly reacted region appeared to be that surrounding the central cavity (5, 12). Generally, it was much more difficult to locate channels in products with higher molar substitution (MS) values as compared with lower-MS modifications because of reduced contrast. Besides penetrating outward from the cavity after passage through channels, another mode of access to the granule matrix is via lateral penetration from channels (4). In the case of higher-MS products, where there is intense labeling of the granule matrix, the mode of reagent penetration, i.e., whether from the cavity outward or laterally from channels, could not be determined. Again, it was concluded that sodium 3-chloro-2-hydroxy-1-propanesulfonate reacts similarly to propylene oxide and that this reagent reacts at a much slower rate than does phosphoryl chloride and has time to penetrate virtually the entire granule before reacting.

Potato starch granules were also reacted with the anionic propylene oxide analog (12). Some derivatized granules had substituent groups distributed throughout the matrix, but in most granules reacted with low levels of the reagent, more intense signals came from concentric layers (Fig. 10). Differences between layers became less discernable as the extent of derivatization increased. It appeared that the reagent solution enters the less-ordered, amorphous layers most readily and reacts there first, but overall, the reaction appeared to be rather uniform (Fig. 11).

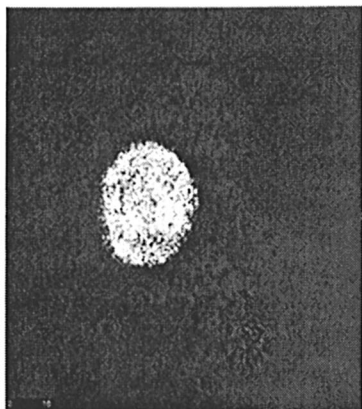


Figure 9. A R-CLSM optical section of the reduced silver salt form of waxy corn starch treated with a relatively large amount of sodium 3-chloro-2-hydroxy-1-propanesulfonate viewed via R-CLSM showing rather, but not completely, homogeneous derivatization. (Reprinted from Cereal Chemistry, Vol. 81, Jonathan A. Gray and James N. BeMiller, Development and Utilization of Reflectance Confocal Laser Scanning Microscopy to Locate Reaction Sites in Modified Starch Granules, p. 284, 2004 with permission from AACC International.)

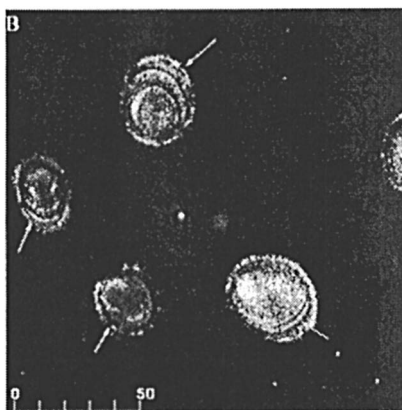


Figure 10. A R-CLSM optical section of granules of potato starch reacted with a low level of sodium 3-chloro-2-hydroxy-1-propanesulfonate. Arrows indicate reacted layers. (Reprinted from Cereal Chemistry, Vol. 81, Jonathan A. Gray and James N. BeMiller, Development and Utilization of Reflectance Confocal Laser Scanning Microscopy to Locate Reaction Sites in Modified Starch Granules, p. 284, 2004 with permission from AACC International.)

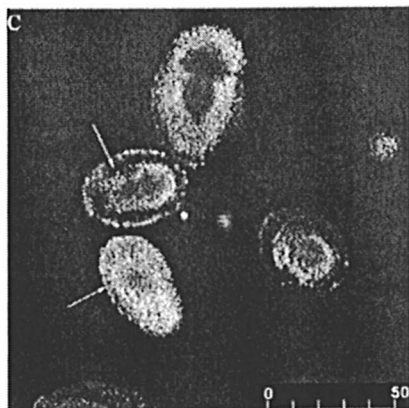


Figure 11. A R-CLSM optical section of granules of potato starch reacted with a higher level (as compared to Fig. 10) of sodium 3-chloro-2-hydroxy-1-propanesulfonate. Arrows indicate a granule with reflections from silver atoms throughout the entire granule (bottom) and a granule with no apparent reaction near the peripheral surface (top). (Reprinted from Cereal Chemistry, Vol. 81, Jonathan A. Gray and James N. BeMiller, Development and Utilization of Reflectance Confocal Laser Scanning Microscopy to Locate Reaction Sites in Modified Starch Granules, p. 285, 2004 with permission from AACC International.)

We concluded that a valid and simple method to locate reactions in starch granules had been developed, that the reactivity of the reagent influences the reaction patterns (which are not identical in all granules), that the presence of channels influences reaction patterns, and that anionic substances/groups are located in granule channels and in the starch matrix (more evident in potato starch).

Relation of Granule Swelling to Reactivity

The factors that affect starch derivatization reactions can be divided into two categories: intrinsic and extrinsic (5). Intrinsic factors are those that are a function of the genetic make-up of the source plant. Extrinsic factors are those related to reaction conditions with the belief that, in general, the more swollen are granules, the more efficient the reaction.

I. Intrinsic factors

A. Granule composition

1. Amylose: amylopectin ratio
2. Fine structures of starch polysaccharides
3. Nature and content of non-carbohydrate components

B. Granule structure

1. Size
2. Shape
3. Macrostructural features (presence or lack of pores and channels)
4. Nature of the outer envelope
5. Organization of starch polymer molecules (supermolecular structures, crystalline lamellae, glassy amorphous regions)

II. Extrinsic factors

A. Nature of reaction medium and reaction conditions

1. pH
2. Temperature
3. Type and concentration of swelling-inhibiting salt added

B. Reagent added

1. Type
2. Concentration

Evidence indicates that, in order for reactions with granular starch to occur, some swelling of the granules must occur (*13*). Support for this hypothesis was obtained when it was found that about 1.8 times as much propylene oxide was needed to achieve the same MS value when a more effective granule swelling inhibitor, viz., potassium citrate, was used in the reaction medium in place of the usual sodium sulfate, i.e., the more swelling that occurs, the more efficient is the reaction (*14*). Others have also found that granule swelling is necessary for efficient derivatization to occur (*15*). It was surmised from these two studies that, since the extent of granule reaction is related to the magnitude of granule swelling, it must be related to the nature of the reaction medium and temperature (*16*).

It was concluded from the cumulative work that granule derivatization is probably a cooperative and concerted process that begins in amorphous regions and proceeds to progressively more crystalline regions of granules (*12*). However, this supposition has been questioned (*17*).

Granule swelling is undoubtedly a function of both intrinsic and extrinsic factors. Probably, the primary intrinsic factor is the organization of the granule matrix. (It is known that two different starches, e.g., corn starch and potato starch, swell to different degrees in the identical environment.) The next logical step was to determine any effects of the different extrinsic factors on the extent and location of sites of derivatization. The R-CLSM method was used in these investigations.

Influence of Reaction Conditions on Starch Granule Derivatization

As a first application of the R-CLSM method, waxy corn starch was reacted with the anionic propylene oxide analog, a reagent that reacts rather uniformly throughout granules, to introduce hydroxypropylsulfonate groups (18). Temperature, pH, and type and concentration of swelling-inhibiting salt were varied. Representative industrial reaction conditions were chosen as the midpoints. Higher and lower temperatures and pH values and lower salt concentrations were used to provide insight as to the effect of each on reaction efficiency, with particular attention to their effect on granule swelling and its relation to reaction efficiency.

It was found that both uniformity of derivatization within granules and MS levels were affected by reaction conditions (Fig. 12). (The R-CLSM method provides only qualitative observations. Therefore, comparisons of amounts of reaction were difficult. Nevertheless, trends in amounts and patterns of reaction when granules were reacted under different conditions were observed.)

In general, increasing the pH from 10.7 to 11.7 increased the observed extent of reaction. It was pointed out that the greater reaction efficiency as the pH increased could be due either to increasing the degree of granule swelling, or to increasing the efficiency of reaction with the derivatizing reagent (via an increase in starch alkoxide concentration), or to a combination of the two. Increasing the temperature from 44°C to 54°C appeared to have little effect in most cases. The type of swelling-inhibiting salt used in the reaction medium did influence reaction efficiency. Granules reacted in the presence of NaCl appeared to be more extensively derivatized than those reacted in the presence of Na₂SO₄, a more effective swelling inhibitor (16), when reactions were done under otherwise identical conditions. Greater derivatization was observed in the presence of a lower concentration of Na₂SO₄ (0.395 m) as compared to a higher concentration (0.527 m). Overall, the results indicated that MS levels achieved are a function of reaction conditions. This finding was confirmed by actual measurement of MS values for the samples reacted in the presence of NaCl. (MS values were determined from sulfur analysis, so samples reacted in the presence of Na₂SO₄ were not used.)

Next, waxy corn starch was reacted under the same conditions used by Gray and BeMiller (18) using propylene oxide, the reagent used industrially, to produce the hydroxypropyl ether to determine the effect of reaction conditions on the extent of derivatization (19). Again, it was found that pH had the greatest effect on reaction efficiency and that temperature had little effect. The differences in MS values for samples hydroxypropylated in the presence of NaCl compared to those hydroxypropylated in the presence of Na₂SO₄ were



Figure 12. R-CLSM optical sections of granules of waxy corn starch reacted with sodium 3-chloro-2-hydroxy-1-propanesulfonate under increasing swelling conditions in the presence of sodium sulfate: A, pH 10.7, 44°C, 0.527 m Na_2SO_4 ; B, pH 11.2, 49°C, 0.527 m Na_2SO_4 ; C, pH 11.7, 54°C, 0.395 m Na_2SO_4 . (Reprinted from *Carbohydrate Polymers*, Vol. 60, Jonathan A. Gray and James N. BeMiller, *Influence of Reaction Conditions on the Location of Reactions in Waxy Maize Starch Granules Reacted with a Propylene Oxide Analog at Low Substitution Levels*, p. 151, 2005 with permission from Elsevier.)

greatest at the lowest pH used (pH 10.7). The MS values ranged from 0.032 to 0.118. The MS value of 0.032 (18% reaction efficiency) was obtained under the poorest swelling conditions [the lowest pH used (pH 10.7), and the lowest temperature used (44°C)] with the exception of that of the lowest concentration (0.471 m) of the less effective swelling-inhibiting salt (NaCl). However, it was found that in most, but not all, cases, samples reacted in the presence of NaCl had lower or equal MS values when compared to those reacted in the presence of Na₂SO₄, in contrast to what was observed by the qualitative method (R-CLSM) which indicated that more derivatization occurred when the reaction was done in the presence of NaCl than in the presence of Na₂SO₄ under identical conditions (18). Both studies indicated that the concentration of salt had very little, if any, effect when NaCl was used. MS values of 0.118 (65% reaction efficiency) were obtained under the best swelling conditions up to the point that granules gelatinized during the reaction. These data clearly showed that pH is the most important factor affecting reaction efficiency. The optimum conditions (of those used) with regards to reaction efficiency and paste characteristics were found to be pH 11.7 and 54°C (129°F) in the presence of Na₂SO₄ as a swelling inhibitor. A typical commercial reaction would be pH 11.2, 49°C (120°F), and 0.527 m Na₂SO₄ (7.5% db, 17% Na₂SO₄•10H₂O).

Uniquenesses and Heterogenities of Starches

Byproducts of the investigations reviewed here are confirmations that each starch is unique and that all populations of starch granules are heterogenous (20).⁴ Because each starch is unique, the differences in patterns of reaction of potato starch granules vs. granules of normal and waxy corn starches are easily discernible (5, 12). Therefore, conclusions based on data obtained on the three types of starch used in these studies (primarily normal and waxy corn starch) might not be applicable to other starches. In fact, we predict that other starches will react differently under identical conditions.

With regards to chemical modification processes (5),⁴ it has been reported that root and tuber starches (starches with B-type x-ray diffraction patterns) are easier to modify chemically than are cereal (A-type x-ray diffraction patterns), or legume starches (C-type patterns). It has also been reported that corn and amaranth starches had different optimum conditions for etherification. The distribution of substituent groups between amylose and amylopectin for normal corn, waxy corn, high-amylose corn, and potato starches was different in each case. The three corn starches underwent acid-catalyzed hydrolysis differently. Heterogenities with regards to penetration of reagents was also observed (4, 21).

Summary and Conclusions

The new, yet still incomplete, understanding of starch granule architecture and how it and reaction conditions influence the degree and pattern of reactions within granules has the potential of leading to development of greater value products via process control.

The presence of channels connecting the outside surface of granules with an internal cavity makes the granules of corn starch and certain other cereal starches unique. The number of channels in corn starch granules varies from granule to granule; therefore the number of channels per granule is an aspect of granule heterogeneity and the average number of channels per granule is another unique macrostructural feature that varies from genotype to genotype.

Where reaction takes place in producing chemically modified starches is influenced by the presence (or absence) of channels. In starches with channels (such as corn starch), reagent solutions primarily pass through the channels to the cavity and then diffuse throughout the granule matrix from the inside out; some lateral diffusion from channels also occurs. Rapidly-reacting reagents (such as phosphoryl chloride) react on surfaces (largely internal surfaces), while slowly-reacting reagents (such as propylene oxide) are able to diffuse throughout granules before reacting. Starches without channels (such as potato starch) react in the same way, except that modifications by highly reactive reagents are concentrated at the outside surface.

Consideration of granule channelization and its influence on starch modification will become increasingly important in efforts to improve modified starches within existing limits of types and amounts of reagents that can be used.

References

1. BeMiller, J.N. *Oyo Toshitsu Kagaku (J. Appl. Glycosci.)* **1997**, *44*, 43.
2. Fannon, J.E.; Gray, J.A.; Gunawan, N.; Huber, K.C.; BeMiller, J.N. *Food Sci. Biotechnol.* **2003**, *12*, 700.
3. Fannon, J.E.; Gray, J.A.; Gunawan, N.; Huber, K.C.; BeMiller, J.N. *Cellulose* **2004**, *11*, 247.
4. Huber, K.C.; BeMiller, J.N. *Carbohydr. Polym.* **2000**, *41*, 269.
5. Huber, K.C.; BeMiller, J.N. *Cereal Chem.* **2001**, *78*, 173.
6. Hall, D.M.; Sayre, J.G. *Text. Res. J.* **1970**, *40*, 256.
7. Fannon, J.E.; Hauber, R.J.; BeMiller, J.N. *Cereal Chem.* **1992**, *69*, 284.
8. Fannon, J.E.; Shull, J.M.; BeMiller, J.N. *Cereal Chem.* **1993**, *70*, 611.
9. Hellman, N.N.; Melvin, E.H. *J. Am. Chem. Soc.* **1950**, *72*, 5186.
10. Huber, K.C.; BeMiller, J.N. *Cereal Chem.* **1997**, *74*, 537.
11. Reichert, E. *The Differentiation and Specificity of Starches in Relation to Genera, Species, etc.*. Carnegie Institute of Washington, Philadelphia, Pennsylvania, **1913**.

12. Gray, J.A.; BeMiller, J.N. *Cereal Chem.* **2004**, *81*, 278.
13. Hauber, R.J.; BeMiller, J.N.; Fannon, J.E. *Starch/Stärke* **1992**, *44*, 323.
14. Shi, X.; BeMiller, J.N. *Carbohydr. Polym.* **2000**, *43*, 333.
15. Kweon, M.R.; Bhirud, P.R.; Sosulski, F.W. *Starch/Stärke* **1996**, *48*, 214.
16. Villwock, V.K.; BeMiller, J.N. *Starch/Stärke* **2005**, *57*, 281; Villwock, V.K. Ph.D. Thesis, Purdue University, **1996**.
17. Han, J.-A.; BeMiller, J.N. *Starch/Stärke* **2005**, in press.
18. Gray, J.A.; BeMiller, J.N. *Carbohydr. Polym.* **2005**, *60*, 147.
19. Han, J.-A.; BeMiller, J.N. unpublished.
20. Ji, Y.; Ao, Z.; Han, J.-A.; Jane, J.-L.; BeMiller, J.N. *Carbohydr. Polym.* **2004**, *57*, 177.
21. Gray, J.A.; BeMiller, J.N. *Cereal Chem.* **2001**, *78*, 236.

Chapter 12

Supramolecular Structures from Reductive Amination of Starch Fragments

Uwe Brasch and Walther Burchard*

Institute of Macromolecular Chemistry, Albert-Ludwig University
of Freiburg, 79104 Freiburg, Germany

ABSTRACT We report the formation of new supramolecular structures formed chemically, but without using group blocking. Potato starch fragments were used, prepared by acid degradation of starch granules in suspensions of alcohols (*Macromolecules* **1995**, *28*, 2363) following a procedure of Fox and Robyt (*Carbohydr. Res.* **1992**, *227*, 163) A series of different molar masses were obtained ranging from $M_w = 37.3 \times 10^3$ g/mol to 80×10^6 g/mol. All samples showed the typical X-ray diffraction pattern of semicrystalline B-starches. The sample of lowest molar mass (LD7, $M_w = 37300$ g/mol) was chosen for coupling reactions of aliphatic amines (C_6 , C_{12} , C_{18}) to the reducing end group of the polysaccharides. The coupling was achieved by reductive amination, and sodium cyanoborohydride ($NaCNBH_3$) was used as a selective reductive reagent. Because of the small size of the LD7 fragment ($R_g \approx 8$ nm) micellation was expected with the alkyl chains forming the hydrophobic core and the branched hydrophilic starch fragments as bulky head groups. However, very large objects were obtained with radii of gyration of $R_g = 175$ - 289 nm and aggregate $M_w = (1.34 - 3.05) \times 10^6$ g/mol. Analysis of the angular dependent light scattering data revealed the internal structure to be formed of aggregates with rodlike segments. X-ray diffraction from powder displayed the characteristic pattern of crystalline V-helices. Apparently the attached alkyl chains form inclusion complexes with the outer side chains of the starch fragment.

Starch is one of the major renewable sources in nature and is abundantly available in the form of granules from cereal grains or potato tubers (1-3). These semicrystalline granules furnish the plant with high density energy storage. These granules have a well organized supramolecular structure with branched amylopectin as the main component, accompanied by a much smaller amount of linear amylose chains. Amylopectin has a very high molar mass with $M_w \approx 70 \times 10^6$ g/mol (4) but amylose is much smaller in size, with molar masses of $M_w = (0.3 - 1.5) \times 10^6$ g/mol. The low price and the high molar mass appear to make amylopectin an ideal starting point for the development of new biodegradable materials in the non-food area, for instance as packing material. Despite these promising aspects the modification required for industrial use is inhibited, mainly by the poor solubility of the native material.

Our interest was directed to the construction of new macromolecular architectures, either by covalent binding of suitable precursors or by a controlled physical aggregation mechanism. Some initial thoughts on possible successful preparation of new architectures may be useful. First, the functionalized precursor should be a macromolecule but still not too large. A large particle has a low diffusion coefficient which can easily reduce a reaction to the diffusion controlled limit, and a kinetically controlled reaction can be much better handled and directed by man. Also, in large flexible macromolecules, functional end groups are often shielded by a cloud of segments from the same macromolecule which slows down the desired reaction. Second, the precursor should have a well characterized structure, as only then can a fairly regular supramolecular structure be expected. The amylopectin molecule has one reducing end group as a focal functionality but a huge excess of non reducing OH-groups, and this barely made it possible to obtain a specific reaction of high yield. Therefore, the first requirement was the preparation of a fairly well defined amylopectin fragment of much smaller size.

We found a suitable reaction in a procedure reported by Fox and Robyt (5) who performed an acid degradation in alcohols, i.e. under controlled condition where the granule crystallinity was never broken up. We repeated this procedure and prepared 11 amylopectin fragments from potato starch (6). The amorphous amylose and the amylopectin in the amorphous layers of the granule are degraded preferentially and then removed by repeated washing with cold water. In four previous papers these fragments were both comprehensively and carefully characterized by static and dynamic light scattering and viscometry. We refer to these papers and suggest them as additional reading (6-9).

Next, we were seeking a selective reaction of the reducing end group which would require no group blocking chemistry. This area has a long history and started with a procedure first developed by Pffannemüller et al. (10-12) In this process the reducing end group of glucose and maltose was activated by oxidation into lactones. These lactones spontaneously converted the aliphatic

primary amines to the corresponding amides, but unfortunately with severely decreasing yield as the chain length became longer. This fact was already observed by Pfannemüller but was quantified with aliphatic amines and maltooligomers from maltose to maltohexaose by Denkinger et al. (13). In particular with hexadecylamine coupled onto maltose, long filamentous micelles were found. After many other approaches we finally found a highly selective coupling reaction for the reducing end group, but this time as an amine, using reductive amination according to Wittig (14), Lane (15) and Lee (16). The reaction is well known in carbohydrate and protein chemistry. The main point is the quick transformation of the intermediate immonium ion into the stable amine, which is achieved efficiently by sodium cyanoborhydride (NaCNBH_3) (17). This reaction has not been used much in polysaccharide chemistry, and it required the procedure to be modified since the longer amines were not soluble in water (see below).

Water solubility of polymers is governed by a delicate balance of hydrophilicity to hydrophobicity. Often a minor change of this balance by incorporating hydrophobic groups causes a drastic change in the solution properties. The hydrophobic groups tend to avoid contact with water which induces a conformational change of the polymer. If possible sterically, spherical micelles will be formed but otherwise the hydrophobic groups or chains have to find another "cage" in which to hide themselves from contact with water. With our branched precursor we did not find micelles but instead a highly aggregated structure of a priori unknown architecture. This fact required a detailed analysis by physico-chemical means, but the approaches may be unfamiliar to polymer scientists, so we will give a fairly detailed outline of procedures. The characterization was made mainly by static and dynamic light scattering (LS). Application of this technique to the study of food polymers was described in a book article by one of the present authors. A summary is given in the Appendix.

Some Structure Properties of the Precursor

The preparation of the precursors by controlled acid degradation in alcohols was described in detail in previous papers (5,6) and will not be reproduced in detail. Here we only wish to emphasize a few essential points. During the degradation process the granule crystallinity was never damaged. This is clear evidence for degradation occurring mainly in the amorphous domains and but also partially in the intercalated layers between the crystalline shells where the highly branched sections of amylopectin are assumed to occur. The predominantly degraded material from the amorphous domains is washed out in cold water, and the partial attack of the intercalated layers should result in a decrease of the branching density, which indeed was found. The amount of amylose, as followed

by the iodine uptake, decreased sharply and was less than 5% for the lowest molar mass sample (6).

Two conformational properties are relevant for judging the structure properties when aliphatic amines were attached to the reducing end group. These are the radius of gyration R_g and the hydrodynamic radius R_h . The former were determined by static LS the other by dynamic LS. Figure 1 shows the molar mass dependence of the radius of R_g and R_h . The exponents in the double logarithmic plot are $\nu_{R_g} = 0.40$ and $\nu_{R_h} = 0.47$. The corresponding radii of gyration for unperturbed hyperbranched macromolecules were predicted to be considerable smaller than the measured ones (curve not shown) which indicates significant segmental stiffness within the measured samples. The lowest fragment of molar mass $M_w = 35000 \text{ g/mol}$ was used for further modification. Its radius of gyration could not accurately be measured but extrapolation gives about a value of $R_g = 8 \text{ nm}$; for the hydrodynamic radius, a value $R_h = 5 \pm 0.5 \text{ nm}$ was found (6).

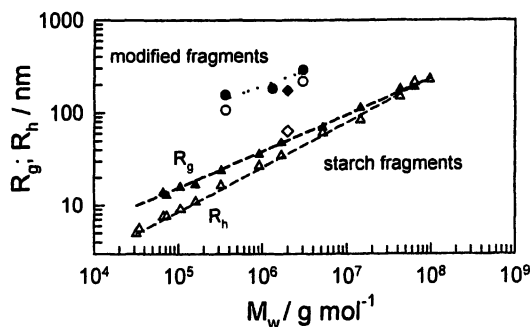


Figure 1: Molar mass dependence of the radius of gyration R_g , and hydrodynamic Radius R_h from 14 different starch fragments and from 4 modified fragments from the lowest fragments with aliphatic amine coupled via to the reducing end group.

Five of the 11 fragments had dimensions of $R_g > 70 \text{ nm}$ and allowed an analysis of the angular dependence of scattered light to be made. Differences in structure become noticeable in the angular dependence of the scattered light mainly in the regime of large values of $R_g q \equiv u$ where $q = (4\pi n_0 / \lambda) \sin(\theta/2)$. This domain is magnified in the Kratky (18) representation where data of the angular dependent particles scattering factor $P(u) = i(\theta)/i(\theta=0)$ are multiplied by u^2 where θ is the scattering angle, related to the scattering vector q . Figure 2 shows the Kratky plots of the particle scattering factor $P(u)$ for several structures at zero concentration. The dashed lines were calculated from the theory of hyperbranched macromolecules taking into account excluded volume interaction (19), the symbols represent the experimental points. The fits to the data gave

branching densities which decreased with the molar mass but were lower than 1%. The measured angular dependence of the scattered light is characteristic of hyperbranched structures. It significantly differs from that of randomly branched macromolecules (20) as found in experiment and predicted by theory (21).

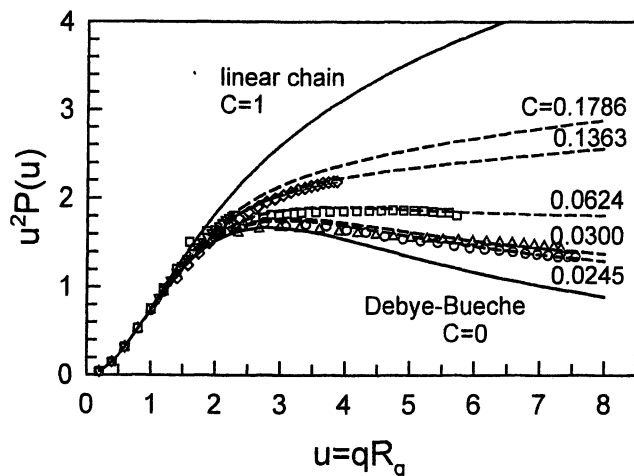


Figure 2: Kratky plots from 5 starch fragments with radii of gyration $R_g > 70$ nm. The values of $1/C$ are proportional to the number of branches per molecule. Dashed lines corresponds to fits for hyperbranched chains under influence of excluded volume interaction (19)

Global Molecular Parameters of Starch Fragments after Covalent Binding of Aliphatic Amines

Because long aliphatic chain amines cannot be dissolved in water, the attachment of long aliphatic amines could not be made in aqueous solution, so a slight modification was necessary. However, the reaction was still possible when the aliphatic amines were added at 50°C as a suspension. After reaction the samples were dialyzed against de-ionized water for several days to remove non reacted amines and the NaCNBH_3 catalyst. The amination of the reducing group is a slow process. Mutarotation has to occur to bring the terminal glucose ring unit into the open aldehyde form before reaction can proceed, so the reacting system was left for at least 100 hours. The samples were carefully analyzed by NMR spectroscopy, elemental analysis and determination of non-reacted reducing end groups. The reducing end-groups (CHO) were effectively determined by the sensitive Somogyi / Nelson technique (22) which has been described in detail in

a previous paper (6). The original procedure is based on water soluble oligo- and polysaccharides but it was also applicable in a mixture of DMSO/H₂O = 9/1 with somewhat lower sensitivity. The two calibration curves for CHO end groups in water and in DMSO/H₂O are shown in Figure 3.

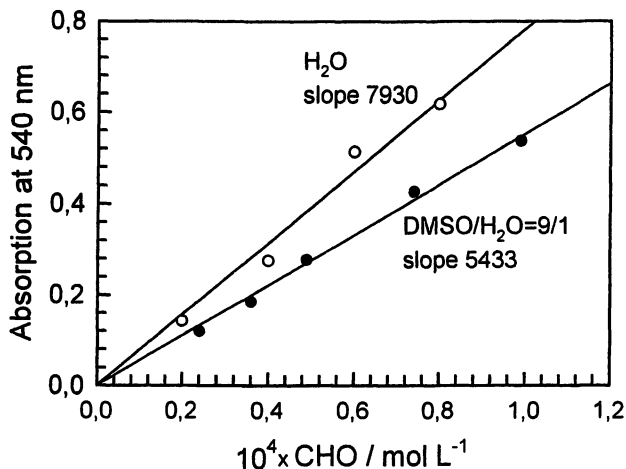


Figure 3: Calibration curves for the reducing end-groups of saccharides according to the Somogyi/Nelson method in H₂O (open) and DMSO/H₂O = 9/1 (solid symbols).

Table 1 gives the measured molecular parameters and the conversion of reducing end-groups. The light scattering measurements were made at 40°C. in DMSO/H₂O = 9/1. The radii of gyration were determined from the initial slope of the q^2 dependence in the Berry plot, $(Kc/R_9)^{0.5}$ (23) which was preferred to than the common Zimm plot (24) because of the high molar mass of the samples. Up to 82 times larger molar masses were obtained and dimensions 58 larger than those of the precursor. The results immediately ruled out spherical micelle formation where an increase in dimension at most by a factor 4.5 would be possible.

Evaluation of the Angular Dependence of Scattered Light

No angular dependence was observed with the starch fragment LD7. The radius of gyration could only be estimated from extrapolation of the line in Figure 1 to the corresponding molar mass and was about $R_g = 8$ nm. In contrast, all samples with coupled aliphatic amine chain exhibited a marked angular dependence and a

very high molar mass. The evaluation of the scattering curve from the Berry plot gave a much higher precision for the molar mass than was possible from the corresponding Zimm plot. The radius of gyration was evaluated from Zimm-, Berry- and Guinier (25) representations of the scattering data applying polynomial fits to find the initial slope (in the Guinier plot $\ln(1/P(q))$ data are plotted against q^2). This was done with the whole set of data but also without the last 15 values at large q -values. The curvature of the angular envelope is less pronounced in the Zimm plot but still gives clear indications for an aggregated structure that deviates significantly from linear chains or common, randomly branched structures (19). At low qR_g values the particle scattering factor only gives information on the average size, not on the shape and internal architecture of the particles.

Table 1

Molar mass M_w , radius of gyration R_g , hydrodynamic radius R_h , ρ -parameter, concentration of non-reacted reducing end groups and conversion as derived from the values of the precursor LD7 and the samples. Filter sizes for R12b1 and R18 were too narrow, and a certain amount was retained on the filter. R12 and R18 denote samples with C12 and C18 aliphatic amines.

Sample	$M_w \times 10^{-3}$ g/mol	R_g nm	R_h nm	$\rho =$ R_g/R_h	$CHO \times 10^{-4}$ mol/g	conversion %	Filter μm
LD7	35	≈ 8	4.5	1.77	1.263	0.00	0.5
R12b1	1340	184	---	---	0.138	88.1	0.2
R12b2	3050	289	217	1.33	0.138	88.1	5.0
R12c1	361	158	108	1.46	0.499	57.1	5.0
R12c2	17.4	---	<10	---	0.499	57.1	5.0
R18	2020	175	64	1.22	0.261	77.5-	0.5

The characteristic structural features appear only at large $qR_g > 2$ values ($R_g > 75$ nm). These characteristics are more apparent when the scattering data are presented in a Kratky (18) or Casassa-Holtzer plot (26) (were $qR_g/Kc\pi = qM_wP(\theta)/\pi$ is plotted against $u = qR_g$) The former is most suited for globular structures i.e. branched or coiled structures of linear chains, the latter gives valuable information on chain stiffness and shows a simple curve for rigid rods, which tends asymptotically to an angular independent plateau (26,27).

Figure 4 presents the Kratky plots for the four samples with $R_g > 75$ nm. Comparison with the curves of Figure 2 shows close similarity up to values of $u = qR_g = 2.5$. These data could be well fitted with the model of hyperbranched

or star-branched chains (6,28). However at larger u -values all samples develop a marked linear increase. Such behavior is familiar to scientists from small angle neutron scattering (SANS) data of linear chains and was interpreted as wormlike chain behavior. According to Kratky-Porod theory (18) this causes an increase at large q -values because of the rodlike behavior of short chain sections. Similar curves were obtained from SANS data of 12-arm star-branched macromolecules and were quantitatively described by a theory of Huber and Burchard (29). Figure 5 shows the theoretical curves for star molecules of increasing arm stiffness.

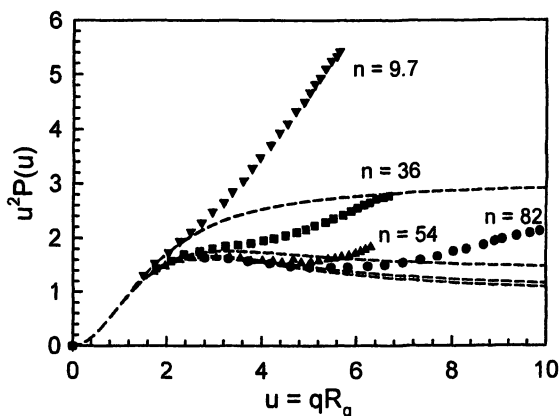


Figure 4 : Kratky plots from 4 modified starch fragments. The numbers on the curves indicate the aggregation factors after the starch fragment LD7 was modified by the coupled amino chain. The dashed line corresponds to fits with the theory of flexible hyperbranched chains (19,20). All curves developed an asymptotic increase, that resembles the behavior of stiff linear chains when the region within Kuhn segments is probed.

The rod-like character of a particle can be checked more specifically in the Casassa-Holtzer representation where $(q/\pi)(R_g/Kc) = (q/\pi)(M_w/P(u))$ is plotted against u (Figure 6). A constant plateau height in the asymptotic regime gives the linear mass density $M_L = M_w/L_w$. At this point of our discussion we have to emphasize that no change or smoothing of the experimental data with any special model has been made. The various plots were only prepared to find out within which framework of known particle structures the experimental data may fit. Once a plateau is obtained in the Casassa-Holtzer plot the linear mass density is an experimentally observed structure parameter since when the molar mass is measured the contour length L_w can also be determined. The data are collected in Table 2 together with the aggregation number derived from the molar mass of the aggregates and the LD7 precursor.

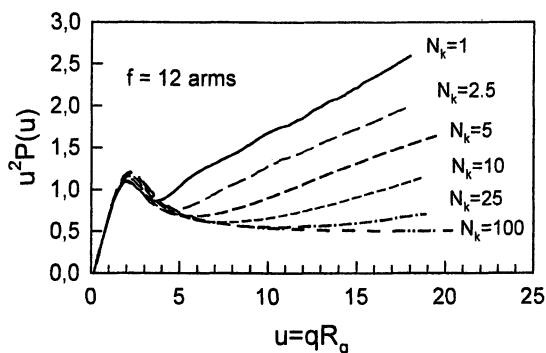


Figure 5 : Kratky plots from a 12-arm star molecules (29) with stiff arms. N_k denotes the number of Kuhn segments per arm. Chain stiffness has no detectable effect on the angular dependence in the regime of light scattering if the chain of one arm contains more than 25 Kuhn segments.

Table 2

Experimental parameters extracted from the asymptotic plateau height in the Casassa-Holtzer plots and degree of polymerization DP_w , radius of gyration R_g and the aggregation number $n_{\text{aggr}} = M_{w,\text{aggr}}/M_{w,\text{LD7}}$. L_w is the contour length.

Sample	DP_w	R_g/nm	$M_L/\text{g}/(\text{mol nm})$	L_w/nm	n_{aggr}	$L_w/n_{\text{aggr}}/\text{nm}$
LD7	321	<10	386	97	1.0	97
R12b1	8234	184	960	1395	33.8	39
R12b2	18741	289	710	1887	81.6	23
R12c1	1831	158	698	517	9.7	53
R18	12400	175	1060	1906	53-8	35

Summary of Experimentally observed Facts

Before turning to interpretation of the experimental observations it is useful to list the observed facts from which we can, without prevarication, draw positive conclusions.

1. The aggregation number varied from $n_{\text{aggr}} = 10 - 82$.
2. The corresponding radii increased by factors 16 - 29.

3. The Kratky plots show similarity to star-molecules with very stiff arms.
4. Linear mass densities were found between $M_L = 698$ and 1060 g/(mol), the corresponding value for randomly coiled amylose is $M_{L,amy} = 385.7$ g/(mol nm), using $l_0 = 0.42$ nm for the bond length of the anhydroglucose unit.
5. The contour length per aggregate subunit L_w/n_{aggr} decreases with the aggregation number.
6. The contour length of the LD7 precursor is $L_{w,LD7} = 0.42 \times DP_{w,LD7} = 97$ nm.

The list gives evidence that, following coupling with aliphatic amines, there is a very strong expansion of the initially fairly flexible branches in LD7. Such expansion is far stronger than can be caused by excluded volume interaction, and the expansion must be based on a marked stiffening by the attached hydrophobic tails. The stiffening is confirmed by the similarity of the angular dependence to that found for stiff star molecules. The linear mass density is 1.8 to 2.7 times larger in the aggregates than in the non modified LD7. Correspondingly the contour length is decreased from 97 nm for LD7 to 54-23 nm for the aggregate subunits.

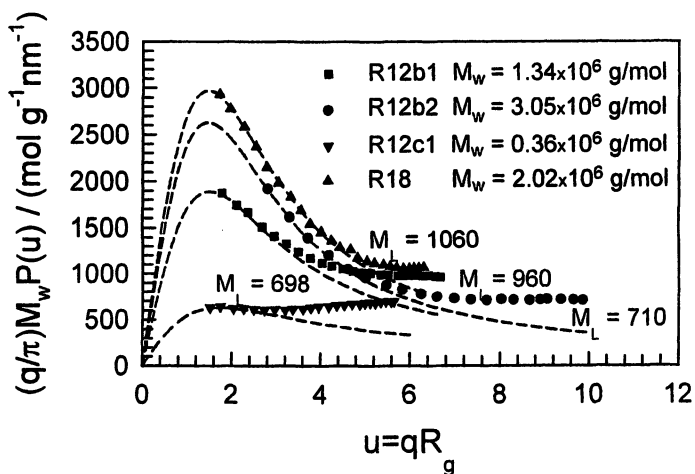


Figure 6: Casassa-Holtzer plots from the same data as in Figure 4. The curves appear to reach a plateau, a feature of rod-like behavior. The numbers on the curves denote the mass per unit length M_L which is a measurable quantity. For further discussion, see text.

Attempt at Interpretation

Apparently the attached aliphatic chain causes a shortening of the overall length which is combined with an increase of the cross section of rodlike segments, and these effects are correlated with aggregation. In our attempt to unearth a model we had to keep in mind that the hydrophobic chains tend to avoid contact with water. Micelle formation would be a most efficient process to conceal the hydrophobic sections, but both, spherical and filamentous micelles have to be excluded. Compared to the size of the hydrophilic head (about 8 nm) the aliphatic chains are with about 1.5 nm for the C12 chain in the stretched conformation, and 2.25 nm for the C18 chain, far too short to allow this structure. Therefore, the aliphatic chains have to find another cage in which to hide themselves from water contact. The only way, we can imagine, that this can be achieved is by inclusion in a helix, i.e. a V-type helix complex similar to the well known one for fatty acids (3). In our search for additional experimental evidence which would confirm or disprove this conjecture we performed X-ray diffraction experiments on powdery samples (Figure 7). The crystalline pattern of B-type double helices in LD7 would be expected but, to our surprise, the modified starch fragments with attached aliphatic amines displayed crystallinity. The pattern differ significantly from that of the B-type of double helices but are identical to that from fatty acid helix inclusion complexes (3), which validates our suggestion derived from light scattering in solution.

The following summary model (see Figure 8) should not be taken literally, because it is based on the oversimplified concept of homogeneously hyperbranched structures(20,30-32), while heterogeneity in branching has been shown in amylopectin (see below). Still it presents an essential feature of how large aggregates can be formed and, simultaneously, bring about complete protection of the aliphatic chains from water contact.

What about alternative models?

Several questions remain open. Some can immediately be answered, but for the remainder we only can make a speculative suggestion. Hopefully other groups with additional techniques may be able to bring further insight.

The first question is based on the possibility that the inclusion complex is already formed before any chemical attachment has taken place. Doubts may be raised about whether such complexes could prevent the chemical reaction, and NMR spectra enabled us to discard this possibility. The free aliphatic chains show the characteristic NH_2 peak at 2.49 ppm, but, in the modified starch fragments, this peak has disappeared and instead of this a new peak at 1.355-1.415 ppm appeared which is assigned to a secondary amine. Admittedly the

formation of an inclusion complex with the non attached amines cannot completely be excluded, but we have to recall that 50 to 80 % of the reducing end groups were consumed by the chemical reaction. Indeed, the hydrophilic primary amine group remains accessible to reaction when the aliphatic chain is enclosed in a helix. Other types of inclusion complexes which could, in addition, cause the observed immense expansion in size, are not known to us

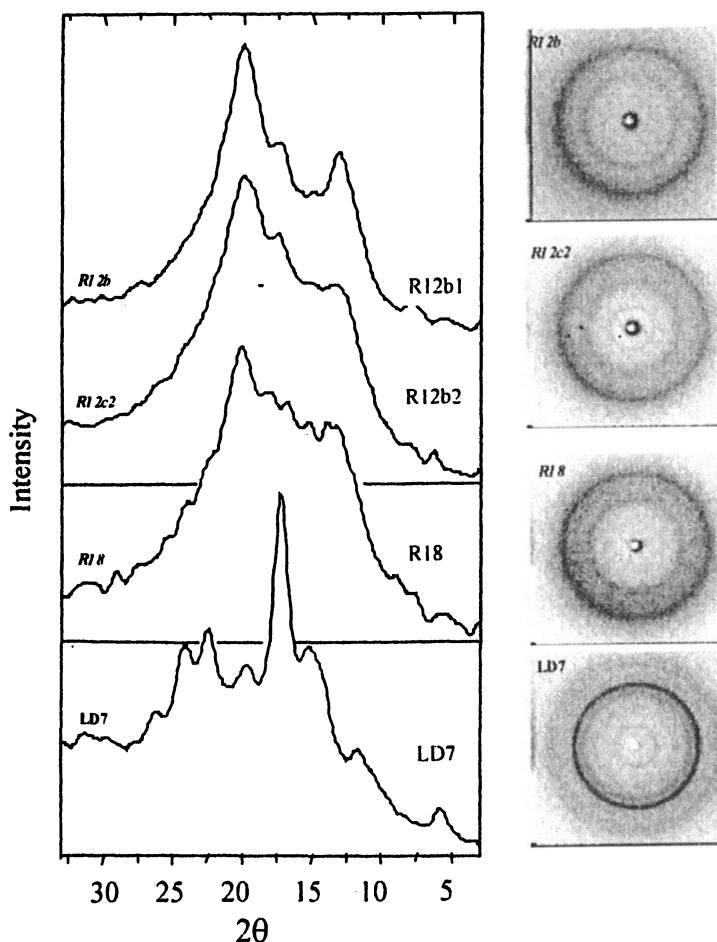


Figure 7 : Diffraction patterns from the powder of the non-modified starch fragment LD7, compared with those from the modified samples with attached amino chains. The former shows the typical pattern of the B-starch modification the latter that of the fatty acid inclusion complex of V-helices (3).

Another doubt can be ruled out. The starch fragments bear an abundance of OH-groups which are predisposed to form hydrogen bonds for instance with another OH group from a second particle, and this could also cause pronounced association. This sort of association is typical for a random cluster formation as were theoretically treated by Flory and Stockmayer (32,33). In previous work we checked this theory experimentally with a number of, chemically different, randomly branched systems (34). The scattering behavior of the aggregated starch fragments deviated radically from that of randomly branched clusters. In the Kratky representation the scattering curve from randomly branched clusters increased continuously with q (34), whereas, with the present samples, a maximum was found around $qR_g = 2$ in full agreement with theoretical predictions for hyperbranched materials (20,35). We can safely discard the occurrence of random branching at the low concentration of the light scattering measurements. However, at concentrations above the overlap concentration a transition was found for amylopectin from the hyperbranching pattern to the scattering behavior of randomly branched clusters (36), as could be anticipated. The question remains to what extent expansion by excluded volume interaction can be distinguished from chain stiffness. This question was implicitly answered by Fujita (37) who demonstrated that excluded volume interaction becomes noticeably effective only if the chain consists at least 50 Kuhn segments. In the range between 20 and 50 Kuhn segments chain stiffness is virtually indistinguishable from excluded volume interaction. However, for chains with less than 10 Kuhn segments cycle formation is scarcely possible, and since this is a precondition for excluded volume interactions, it can be neglected.

So far these conclusions could be made, for linear and star-branched chains. Recently, the theory of chain stiffness has been extended to dendritic macromolecules with stiff linear spacer chains of various rigidity between two generations (38). The effect of stiffness was found to be more pronounced in the dendrimers than in star-branched chains and would give a better fit of the experimental data of the present modified starch fragments. The application of the theory to hyperbranched structures appears possible, but is complicated and is presently work in progress.

We also wonder what may be the reason of the change from rather flexible starch fragments to those of overwhelming rigidity after fairly minor modification.

A V-type helix with enclosed hydrophobic chains will behave like a rod, but the aliphatic chains are comparatively short, and therefore broken-rod behavior with many short rod sections could be expected. So far, we cannot give a definite answer, but experimental findings suggest a cooperative effect of the filled short helical sections which induce the formation of the empty V-type helix conformation. This view requires more detailed theoretical development in close relation to the crystalline amylopectin structure that recently was deduced by Donald et al. (39,40) from carefully analyzed X-ray diffraction patterns of native

amylopectin. According to this model amylopectin is not only heterogeneously branched but, superimposed on the crystalline packing of double helices, so that a superhelical arrangement seemed to be present.

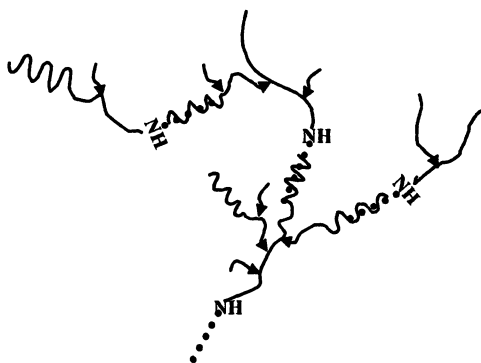


Figure 8: Possible model which prevents contact of the aliphatic chains with water is in agreement with the diffraction pattern of fatty acids, and preserves the hyperbranched character. The observed high chain stiffness may arise from a cooperative effect that extends over two or more aggregation generations.

References

1. Banks, W.; Greenwood, C. T. *Starch and its Components*, Edinburgh University Press, Edinburgh 1975.
2. Whistler, R. L.; BeMiller, J. N.; Paschall, E. F. *Starch: Chemistry and Technology*, Academic Press, Orlando 1984, second edition.
3. Guilbot, A.; Mercier, Ch. *Starch in: The Polysaccharides*, Apinal, G. O., Ed., Academic Press, Orlando 1985, p. 209.
4. Aberle, T.; Burchard, W.; Vorwerg, W.; Radosta, S. *Starch/Stärke* 1994, 46, 329.
5. Fox, J. D.; Robyt, J. F. *Carbohydr. Res.* 1992, 227, 162.
6. Galinsky, G.; Burchard, W. *Macromolecules* 1995, 28, 2363.
7. Galinsky, G.; Burchard, W. *Macromolecules* 1996, 29, 1498.
8. Galinsky, G.; Burchard, W. *Macromolecules* 1997, 30, 4445.
9. Galinsky, G.; Burchard, W. *Macromolecules* 1997, 30, 6966.
10. Pfannemüller, B. *Neue Polymere aus Polysacchariden*, in: *Polysaccharide, Eigenschaften und Nutzung*. Burchard, W., Ed., Springer Verlag, Berlin 1985, p. 280.
11. Emmerling, E. N.; Pfannemüller, B. *Makromol. Chem.* 1978, 178, 691.

12. Emmerling, E. N.; Pfannemüller, B. (a) *Makromol. Chem.* 1983, 184, 1441; (b) *Colloid Polym. Sci.* 1983, 261, 677.
13. Denkinger, P.; Burchard, W.; Kunz, M. *J. Phys. Chem.* 1989, 93, 1428.
14. Wittig, G. *Liebigs Ann. Chem.* 1951, 573, 209.
15. Lane, C. F. *Synthesis* 1975, 135.
16. Lee, R. T.; Lee, Y. C. *Biochemistry* 1980, 19, 156.
17. Simon, K.; Warren, G. *Adv. Prot. Chem.* 1984, 36, 79.
18. Kratky, O.; Porod, G. *Rec. Trav. Chim.* 1949, 68, 1106; *J. Colloid Sci.* 1949, 4, 35.
19. Burchard, W. *Macromolecules* 2004, 37, 387.
20. Burchard, W. *Macromolecules* 1972, 5, 604.
21. Kajiwara, K.; Burchard, W.; Gordon, M. *Brit. Polym. J.* 1970, 2,
22. Somogyi, M. *J. Biol. Chem.* 1937, 117, 771; (b) Nelson, N. *J. Biol. Chem.* 1944, 153, 375.
23. Berry, G. C. *J. Chem. Phys.* 1966, 44, 4550.
24. Zimm, B. H. *J. Chem. Phys.* 1948, 16, 1099.
25. Guinier, A.; Fournet, G. *Small Angle Scattering of X-Rays*, Wiley, New York 1955.
26. Casassa, E. F. *J. Chem. Phys.* 1955, 23, 596.
27. Schmidt, M.; Paradossi, G.; Burchard, W. *Makromol. Chem., Rapid Commun.* 1985, 6, 767.
28. Burchard, W. *Macromolecules* 1977, 10, 919.
29. Huber, K.; Burchard, W. *Macromolecules* 1989, 22, 3302.
30. Meyer, K. H.; Bernfeld, P. *Helv. Chim. Acta* 1940, 23, 805.
31. Erlander, S. R.; French, D. *J. Polym. Sci.* 1956, 20, 7.
32. Flory, P. J. *Principles of Polymer Chemistry*, Cornell University Press, Ithaca, N.Y., 1953, Chapt. 9.
33. Stockmayer, W. H. *J. Chem. Phys.* 1943, 11, 45; 1944, 12, 125.
34. Trappe, V.; Bauer, J.; Weissmüller, M.; Burchard, W. *Macromolecules* 1997, 30, 2365.
35. Burchard, W. *Adv. Polym. Sci.* 1983, 48, 1.
36. Aberle, L. B.; Kleemeier, M.; Hennemann, O.-D.; Burchard, W. *Macromolecules* 2002, 35, 1877.
37. Fujita, H. *Macromolecules* 1988, 21, 179.
38. Burchard, W. Manuscript in preparation.
39. Waigh, T. A.; Perry, P.; Riekel, C.; Gidley, M.; Donald, A. M. *Macromolecules* 1998, 31, 7980.
40. Waigh, T. A.; Donald, A. M.; Heidelbach, F.; Riekel, C.; Gidley, M. *Biopolymers* 1999, 49, 91.
41. Burchard, W. *Light Scattering in: Ross-Murphy, S. B. (ed) Physical Techniques for the Study of Food Biopolymers*, Blackie Academic & Professional London 1994., Chapt 4.

Appendix: Summary of some Light Scattering Properties (41).

Characterization of large particles by static light scattering (LS) requires measurements of the absolute scattering intensity in terms of Rayleigh ratios $R_\theta = r^2 i(\theta)/I$, where $i(\theta)$ is the scattering intensity at the scattering angle θ and I the primary beam intensity, both measured in counts of photons, and r is the distance of the detector from scattering volume. Scattering angles between 30° and 145° are realized with conventional LS goniometers. The absolute scattering intensity at zero scattering angle and in the limit of zero concentration is given by $R_\theta = KcM_w$, where M_w is the weight average molar mass of the particle, c the concentration and K a contrast factor. The angular dependence results from interference among the scattering rays emitted by the various scattering points (segments) of the particle, and is a characteristic function of shape and internal particle structure. The ratio $P(q) = i(q)/i(q=0)$, the so-called particle scattering factor, could be calculated analytically for special structures. Here the value of the scattering vector $q = (4\pi/\lambda)\sin(\theta/2)$ is introduced which is related to the scattering angle θ , and λ is the wavelength of the light in the solution. The parameter qR_g has no dimension and represents the average phase difference among the scattering rays. All particle scattering factors can be expressed in terms of $u = qR_g$. The initial part of $1/P(q)$ as a function of q^2 is universal for all structures and its slope $(1/3) R_g^2$ is defined by the mean square radius of gyration, so the radius of gyration can be measured without knowing the structure. At large $u = qR_g$ typical structural features are displayed. These characteristics can be discriminated quantitatively in special plots of the measured data. Most efficient are the Kratky and the Casassa-Holtzer plots, the latter is especially adapted for a quantitative evaluation of stiff to rodlike behavior of chains (see text).

In dynamic LS the scattering intensity is measured in very short time intervals ($>10^{-6}$ s), whereas in static LS the time interval is much larger than the thermal concentration fluctuations. By means of a so-called autocorrelator a time correlation function is measured which decays exponentially with time. The initial decay constant $\Gamma(q) = q^2 D(q)$ defines the apparent mutual diffusion coefficient. After extrapolation of $D(q)$ to $q = 0$ and, in the limit of zero concentration, the translation coefficient $D_{\text{trans}} = kT/(6\pi\eta_0 R_h)$ is obtained, and this determines the hydrodynamic radius R_h via the Stokes-Einstein relationship. The ratio of the two radii R_g/R_h depends on the segment density in the particle and is a valuable parameter in the characterization of structures (35,41). LS is a non-invasive technique and allows measurements of the particles under thermodynamic equilibrium, and even the dynamics are not perturbed by external forces. Over and above the outer shape of such particles, which can be visualised by say cryo-electron microscopy (cryo-TEM), LS probes the internal structure.

Chapter 13

Pectin: Networks, Clusters, and Molecules

Marshall L. Fishman¹, Peter H. Cooke², Hoa K. Chau¹,
David R. Coffin¹, and Arland T. Hotchkiss, Jr.¹

¹Crop Conversion Science and Engineering and ²Core Technologies,
Eastern Regional Research Center, Agricultural Research Service,
U.S. Department of Agriculture, 600 East Mermaid Lane,
Wyndmoor, PA 19038

Time dependent microwave assisted extractions of pectin from lime and orange albedo, have revealed that with increasing time of heating, molar mass and size decreased. In contrast, Mark-Houwink exponents, a measure of the rate of change of the molar volume with molar mass, increased with time. Based on these experiments, it is hypothesized that pectin network structures gradually break down during the extraction process with increasing heating time. Initially networks degenerate to partially formed networks (clusters or branched structures) and finally to a mixture of linear molecules in the shape of rods, segmented rods and kinked rods. Additional evidence for this model was obtained from electron micrographs of pectin deposited on mica from solution which showed the presence of all the structures described above. Furthermore, pectin imaged in native sugar acid gels by atomic force also revealed that pectin existed in these gels as partially formed networks.

Pectin is a heterogenous polysaccharide found in the cell walls of most if not all higher plants (1). About 60 to 90 % of fruit pectin is comprised of (1→4) linked, α -D-galacturonic acid and its methyl ester, i.e. homogalacturonan (HG) (2, 3). Some HGs contain pendant α -D-xylose units. Also contained in pectin is rhamnogalacturonan I which has arabinan, galactan and arabinogalactan side chains. These constituents account for most of the monosaccharide units present in pectin preparations. Plant cell wall functions attributed to pectin include governing cell wall porosity, modulating cell wall pH and charge, regulating inter cell adhesion at the middle lamella and signaling to plant cells the presence of foreign bodies such as symbiotic organisms, pathogens and insects (1). Numerous workers have researched the various activities of pectin fragments as nutraceuticals (4). Some of these activities include immunostimulation, anti-metastasis, hypoglycemic and cholesterol lowering effects. The ability of pectin to gel and texturize unprocessed and processed foods is its most important food property. The degree of methyl esterification (DE) in commercial citrus pectins may range from about 17 to 73. The DE of pectin depends on the source and method of extraction. Commercial citrus pectin has a DE of about 72-77% and is often used to make high methoxy sugar acid gels (SAG) (5). The object of this review is to correlate the structure of high methoxy pectin in solution ($DM \approx 73$) with that which is in SAGs.

Experimental

Materials

Peach pectin extraction for analysis by electron microscopy has been described previously (6). Briefly, cell walls were obtained from the mesocarp of "Redskin" peaches which were harvested 140 days after the tree flowered. Mildly extracted alkaline soluble pectin (ASP) was obtained from the cell walls after removal of chelate soluble pectin. Extracted ASP was dialyzed against water and lyophilized.

Albedo from early Florida Valencia oranges (EVO) and Florida tropical seedless limes (TSL) was flash extracted by microwave heating, under acid conditions as described before (5). Pectin was extracted by microwave heating in a CEM, model MDS-2000 microwave sample preparation system (CEM Corp., Matthews, NC). Samples were irradiated with 630 watts of microwave power at a frequency of 2450 MHz. For each experiment, six equally spaced cells were placed in the sample holder, a rotating carousel. One vessel was equipped with temperature and pressure sensing devices which measured and controlled the

temperature and pressure within the cell. Time of irradiation varied between 1 and 10 min followed by rapid cooling in a cold water bath to room temperature. The maximum allowed pressure level within the cell was set at 52 ± 2 psi and the maximum temperature within the cell was set at 195°C . Experiments were run with HCl at pH 2.0 prior to addition of albedo. Cells were loaded with 1 g of albedo dispersed in 25 mL of acid solution. Solubilized pectin was precipitated with 70% isopropyl alcohol (IPA), washed once with 70% IPA and once with 100% IPA. Finally, the sample was vacuum dried at room temperature and prepared for chromatography. Percentage of galacturonic acid content (7) and degree of methyl esterification were determined (8) for selected pectin samples.

Electron Microscopy

Preparation and imaging of peach pectin by transmission electron microscopy (TEM) has been described (6). Peach pectin was dissolved in water, 50 mM NaCl or 50% aqueous glycerol at 10 or 100 $\mu\text{g}/\text{mL}$. Ten μL aliquots were sandwiched between sheets of cleaved mica. The mica sandwich was allowed to set for 10-30 min, peeled apart, vacuum dried for 60 min at 5×10^{-6} Torr., rotary shadowed with platinum at an angle of 5-8 degrees and coated with a thin layer of carbon. The coated replicas were floated off the mica onto water, mounted on grids and imaged by TEM in a Zeiss 10B electron microscope (Thornwood, NY).

Atomic Force Microscopy

Gels from citrus pectins extracted from albedo were prepared and imaged as described previously (9).

The final composition (w/w) of the gels was 0.25% pectin, 65% sucrose and 35% of buffer. Preliminary experiments revealed that the pH of maximum gel strength was 3.0 for commercial citrus pectin, 3.2 for orange albedo pectin and 3.5 for lime albedo pectin. Gel strengths were determined with a Stable Micro Systems TA-XT2 Texture Analyzer (Texture Technologies Corp, Scarsdale, NY).

A thin (~1 mm) slice of transparent gel was cut manually with a stainless steel razor blade from a cm-size sample of gel, scooped from the center of the casting jar. A freshly cleaved 10 mm diameter disk of mica was applied to the cut surface of the gel. After 5 to 10 min, the disk was peeled off the gel surface and mounted in a Multimode Scanning Probe microscope with a Nanoscope IIIa controller, operated as an atomic force microscope in the Tapping Mode (Veeco Instruments, Santa Barbara, CA). The thin layer of pectin adhering to the mica

surface was scanned with the AFM operating in the intermittent contact mode using tapping mode etched silicon probes (TESP). The cantilever controls, namely drive frequency, amplitude, gains, and amplitude set point ratio (r_{sp}) were adjusted to give a phase image with the clearest image details. Values of r_{sp} used in this study were about 0.95.

Images were analyzed by software version 5.12 rev. B which is described in the Command Reference Manual supplied by the manufacturer. Lengths, widths and areas of strands and pores were determined by particle analysis. Prior to particle analysis, low-pass filtering was applied to reduce background noise and high-pass filtering was applied to highlight the objects of interest which are delineated from the background as areas of rapidly changing height or phase.

Size Exclusion Chromatography (SEC)

SEC was performed as before (5). Sample injection volume was 200 μL , mobile phase was 0.05 M NaNO_3 , flow rate was 0.7 mL/min. Columns were thermostatted at 45°C by immersing them in a water bath.

The chromatography system consisted of a degasser, autosampler, in-line membrane filter, pre- and post column set guards, three chromatography columns, multi angle laser light scattering detector (MALLS), viscometer detector and refractive index detector. The serially placed chromatography columns were, two PL- Aquagel OH-60 columns and one PL-Aquagel OH-40 (Polymer Laboratories, Amherst, MA). These columns have been found to fractionate over the range 1.1×10^7 to 1×10^4 g/mole for pectins. (10) Each column is 7.5 mm I. D. \times 300 mm length.

The electronic outputs from the MALLS DRI and DP detectors were processed by Viscotek TriSec 3.0 GPC software. and with ASTRA™ (v. 4.90.08) software. A dn/dc value of 0.130 mL/g at 633 nm was determined using acid extracted lime pectin as the source. The method for measuring dn/dc was described previously (11).

Results and Discussion

Pectin Structure Visualized by Electron Microscopy

Rotary shadowed micrographs of pectin isolated from peaches and imaged from dilute solution revealed for the first time that pectin dissolved in water at 10 $\mu\text{g/mL}$ formed circular shaped networks (Figure 1A) (6). Furthermore, these

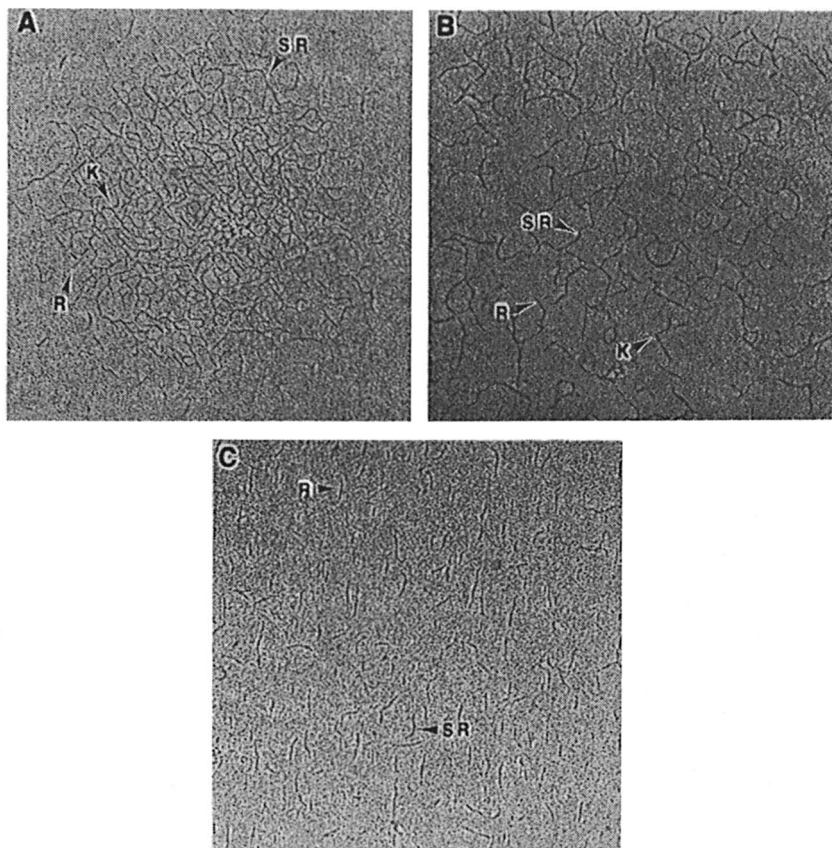


Figure 1. Rotary shadowed peach pectins which were dried and replicated from (A) water, (B) 5 mM NaCl, (C) 50% aqueous glycerol. (R) rods, (SR) segmented rods, (K) kinked rods. (Reproduced from reference 6).

networks were partially broken down into clusters or into branched structures when peach pectin was imaged from 5 mM NaCl (Figure 1B). Imaging peach pectin from 50 mM NaCl or 50% aqueous glycerol (Figure 1C) reduced the clusters to linear objects in the form of rods (R), kinked rods (K) or segmented rods (SR). Closely examining (Figure 1A) reveals that these linear objects (R, K, SR) are integrated into the network. If peach pectin dissolved at 100 $\mu\text{g}/\text{mL}$ is imaged from water, sheets of networks can be imaged (Figure 2) (12).

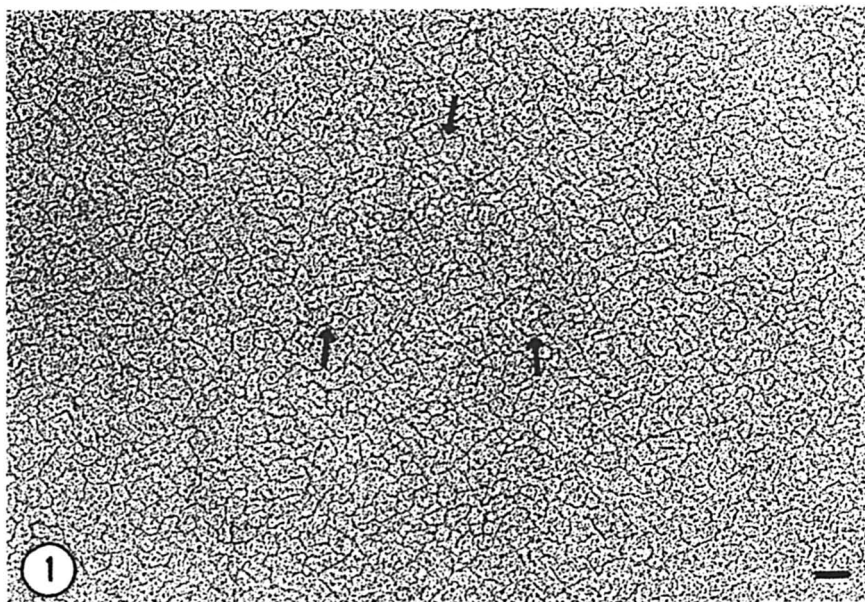


Figure 2. Portion of a sheet of pectin network dried from water at high concentration (100 $\mu\text{g/mL}$). Arrows indicate interconnected subunits of rodlike, segmented rodlike, and kinked rodlike components which define open polygonal spaces. (Reproduced from reference 12).

The ability NaCl, or glycerol to dissociate pectin networks into linear objects leads one to conclude that pectin networks are held together largely by hydrogen bonds and that the linear objects may be considered to be hydrogen bonded subunits of the networks. The multimodal nature of pectin molar mass or size distributions obtained by HPSEC experiments could be construed as evidence for the sub unit structure of pectin (2, 6, 13, 14, 15).

Physico-Chemical Properties of Pectin in Solution

Measurements were made in dilute solution to determine if these would be consistent with results from microscopic imaging. Previously, we have developed a microwave flash extraction method to extract pectin from orange and lime albedo (3, 5). In the course of this method development, we measured the effect of heating time on pectin structure using HPSEC with on-line multi-angle light scattering and viscosity detectors. In Figure 3 (5) we have plotted the effect of heating time on the weight average molar mass (M_w), intrinsic viscosity ($[\eta_w]$) and Z-average radius of gyration (R_{gz}) of pectin extracted from lime

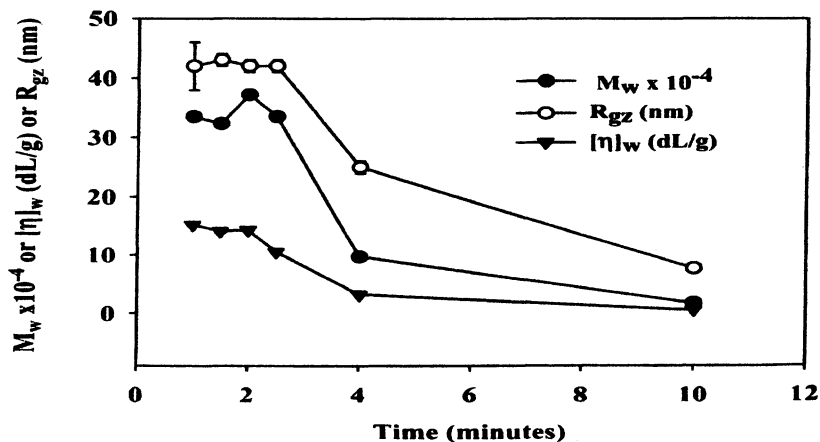


Figure 3. Effect of heating time on lime pectin properties. (Reproduced from reference 5).

albedo. The values of these three properties decreased with time. Molar mass distributions and Mark-Houwink plots for lime pectin at various heating times are in Figure 4 and Figure 5, respectively. Similar plots were obtained for pectin extracted from orange albedo (3).

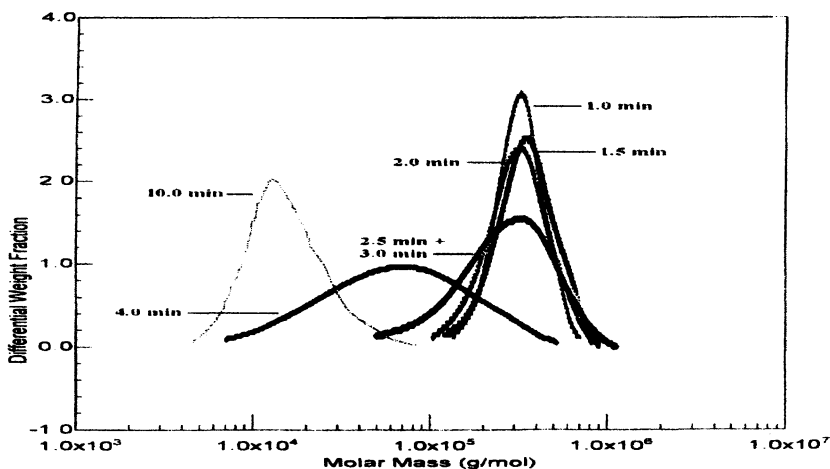


Figure 4. Overlaid differential weight fractions against molar mass for lime pectins heated during extraction from 1 to 10 min. (Reproduced from reference 5).

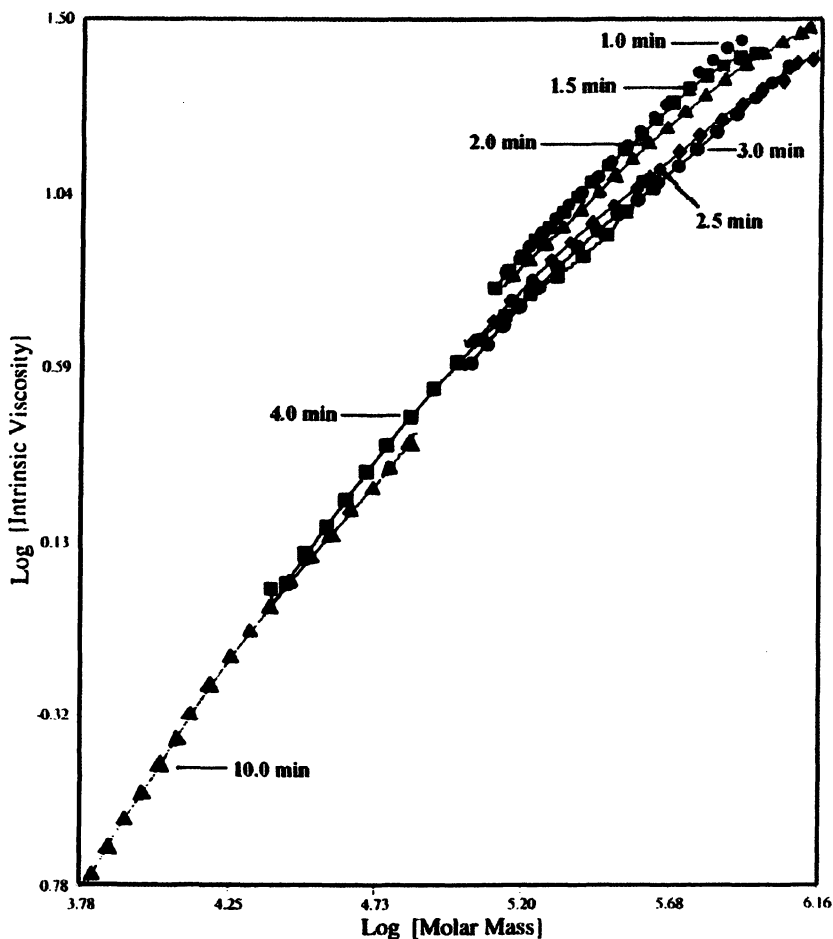


Figure 5. Overlaid Mark-Houwink plots for lime pectins heated during extraction from 1 to 10 min. (Reproduced from reference 5).

The results of some of the properties obtained from HPSEC experiments for pectin from lime and orange are in Table I. For both kinds of pectin, the slopes of $\log [\eta]$ against $\log M$ (e.g. Figure 5) for different heating times are found in columns under the heading "a". These "a" values are termed Mark-Houwink (M-H) exponents and are a measure of the molecular compactness of a macromolecule. The units of $[\eta]$, the ordinate of the M-H plot, are dL/g or volume/unit mass whereas the units of the abscissa are molar mass. Thus the slope or "a" value for the M-H plot is a measure of the change in molecular

volume with molar mass. The value of $[\eta]$ for a hard sphere is proportional to $M^{1/3}$, a random coil is proportional to $M^{1/2}$, and a rod is proportional to $M^{1.8}$. Thus a hard sphere is more compact than a random coil which in turn is more compact than a rod because in each case the volume changes more slowly with molar mass. Nevertheless, the compactness of a molecule may not uniquely define its shape because it is possible that two or more shapes with equal molar masses could occupy the same volume. Typically, the smaller the M-H value, the more compact the molecule is and conversely the larger the M-H value, the less

Table I. Comparison of Molecular Properties of Pectin from Lime and Orange Albedo

Time ^b min	Lime				Orange ^a			
	M_w $\times 10^{-3}$	R_{gz}^c nm	η_w dL/g	a^d	M_w $\times 10^{-3}$	R_{gz}^c nm	η_w dL/g	a^d
1	335(2) ^e	42(4)	15.2(0.1)	0.78				
1.5	323(1)	43(1)	14.1(0.3)	0.77				
2	372(4)	42(1)	14.3(0.1)	0.73				
2.5	335(8)	42(1)	10.5(0.1)	0.71	394(22)	38(1)	10.8(0.1)	0.71
3	311(10)	38(4)	9.5(0.1)	0.74	373(11)	33(1)	7.7(0.5)	0.63
4	97(1)	25(1)	3.2(0.1)	0.94	132(11)	35(5)	4.8(0.1)	0.75
5					58(7)	19(1) ^f	1.8(0.2)	0.98
6					51(5)	15(1) ^f	1.4(0.1)	0.99
10	17(1)	7.7(0.2) ^f	0.55(0.02)	1.18				

^aData taken from reference 3.

^bExtraction time.

^cRadius of gyration, z average

^dMark-Houwink exponent.

^eStandard deviation of triplicate analysis.

^fDetermined by LS/Viscometry method.

compact the molecule is. Thus a random coil in an ideal solution will have an M-H value of 0.5 whereas a rod-like molecule will have M-H values greater than 1 (16). M-H exponents are plotted against M_w values in Figure 6 for lime and orange pectin. For both kinds of pectin, the M-H exponent tends to increase with decreasing molar mass. This behavior indicates increasing compactness with decreasing molar mass which is consistent with the progressive dissociation of a network into its component parts.

We note that the M-H plots are concave down in Figure 5, so that the M-H exponent is an average value for two or more shapes. In the case of orange pectin, the M-H plots show even more downward concavity than lime pectin

(3, 17). Integration by parts of the chromatograms revealed that the high molar mass end may have M-H exponents ranging from 0.14 to 0.45 whereas the low molar mass end may have M-H exponents ranging from about 0.92 to 1.57. M-H exponents for the high molar mass end are consistent with network or with branched structures such as shown in Figure 1A or 1B whereas M-H exponents for the low molar mass end are consistent linear structures shown in 1C. Thus we conclude that hydrogen bond breaking solvents or heating pectin in an acid environment will dissociate network or branched structures held together by hydrogen bonds.

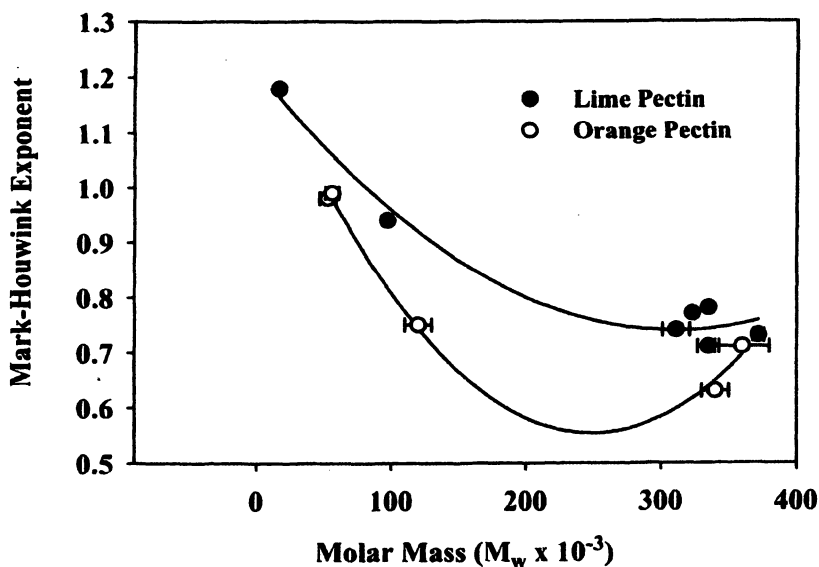


Figure 6. Change in shape as function of time of heating as related to molar mass changes (Reproduced from reference 5).

Structure of a Pectin High Methoxy Sugar Acid Gels (SAG) Visualized by Atomic Force Microscopy (AFM)

Height and phase-shift images of atomic force micrographs of a SAG made from commercial citrus pectin (CCP) are shown in Figure 7A and 7B respectively. Comparable images were obtained from lime (LAP) and orange albedo pectin (OAP) (9). The interstitial fluid (yellow areas) in the height image is above the strands (brown areas). The strands (yellow areas) in the phase-shift image exhibit stronger tip-sample interactions than the interstitial fluid (brown areas.) Because pectin gels are inherently sticky, the sample-tip interaction is

expected to be an attractive force. Thus the AFM image is one of a network of sticky strands sitting in a trough surrounded by a viscous interstitial fluid. In Figure 8A-C are strands electronically thinned (i.e. filtered) by an algorithm (Image-Pro Plus 2, Media Cybernetics, Silver Spring, MD) which iteratively removes pixel layer by layer until only a single layer of pixels remains. Phase images such as that of Figure 7B are the source images for Figure 8. Possibly, these images reveal the pectin framework upon which sugar is adsorbed. Measurements of strand and pore areas for the entire field revealed that for CCP, OAP and LAP, strands comprised 56%, 57% and 54% of the field respectively (9). Considering that the ratio of sucrose to pectin in the gel is about 260:1 (w/w) it is rather unlikely that strands of pectin could take up that much area of the gel unless sucrose was adsorbed to pectin strands. It should be noted that the geometry of probe tips is such that the width of strands in crevices tend to be underestimated whereas high pore areas tend to be overestimated (9). Therefore the relative strand area may be even greater than given above.

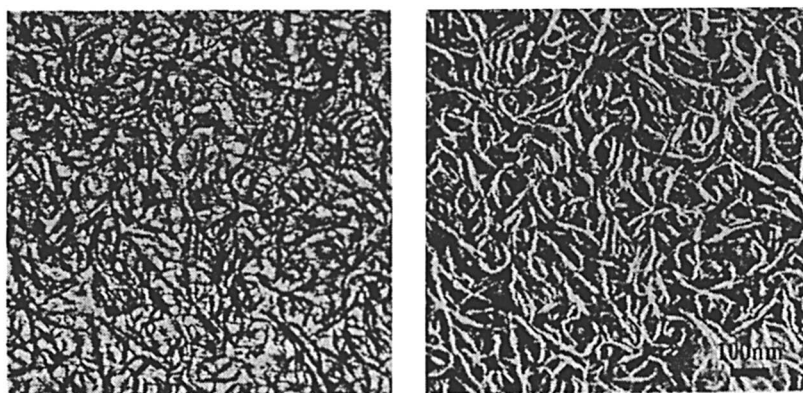


Figure 7. Matching images of (A) height and (B) phase-shift of an acid-gel made from commercial citrus pectin (CCP). The organization of thin clefts or depressions in the surface of the gel in (A) corresponds to the arrangement of phase-shifted or adhesive areas in (B). (Reproduced from reference 9).
(See page 3 of color inserts.)

Visual comparison of Figures 8A-C revealed that the density of pectin chains increased somewhat in the order LAP>OAP>CCP. Interestingly, the maximum value of gel strength at constant amount of pectin and sucrose increased in the same order (5).

It is pertinent to the objective of this research that the partially formed network structures visible in Figure 8 (particularly, Figure 8A) are similar to the clusters or branched structures visualized in 5 mM NaCl by rotary shadowed



Figure 8. Electronically thinned strands from phase images of gels. (A) commercial citrus pectin, CCP; (B) orange albedo pectin, OAP; (C) lime albedo pectin, LAP. (R) rods., (SR) segmented rods, (KR) kinked rods. (Reproduced from reference 9).

electron micrographs (see Figure 1B). Furthermore, visible in Figure 8 are the rod, kinked rod and segmented rod structures visible in Figure 1C. Moreover, these structures visualized by microscopy are consistent with the trend in Mark-Houwink exponents obtained with time of heating experiments.

Conclusions

We may conclude from this work that the partially formed or open network structure visualized in Figure 1B is a fluid precursor to the pectin gel structure visualized in Figure 8. Also the large quantity of sucrose present is responsible for fixation of the pectin into an open gel network. The mechanism by which this fixation occurs is akin to preferential solvation of the pectin backbone with sucrose. In addition, the unique property of pectin SAGs to form pressure sensitive, spreadable gels is probably a result of the network being held together by weak secondary forces, namely hydrogen bonds and possibly hydrophobic interactions (18).

References

1. Carpita, N.; McCann, M. C. In *Biochemistry and Molecular Biology of Plants*; Buchanan, B., Ed.; American Society of Plant Physiologists: Rockville, MD, 2000; pp 52-108.
2. Fishman, M. L.; Levaj, B; Gillespie, D.; Scorza, R. *J. Amer. Soc. Hort. Sci.* **1993**, *118*, 343-349.
3. Fishman, M. L.; Chau, H. K.; Hoagland, P.; Ayyad, K. *Carbohydr. Res.* **2000**, *323*, 126-138.
4. Yamada, H. In *Pectins and Pectinases*; Voragen, A. G. J., Visser, J., Eds.; Elsevier: Amsterdam, 1996; pp 173-190.
5. Fishman, M. L.; Chau, H. K.; Coffin, D. R.; Hotchkiss, A. T. In *Advances in Pectin and Pectinase Research*; Voragen, F., Schols, H., Visser, R., Eds.; Kluwer Academic Publishers: Dordrecht, 2003; pp 107-122.
6. Fishman, M. L.; Cooke, P.; Levja, B.; Gillespie, D. T.; Sondey, S. M.; Scorza, R. *Arch. Biochem. Biophys.* **1992**, *253*, 253-260.
7. Tullia, M. C. C.; Filisetti-Cozzi, T; Carpita, N.C. *Anal. Biochem.* **1991**, *197*, 157-162.
8. Voragen, A. J. G.; Schols, H. A.; Pilnik, W. *Food Hydrocolloids* **1986**, *1*, 65-70.
9. Fishman, M. L.; Cooke, P. H.; Coffin, D. R. *Biomacromolecules*, **2004**, *5*, 334-341.

10. Fishman, M. L.; Chau, H. K.; Kolpak, F.; Brady, J. J. *J. Agr. Food Chem.* **2001**, *49*, 4494-4501.
11. Fishman, M. L.; Cescutti, P.; Fett, W. F.; Hoagland, P. D.; Chau, H. K. *Carbohydr. Polym.* **1997**, *32*, 213-221.
12. Fishman, M. L.; Cooke, P.; Hotchkiss, A.; Damert, W. *Carbohydr. Res.* **1993**, *248*, 303-316.
13. Fishman, M. L.; Gillespie, D. T.; Sondey, S. M.; *Carbohydr. Res.* **1991**, *215*, 91-104.
14. Fishman, M. L.; El-Atawy, Y. S.; Gillespie, D. T.; Hicks, K. B. *Carbohydr. Polym.* **1991**, *15*, 89-104.
15. Fishman, M. L.; Gross, K. C.; Gillespie, D. T.; Sondey, S. M. *Arch. Biochem. Biophys.* **1989**, *274*, 179-191.
16. Mays, J. W. In *Modern Methods of Polymer Characterization*; Barth, H. G.; Mays, J. W., Eds.; John Wiley & Sons: New York, 1991; pp 227-269.
17. Fishman, M. L.; Walker, P. N.; Chau, H. K. *Biomacromolecules*, **2003**, *4*, 880-889.
18. Oakenfull, D. G. In *Chemistry and Technology of Pectin*; Walter, R. H., Ed.; Academic Press: San Diego, CA, 1991; pp 87-108.

Chapter 14

Extraction and Characterization of Pectin from Novel Sources

**Juan C. Contreras-Esquivel^{1,2,*}, Judith D. Espinoza-Pérez²,
Julio C. Montanez², Ana V. Charles-Rodríguez^{1,2},
Jacqueline Renovato², Cristóbal N. Aguilar¹,
Raúl Rodríguez-Herrera¹, and Louise Wicker³**

¹Food Research Department, School of Chemistry, Universidad Autónoma de Coahuila, P.O. Box 252, Saltillo, Coahuila 25000, Mexico

²Research and Development Center, Coyotefoods, Biopolymer and Biotechnology Company, Simón Bolívar 851-A, Saltillo, Coahuila 25000, Mexico

³Department of Food Science and Technology, University of Georgia, Athens, GA 30602 (lwicker@uga.edu)

*Corresponding author: jcontrer@usquim.uadec.mx

Jicama, cactus and tejocote pulps, prickly pear and mango pomaces were tested as new alternative raw materials for pectin extraction. Prior to selecting the extractant solution, a preview step was suggested the characterization of the raw material using FTIR spectroscopy. Knowing its fingerprint map, it can be inferred which extractant solution can be used. An autoclaving method was applied for 10 min to extract pectin using water, sodium hexamethaphosphate and citric acid. Pectin yield was calculated on a dry weight basis. For jicama pulp, cactus pulp and prickly pear pomace, the highest yields were obtained using sodium hexamethaphosphate. The maximum pectin yield obtained was 40% with jicama pulp. Infrared spectroscopy analysis showed that pectic substances extracted with sodium hexamethaphosphate under described conditions had a low degree of methoxylation. Mango pectin was extracted obtaining high yields (39%) with citric acid. The highest extraction yield of tejocote pectin was 20% using citric acid.

Pectin is a heterogeneous complex polysaccharide present in plant cell walls, having important roles in the plant physiology. Its composition varies with the source and the conditions applied during isolation. The major constituents are the linear sequences of 1,4-linked α -D-galactopyranosyluronic acid with some carboxyl groups esterified with methanol. The proportion of methyl-esterified galacturonic acid subunits influences the functional properties of the pectin. Commercial pectins are divided into low-methoxyl and high-methoxyl pectins (1,2). Pectic structure involved two domains: galacturonans (homogalacturonan, xylogalacturonan and rhamnogalacturonan type II) and rhamnogalacturonan type I. Detailed information and elaborate models of pectin structure can be found in recent reviews (3).

Pectic substances are important in food, medical and cosmetic industries. Pectins are mostly used by the food industry in the jam, marmalades and jelly manufacture. They are applied in confectionery gums, and in a minor level in sauces, dressings and flavored syrups production. Also they are used as stabilizers of fermented and acidified milks, fruit yogurts and related foods. In the cosmetic industry, they act as protective colloids in cosmetic emulsions. Finally in the medical area, they are used in the manufacture of surgical dressings (4). Pectin production depends on a number of factors, including access to raw materials, water, energy and effluent disposal at reasonable prices (5). Selection of alternative sources for pectin production depends on quantity, quality, availability, endogenous physicochemical characteristics and specific required applications. The commercial value of the rich agroindustrial wastes in pectin substances depends on great extent of the quality and quantity of pectin that can be extracted. Their classification also allows selecting the extractant to carry out mixtures and obtain uniformity in the product (6).

Current raw materials for commercial pectin extraction include the solid by-products generated by the juice industry, especially of citrus fruits (peel from lemon, mandarin, orange and grapefruit) and apples (residue or baggase). Other minor pectin sources are: the pulp of sugar beet and sunflower. The commercial extraction of sunflower pectin has been reported in China, Germany and India (7), while the pectin production starting from sugar-beet pulp has been described in the former Soviet-Union and Germany (8). Pectin extraction from alternative materials not only helps to reduce the costs of production of diverse nutritious products, but also it allows the utilization of agroindustrial residuals, generally considered as environmental pollutants. To consider a material as an alternative source of pectin, it must have a pectin yield superior to 10% on a dry weight basis (9). In Mexico, commercial pectin is obtained from lime or lemon pomace, meanwhile alternative raw materials such as coffee, mango, passion fruit, cactus (nopal and prickly pear) wastes and tejocote pulp are being considered (10).

In conventional pectin extraction, hot acid solution (pH 1.0-2.5; temperature 60-90 °C) is frequently applied to extract highly methoxylated pectin from the cell wall (5). Technologically, pectic substances can be extracted by chemical, biological or physical methods (Figure 1).

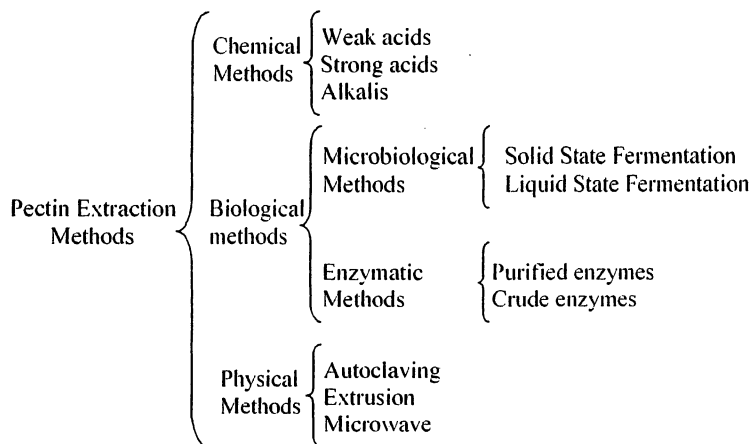


Figure 1. Pectin extraction methods

Currently commercial pectins are extracted by chemical methods followed by different modifications depending on the application to which they are directed. The chemical structure of acid-extracted pectins has been extensively investigated (11). Disadvantages of the chemical pectin extraction methods includes environmental pollution and susceptibility of extraction reactors and equipment to corrosion (12). Biological (fermentation or enzyme) methods are considered as alternative procedures for releasing pectin because these processes are non-polluting and the reaction conditions are not severe. For the enzymatic extraction of pectin, diverse polysaccharidases (i.e. polygalacturonases, xylanases, cellulases, rhamnogalacturonases, etc.) have been employed either as purified enzymes or crude extracts (13,14). Biological methods are subdivided in microbiological (fermentative) and enzymatic processes (13-16). Solid (17) and liquid (18) extraction systems have been developed. Microbiological extraction releases pectin by microorganisms that produce endopolygalacturonases. But an energy increment is generated in the bioreactor to maintain the operational conditions, such as mixing or aeration. In addition, viscosity increases as the pectin is extracted. This extraction requires long times (more than 36 h). Enzymatic extraction is used as an analytical tool, although from both biological methods, this one has great industrial potential.

Pectin extraction enzymes of microbiological origin are used with commercial purposes, already they are purified or in raw extracts coming from yeasts, bacteria or filamentous fungi. Due to the structural knowledge of enzymes, they can be applied in a specific way to permit the release of pectins of high molecular weight. The enzymatic method is expensive due to the enzymatic isolation and to the long extraction time required to solubilize the pectin. The high costs are due mainly to the catalyst, however the search of new enzymes and their production for genetic technology would reduce significantly the operation costs (19). Among physical methods to extract pectin, autoclaving is a recent development with the great advantage of reduced extraction time from 60 min to 5 or 10 min (20) and is a clean extractant method in combination with citric acid (21). In extrusion, water is used to extract pectins of molecular weight similar to those extracted with acids (22-24). Also microwave energy has been applied recently to the pectin extraction from diverse raw materials producing numerous papers, which report the optimum conditions of this process. Similar to extrusion, microwaves processes offer a reduction on time extraction, high yield and high quality of the pectin extraction (25-27). In this chapter, we apply the autoclaving method to extract pectins from novel raw materials and determine the yield and some physicochemical characteristics of the extracted pectins.

Materials and Methods

Raw materials

Tejocote (Flortex) and nopal powder were purchased from Alimenta S de R.L., Michoacán, Mexico and IDEAL Corporation, S.A. de C.V., Mexico, respectively. Mango, prickly pear and jicama were acquired in the local market of the city of Saltillo, Coahuila, Mexico. Lime pomace was procured by Danisco Ingredients, Mexico. Pectic galactan from potato and high methoxyl citrus pectin were purchased from Megazyme, Ireland and CP Kelco, USA, respectively.

Preparation of pomaces

The mango fruits were washed thoroughly in a running tap water. The peels were cleaned manually with a knife to remove the adhering pulp and steam blanched for 5 minutes. Blanched peels were washed twice with tap water and twice with distilled water to leach water soluble solids. After that, they were dried in an oven (60 °C for 12 h). Jicama roots were washed, peeled and cut into cubes of 2×2×1.5 cm (28). The juice was obtained using an industrial juice

extractor (Cafeteras Internacionales SA de CV, Mexico). The remainder was pressed to eliminate residual juice, and then it is was steam blanched by 15 minutes, leached twice with distilled water and washed three times with 95% ethanol, pressed and dried at 40 °C. Prickly pear pomace was prepared according to Terrazas *et al.* (29)

Pectin extraction and downstream processing

The pomace was mixed with agent extractant solution (citric acid, pH 2.3, 1.0%, sodium hexamethaphosphate 1.0% or water) and placed in a glass vessel covered with aluminum foil. The ratio of pomace to extractant was 1:40 to lime, mango, nopal, prickly pear, and the ratio was 1:75 for jicama. Pomaces were autoclaved for 10 min at 121°C (2 atm) and cooled in an ice-water bath. After extraction for a given period of time, insoluble material was separated by sequential filtration through a muslin cloth and Whatman filter paper No. 1 under vacuum. The pectin was precipitated by adding 2 volumes of 95% ethanol to 1 volume of extract. The precipitate was recovered by filtration, dried at 40°C, milled with a mortar and stored at room temperature until use.

Fourier transform infrared (FTIR) spectroscopy and molecular characterization of mango pectins

A FTIR spectrometer (Spectrum GX, PerkinElmer, Boston, MA) equipped with a Golden-gate single reflection attenuated total reflectance (ATR) accessory (SensIR Technologies, part number 071-1305) placed with the sample compartment was used for the powders and pectin analysis. The FTIR spectral regions used were 4000-670 cm^{-1} . Spectra were collected by co-adding 35 scans at a resolution of 4.0 cm^{-1} . The weight-average molecular weight (M_w) and radius of gyration (R_G) were examined by gel permeation chromatography in-line with multi-angle light-scattering measurements and reflective index detectors (30).

Results and Discussion

Pomace characterization by FTIR spectroscopy

Before selecting the extractant solution, a preview step is suggested, the characterization of the raw material using FTIR spectroscopy. Knowing its fingerprint map, it can be inferred which extractant solution can be used. For example, for a pectin linked by covalent bonds, the use of an acid must be

selected and in the case of a pectin ionic linked, chelating agents such as sodium hexamethaphosphate is recommended. FTIR spectroscopy has been extensively applied to determine the intensity of specific bonds and functional groups within a polymeric structure (31,32) and to plant cell wall analysis (33,34). However, very few studies have been applied FTIR to examine characteristics in the raw materials for pectin industry (35). For this reason, in the present work, FTIR was used to generate a specific spectral fingerprint for the complex plant cell walls under investigation. The spectral fingerprint could be used to estimate the extractant solution required to hydrolyze either covalent or ionic linkages. In addition, we generated a spectral fingerprint for a commercial pomace (lime) widely used in the pectin industry and compared it to pectins extracted from novel alternative raw materials (tejocote and nopal pulp, mango, jicama and prickly pear pomaces) under study. In Figure 2, FTIR spectra for both commercial and alternative pomaces are shown. The vibrational characteristics of mono- and polysaccharides generally dominate the region between 1200 and 900 cm^{-1} because of the C-O stretch bonds related to sugars. Also, the carbonyl absorption bands at 1650 and 1750 cm^{-1} belong to free and esterified carboxyl groups, respectively. FTIR spectrum from Mexican lime pomace, mango pomace and tejocote pulp were different from prickly pear pomace, nopal pulp and jicama pomace. The FTIR spectra revealed that all samples were enriched in wavenumbers characteristic of uronic acids. The main differences between raw materials were observed in the region of 1750 and 1650 cm^{-1} . Tejocote pulp and mango pomaces showed similarity with the Mexican lime pomace fingerprint pattern, indicating the presence of an endogenous pectin with a higher methoxyl content (1750 cm^{-1}). Whereas the absence of absorption in the region of 1750 cm^{-1} in the samples of jicama, nopal and prickly pear pomaces denoted the absence of methoxyl groups, indicating that these materials have endogenous low methoxyl pectins. Prickly pear pomace and nopal pulp showed an intense band at 1650 cm^{-1} assigned to carbonyl, acetyl and feruloyl groups (32,36).

Pectin yields from novel sources

Based on the analysis of the FTIR spectra of the novel alternative raw materials, we established the type of extractant solution. Mexican lime pomace, tejocote pulp and mango pomace were extracted with water or citric acid because of their higher methoxyl content. Meanwhile jicama, nopal and prickly pear were extracted with sodium hexamethaphosphate due to their low methoxyl content. The next step was to realize the autoclaving extraction process where the effect of the type of extractant solution, its concentration and the time extraction were studied. Values of pectin yields from the studied novel sources are summarized in Table I.

Table 1. Pectin yields from alternative and commercial raw materials for pectin industry

<i>Pectin Source</i>	<i>Extractant</i>	<i>Concentration (%)</i>	<i>Extraction time (min)</i>	<i>Pectin yield (%)</i>
Mango pomace	Water	-	10	25.97 ± 1.01
	Citric Acid	0.5	10	22.82 ± 0.46
	Citric Acid	1.0	10	28.00 ± 4.11
Tejocote pomace	Citric Acid	1.0	20	39.05 ± 0.61
	Water	-	10	12.59 ± 1.25
	Citric Acid	1.0	10	19.83 ± 2.77
Prickly pear pomace	Water	-	10	0.0
	Sodium hexamethaphosphate	1.0	10	38.80 ± 1.06
Nopal pulp	Water	-	10	0.0
	Sodium hexamethaphosphate	1.0	10	46.00 ± 2.13
Jicama pomace	Water	-	10	0.0
	Sodium hexamethaphosphate	1.0	10	40.00 ± 1.25
Lime	Citric Acid	1.0	10	28.13

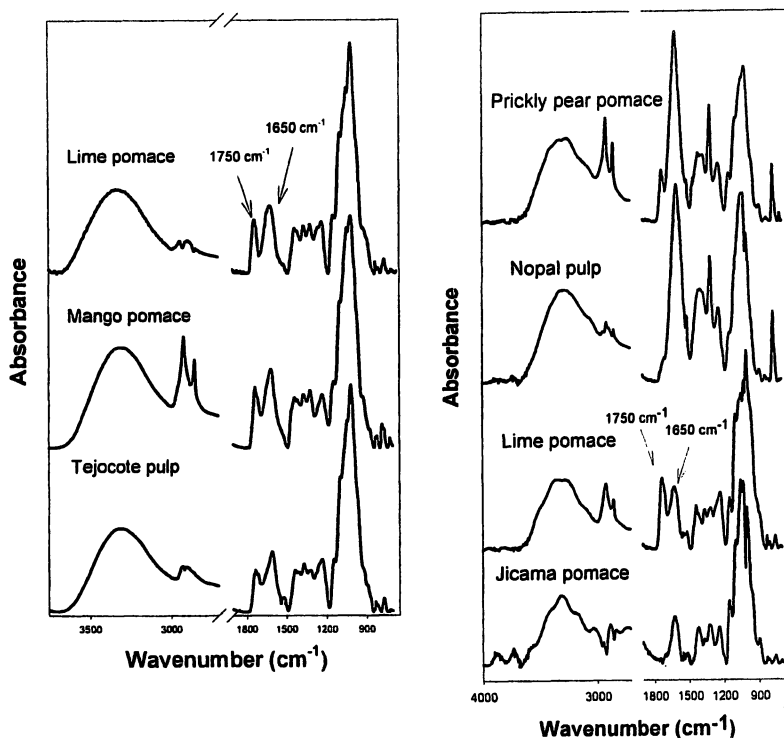


Figure 2. FTIR spectra of pomaces. The carbonyl absorption bands at 1650 and 1750 cm^{-1} belong to free and esterified carboxyl groups, respectively.

For mango pomace, there was not a significant difference between the obtained yield from the treatments with water and citric acid 0.5% for 10 min, but yield increased when pomace was extracted with 1% citric acid for 10 min. The treatment with citric acid 1.0% for 20 min had the highest yield (39.05%). Similarly, mango pectin yields (5.8–24%) were obtained by Kratchanova *et al.* (37) by using an acid extraction. Tejocote pulp yield was higher (20%) when 1% citric acid solution for 10 min was applied. There are only some reports related to tejocote pectin extraction, by example Pedroza-Islas *et al.* (38) worked with an acid extraction obtaining a yield of 22%. Prickly pear pomace pectin showed a high yield (39%) using a sodium hexamethaphosphate solution 1% by 10 min and not extraction was realized when water was used. Low prickly pear pectin yields were found by Forni *et al.* (39) using also an acid

prickly pear pectin yields were found by Forni *et al.* (39) using also an acid extraction, whereas the yield that we obtained (39%) is higher from that obtained for commercial lime pomace (28%). By the other side, at nopal pulp and jicama pomace, water did not promoted the pectin extraction. But both raw materials were analyzed using sodium hexamethaphosphate 1% by 10 min, the resulted yields were of 38 and 46%, respectively. For lime, only citric acid 1% by 10 min was used finding a pectin yield similar to that from mango pomace (26% with water) at the same conditions. From all these results it is important to remark that our proposition of characterizing the pomaces generated an advantages that was reflected in the high yields extraction. By this way, those raw materials that showed FTIR spectra free of methoxyl groups at the carbonyl (1750cm^{-1}) presented higher pectin yield extraction when sodium hexamethaphosphate was used instead of water. Comparing the yield extraction generated at this report with those from the literature (36-39) it can be established that, although in some cases the yields extraction were similar, our proposal extraction method extraction does not present the disadvantages of the acid extraction method (pH 1.5, $85\text{ }^{\circ}\text{C}$, 60 min) such as the longer extraction time and the use of a corrosive and pollutant extractant solution.

Pectin characterization

The FTIR technique also was used successfully to characterize partially the extracted pectins from the different raw materials (40). A pectin FTIR spectra has characteristic regions: O-H stretching band ($3100\text{-}3600\text{ cm}^{-1}$) in which the absorption is due to the inter hydrogen bonding of the galacturonic acid polymer; C-H stretching bands ($2800\text{-}3000\text{ cm}^{-1}$) that includes CH, CH₂ and CH₃ stretching and bending vibrations; as well as the region $1200\text{-}1800$ the state of carboxylic groups (40-42). However, the region between $1000\text{-}2000\text{ cm}^{-1}$ identified the major chemical groups in pectins and provide structural information that could be used to compare different types of pectin (43-45).

The spectra in Figure 3 illustrate characteristics of novel and commercial pectins. Comparing spectra of jicama and prickly pear pectins with Mexican lime pectin a noticeable decrease of the carboxyl peak was noticed at 1750 cm^{-1} . This decrease indicated the absence of methyl esterification. Whereas the nopal sample did not show a typical FTIR spectral pattern of pectin due to the absence of absorption in the region of 1750 and 1650 cm^{-1} . By this reason, the nopal polysaccharide spectrum was compared with the spectra of a purified pectic galactan from potato and both spectra showed great similarity (data non-shown).

This result suggested that the polysaccharide extracted from nopal pulp was not pectin. At this point, it is also important to mention that pectic galactan sources are limited and the yields are lower like in tepary bean (3.61%) (46). As mentioned earlier, yield of nopal pectin galactan was of 46%. Mexican lime pectin showed a typical FTIR pattern of high methoxyl pectin. No significant differences were observed in the FTIR spectra of mango and tejocote pectin compared with lime as is shown in Figure 3. When the tejocote pectin was extracted with citric acid or water, the FTIR spectra did not show difference (data non-shown). This demonstrates that the methoxyl groups present in extracted tejocote pectin was not affected during treatment with citric acid under autoclaving process. The same profile of FTIR spectra was observed in mango pectins under the different extraction conditions. Contreras-Esquivel *et al.* (21) demonstrated that the methoxylation degree of passion fruit pectin did not decrease with an increase in extraction time by autoclaving. Jicama pectin showed a typical FTIR spectra profile of a low methoxyl pectin. The jicama pectin showed a contamination with starch, which may account for the higher pectin yield. As a consequence, to obtain a pure pectin it is advisable to eliminate the jicama starch either by physical, chemical or enzymatic methods. The FTIR pattern of low methoxyl pectin was also observed for prickly pear pectin.

Molecular characterization of mango pectin

Figure 4 is a plot of differential molar mass calculated from gel permeation chromatography-multi-angle light scattering (GPC-MALLS) detector of the commercial citrus pectin and the mango pectin. It can be observed that commercial citrus pectin revealed the same pattern of mango pectin extracted with water by autoclaving at the differential weight fraction versus molar mass curves. Mango pectin showed a similar homogeneity within the same interval at the size of molecular weights of the citrus pectin, which is what the industry requires. As shown in Figure 4a, the molecular weight of commercial citrus pectin and mango pectin extracted with water were inside the interval of 2.84×10^5 g/mol and 2.80×10^5 g/mol, respectively, which were agreed with the absolute molecular weight interval for commercial citrus pectin reported previously by Corredig *et al.* (30). Oosterveld (47) also obtained by the autoclaving method a homogeneous molecular weight distribution of polysaccharides extracted from sugar bean pulp. While mango pectin sample extracted with citric acid at 0.5% showed a heterogeneity distribution of molecular weights indicating an important depolymerization by effect of acid

(Figure 4b). The region of low distribution molecular weight showed a minor dispersion that those of the high distribution molecular weight region.

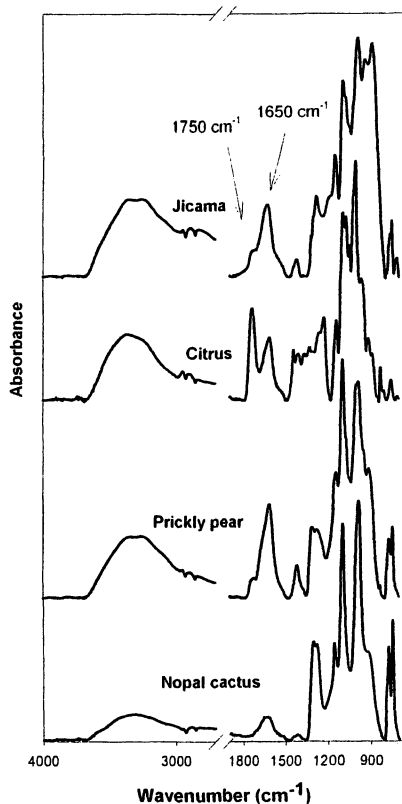


Figure 3. FTIR spectra of non-traditional pectic polysaccharides extracted by autoclaving methods compared with commercial citrus pectin

As a result, it is recommended to characterize this region specifically in order to know in what way the citric acid modify the structure of the pectin. Passion fruit pectin has been extracted by autoclaving using citric acid (1%), nevertheless homogeneous polymers were obtained (21). Kim *et al.* (48) described the decrease of molecular weight by GPC-MALLS attributed to the chemical depolymerization when mandarin pectin was extracted with citric acid instead of water. The radius of gyration of pectins depends of variables such as

mobile phase; method of purification; chemical modification and methoxyl content (48). The radius of gyration (R_G) of mango pectin (R_G 33.1 nm) was similar to that of citrus pectin (R_G 27.8 nm) (49). Fishman *et al.* (50) determined the radius of gyration of pectin extracted from lime by microwave heating under pressure, founding values of 42 nm with a time extraction of 3 min.

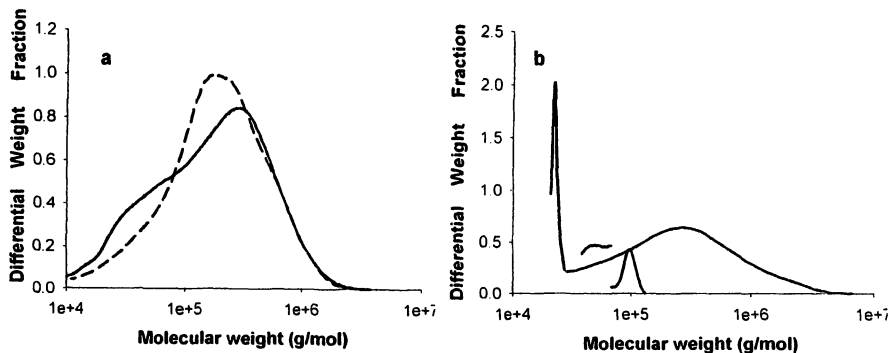


Figure 4. a) Molecular weight distributions of citrus pectin (long dash) and mango pectin extracted by 10 minutes with water (solid line), b) mango pectin extracted by 10 minutes with citric acid 0.5% (solid line).

The molecular characteristics of mango pectins extracted by autoclaving with water showed similarity with commercial citrus pectin. As a result, it is recommended to characterize this region specifically in order to know in what way the citric acid modify the structure of the pectin.

Conclusions

Jicama, mango, nopal, prickly pear and tejocote pomaces are raw materials of commercial relevancy in the pectin industry, since the quality and quantity of endogenous pectic polysaccharides that can be extracted is comparable with those obtained from citrus pomace. The present work demonstrated that FTIR spectroscopy could be used as an efficient tool to characterize the raw material for pectin industry, as well as to select the adequate chemical agent to release the pectic polysaccharides. Jicama and prickly pear pomaces can be considered

as new commercial sources of low methoxyl pectins, while mango and tejocote pomace can be considered as high methoxyl pectins. Nopal pomace is a raw material for arabinogalactan large-scale production.

Acknowledgments

Part of the work on this paper was done during the visit of JCCE and AVCR to the DFST at UGA. A joint international cooperation between National Council for Science and Technology (CONACyT), Mexico - and National Science Foundation (NSF), USA supported this research. This work also was partially supported by CONACyT-Fondos Mixtos Hidalgo (Project HGO-2002-C01-8736).

References

1. Rolin, C. In *Pectins and Their Manipulation*. Editors: Seymour, G.B.; Knox, J.P., Eds.; Blackwell Publishing Ltd: Oxford, UK, 2002; pp 222-241.
2. Voragen, A. G. J.; Pilnik, W.; Thibault, J.-F.; Axelos, M. A.V.; Renard, C.M.G. In *Food Science and Technology* (New York, NY, United States) 1995, 67, 287-339.
3. Voragen, F.; Schols, H.; Visser, R. In *Advances in Pectin and Pectinase Research*, 2003; (Kluwer Academic Publishers: Dordrecht, Neth.), pp.1-504.
4. Liu, L.S.; Kramer, W.H.; Fishman, M.L.; Hicks, K.B. *Recent Developments in Carbohydrate Research* 2003, 1, 181-194.
5. May, C.D. *Carbohydrate Polymers* 1990, 12, 79-99.
6. Francis, B.J.; Bell, J.M.K. *Trop. Sci.* 1975, 17, 25-44.
7. Wiesenborn, D. P.; Wang, J.; Chang, K. C.; Schwarz, J. G. *Industrial Crops and Products*, 1999, 9, 171-181.
8. Potter, R. S. *Process Biochem.* 1966, 1, 378-84
9. Mohamed, S.; Hasan, Z. *ASEAN Food J.* 1995, 10, 43-50
10. Contreras-Esquivel, J.C. In *La Investigación y Desarrollo Tecnológico*. CONACyT: Saltillo, Coahuila, México. 1995; pp:30-43.
11. Kravtchenko, T. P.; Voragen, A. G. J.; Pilnik, W. *Carbohydrate Polymers*, 1992, 19, 115-124.
12. Proverbio, E.; Bonaccorsi, L. M. *Engineering Failure Analysis*, 2002, 9, 613-620.
13. Hwang, J.; Pyun, Y. R.; Kokini, J. L. *Food Hydrocolloids* 1993, 7, 39-53.
14. Contreras-Esquivel, J.C.; Hours, R.A.; Aguilar, C.N.; Reyes-Vega, M.L.; Romero, J. *Arch Latinoam Nutr.* 1997, 47, 208-16.

15. Sakamoto, T.; Kawasaki, H.; Sakai, T. *Applied Biological Science* **1998**, *4*, 89-105.
16. Contreras Esquivel, J. C.; Voget, C. E. *J. Biotechnol.* **2004**, *110*, 21-28.
17. Khodzhaeva, M. A.; Turakhozhaev, M. T.; Kristallovich, E. L.; Abdullaev, N. D.; Azimkhodzhaeva, M. N. *Khimiya Prirodnikh Soedinenii* **1996**, *1*, 3-6.
18. Sakai, T.; Okushima, M. *Appl. Environ. Microbiol.* **1980**, *39*, 908-912.
19. Dalboge, H. *FEMS Microbiology Reviews* **1997**, *21*, 29-42.
20. Fishman, M.L.; Walker, P.N.; Chau, H.K.; Hotchkiss, A.T. *Biomacromolecules* **2003**, *4*, 880-889.
21. Contreras-Esquivel, J.C., Montañez-Saenz, J.C.; Brandelli, A.; Aguilar, C.N.; Renard, C.M.G.C. In *Proceedings of Annual Meeting XV Congreso Nacional de Polimeros*, Acapulco, Guerrero, Mexico. 2002; pp 684-685.
22. Ralet, M.-C.; Thibault, J.-F. *Carbohydr. Res.* **1994**, *260*, 283-96
23. Hwang, J.K. *Food Sci. Biotechnol.* **2001**, *10*, 455-459.
24. Shin, H.H.; Kim, C.T.; Cho, Y.J.; Hwang, J.K. *Food Sci. Biotechnol.* **2005**, *14*, 28-31.
25. Hou, C.; Liu, Z.; Chen, Z. *J. Zhengzhou Institute of Technology* **1999**, *20*, 8-11.
26. Fishman, M. L.; Chau, H. K.; Hoagland, P.; Ayyad, K. *Carbohydr. Res.* **2000**, *323*, 126-138.
27. Manabe, M.; Naohara, J.; Sato, T.; Okada, J. *Nippon Shokuhin Kogyo Gakkaishi* **1988**, *35*, 497-501.
28. Mudahar and Jen, *J. Food Sci.* **1991**, *56*, 977-980.
29. Terrazas, J.J.; Basurto-Ortiz, R.I.; Montañez-Saenz, J.C.; Aguilar, C.N.; Reyes-Vega, M.L.; Contreras-Esquivel, J.C. IFT 2002 Annual Meeting, Book abstract 15E.
30. Corredig, M.; Kerr, W.; Wicker, L. *Food Hydrocoll.* **2000**, *14*, 41-47.
31. Chauhan, S.; Aggarwal, P.; Karmarkar, K.; Pandey, K. *Holz als Roh-und Werkstoff*, **2001**, *59*, 250-253.
32. Tjeerdsma, B.; Militz, H. *Holz als Roh-und Werkstoff*, **2005**, *63*, 102-111.
33. Belton, P.; Kemsley E.; McCann, M.; Ttotis, S.; Wilson, R.; Delgadillo, I. *Food Chem.* **1995** *54*, 437-441.
34. Zeier, J.; Schreiber, L. *Planta*, **1999**, *209*, 537-542.
35. Barron, C.; Parker, M.; Mills, C.; Rouau X.; Wilson R. *Planta*, **2005**, *220*, 667-677.
36. Synytsya, A.; Copíková, J.; Jankovská, P. *Association AVH 9 Simposium. Reims, mars* **2002**, 4-9.
37. Kratchanova, M.; Bénémou, C.; Kratchanov, C. *Carbohydr. Polym.* **1991**, *15*, 271-282.
38. Pedroza-Islas, R.; Aguilar- Esperanza, E.; Vernon-Carter, E. *Rev. Esp. Tecnol. Alim.* **1995**, *35*, 151-156.
39. Forni, E.; Penci, M.; Polesello, A. *Carbohydr. Polym.* **1994**, *23*, 231-234.

40. Kammev, A.; Colina, M.; Rodriguez, J.; Ptitchkina, N.; Ignatov, V. *Food Hydrocoll.* **1998**, *12*, 263-271.
41. Marry, M.; McCan M.; Kolpak, F.; White, A. *J. Sci. Food Agric.* **2000**, *80*, 17-28.
42. Filippov, M. *Food Hydrocoll.* **1992**, *6*, 115-142.
43. Gnanasambandam, R.; Proctor, A. *Food Chem.* **2000**, *68*, 327-332.
44. Kalapathy, U. Proctor, A. *Food Chem.* **2001**, *73*, 393-396.
45. Karurakova, M.; Capek, P.; Sasinkova, V., wellner, N.; Ebringerova, A. *Carbohydr. Polym.* **2000**, *43*, 195-203.
46. Chang, K.J. *Food Sci. Biotechnol.* **1995**, *4*, 1-6.
47. Oosterveld, L. PhD thesis, Wageningen Agricultural University, Wageningen, The Netherlands, 1997.
48. Kim, D.H., Kim, D.G.; Lee, D.Y.; Kim, K.E.; Kim, C.W. *Food Sci. Biotechnol.* **2000**, *9*, 95-98.
49. Fishman, M.L.; Pfeffer, P.E.; Barford, R.A., Donner, L.W. *J. Agric. Food Chem.* **1984**, *32*, 372-378.
50. Fishman, M.L.; Chau, H.K. Coffin, D.R., Hotchkiss, A.T. In *Advances in Pectin and Pectinase Research*, 2003; Kluwer Academic Publishers: Dordrecht, Neth., pp 107-122.

Chapter 15

Pectinmethylesterase Modification to Produce Charge Modified Citrus Pectin

Yookyung Kim¹ and Louise Wicker^{2,*}

¹Research Food Technologist, Agricultural Research Service,
U.S. Department of Agriculture, Athens, GA 30605

²Department of Food Science and Technology, University of Georgia,
Athens, GA 30602 (lwicker@uga.edu)

Valencia orange pectinmethylesterase (PME) isozymes that are involved in de-stabilization of orange juice cloud, were partially purified and used to de-esterify commercial pectin. Based on SDS PAGE, the PME isozymes contained proteins at 36 kDa and 13 kDa or 36 kDa and 27 kDa. Control and PME-modified pectin that was de-esterified by less than 10%, were compared for molecular weight, charge, charge distribution and calcium sensitivity. Modified pectins were more heterogeneous based on elution from anion exchange chromatography and had a greater population of pectin that eluted at higher salt concentration. Only modified pectins were calcium sensitive. A negative ζ -potential value was observed for all pectins at pH values between 4.0 and 7.0, and modified pectins had a more negative ζ -potential value. Potentially, different PME isozyme activities will impact differently colloidal stability of juices and juice beverages that is dependent on total charge and charge distribution of pectins.

Pectin is an anionic polymer consisting of partially esterified α (1-4)-D-galacturonic acid residues, forming a homogalacturon backbone. The presence of 1,2 linked L-rhamnose residues form rhamnogalacturonan I and II and are the site for attachment of neutral sugar side chains. (1) Intrinsic factors such as average charge and charge distribution, average molecular weight (MW) and distribution of MW, number and size of neutral sugar side chains, extrinsic factors, such as ionic strength, pH, temperature, co-solutes have an effect on functionality of pectin. Pectins are broadly classified, according to the average degree of esterification (DE), as high-methoxyl pectin (HMP, > 50% DE) and low-methoxyl pectin (LMP, < 50% DE) (1).

Pectin methyl-esterase (PME, E.C. 3.1.1.11) catalyses the demethoxylation of esterified pectins by (1) a single-chain mechanism, where the binding of the enzyme is followed by a conversion of all contiguous substrate sites on the homogalacturonan; (2) a multi-chain mechanism, where the enzyme-substrate complex dissociates after each reaction, resulting in deesterification of only one residue for each attack; (3) a multi-attack mechanism, in which the enzyme catalyses the deesterification of a limited number of consecutive residues for every active enzyme complex formed (2, 3). Conventionally, acidic microbial (*Aspergillus spp.*) PMEs de-esterify pectins with a random distribution of free carboxyl groups (multiple chain mechanism), while alkaline PMEs from higher plants and fungi (*Trichoderma reesei*) de-esterify pectin consecutively linearly (single chain mechanism) and result in a blockwise arrangement of free carboxyl groups on pectin (4-8). Initiation of de-esterification introduces block-structures of adjacent free galacturonic acid units on the HG backbone and changes in calcium sensitivity characteristics of HM pectins (9-13). Some plant PMEs have the capacity to remove a limited number of methyl esters per reaction, giving rise to short, de-esterified blocks (14). The action pattern of apple PMEs at pH 7.5 consisted of blockwise, single chain mechanism, while the action at pH 4.5 was blockwise, but with shorter blocks, on multiple chains.

Multiple PME isozymes are present in plant tissue, and individual isozymes can be distinguished by expression patterns as well as physical and biochemical properties (15). These differences in PME properties are likely to result in differences in quality of pectin containing foods and beverages and modification of pectin. Versteeg et al. (16) isolated a PME isozyme in Navel orange that was thermostable (TS-) and rapidly clarified juice. Thermolabile (TL-) PMEs destabilized the cloud very slowly or not at all. In Valencia orange, four PME activity peaks were resolved by Heparin-Sepharose chromatography (17). One of four PME isozymes did not affect orange juice cloud, while the other three isozymes destabilized orange juice cloud at varying rates. Wicker et al. (18) reported clarification of citrus juices by TL-PME from Valencia pulp only in the presence of cations. TL-PME containing 36 kDa and 27 kDa peptides clarified juice faster than TL-PME containing 36 kDa and 13 kDa peptides (19). The molecular characterization of PME peptides and use of enzymatically homogenous PMEs was stressed by Savary et al. (20). Use of well defined PMEs is an important tool to effectively and consistently prepare charge

modified pectins (Savary personal communication). The task is complex, considering the differences in clades of plant, fungal and bacterial PME and paucity of significant strictly conserved amino acid residues (21).

Gelling activity is perhaps the most common functional property of pectin for industrial applications, but the interaction of pectin with cations, such as calcium and proteins, has great potential in the food and pharmaceutical industries. Different gel strength and gel properties of LM pectins with similar ester contents prepared by different de-esterification procedures has been well established (22-25). Considerable effort to create and define tailored pectins for specific functionality is the focus of more recent research. Efforts to alter and quantify changes in GalA content, ratio to neutral sugar content, molar mass, charge, intra- and intermolecular methyl ester charge distribution, homogeneity and other intrinsic parameters form the basis for prediction of pectin function.

The greatest activity in pectin modification has been to more modify and characterize the inter- and intramolecular charge distribution on the homogalacturonan backbone. One approach described as enzymatic fingerprinting with endo-pectin lyase and endopolygalacturonase was used to differentiate the patterns of de-esterification by plant and fungal PMEs and base (12). Taking advantage of the ability of low ester pectins to crosslink calcium and form gels, the degree and pattern of de-esterification by PME was assessed. Calcium mediated gels formed from pectins that contained homogalacturonan domains, with different degrees and patterns of methyl-ester group distribution, had different elasticity and response to compressive strain (26). The gel strength of pectins with similar DE values but different distribution patterns was nearly 3-fold higher in plant than fungal PME modified pectin. Pectin with 12% lower DE, but similar distribution pattern, formed a 10-fold stronger gel. Elasticity of gels was correlated with decreasing DE. A 6.5% DE decrease of a non-calcium-sensitive citrus pectin by a salt-dependent PME from orange fruit rag tissue increased the calcium sensitivity (9) as did a heat stable isozyme of PME (27). Heterogeneity of charge density was greater in plant PME de-esterified pectins compared to fungal PME or base de-esterified pectins (28). Pectins de-esterified by plant PME had a different response to calcium. Unlike fungal PME or base de-esterified pectins, experimental calcium transport parameters for plant PME de-esterified pectins were markedly less than predicted values, which was attributed to blockwise de-esterification (29). Blocks in sugar beet pectin formed by plant PME allowed the formation of calcium-pectinate precipitates in concentrated mediums for high DE, even though these blocks were not long enough to induce abnormal polyelectrolyte behavior or to promote dimerization of pectic molecules in dilute solution (30). The diversity of interchain, multi attack mechanisms by plant PMEs was noted by Ralet and Thibault (31) who observed that progressive dimerization with decreasing DE of plant PME de-esterified lime pectin and attributed it to a very large charge density.

A different approach (32) to characterization of charge distribution included degree of blockiness or relative amount of di- or tri- to total non-methylesterified GalA residues (33), the size of the blocks as estimated by sensitivity to endo-PG attack (34) and ratio of esterified to non-esterified GalA

oligomers (35). In an application to differentiate and characterize commercial pectins (36), these methods did not fully explain differences in functional behavior between two chemically similar pectins. Further progress to prepare HG populations that were homogenous in molar mass and charge density were described (31, 37). PME modified pectins were sequentially fractionated by size and charge. The main fraction from IEX was degraded by side chain and backbone degrading enzymes before further anion exchange chromatography. The final fraction was estimated to be homogenous in terms of molar mass and charge density (37). The products are to be further tested in interaction studies. Non-gelling applications of pectins and potential application of modified pectins include stabilization of flavor oils in beverages, acidified dairy drinks, emulsion and development of drug delivery systems (38-41). Charge modified pectins interact more strongly with calcium and other cations, such as proteins and are likely to influence the use of pectin as a gelling agent or stabilizer in juice and protein containing beverages. In this work, we describe recent efforts to modify citrus pectin with PME extracted from Valencia pulp. The results assist in interpreting different effects of PME enzymes on citrus juice pectin and potential application to understanding cloud loss and protein interactions in juice beverage formations.

Materials and Methods

PME Isolation and Pectin Modification

PME was extracted from Valencia pulp (Citrus World, Lake Wales, FL) and used to modify 72% DE pectin (CP Kelco, San Diego, CA) as described by Kim et al. (42). Briefly, PME that did not bind SP cation exchange column (Amersham Pharmacia Biotech, Uppsala, Sweden) was collected in the void volume and applied to a heparin (HP) column. PME that did not bind SP, nor HP column was denoted as U-PME; PME that did not bind SP, but did bind heparin and was eluted with a salt gradient, was denoted as B-PME. After SDS-PAGE analysis with a PhastSystem, it was observed that U-PME contained 36,000 and 27,000 peptides and B-PME contained 36,000 and 13,000 peptides. Pectins that were not modified, modified by U-PME, or B-PME were denoted O-Pectin, U-Pectin, or B-Pectin, respectively.

Pectin was modified as described by Hunter et al. (43) or as described by Kim et al. (42) Briefly, 2% pectin with 0.1M NaCl, adjusted to pH 7.5 with NaOH was held at 30°C after the addition of a known amount of PME. The pH was maintained at 7.5 for a period of time that was estimated by the total units of activity of PME. The reaction was stopped by pH adjustment to 5.0, addition and boiling in ethanol.

Pectin Characterization

Either original or modified pectin in 0.5M acetate, pH 5.0 was loaded onto a Macro-Prep High Q Support (Bio-Rad, Hercules, CA) IEX column and eluted with a linear gradient to 1.3M acetate, pH 5.0 at a flow rate of 12 mL/min (43). Depending on the elution profile, samples were pooled to generate sufficient sample for analysis, dialyzed against deionized water and freeze dried. Original and modified pectin was characterized for galacturonic acid content by m-phenyl phenol assay, DE by FTIR, MW by SEC-MALLS, as described by Hunter et al. (43), and surface charge by zeta potential, charge and charge distribution by NMR (42). Gelling properties of pectin dispersions were assessed using a Texture Profile Analysis (TA-XT2i, Texture Technologies Corp, Scarsdale, NY, (43) or a Controlled Stress Dynamic Rheometer™ (Rheometrics, Piscataway, NJ, USA) equipped with a cone and plate device (44).

Results and Discussion

Partially purified PME from Valencia juice sacs clarify citrus juices at different rates and with little correlation with total PME activity (13, 18, 19). In an approach that had the original objective to explain PME role in clarification of citrus juice and to understand pectin stabilization of acidified milk drinks, partially purified PME preparations have been used in this research.

Initial efforts to de-esterify and characterize charge modified pectins by ion exchange chromatography resulted in heterogenous dispersions of pectin (Figure 1). (43) The original or mother pectin, 72% DE, had two populations that eluted with increasing sodium chloride concentration (data not shown). In B-PME modified pectin, 67% DE, there was less of the population with lower affinity for the anion exchanger than in the original pectin. (43) In subsequent research, it was shown that the pattern of elution from ion exchange was similar for B-PME or U-PME modified pectins, but the %DE varied from an average value of 62% to higher and lower values of %DE in the populations. (42) A greater proportion of charge modified pectin eluted at higher sodium chloride concentration. Pooled fractions of eluted pectin were characterized for MW and gelling properties. Unfractionated pectin, modified by B-PME, had an average DE of 67% and pooled fractions from ion exchange ranged from 69 to 64% DE as indicated on Figure 1 (43). For pectin that was not modified or modified by U-PME or B-PME, the change in %DE of U-PME and B-PME modified pectins (62% target DE) for the elution sequence of pooled IEX fractions is depicted in Figure 2. In general, the %DE declined with fraction number, especially for the original pectin. The average %DE of U-pectin or B-pectin was nearly constant for fractions 2, 3, and 4. The %DE for both modified pectins, Fraction 5, was less than earlier eluting fractions.

The MW of original pectin and pectin modified by B-PME or U-PME was not significantly different (Figure 3). This result is in concurrence with earlier reports results that Valencia PME de-esterification does not result in loss of MW

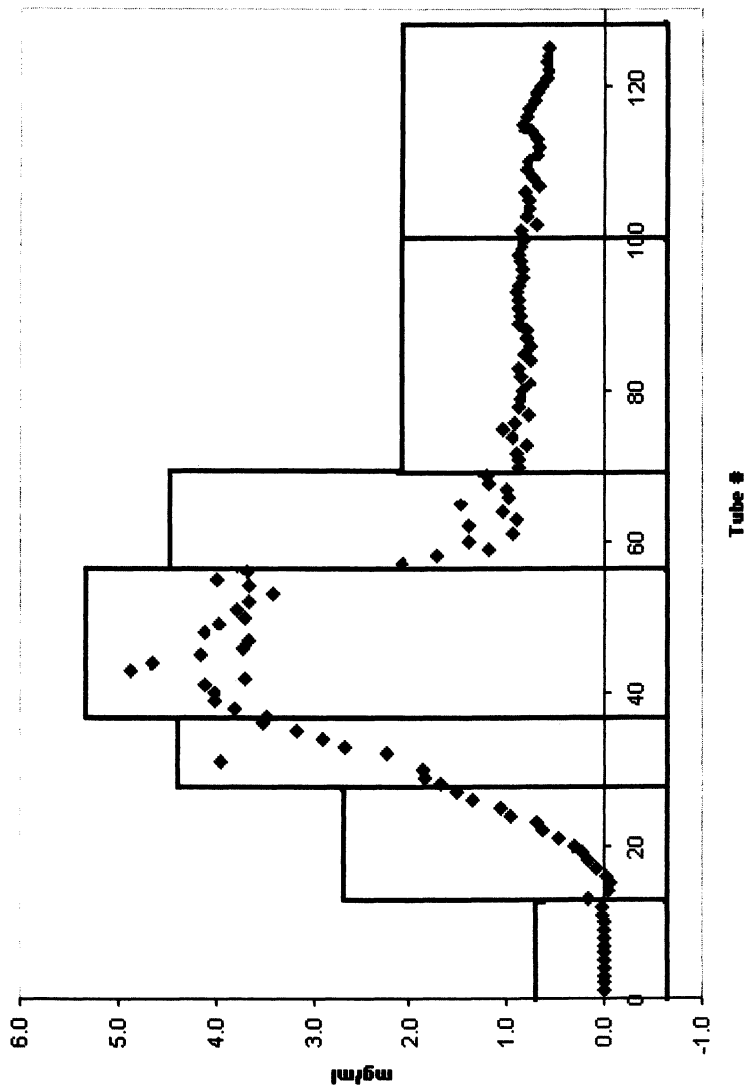


Figure 1. Ion exchange chromatography elution profile by mg/mL uronic acid. The pooled fractions are depicted by blocks on the graph, with the tubes represented below and %DE for each fraction given above. Adapted from Hunter et al. 2005 (43).

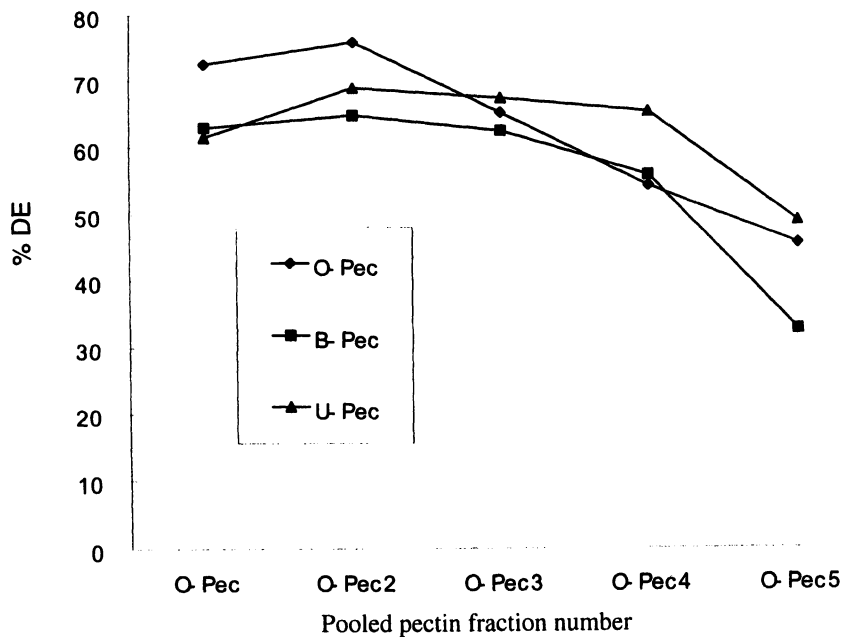


Figure 2. Degree of esterification (%DE) of unfractionated and fractionated pectin samples. (O-Pectin): original pectin. (B-Pectin): SP-unbound and HP-bound PME modified pectin. (U-Pectin): SP-unbound and HP unbound PME modified pectin. Pectins were pooled into five fractions based on IEX elution. Pectin modification is as described by Kim et al. {Kim, 2005 #4625}

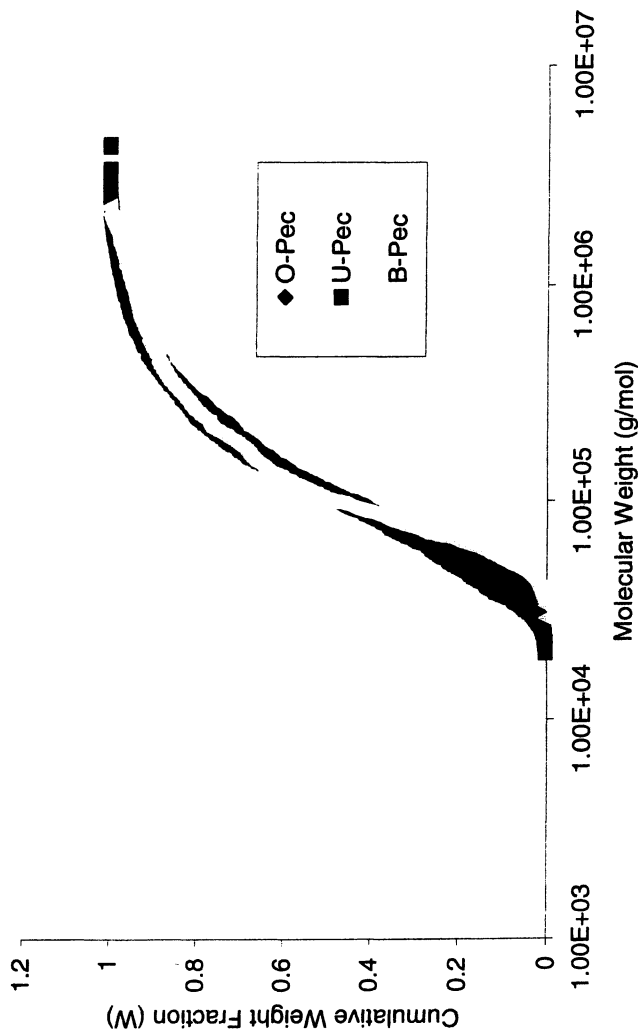


Figure 3. Cumulative weight fraction plotted against molecular weight of unfractionated pectin samples. (O-Pectin): original pectin. (B-Pectin): SP-unbound and HP bound pectin. (U-Pectin): SP-unbound and HP unbound pectin. Pectin modification is as described by Kim et al. {Kim, 2005 #4625} (See page 3 of color inserts.)

(11, 45). However, a lower MW was observed in pooled fractions or original or modified pectin, collected after IEX chromatography. The lower MW in the fractions after ion exchange of modified and original pectin compared to unfractionated pectin, may be related to the loss of larger MW aggregates that are lost by filtration or by irreversible binding to the column. In contrast to the MW results, there was no significant difference in viscosity of differently modified pectins, although the viscosity of the two modified pectins were significantly higher than the original pectin (44).

Pectins that were modified by B-PME formed gels in the presence of calcium. Modified, unfractionated pectin as well as pectin fractions formed gels (Table I). The hardness of the gels varied with fraction number, but high variation was observed in duplicate samples. The high variation may be related to the relatively small decrease in DE from 72% to 67% DE. Significant increases in hardness were observed in gels that were prepared from fractions of pectin that was modified to 62% DE (44).

Pectins that were modified by U-PME and B-PME were unique with respect to charge distribution (42) and gel properties (44). Based on the NMR profile and frequencies of monad, dyad and triads of unfractionated and fractionated pectins, both U-PME and B-PME modified pectin in a blockwise manner, but the mechanism was different between the two PMEs. A 2-fold increase in F_{GGG} fraction (contiguous de-esterified blocks), both B-PME and U-PME created blockwise de-esterification pattern of different length. Within the IEX fractions of O-, B-, or U-pectin, differences in the monad, dyad, and triad frequencies were reported that were consistent with blocks of de-esterified regions but the frequency varied between the pectins. Additionally, the surface charge or zeta potential, especially with increase in pH and the viscoelastic properties were unique for U-Pectin and B-Pectin (44).

U-PME and B-PME from Valencia are useful to modify charge, generate calcium reactive pectin, and expand the potential use for pectins in the food and beverage industry. U-PME created a more reactive pectin that had an overall lower net negative surface charge, that affected more pectin chains in the population and created greater gel strength (44). Collectively with earlier research on clarification of juices, it is apparent that one reason Valencia PME isozymes differ in rate of clarification is related to the mechanism of de-esterification. PME fractions that contained the 36,000 and 27,000 dalton peptides (U-PME) clarified juices faster and created more reactive modified pectin. PME fractions that contained the 36,000 and 13,000 peptides (B-PME) also de-esterified pectin in a blockwise manner, but did not cause rapid clarification of juices. The origin of these PME fragments and the role of the 36,000 peptide alone in juice clarification remains to be elucidated.

Table I. Texture profile analysis data of the pectin and pectin fractions^a

<i>Fraction</i>	<i>Original</i>	<i>Modified</i>	<i>Fraction</i> 14-27	<i>Fraction</i> 28-37	<i>Fraction</i> 38-56	<i>Fraction</i> 57-69	<i>Fraction</i> 70-99	<i>Fraction</i> 100-125
GalA	0.62	0.56	0.57	0.60	0.69	0.65	0.49	0.60
Hardness, g	No gel	70.6	53.2	55.9	64.5	149.5	87.8	36.8

^aPectin modified by B-PMME. Adapted from Hunter et al. 2005 (43)

References

1. Voragen, A. G. J.; Pilnik, W.; Thibault, J. F.; Axelos, M. A. V.; Renard, C. M. G. C. In *Food Polysaccharides and Their Applications*; Stephen, A. M., Ed. Marcel Dekker, Inc: New York, 1995; Vol. 67, pp 287-339.
2. Grasdalen, H.; Andersen, A. K.; Larsen, B. *Carbohydr. Res.* **1996**, *289*, 105-114.
3. Greenwood, C. T.; Milne, E. A. *Advances in Carbohydrate Chemistry and Biochemistry* **1968**, *23*, 281-366.
4. de Vries, J. A.; Hansen, M.; Soderberg, J.; Glahn, P. E.; Pedersen, J. K. *Carbohydr. Polym.* **1986**, *6*, 165-176.
5. de Vries, J. A.; Rombouts, F. M.; Voragen, A. G. J.; Pilnik, W. *Carbohydr. Polym.* **1983**, *3*, 245-248.
6. Thibault, J. F.; Rinaudo, M. *Biopolymers* **1985**, *24*, 2131-2143.
7. Tuerana, C. E.; Taylor, A. J.; Mitchell, J. R. *Carbohydr. Polym.* **1982**, *2*, 193-203.
8. Tuerana, C. E.; Taylor, A. J.; Mitchell, J. R. *J. Sci. Food Agric.* **1984**, *35*, 797-804.
9. Cameron, R. G.; Savary, B. J.; Hotchkiss, A. T.; Fishman, M. L.; Chau, H. K.; Baker, R. A.; Grohmann, K. *J. Agric. Food Chem.* **2003**, *51*, 2070-2075.
10. Christensen, T. M. I. E.; Nielsen, J. E.; Kreiberg, J. D.; Rasmussen, P.; Mikkelsen, J. D. *Planta* **1998**, *206*, 493-503.
11. Hotchkiss, A. T.; Savary, B. J.; Cameron, R. G.; Chau, H. K.; Brouillette, J.; Luzio, G. A.; Fishman, M. L. *J. Agric. Food Chem.* **2002**, *50*, 2931-2937.
12. Limberg, G.; Korner, R.; Buchholt, H. C.; Christensen, T. M. I. E.; Roepstorff, P.; Mikkelsen, J. D. *Carbohydr. Res.* **2000**, *327*, 293-307.
13. Wicker, L.; Ackerley, J. L.; Hunter, J. L. *Food Hydrocolloids* **2003**, *17*, 809-814.
14. Denes, J. M.; Baron, A.; Renard, C. M. G. C.; Pean, C.; Drilleau, J. F. *Carbohydr. Res.* **2000**, *327*, 385-393.
15. Bordenave, M. In *Modern Methods of Plant Analysis*; Linskens, H. F., Ed. Springer: New York, 1996; Vol. 17, pp 165-180.
16. Versteeg, C.; Rombouts, F. M.; Spaansen, C. H.; Pilnik, W. *J. Food Sci.* **1980**, *45*, 969-971.
17. Cameron, R. G.; Baker, R. A.; Grohmann, K. *J. Food Sci.* **1998**, *63*, 253-256.
18. Wicker, L.; Ackerley, J. L.; Corredig, M. *J. Agric. Food Chem.* **2002**, *50*, 4091-4095.
19. Ackerley, J.; Corredig, M.; Wicker, L. *J. Food Sci.* **2002**, *67*, 2529-2533.
20. Savary, B. J.; Hotchkiss, A. T.; Cameron, R. G. *J. Agric. Food Chem.* **2002**, *50*, 3553-3558.
21. Markovic, O.; Janecek, S. *Carbohydr. Res.* **2004**, *339*, 2281-2295.

22. Heri, W.; Deuel, H.; Neukom, H. *Helv. Chim. Acta* **1961**, *44*, 1945-1949.
23. Kertesz, Z. I. In *The Pectic Substances*; Interscience Publishers: New York, 1951; pp 94-129.
24. Kohn, R.; Furda, I.; Kopec, Z. *Collect. Czech. Chem. Commun.* **1968**, *33*, 264-269.
25. Powell, D. A.; Morris, E. R.; Gidley, M. J.; Rees, D. A. *J. Mol. Biol.* **1982**, *155*, 517-531.
26. Willats, W. G. T.; Orfila, C.; Limberg, G.; Buchholt, H. C.; van Alebeek, G. J. W. M.; Voragen, A. G. J.; Marcus, S. E.; Christensen, T. M. I. E.; Mikkelsen, J. D.; Murray, B. S.; Knox, J. P. *J. Biol. Chem.* **2001**, *276*, 19404-19413.
27. Cameron, R. G.; Savary, B. J.; Hotchkiss, A. T.; Fishman, M. L. *J. Agric. Food Chem.* **2005**, *53*, 2255-226-.
28. Ralet, M. C.; Bonnin, E.; Thibault, J. F. *J. Chromatogr. B Anal. Technol. Biomed. Life Sci.* **2001**, *753*, 157-166.
29. Ralet, M. C.; Dronnet, V.; Buchholt, H. C.; Thibault, J. F. *Carbohydr. Res.* **2001**, *336*, 117-125.
30. Ralet, M. C.; Crepeau, M. J.; Buchholt, H. C.; Thibault, J. F. *Biochem. Eng. J.* **2003**, *16*, 191-201.
31. Ralet, M. C.; Thibault, J. F. *Biomacromolecules* **2002**, *3*, 917-925.
32. Daas, P. J. H.; Albeek, G. J. W. M.; Voragen, A. G. J.; Schols, H. A. In *Gums and Stabilizers for the Food Industry*; Williams, P. A.; Phillips, G. O., Eds. Royal Society of Chemistry: 1999; pp 3-18.
33. Daas, P. J. H.; Arisz, P. W.; Schols, H. A.; De Ruiter, G. A.; Voragen, A. G. J. *Anal. Biochem.* **1998**, *257*, 195-202.
34. Daas, P. J. H.; Voragen, A. G. J.; Schols, H. A. *Carbohydr. Res.* **2000**, *326*, 120-129.
35. Daas, P. J. H.; Voragen, A. G. J.; Schols, H. A. *Biopolymers* **2001**, *58*, 195-203.
36. Guillotin, S. E.; Bakx, E. J.; Boulenguer, P.; Mazoyer, J.; Schols, H. A.; Voragen, A. G. J. *Carbohydr. Polym.* **2005**, *60*, 391-398.
37. Hellin, P.; Ralet, M. C.; Bonnin, E.; Thibault, J. F. *Carbohydr. Polym.* **2005**, *60*, 307-317.
38. Buchholt, H. C.; Christensen, T. M. I. E.; Fallesen, B.; Ralet, M. C.; Thibault, J. F. *Carbohydr. Polym.* **2004**, *58*, 149-161.
39. Benichou, A.; Aserin, A.; Garti, N. *J. Dispersion Sci. Technol.* **2002**, *23*, 93-123.
40. Garti, N.; Wicker, L., In *American Chemical Society, 229th Annual Meeting*, Amer Chemical Soc: 2005.

41. Kazmierski, M.; Wicker, L.; Corredig, M. *J. Food Sci.* **2003**, *68*, 1673-1679.
42. Kim, Y. K.; Teng, Q.; Wicker, L. *Carbohydr. Res.* **2005**.
43. Hunter, J. L.; Thomas, A.; de Haseth, J.; Wicker, L. *Food Hydrocolloids* **2005**.
44. Kim, Y. K.; Wicker, L. *J. Agric. Food Chem.* **2005**.
45. Hunter, J. L.; Wicker, L. *J. Sci. Food Agric.* **2005**.

Chapter 16

Chemical Composition of an Effective Emulsifier Subfraction of Gum Arabic

Madhav P. Yadav¹ and Eugene A. Nothnagel²

¹Eastern Regional Research Center, Agricultural Research Service,
U.S. Department of Agriculture, 600 East Mermaid Lane,
Wyndmoor, PA 19038

²Department of Botany and Plant Sciences, University of California,
Riverside, CA 92521

Gum arabic, which is principally a mixture of polysaccharides and arabinogalactan-proteins (AGPs), contains trace levels of lipids. This report explores the hypothesis that these lipids are attached to the gum arabic AGPs as glycosylphosphatidylinositol (GPI) lipids, or in some other way, and make a significant contribution to the emulsifying properties of gum arabic. Treatment of gum arabic with nitrous acid, which cleaves the GPI oligosaccharide, decreased the emulsion stabilizing capacity of gum arabic. Treatment with 50% aqueous HF at 0°C also resulted in diminished emulsion stabilizing properties of gum arabic, but this effect could not be unambiguously attributed to lipid cleavage because the HF also caused other structural changes, as indicated by a significant reduction in arabinose content. The subfraction of gum arabic components (\approx 1-3%) that adsorb at the surface of oil droplets has a higher abundance of GPI linker components and much higher relative lipid content than the whole gum.

Keywords: Emulsions; Emulsion activity; Emulsion stability; Emulsifier; Glycosylphosphatidylinositol (GPI) lipid anchor; GPI lipid linker oligosaccharide; Arabinogalactan-proteins

Introduction

Gum arabic, an exudate from *Acacia senegal* or *Acacia seyal* trees (1), is a widely used industrial gum. In ancient times gum arabic was used as an adhesive when wrapping mummies and as a binder in preparing mineral paints for hieroglyphs (2), but presently it is more important as an emulsifier in the food and pharmaceutical industries. Gum arabic is considered to be an excellent gum for use in beverage emulsion systems (3).

Some emulsifiers are polymers that increase viscosity, slow the rate of oil droplet coalescence, and thereby stabilize oil-in-water emulsions (Figure 1A).

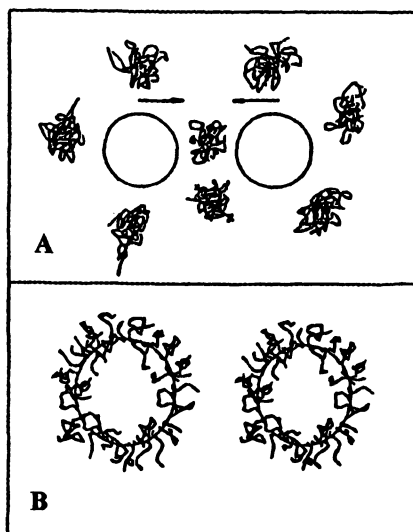


Figure 1. Stabilization of oil droplets by (A) an emulsifier that increases viscosity and slows oil droplet coalescence or by (B) an emulsifier that adsorbs at the oil-water interface and prevents oil droplet fusion. (Reproduced with permission from reference 3. Copyright 1999 Taylor and Francis Group, LLC., <http://www.taylorandfrancis.com>.)

Other emulsifiers are amphipathic molecules that adsorb at the oil-water interface, prevent oil droplet fusion, and thereby stabilize oil-in-water emulsions (Figure 1B).

In the case of gum arabic, an emulsifier of type 1B, the absorbed material has been shown to be high mass polysaccharide that also contains most of the protein in gum arabic. When treated with a protease, gum arabic loses its emulsifying activity, and so the protein component has been recognized as key to emulsification (4). A current model suggests that the protein component of gum arabic contains a hydrophobic polypeptide domain that anchors into the oil droplet while the hydrophilic polysaccharide extends into the surrounding water (Figure 2).

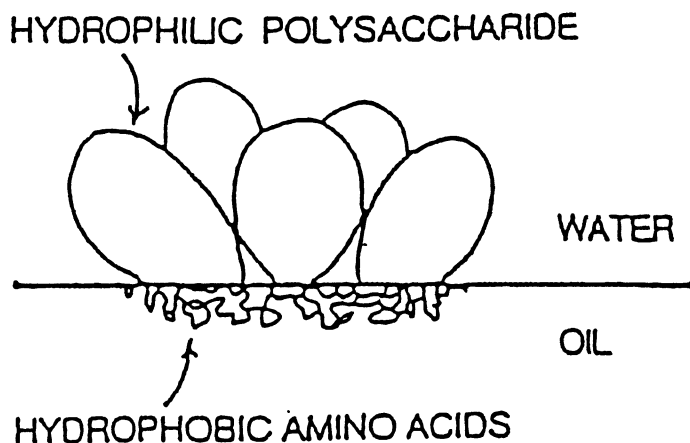


Figure 2. Model of gum arabic localization at an oil-water interface. (Reproduced with permission from reference 5. Copyright 1990 Oxford University Press.)

When chemically analyzed, gum arabic is found to be a complex mixture of macromolecules with molecular weights ranging from 250 kDa to 1,450 kDa. The composition varies somewhat from batch-to-batch but is typically rich in carbohydrate, with 42% (w/w) galactosyl (Gal), 27% arabinosyl (Ara), 15% rhamnosyl (Rha), 14.5% glucuronosyl (GlcA), and 1.5% 4-*O*-methylglucuronosyl (4-*O*-Me-GlcA) residues in gum arabic from *Acacia senegal*; and 38% Gal, 46% Ara, 4% Rha, 6.5% GlcA, and 5.5% 4-*O*-Me-GlcA residues in gum arabic from *Acacia seyal* (1). The protein content is typically about 2% with Hyp, Pro, and Ser residues being relatively most abundant (6).

Arabinogalactan-proteins (AGPs) are major components in the mixture that comprises gum arabic (6). Widely distributed throughout the plant kingdom, AGPs are present in leaves, stems, roots, floral parts and seeds. These complex

proteoglycans are hypothesized to function as markers of cell identity or as signals in development (7). Across the plant kingdom, the size of AGPs varies from 60 to 300 kDa with carbohydrate typically accounting for 90 to 95% of this mass. The glycan chains are highly branched with (1→3)- β -Gal backbones and (1→6)- β -Gal side chains. The side chains in turn carry large amounts of α -Ara residues and lesser amounts of other sugars. The core polypeptide of AGPs is typically rich in Hyp, Ala, Ser, Thr, and Gly residues. Many AGPs are synthesized with a glycosylphosphatidylinositol (GPI) lipid anchor (8-10). The lipid portion of the GPI anchor is a ceramide consisting of predominantly tetracosanoic acid (C24:0) and phytosphingosine (9). The core structure of the GPI anchor on *Pyrus communis* AGPs, as reported by Oxley and Basic (11), is shown in Figure 3. Some of the *P. communis* GPI cores carry a β -D-Gal-(1→4) substitution on the mannosyl (Man) residue adjacent to the glucosaminyl (GlcN) residue.

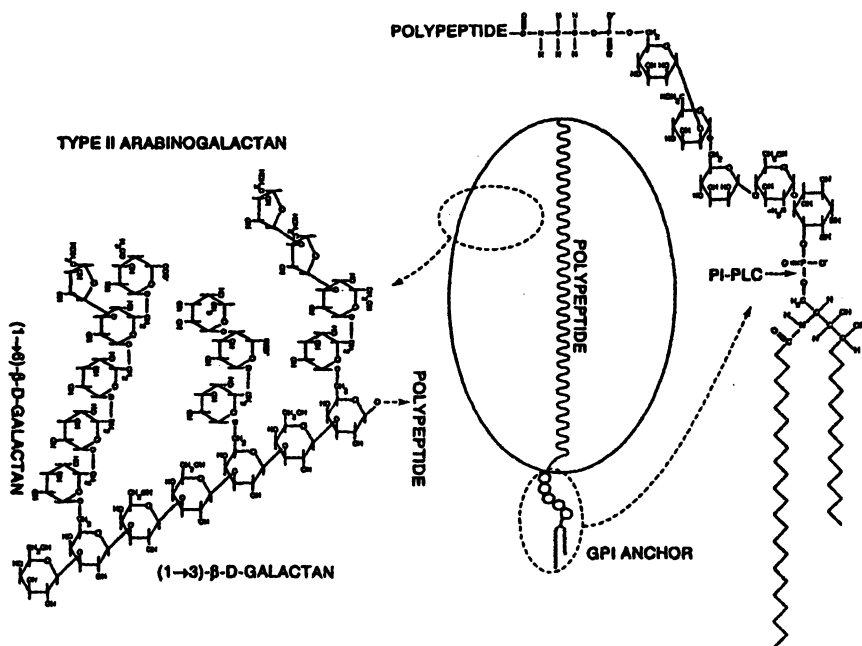


Figure 3. Hypothetical model of the structure of an arabinogalactan-protein (AGP). (Reproduced with permission from reference 7. Copyright 1999 Elsevier Ltd.)

The GPI lipid anchor attaches AGPs to the plant plasma membrane and appears to be cut by a phosphatidylinositol-specific phospholipase C (PI-PLC, Figure 3) or a GPI-specific phospholipase D (which cleaves the phosphate and inositol (Inos) residue) to release AGPs from the membrane into the cell wall space (9,11).

Hypothesis

A small proportion of the AGPs present in gum arabic carry GPI lipids, and it is these lipid-containing AGPs that are primarily responsible for the valuable emulsifying properties of gum arabic.

Materials and Methods

Materials

Gum arabic was obtained from TIC Gums (Belcamp, MD) (samples A and B) or Sigma Chemical (St. Louis, MO) (sample C). Cold-pressed orange oil was obtained from Sunkist Growers (Ontario, CA). Hexadecane (99%) was from Aldrich Chemical (Milwaukee, WI). The Tenbroeck tissue grinder (15 ml volume, 0.15 mm clearance between the ground-glass surfaces) was purchased from Wheaton Scientific Products (Millville, NJ).

Chemical Analyses of Gum Arabic

Sugar and lipid compositions were determined as described by Svetek et al. (9). Elemental analyses were performed by Desert Analytics Inc. (Tucson, AZ).

Chemical Treatment of Gum Arabic

Nitrous acid deamination and aqueous hydrofluoric acid dephosphorylation of gum arabic were done as described (12). Nitrous acid (0.25 M) was generated by adding sodium nitrite to a solution of gum arabic in 0.2 M sodium acetate buffer (pH 3.7) and allowed to react for 5 hours at 23°C. Aqueous 50% (w/w) HF was applied to gum arabic for 49 hours at 0°C or -12°C.

Assay of Emulsifying Activity and Stability

A stock solution of 20-30% (w/w) gum arabic in 0.02% (w/v) sodium benzoate was prepared by adding gum arabic powder and sodium benzoate to water and then gently stirring overnight to produce a homogeneous solution (13). This gum arabic stock solution and additional water were mixed in various proportions with orange oil (typical overall formulation: 1 g orange oil, 1 g gum arabic, and 3 g water) and then homogenized by 15 strokes in a Tenbroeck tissue grinder. No weighting agent was used. The resulting homogenate was diluted 500X into 0.02% (w/v) sodium azide in water. The optical density (1 cm pathlength cuvette, distilled water as the blank) of the diluted emulsion was measured immediately at 650 nm, and then the emulsion was transferred into a separatory funnel for gravity separation at 23°C without agitation. After 24 hours, 37.5% of the total volume of the solution was carefully (to avoid remixing) drained from the bottom of the funnel and discarded. The next 25% of the volume of solution was then carefully drained from the bottom of the funnel. Once collected, this 25% middle fraction was gently swirled to homogeneity, and its optical density was measured at 650 nm. Using the Pearce and Kinsella turbidometric method (14), the optical densities enabled relative comparison of emulsifying properties between different preparations. In particular, the optical density measured immediately after emulsification (0 hours) indicates relative emulsifying activity, with bigger optical density corresponding to greater activity. The optical density measured at 24 hours after emulsification indicates relative emulsion stability (13, 14).

Separation of Gum Arabic Subfraction Associated with Oil Droplets in a Floating Creamy Layer

Emulsions were prepared as described above except hexadecane was used in place of orange oil, and the dilution of the homogenate from the Tenbroeck tissue grinder was 20X into 3 M KBr with 0.02% (w/v) sodium azide, pH 7. Ten diluted batches from the tissue grinder, each approximately 99 ml, were combined in a 1000 ml separatory funnel and allowed to separate under gravity at 23°C without agitation. Separation was continued for 5 days until most of the emulsion had gathered in a creamy layer at the top of the separatory funnel and a clear lower layer contained most of the gum arabic. The lower layer was carefully drained from the bottom of the funnel and discarded. The creamy layer was collected and transferred to a centrifuge bottle. The separatory funnel was rinsed with 10 ml water and then several aliquots of isopropanol totaling 200 ml. These water and isopropanol rinses were pooled with the creamy layer in the centrifuge bottle. The isopropanol broke the emulsion and generated a precipitate which was collected by centrifugation (30 minutes at 3000 g). The

precipitate was further washed by centrifugation with 100 ml isopropanol (2X), 100 ml hexane (1X), and 100 ml 2:1 (v/v) chloroform: methanol (2X). The final pellet was dried, dissolved in water, dialyzed extensively against distilled water, and lyophilized. Recovery of lyophilized material was typically 0.5 to 3% of the starting weight of gum arabic

Results and Discussion

All three starting gum arabic samples contained Inos, GlcN, Man, and fatty acids (Table I) which are the anticipated GPI components (Figure 3). In the gums obtained from the suppliers, the levels of Inos and Man were stoichiometrically adequate, and the levels of GlcN were more than adequate, for roughly one-third to one-half of the gum arabic molecules to have GPI linker cores (Table I). The lipid contents, however, were less abundant than these characteristic sugar residues of the GPI linker core. In sample B, which was marketed as a good emulsifier, the amount of fatty acid was sufficient for only

Table I. Chemical Analysis of Three Gum Arabic Samples

Component	Sample A		Sample B		Sample C	
	Whole	Creamy	Whole	Creamy	Whole	Creamy
<i>Major Glycosyl Residues (weight% of total carbohydrate)</i>						
Gal	43.9	43.5	36.1	40.2	37.4	39.6
Ara	25.9	24.7	41.1	34.2	29.6	26.1
Rha	10.8	12.5	3.5	3.4	12.7	13.0
GlcA	17.9	14.9	18.0	15.6	18.4	17.5
<i>Elemental Composition (% weight/weight)</i>						
C	42.0	42.0	41.9	41.9	41.6	40.9
H	5.8	5.9	6.0	5.7	6.1	5.7
N	0.47	2.2	0.18	1.8	0.37	2.2
P	0.003	0.005	0.004	0.005	0.003	0.011
<i>Molar Ratios of GPI Lipid Components to Gum Arabic (GA) Molecules (nmol/nmol gum arabic)</i>						
Inos/GA	0.42	0.56	0.32	1.1	0.47	0.81
GlcN/GA	8.3	16	4.7	54	7.4	18
Man/GA	2.7	22	1.4	52	1.7	20
Fatty acid/GA	0.009	0.19	0.020	0.20	0.031	0.20

NOTE: Each sample was analyzed in the whole form as obtained from the supplier and as the subfraction from the creamy layer obtained by flotation of an emulsion in 3 M KBr. Fatty acids include species C16:0 through C30:0. P detection was at the limits of sensitivity and thus should be considered an approximation. Molar ratios were calculated assuming 384 kDa average molecular weight (1) and 98% (6) carbohydrate content for gum arabic.

2% (or 1% if two fatty acids each) of the gum arabic molecules to carry a lipid. This proportion of fatty acid, however, agrees with the earlier observation (4) that only 1-2% of the applied gum arabic was adsorbed at the oil-water interface in an oil-in-water emulsion stabilized with gum arabic. Accordingly, sample C with its slightly higher lipid content would be predicted to be an even better emulsifier than sample B.

All three samples exhibited emulsifying activity and stability (Table II). Although the supplier pretested and certified gum B for use as an emulsifier, gum A from the same supplier was equally good at 0 hours and superior after 24 hours. Gum C, which had the highest fatty acid content (Table I), was the best emulsifier at 0 hours, which is consistent with the role of GPI lipid anchors in emulsification.

Table II. Emulsifier Activities and Stabilities of Gum Arabic Samples A-C

Gum	Gum/Orange Oil (w/w)	Optical Density at 650 nm	
		At 0 hours	At 24 hours
No gum	0.00	0.076 ± 0.022	0.0007 ± 0.0006
Sample A	0.508	0.292 ± 0.028	0.048 ± 0.006
	0.773	0.427 ± 0.051	0.096 ± 0.022
Sample B	0.508	0.291 ± 0.034	0.035 ± 0.010
	0.773	0.407 ± 0.033	0.063 ± 0.003
Sample C	0.508	0.332 ± 0.042	0.044 ± 0.007
	0.773	0.479 ± 0.078	0.105 ± 0.020

NOTE: Higher optical density indicates greater emulsifier activity or stability measured at 0 or 24 hours, respectively, after emulsification. Emulsions prepared without gum were the controls. Each datum is the average of three trials ± standard deviation.

To further test the hypothesis that GPI lipids on AGPs in gum arabic are important in emulsifier activity, chemical treatments were applied to cleave the lipid from the GPI linker core. Treatment of GPI-containing molecules with NaNO_2 at pH 3.7 generates nitrous acid which attacks and cleaves primary amino groups, resulting in cleavage of the GPI linker oligosaccharide at the GlcN residue (12). Gum arabic sample C, which was a good emulsifier (Table II), was selected for these experiments. Compared to native (as obtained from the supplier) gum arabic, the nitrous acid-treated gum arabic was greatly diminished in both emulsion activity and stabilization (Table III). The general structure of the gum arabic molecules was not greatly altered by the nitrous acid treatment, as judged by comparison of glycosyl composition with the native material (Table IV). As expected, the nitrous acid-treated gum arabic seemed to be slightly diminished in both N and P content. If gum arabic molecules are assumed to have an average size of 384 kDa and contain an average of one P atom per molecule, then the expected P content would be 0.008% (w/w).

Table III. Emulsifier Activities and Stabilities of Gum Arabic Sample C after Chemical Treatments Designed to Cleave GPI Lipid Anchors

Gum Treatment	Gum/Orange Oil (w/w)	Optical Density at 650 nm	
		At 0 hours	At 24 hours
No gum	0.00	0.051 ± 0.022	0.0011 ± 0.0020
Native	0.508	0.369 ± 0.074	0.057 ± 0.021
	0.773	0.468 ± 0.060	0.117 ± 0.021
Nitrous acid	0.508	0.098 ± 0.014	0.008 ± 0.002
	0.773	0.160 ± 0.012	0.023 ± 0.002
HF, -12°C	0.508	0.430 ± 0.068	0.091 ± 0.022
	0.773	0.306 ± 0.050	0.087 ± 0.013
HF, 0°C	0.508	0.115 ± 0.004	0.023 ± 0.006
	0.773	0.132 ± 0.014	0.040 ± 0.005

NOTE: Higher optical density indicates greater emulsifier activity or stability measured at 0 or 24 hours, respectively, after emulsification. Emulsions prepared without gum were the controls. Each datum is the average of three to six trials ± standard deviation.

Table IV. Analysis of Chemically-Treated Gum Arabic Sample C

Component	Gum Treatment			
	Native	Nitrous Acid	HF, -12°C	HF, 0°C
<i>Major Glycosyl Residues</i>		<i>(weight% of total carbohydrate)</i>		
Gal	37.4	31.5	34.5	29.3
Ara	29.6	32.0	25.5	4.2
Rha	12.7	14.7	14.7	18.8
GlcA	18.4	20.3	22.9	40.3
<i>Elemental Composition</i>		<i>(% weight/weight)</i>		
C	41.6	41.4	40.7	ND
H	6.1	6.0	6.0	ND
N	0.37	0.20	0.38	ND
P	0.003	0.001	0.005	ND

NOTE: P detection was at the limits of sensitivity and thus should be considered an approximation. ND, not determined.

Under appropriate conditions, 50% aqueous HF is reasonably specific for dephosphorylation cleavage at both ends of the GPI linker oligosaccharide (12). After treatment with HF under the usual conditions of 0°C for 50-60 hours, emulsifying activity and stability of gum arabic were considerably diminished (Table III). This treatment also clearly had undesirable effects on the glycosyl composition (Table IV), however, so treatment with 50% HF was tested at a lower temperature, -12°C. The -12°C HF treatment seemed to have only small effects on the glycosyl composition of gum arabic (Table IV), but it likewise had no significant effect on emulsification properties (Table III). Thus far we have been unsuccessful in finding a temperature between 0 and -12°C at which emulsifying activity is lost but carbohydrate content is maintained.

These results involving chemical treatments, especially the nitrous acid treatment, are generally consistent with the hypothesis that GPI lipid anchors make an important contribution to the emulsifying activity of gum arabic. From earlier work the active emulsifying components are expected to amount to only 1-2% of gum arabic (4), however, and the preponderance of inactive material is a confounding factor in these experiments. Thus, a flotation procedure was developed for the bulk purification of gum arabic components that adsorb to oil droplets. This procedure was applied to gum samples A, B, and C, and in each case the recovery of gum components from the floating creamy layer was 0.65 to 0.75% of the total gum emulsified with the hexadecane oil.

For all three gum samples A, B, and C, the major glycosyl residues in the gum components adsorbed to the hexadecane droplets in the creamy layer were present at abundances similar to those in the whole gum (Table I). The minor glycosyl residues Man and GlcN, which occur in the GPI linker oligosaccharide (Figure 3) and in *N*-glycans of glycoproteins, were much more abundant in the gum components from the creamy layers than in the whole gums. Inositol also seemed to be somewhat more abundant in the components from the creamy layers, although we regard quantitation of Inos to be less precise than for the other sugars. The C and H elemental contents were similar between the whole gums and the components from the creamy layers, but N was distinctly more abundant in the components from the creamy layers. This increase in N content was larger than could be accounted for by the increase in GlcN content, thus indicating higher protein content in the components from the creamy layers. Phosphorous content was near the lower limit of detectability in all samples, and thus no reliable conclusion could be drawn regarding differences in P content.

The comparative lipid contents of the whole gums and the components from the creamy layers were of greatest interest with regard to testing the hypothesis of this project. Consistent with the hypothesis, the gum components adsorbed to the hexadecane droplets had much higher lipid contents than did the whole gums (Table I). It must be noted that the shorter fatty acids (C16:0-C20:0) are common laboratory contaminants, and thus it was necessary in these experiments to analyze blank samples to obtain background subtraction factors.

The resulting corrections were large for the C16:0-C20:0 fatty acids and thus limited the precision with which the abundances of these shorter fatty acids could be measured. This limitation did not arise in the measurement of longer fatty acids (C22:0-C30:0), which were not found as laboratory contaminants but were found to be much more abundant in the creamy layers than in the corresponding whole gums.

Conclusions

The results of this study could be consistent with the hypothesis that some AGPs in gum arabic contain intact GPI lipid anchors that make a significant contribution to the emulsifying action of the gum. Long chain bases, which are expected components of GPI anchors (Figure 3), were not detected in this study and thus remain as an outstanding issue relative to the hypothesis.

Acknowledgement

This work was supported by award number 2001-35503-10027 to E.A.N. from the NRI Competitive Grants Program/USDA. Mention of trade names or commercial products in this article is solely for the purpose of providing specific information and does not imply recommendation or endorsement by the U.S. Department of Agriculture.

References

1. Islam, A. M.; Phillips, G. O.; Sljivo, A.; Snowden, M. J.; Williams, P. A. *Food Hydrocolloids* **1997**, *11*, 493-505.
2. Whistler, R. L. In *Industrial Gums, Polysaccharides and Their Derivatives*; Whistler, R. L.; BeMiller, J. N., Eds.; Academic Press: San Diego, CA, 1997; pp 309-339.
3. Garti, N. *J. Dispersion Sci. Tech.* **1999**, *20*, 327-355.
4. Randall, R. C.; Phillips, G. O.; Williams, P. A. *Food Hydrocolloids* **1988**, *2*, 131-140.
5. Williams, P. A.; Phillips, G. O.; Randall, R. C. In *Gums and Stabilisers for the Food Industry*; Phillips, G. O.; Wedlock, D. J.; Williams, P. A., Eds.; IRL Press: Oxford, UK, 1990; Vol. 5, pp 25-36.
6. Akiyama, Y.; Eda, S.; Kato, K. *Agric. Biol. Chem.* **1984**, *48*, 235-237.
7. Serpe, M. D.; Nothnagel, E. A. *Adv. Bot. Res.* **1999**, *30*, 207-289.
8. Youl, J. J.; Bacic, A.; Oxley, D. *Proc. Natl. Acad. Sci. U.S.A.* **1998**, *95*, 7921-7926.

9. Svetek, J.; Yadav, M. P.; Nothnagel, E. A. *J. Biol. Chem.* **1999**, *274*, 14724-14733.
10. Sherrier, D. J.; Prime, T. A.; Dupree, P. *Electrophoresis* **1999**, *20*, 2027-2035.
11. Oxley, D.; Bacic, A. *Proc. Natl. Acad. Sci. USA* **1999**, *96*, 14246-14251.
12. Menon, A. K. *Methods Enzymol.* **1994**, *230*, 418-442.
13. Buffo, R. A.; Reineccius, G. A.; Oehlert, G. W. *Food Hydrocolloids*, **2001**, *15*, 53-66.
14. Pearce, K. N.; Kinsella, J. E. *J. Agric. Food Chem.* **1978**, *26*, 716-723.

Chapter 17

Characterization of Functionalized Electroactive Biopolymers

Victoria L. Finkenstadt* and J. L. Willett

Plant Polymer Research, National Center for Agricultural Utilization
Research, U.S. Department of Agriculture, 1815 North University Street,
Peoria, IL 61604

*Corresponding author: finkenvl@ncaur.usda.gov

Biopolymers have the potential for use as a matrix for applications such as controlled release devices and environmentally sensitive membranes. Renewable resources can be utilized as polymer matrices for electroactive material. Natural polymers are generally more environmentally-friendly and biocompatible than existing synthetic products. Thermoplastic starch is naturally insulative; however, the chemical, electrical, and mechanical properties of the biopolymer matrix can be tailored for specific functionality in a continuous process utilizing reactive extrusion. Conductance can be measured in the solid state by a direct-current resistance method. Ion-conducting materials, produced by doping thermoplastic starch and biopolymers with metal halides, have 3 orders of magnitude greater conductance than native materials. There is a correlation between polymer mobility and conductance. We have investigated several types of starch of different origin, derivatized starches, and plant or microbial biopolymers with ionic functional groups. The conductance approaches the level of synthetic polymer electrolytes.

Introduction

Electroactive polymers (EAPs) are a new class of materials. EAPs are plastics that conduct small amounts of electricity either electronically or ionically. Intrinsically conductive polymers (ICPs) conduct electricity by virtue of their unpaired electrons associated with carbon-carbon conjugated double bonds. Recently, biopolymers have been shown to be able to conduct electricity using an ion-conduction mechanism. This work concentrates on solid-state materials that are less than 30% moisture by weight. Thermoplastic corn starch and other biopolymers are naturally insulative; however, ionic functional groups can mediate the level of conductance (1). Starch is a biodegradable, renewable resource and is composed of a mixture of two polysaccharides. Amylose is a linear polymer of $\alpha(1\rightarrow4)$ linked glucose. Amylopectin is a highly branched polysaccharide composed of $\alpha(1\rightarrow6)$ linked amylose chains. Native starch is packaged into granules and the plastic properties of starch are only exhibited when the granular structure is broken down by mechanical and thermal means. The incorporation of salts that can be solvated by the polymer matrix increase conductance of the resulting films (2). Plastics that are electrically active have several uses that are listed in Table 1.

Table 1. Applications of electroactive biopolymers

Solid polymer electrolytes	Chemical biosensors
Energy transfer devices	Chelation of minerals
Anticorrosion	Biocatalysis
Photochemistry	Polymer-drug conjugates
Environmental sensitivity	Solar energy utilization
Drug targeting & delivery	Biocompatible biomaterials

Materials and Methods

Starches. Commercially available starches were used. Ambient moisture was approximately 9% weight basis. Salts were obtained from Sigma. They were dissolved in water which was used as a plasticizer for producing thermoplastic starch. Salt content was calculated on a molar basis. The starch-water and starch-salt-water mixture was blended using a commercially available mixer and refrigerated overnight to distributed moisture uniformly. Water content was controlled initially by formulation and then by storing the samples in controlled temperature and humidity environments. Moisture content was measured using a gravimetric moisture balance.

Extrusion. Batches were extruded using a Brabender single-screw extruder with four temperature zones (profile: 80°-90°-110°C and a die temperature of 100°C). A 3:1 high shear mixing zone screw was employed. Ribbons (100 mm wide and approximately 0.5 mm thick) were extruded using a hangar-type die.

Resistance. Electrical resistance (R, ohms) was measured by a Keithley constant current source and an ElectroTech Systems four-point probe at room temperature and humidity according to ASTM D-257. A direct current technique was used (3). Conductance is equal to 1/R, corrected for volume, and reported as Siemens per centimeter (S/cm). For clarity on plots, the log of conductance is reported.

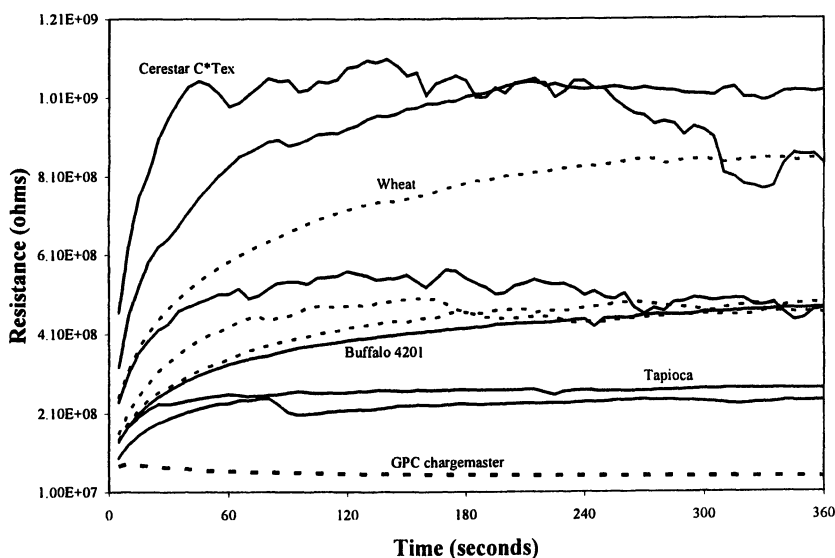


Figure 1: Resistance (in ohms) of native starches with ambient moisture content of less than 10% w/w. From top to bottom: Cerestar C*Tex, Cerestar C*PolarTex, MGP Wheat, GPC D-17F, Olgivic Wheat, Staley Kolguard, CPC International Buffalo 4201 Corn, Tapioca, Cerestar C*EmCap; and GPC Chargemaster.¹

¹ Names are necessary to report factually on available data; however, the USDA neither guarantees nor warrants the standard of the product, and the use of the name by USDA implies no approval of the product to the exclusion of others that also may be suitable.

Results and Discussion

Different native starches have different initial resistance depending on its ionic character. Figure 1 shows the electrical resistance of several starches in their native form using a powder cell electrode attachment. For efficiency and cost, Buffalo 4201 corn starch (CPC International) was chosen as the base material for ion-conductive materials.

Moisture content plays a role in the conductance of a material especially for water-sensitive materials like starch (3). The contribution of moisture to the conductance of thermoplastic starch tails off above 30% w/w moisture (Figure 2). In most cases, water can be replaced by another plasticizer such as glycerol. In the work with the metal halides, the moisture content was kept to less than 20% weight basis (4).

Incorporating metal halides into thermoplastic starch (called doping) plasticizes the material. Metal halide concentration was evaluated on a mole basis. The weight of each metal halide varied significantly although the number of ions remained the same. The flexibility, represented by elongation, increases as the amount of metal halide is increased (Figure 3). Looking at lithium iodide (LiI) in Figure 3, there is a 300% increase in elongation with a 3-fold increase in metal halide concentration. Large anions (i.e. I⁻) seem to have a plasticization effect on

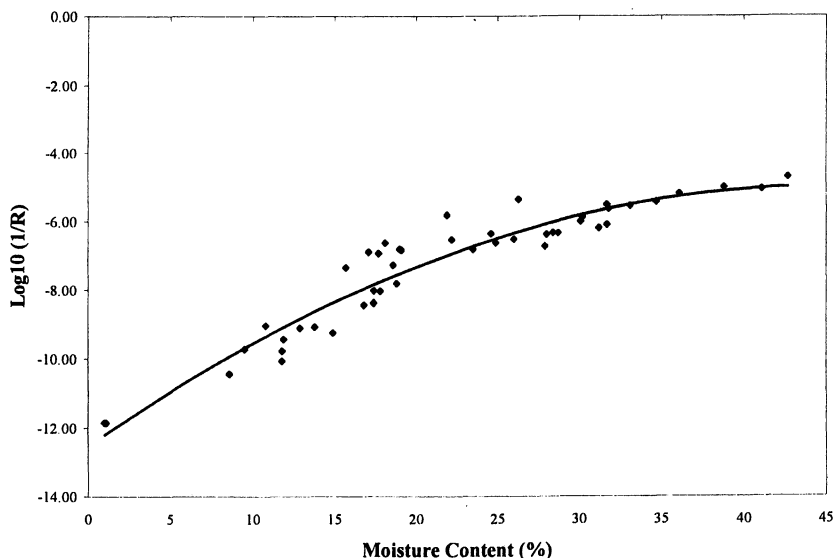


Figure 2: Relationship of conductance to moisture content for extruded thermoplastic starch using water as the sole plasticizer.

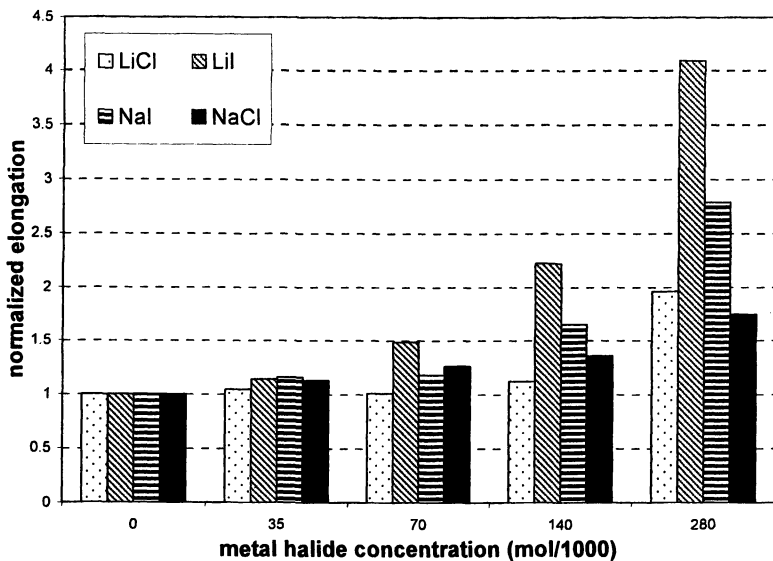


Figure 3. Elongation (normalized to a TPS control) versus metal halide concentration for thermoplastic starch. Moisture content is approx. 15% w/w.

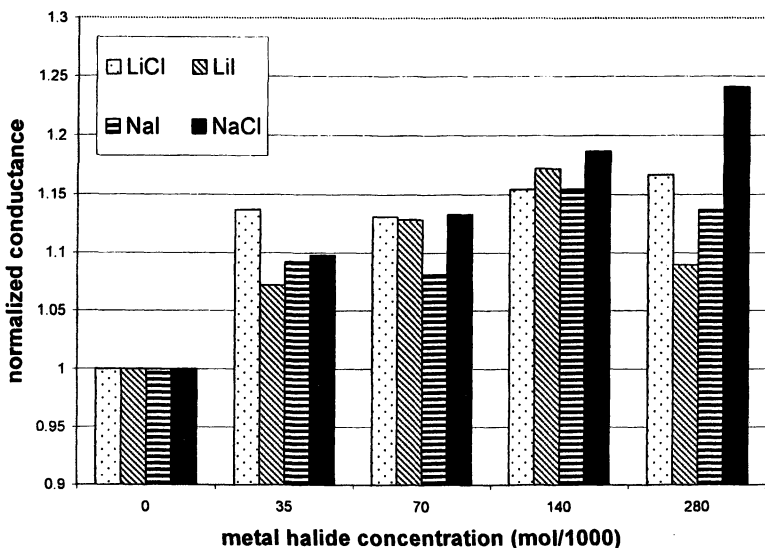


Figure 4. Conductance (normalized to a TPS control) versus metal halide concentration for thermoplastic starch. Moisture content is approx. 15% w/w.

thermoplastic starch. The moisture content for all samples is approximately 15% w/w so the hydrophilic nature of the metal halide is not a contributing factor. Tensile strength (data not shown) steadily decreases with increasing metal halide content.

The mobility of the polymer chains in thermoplastic starch plays a role in the conductivity mechanism, allowing cations to flow more freely in the system. Increasing the amount of metal halide in the system increases the conductance, but only to a certain degree. Figure 4 shows the effect on conductance from metal halide type and amount. In this case, a 10% increase is comparable to an order of magnitude ($\times 10$) increase in conductance. There seems to be a concentration effect related to material integrity. In order to tailor conductance, one can control the type and amount of metal halide in the system. Examining Figure 4 shows that for equal amounts of metal halide, the effect on conductance is different. For example, using lithium chloride in small amounts increases conductance better than similar amounts of other metal halides.

Conclusion

Thermoplastic starch, normally insulative, can be made electrically conductive using metal halide salts. The mode of conductance is ionic in nature. Polymer flexibility and salt content determine the final conductance value for thermoplastic starch. Relatively high conductance and mechanical integrity of the electroactive biopolymer system indicates that metal halide doped thermoplastic starch can be used as a solid polymer electrolytes.

References

1. Finkenstadt, V.L. *Applied Microbiology and Biotechnology*. **2005**, 67, 735-745.
2. Finkenstadt, V.L.; Willett, J.L. *Polymeric Materials: Science and Engineering*. **2001**, 85, 619-620.
3. Finkenstadt, V.L.; Willett, J.L. *Carbohydrate Polymers*. **2004**, 55, 149-154.
4. Finkenstadt, V.L. Willett, J.L. *Journals of Polymers and the Environment*. **2004**, 12, 43-46.

Chapter 18

Functionalizing Chitosan Using Tyrosinase: From the Construction of Bio-Based Products to the Assembly of Stimuli-Responsive Materials for Biofabrication

Gregory F. Payne^{1,*} and Tianhong Chen^{1,2}

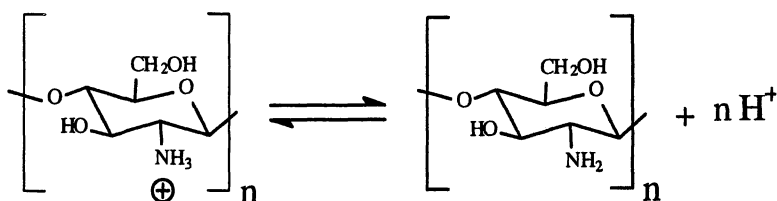
¹Center for Biosystems Research, University of Maryland Biotechnology Institute, 5115 Plant Sciences Building, College Park, MD 20742-4450

²Current address: TA Instruments, 109 Lukens Drive, New Castle, DE 19720

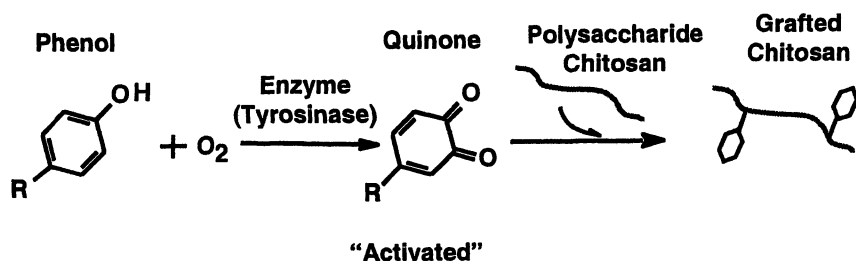
*Corresponding author: payne@umbi.umd.edu

Tyrosinase is a versatile enzyme that oxidizes a broad range of substrates that include low molecular weight phenols, peptides that contain tyrosine, and proteins with accessible tyrosine residues. The products of tyrosinase-catalyzed reactions are reactive *o*-quinones (or *o*-quinone residues) that can undergo uncatalyzed reactions with various nucleophiles. We are studying the use tyrosinase to generate quinones to undergo grafting reactions with the aminopolysaccharide chitosan. Initially, our goal was to demonstrate that tyrosinase could initiate the grafting of various plant phenols onto chitosan to create functional polymers from bio-based renewable resources. More recently, we are examining how tyrosinase can be enlisted to generate protein-chitosan conjugates with stimuli-responsive properties. Here we review our group's efforts over the last decade.

Chitosan is an aminopolysaccharide derived from chitin. The distinctive feature of chitosan is that it has primary amines at nearly every repeating residue, and these primary amines confer two important properties. At low pH, these amines are protonated making chitosan a water-soluble cationic polyelectrolyte. Raising the pH above about 6.3 leads to deprotonation of these amines, a reduction in chitosan's charge and ultimately to chitosan becoming insoluble. Thus, the first important property conferred by chitosan's primary amines is the pH-responsive solubility. Secondly, these amines are nucleophilic allowing chitosan to be derivatized using a range of electrophilic reagents.



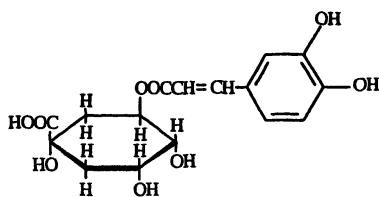
In our studies, we are derivatizing chitosan using the enzyme tyrosinase to *in situ*-generate the electrophile that subsequently reacts with chitosan. Tyrosinases, and related phenol oxidases, are ubiquitous in nature. These enzymes oxidize a diverse range of phenolic reactants using molecular oxygen as the oxidant (i.e. complex cofactors are not required for this oxidation). The product of this oxidation is an *o*-quinone that is reactive – it diffuses from the enzyme's active site and can undergo a cascade of uncatalyzed reactions. These reactions are familiar for their role in the enzymatic browning of foods, but these reactions are also integral to various natural processes - the hardening of the insect integument (i.e. quinone tanning) and the setting of the mussel's water-resistant adhesive. For the last decade, our group has been examining how tyrosinase can be enlisted to initiate reactions that lead to the grafting of functionalizing moieties onto chitosan's backbone.⁽¹⁾ Our hope when we started was that tyrosinase would provide an environmentally-friendly means to confer useful functional properties to chitosan – that is, to create useful bio-based products from renewable natural resources.



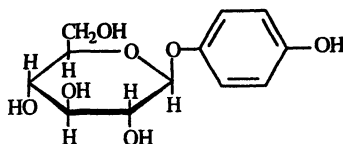
Tyrosinase-catalyzed modification with low molecular weight natural phenols

The suggestion that tyrosinase could provide a generic means to derivatize chitosan is supported by the facts that; (i) a diverse array of phenolic compounds are abundantly available from nature (i.e. plant phenols), and (ii) tyrosinases have a broad substrate range for phenols. To demonstrate the broad potential, we have performed reactions with various low molecular weight natural phenols and observed a variety of functional properties can be conferred to chitosan. In one of our early studies, we grafted chlorogenic acid onto chitosan. The name, chlorogenic acid, is a misnomer as this phenol has no chlorines in its structure. Rather, chlorogenic acid is a natural product that is abundant in coffee. The tyrosinase-catalyzed grafting of chlorogenic acid to chitosan yielded a derivative that was soluble under acid conditions but insoluble under neutral conditions (characteristic of chitosan). Unlike chitosan, however, the chlorogenic acid-modified chitosan became soluble under mildly basic conditions – presumably due to the hydrophilic and acidic functionality of the quinic acid moiety of chlorogenic acid.(2)

Arbutin is a natural phenol found in pears. When this phenol was reacted with tyrosinase in the presence of low concentrations of chitosan (0.5 %), the solution was observed to undergo gel formation.(3) Similarly, reactions between tyrosinase, dopamine and chitosan led to gel formation, and when this reaction was performed between two surfaces, the surfaces were bonded together even when “curing” occurred under wet conditions.(4)



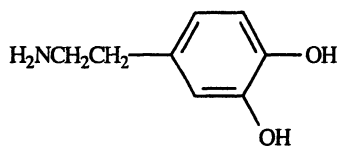
Chlorogenic Acid



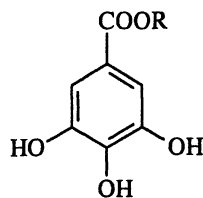
Arbutin

Gallates are abundant in tannins and various gallate esters are used as food antioxidants. We observed that gallates could be oxidized by tyrosinase although our results suggest that the gallate ester concentration has a significant effect on the reactions in this system (either the enzymatic and/or non-enzymatic reactions).(5) To react the hydrophobic octylgallate with tyrosinase we used a 30 % ethanol-water solution and performed the reaction in the presence of a chitosan film (i.e. chitosan modification was performed heterogeneously). After

reaction, the films were washed extensively, dried and then the contact angle was measured. These measurements indicate that the surface of the octylgallate modified-chitosan films was more hydrophobic than the surface of the unmodified chitosan film.(6)

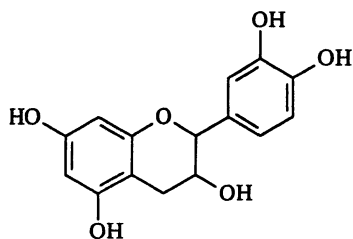


**Dihydroxyphenethylamine
(Dopamine)**



Gallate Ester

In a final example, we examined the tyrosinase-catalyzed modification of chitosan with catechin. After reaction, the polymer was purified by a series of precipitation, washing and resolubilization steps. Rheological measurements on the re-dissolved polymer indicated that the catechin-modified chitosan offers associative thickening properties.(7)

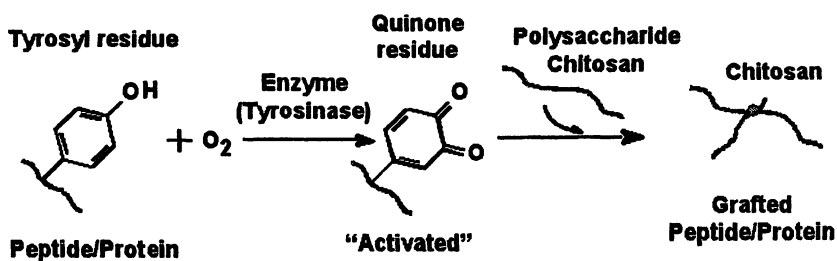


Catechin

The above results indicate that a broad range of low molecular weight phenols can be enzymatically-grafted onto chitosan to yield modified chitosans with various functional properties. Thus, tyrosinase allows access to the diversity of natural phenols available from plants and provides a facile means for creating functional chitosan derivatives. While these studies did not focus on the covalent linkage between the phenol and chitosan, chemical evidence based on mass spectrometry is consistent with the formation of either (or both) Michael-type adducts or Schiff-bases.(7)

Extending tyrosinase-catalyzed modification to peptides and proteins

Tyrosinase's activity is not confined to low molecular weight phenols – rather tyrosinase can oxidize the phenolic moieties (i.e. the tyrosine residues) of peptides and proteins. Thus, tyrosinase can access an even broader palate of compounds for grafting onto chitosan. Recent studies demonstrated that a model di-peptide (Tyr-Ala) could be enzymatically-grafted to chitosan. Further, peptides from casein hydrolyzate could be enzymatically grafted onto chitosan without the need for purification of the peptides from this complex mixture. Thus, the molecular recognition capabilities of tyrosinase can be exploited to selectively oxidize only peptides that have tyrosine residues – potentially this molecular recognition capability might eliminate the need for fractionation/purification of the peptide raw materials. Rheological studies with this peptide-modified chitosan indicated that it offered associative thickening properties.(8)



In addition to recognizing and reacting with tyrosine residues of peptides, the enzyme can oxidize accessible tyrosine residues on proteins. Once these residues are "activated", by conversion into *o*-quinone residues, they can be grafted onto chitosan to yield protein-chitosan conjugates. This was first demonstrated using the open-chain protein gelatin that has a small fraction of tyrosine residues localized to its telopeptide region. The addition of tyrosinase to a gelatin-chitosan blend was observed to result in a sol-gel transition to yield a relatively weak gel.(9,10) Interestingly, the tyrosinase-catalyzed gelatin-chitosan gels could be reversibly strengthened by cooling below the transition temperature that gelatin solutions normally undergo gel formation. This result suggests that tyrosinase-catalyzed reactions do not destroy gelatin's ability to undergo coil-to-triple helix transitions. Also interesting is that the gelatin-chitosan gel is transient and spontaneously breaks over time in processes that appears to follow percolation-type physical models.(11)

The ability of tyrosinase to initiate the grafting of peptides and proteins allows a broad range of bio-based products to be grafted onto chitosan. Importantly, the results with gelatin demonstrate that protein grafting is achieved with retention of structural characteristics important for functionality (i.e. gelatin's ability to undergo coil-to-helix transition). Also important is that the macromolecular conjugate offers characteristics unique from those of the starting materials (i.e. the tyrosinase-catalyzed gelatin-chitosan gel forms a transient network).

To further extend the tyrosinase-initiated grafting of proteins to chitosan, we collaborated with Dr. Bentley's group who engineered a green fluorescent protein (GFP) to have a C-terminal penta-tyrosine tail. It was reasoned that this tail would provide additional tyrosine residues in an unstructured region that would be readily accessible for tyrosinase-catalyzed activation. Results demonstrated that this GFP construct could be grafted onto the chitosan backbone and the GFP-chitosan conjugate retained the fluorescent properties characteristic of the protein. In addition, the conjugate also possesses the pH-responsive solubility that is characteristic of chitosan.⁽¹²⁾ Thus, tyrosinase permits the facile conjugation of proteins to chitosan to yield a conjugate with a combination of properties contributed by each of the biomacromolecules.

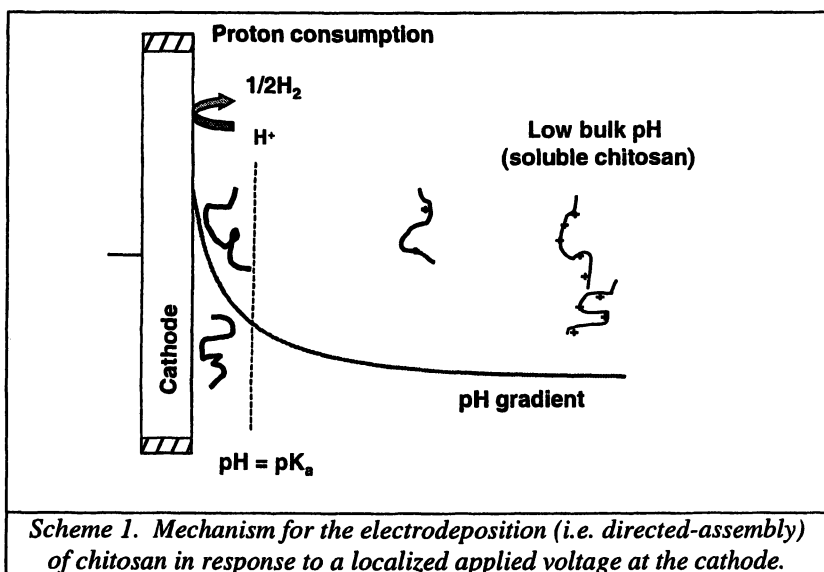
Exploiting chitosan's stimuli-responsive properties to direct the assembly of protein-chitosan conjugates

Through a series of collaborations, we are exploring the concept of biofabrication - the use of biological materials for micro/nano-scale fabrication.⁽¹³⁾ A key motivation for biofabrication is the recognition that many biological materials can self-assemble - potentially offering a "bottom-up" approach to constructing precise structures at the nanoscale. However, biological materials offer more than *self-assembly* capabilities. The ability of biological materials to be acted upon by precise biocatalysts (i.e. enzymes) allows macromolecular structures to be built through *enzymatic-assembly*. Tyrosinase-mediated conjugation of proteins to chitosan provides an example of such an enzymatic-assembly operation.

Another feature of biological polymers is that they are generally charged and therefore can respond to applied electrical signals. We are exploiting chitosan's pH-dependent electrostatic properties to direct its assembly in response to locally-applied electrical signals. Scheme 1 shows the mechanism for chitosan's *directed-assembly*. At a cathode surface, protons can be electrochemically reduced generating a localized pH-gradient. Chitosan chains that experience a localized pH that exceeds its pKa (≈ 6.3) will become insoluble

and will deposit at the cathode surface. After electrodeposition, the deposited chitosan film can be rinsed and neutralized after which it will remain deposited as a thin film (these films can be re-dissolved by rinsing with mild acid).^(14,15)

There are two important features of chitosan's directed-assembly (i.e. electrodeposition). First, electrodeposition does not require macroscopic electrodes but has been performed on microscopic cathode surfaces that have been patterned onto silicon wafers⁽¹⁶⁾ or onto the surfaces of microfluidic channels.⁽¹⁷⁾ With these microfabricated devices, the applied electrical signals can be controlled spatially (by the initial patterning of the electrodes) and temporally (based on when the voltage is applied), allowing the directed-assembly of chitosan to be well-controlled in space and time. The second important feature of this electrodeposition, is that protein-chitosan conjugates that retain chitosan's pH-responsive solubility can also be directed to assemble in response to localized electrical signals. In fact, recent studies have demonstrated that separate proteins can be guided to sequentially-assemble at different addresses (i.e. different electrode surfaces).⁽¹⁸⁾



While our studies are on-going, chitosan appears to provide unique properties for biofabrication. Its nucleophilic amines permit the enzymatic-assembly of proteins onto its backbone (via tyrosinase-mediated reactions). And, its pH-responsive solubility allows the directed-assembly of protein-chitosan conjugates at specific addresses (in response to localized electrical stimuli).

Conclusions

Tyrosinase's broad substrate range enables a diverse array of substrates (phenols, peptides and proteins) to be grafted onto chitosan to create bio-based polymeric products with a variety of macromolecular architectures and functional properties. In many cases, the substrates could be obtained as by-products from food processing or agricultural operations - potentially providing value-added opportunities for these renewable resources. Further, many of these substrates are obtained from edible materials such that all components in some systems (i.e. chitosan, tyrosinase, and the substrate) could be food-grade while products derived from these components would be expected to offer safety and environmental benefits. Finally, tyrosinase is simple to use with reactions occurring under mild conditions without the need for reactive reagents (the reactive *o*-quinone is *in situ*-generated by the enzyme). Thus, tyrosinase provides interesting means to graft substrates to chitosan to create functional bio-based products.

Tyrosinase's amino-acid-residue-specificity provides an interesting opportunity to enzymatically-assemble protein-chitosan conjugates with defined macromolecular architectures. Importantly, tyrosinase-mediated conjugation is performed under sufficiently mild conditions that the protein retains structural features critical to functional properties. Further, molecular biological methods can be enlisted to add accessible tyrosine residues to proteins (i.e. through tyrosine-rich fusion tags) suggesting that tyrosinase-mediated conjugation could provide a generic construction method. Potentially, such fusion tags could also allow control of the protein's orientation with respect to chitosan backbone. In addition to offering properties characteristic of the protein, the protein-chitosan conjugates may offer the pH-responsive properties characteristic of chitosan. These pH-responsive properties have been shown to allow conjugates to be directed to assemble in response to localized electrical signals. Thus, our hope is that tyrosinase mediated coupling to chitosan will emerge as an enabling technique for biofabrication.

Acknowledgements

Financial support was provided by the United States Department of Agriculture (2001-35504-10667) and the National Science Foundation (grant BES-0114790).

References

1. Payne, G.F.; Chaubal, M.V.; Barbari, T.A. Enzyme-catalysed polymer modification: Reaction of phenolic compounds with chitosan films. *Polymer* **1996**, *37*, 4643-4648.
2. Kumar, G.; Smith, P.J.; Payne, G.F. Enzymatic grafting of a natural product onto chitosan to confer water solubility under basic conditions. *Biotechnol. Bioeng.* **1999**, *63*, 154-165.
3. Aberg, C.M.; Chen, T.; Payne, G.F. Renewable resources and enzymatic processes to create functional polymers: Adapting materials and reactions from food processing. *J. of Polymers and the Environ.* **2002**, *10*, 77-84.
4. Yamada, K.; Chen, T.H.; Kumar, G.; Vesnovsky, O.; Topoleski, L.D.T.; Payne, G.F. Chitosan based water-resistant adhesive. Analogy to mussel glue. *Biomacromolecules* **2000**, *1*, 252-258.
5. Chen, T.H.; Vazquez-Duhalt, R.; Wu, C.F.; Bentley, W.E.; Payne, G.F. Combinatorial screening for enzyme-mediated coupling. Tyrosinase-catalyzed coupling to create protein-chitosan conjugates. *Biomacromolecules* **2001**, *2*, 456-462.
6. Govar, C.J.; Chen, T.H.; Liu, N.C.; Harris, M.T.; Payne, G.F. Grafting renewable chemicals to functionalize chitosan. In *Biocatalysis in Polymer Science*, 2003; pp 231-242.
7. Wu, L.-Q.; Embree, H.D.; Balgley, B.M.; Smith, P.J.; Payne, G.F. Utilizing renewable resources to create functional polymers: Chitosan-based associative thickener. *Environ Sci. & Technol.* **2002**, *36*, 3446-3454.
8. Aberg, C.M.; Chen, T.H.; Olumide, A.; Raghavan, S.R.; Payne, G.F. Enzymatic grafting of peptides from casein hydrolysate to chitosan. potential for value-added byproducts from food-processing wastes. *J. Agric. Food Chem.* **2004**, *52*, 788-793.
9. Chen, T.H.; Embree, H.D.; Wu, L.-Q.; Payne, G.F. In vitro protein-polysaccharide conjugation: tyrosinase catalyzed conjugation of gelatin and chitosan. *Biopolymers* **2002**, *64*, 292-302.

10. Chen, T.; Embree, H.D.; Brown, E.M.; Taylor, M.M.; Payne, G.F. Enzyme-Catalyzed Gel Formation of Gelatin and Chitosan: Potential for in situ Applications. *Biomaterials* **2003**, *24*, 2831-2841.
11. Kostko, A.F.; Chen, T.; Payne, G.F.; Anisimov, M.A. Dynamic Light-scattering monitoring of a transient biopolymer gel. *Physica A* **2003**, *323*, 124-138.
12. Chen, T.H.; Small, D.A.; Wu, L.-Q.; Rubloff, G.W.; Ghodssi, R.; Vazquez-Duhalt, R.; Bentley, W.E.; Payne, G.F. Nature-inspired creation of protein-polysaccharide conjugate and its subsequent assembly onto a patterned surface. *Langmuir* **2003**, *19*, 9382-9386.
13. Wu, L.-Q.; Payne, G.F. Biofabrication: using biological materials and biocatalysts to construct nanostructured assemblies. *Trends Biotechnol.* **2004**, *22*, 593-599.
14. Wu, L.-Q.; Gadre, A.P.; Yi, H.M.; Kastantin, M.J.; Rubloff, G.W.; Bentley, W.E.; Payne, G.F.; Ghodssi, R. Voltage-dependent assembly of the polysaccharide chitosan onto an electrode surface. *Langmuir* **2002**, *18*, 8620-8625.
15. Fernandes, R.; Wu, L.-Q.; Chen, T.H.; Yi, H.M.; Rubloff, G.W.; Ghodssi, R.; Bentley, W.E.; Payne, G.F. Electrochemically induced deposition of a polysaccharide hydrogel onto a patterned surface. *Langmuir* **2003**, *19*, 4058-4062.
16. Wu, L.-Q.; Yi, H.M.; Li, S.; Rubloff, G.W.; Bentley, W.E.; Ghodssi, R.; Payne, G.F. Spatially selective deposition of a reactive polysaccharide layer onto a patterned template. *Langmuir* **2003**, *19*, 519-524.
17. Kastantin, M.J.; Li, S.; Gadre, A.P.; Wu, L.-Q.; Bentley, W.E.; Payne, G.F.; Rubloff, G.W.; Ghodssi, R. Integrated fabrication of polymeric devices for biological applications. *Sensors and Materials* **2003**, *15*, 295-311.
18. Yi, H.M.; Wu, L.-Q.; Ghodssi, R.; Rubloff, G.W.; Payne, G.F.; Bentley, W.E. Signal-directed sequential assembly of biomolecules on patterned surfaces. *Langmuir* **2005**, *21*, 2104-2107.

Chapter 19

Pectin-Based Networks for Non-Food Applications

**LinShu Liu, Michael Tunick, Marshall L. Fishman, Kevin B. Hicks,
Peter H. Cooke, and David R. Coffin**

**Eastern Regional Research Center, Agricultural Research Service,
U.S. Department of Agriculture, 600 East Mermaid Lane,
Wyndmoor, PA 19038**

Two types of pectin based composite networks were prepared and evaluated in this study: (I) Pectin-protein composite films and (II) Pectin gels incorporated with silicate nanoparticles. The structural and mechanical characterizations indicated that the properties of the composite films could be controlled by altering the compositions and the ratios of components, or by cross-linking. The pectin-silicate gels were loaded onto the surfaces of paper strips to form a coating layer. The coating layer enhanced the flame retardancy and was able to retain the basic functionalities of the papers.

Pectin is a cell wall polysaccharide found in vegetables, fruits, and other higher plants. Residues from agricultural processing, such as apple pomace, citrus fruit peels and sugar beet pulp, contain a large amount of pectin and are the main source of commercially available pectin. It is estimated that about $5.5\text{--}8.8 \times 10^5$ dry tons of pectin could be annually produced from the by-products of the U.S. beet sugar and fruit juice industries. Profitable utilization of these enormous quantities of pectin is critical for the future profitability of agribusiness and rural development. Traditionally, pectin is used as gelling and thickening reagent in food industries. However, only a small portion of the

commercially available pectin, about 8 million pounds, could be consumed by the U.S. food market. Furthermore, the requirement of the U.S. food market for pectin grows very slowly and is almost saturated. The efforts to explore the new uses of pectin for non-food applications may present a new strategy to develop a broad market for this polysaccharide. This is because of (I) the wide diversity and rapid growth of non-food markets; (II) the unique functionalities of pectin; and (III) the potential of pectin to be modified into a variety of derivatives.

A spectrum of pectin based non-food applications has been developed in our laboratory. Plasticized pectin/starch films and pectin/poly(vinyl alcohol) blends were introduced as a biodegradable membrane and characterized for pharmaceutical use and as packaging materials (1-3). Pectin formulations are currently examined *in vivo* as prebiotics (4). Pectin derived microparticles, 3-D porous structures, or gels were studied for the controlled release of active substances and tissue engineering (5-7). In this chapter, we outline the most recent developments of pectin related non-food applications conducted by our research team.

Pectin-protein composite films

Pectin, as a group of complex polysaccharides, consists primarily of blocks of (1-4)- α -galacturonic acid residues interrupted by single (1-2)- α -rhamnose units in the backbone, to which are attached branch chains of (1-5)- α -L-arabinan or arabinogalactan. The conditions under which pectin forms gels are determined by its structure. Low methoxyl pectins with the degree of esterification (D.E.) from 25 to 50% will form a gel in presence of divalent cations, high methoxyl pectin with the D.E. value from 50 to 80% will form gels in the presence of sugar and/or acid. Typically, materials which gel are also good film formers. The potential uses of pectin films include drug encapsulation, recyclable packing materials, and coatings for foods and papers (8-12). The inclusion of divalent metal ions, synthetic polymers, proteins and other biopolymers into the pectin formulations alters the physical and mechanical properties of resultant composites. Therefore, new uses of pectin could be developed through the better control of film properties by incorporation into pectin of the materials mentioned above.

Fabrication and characterization of pectin-protein composite films.

Composite films were prepared by combining various proteins and a plasticizer, glycerol, with pectin as described previously (1). The proteins used in this study were bovine serum albumin (BSA) or chicken egg albumin (CEA),

gelatin from cold water fish skin (FSG), bovine skin (type B, BGB), or porcine skin (type A, PGA), and a plant protein from soybean flour (SBF). The amounts of each component in 140 ml of distilled water were: pectin 5.0-2.5 g, glycerin 6.0 g, and protein 1.5-3.0 g. In some experiments, the films were further treated with 0.1% glutaraldehyde in ethanol at room temperature overnight.

For structural characterization, proteins were labeled with fluorescent red 646 dye prior to blending with pectin. Samples of the films were glued to microscope slides and examined on a model TCS-SP laser scanning confocal microscope (Leica Microsystems, Exton, PA). The parameters for the image acquisition were set at 640/666 nm (excitation/emission) for confocal fluorescence of the proteins and at 425/475 nm for the autofluorescence intensity of pectin in two channels.

Mechanical properties of resultant composite films were investigated by measuring their storage modulus (E'), loss modulus (E'') and loss tangent ($\tan \delta$). The small deformation thermal dynamic mechanical analysis (TDMA) was performed on a Rheometric Scientific RSA II Solids Analyzer (Rheometric Scientific, Piscataway, NJ) using a film-testing fixture at the following setting: nominal strain, 0.1%; applied frequency, 10 rad/s; temperature, ranging from -100 °C to 200 °C; heating rate, 10 °C/min; gap between the jaws at the beginning of each test, 23.0 mm.

Mechanical testing was also performed by the use of a Sintech 1/G universal testing machine (MTS Systems, Eden Prairie, MN) at room temperature. Both ends of a sample strip were held in place with pneumatic grips, length and thickness were entered, and the strips underwent tensile deformation until breakage. The initial slope of the force-time curve was calculated by the instrument's software.

The water resistance of the films were determined by measuring the weight change after the films were equilibrated at the relative humidity of 22% (over drierite) or at 95% (over water) in a desiccator at room temperature for 2 weeks.

Structural properties of pectin-protein composite films.

The composite films have a two-phase, interpenetrating network structure as revealed by confocal scanning microscopy (Fig. 1). The pectin in composite film blends formed a continuous, uneven phase, consisting of numerous small crevices and ridges at a size less than 1 μm , just as shown in pure pectin films (13). Protein appeared to be fairly distributed into the pectin structures and embedded in the pectin matrices. This was seen for all pectin-protein blends tested in this study, indicating that blending the mixtures of pectin and proteins resulted in a compatible composite. For the composites consisting of BSA, CEA, FSG, BGB, or PGA, the films appeared smooth and transparent by casual

observation. For those obtained from SBF, irregular particles ranging from 2 to 6 μm in size were uniformly distributed within the pectin phase. The films were rough, dense and brittle in appearance. This may be attributed to the minor components in soybean flour, such as insoluble polysaccharides and fat. In general, in comparison with the films prepared from the mixture of pectin and starch, where the starch is acting more as a filler than as a secondary polymeric component, the substitution of starch with protein seems to introduce a more compatible composite film.

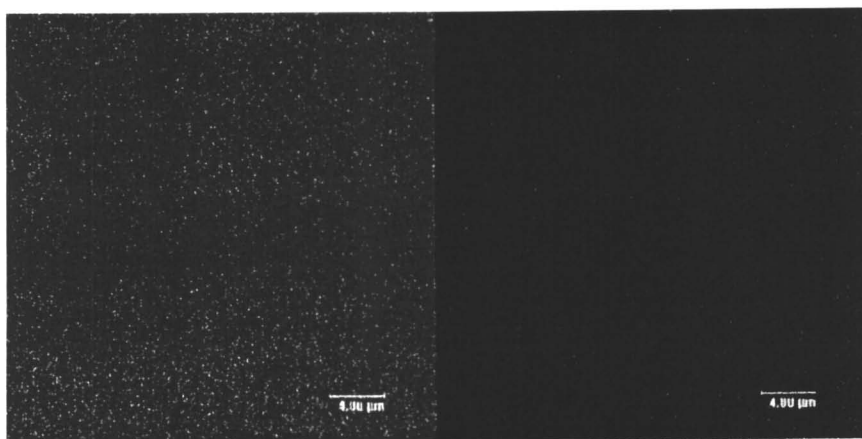


Figure 1. Averaged confocal fluorescence image of pectin-BSA composite films
Left: pectin networks, *ex/em*, 425/475nm; right: BSA networks, 640/666 nm.
(See page 4 of color inserts.)

Physical properties of pectin-protein composite films.

As a complement to microscopic examination, structural characteristics of the films were investigated by TDMA. The method was used to determine interactions among components by measuring the E' , E'' and $\tan \delta$ after sample underwent a small sinusoidal deformation. Figure 2 shows the effect of the substitution of starch with protein CEA on the storage modulus and loss modulus of the composite films. There are some similarities in the trends of the temperature-dependent dynamic mechanical characteristics between the pectin-CEA film and the pectin-starch film. However, as the temperature increased, the difference between E' value and E'' values gradually became less and less for pectin-CEA film in comparison with that for pectin-starch film. This difference was more obvious at around ambient temperature.

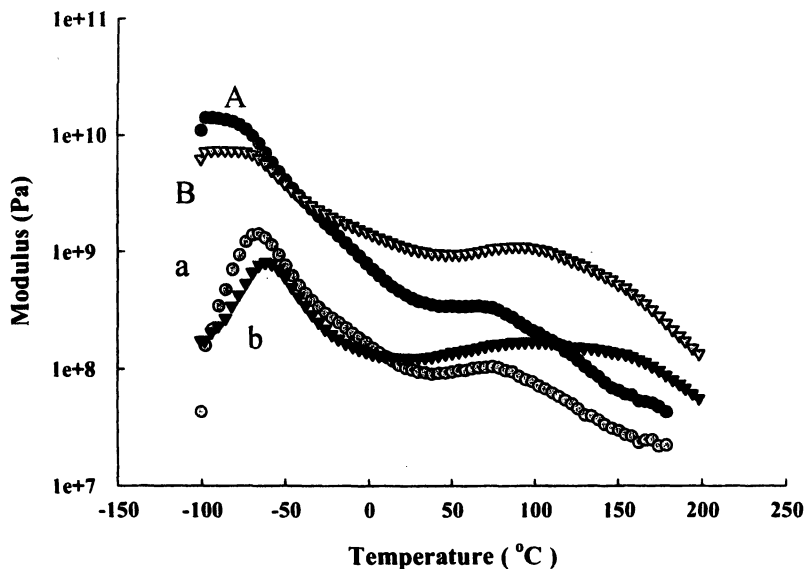


Figure 2. Effect of the substitution of starch (B, b) with CEA (A, a) on storage modulus (A, B) and loss modulus (a, b) for pectin composite films. (See page 4 of color inserts.)

Storage modulus is a measure of the energy stored and recovered; whereas loss modulus is a measure of the energy dissipated per cycle of deformation. The closer the values of E' and E'' , the more flexible the films are. These results suggest a more flexible thermoplastic material by the substitution of rigid starch granules with denatured, uncoiled CEA macromolecules. This trend was seen for all tested pectin-protein composite films (Table 1). This may be of interest to scientists and engineers involved in drug encapsulation processing, where the flexibility of films is important. Although flexible films usually can be obtained by increasing the processing temperature appropriately, a higher temperature is harmful to most bioactive compounds and is more costly. Thus, processing at ambient temperature is favored over operating at higher temperatures.

The effect of incorporating proteins into plasticized pectin films on their mechanical properties was also evaluated by an universal testing machine. This was done by measuring their maximal elongation and tensile strength. As shown in Figure 3, the substitution of starch with various proteins dramatically increased the values of maximal elongation; meanwhile, the tensile strength was retained or even enhanced (Fig. 3).

Table I. Effect of Proteins on $\tan \delta$ of pectin composite films

<i>Proteins</i>	<i>Loss tangent (E''/E')</i>
CEA	0.289 ± 0.050
BSA	0.330 ± 0.040
BGB	0.348 ± 0.023
FSG	0.293 ± 0.019
PGA	0.342 ± 0.028
SBF	0.308 ± 0.030
Control: Starch	0.159 ± 0.004

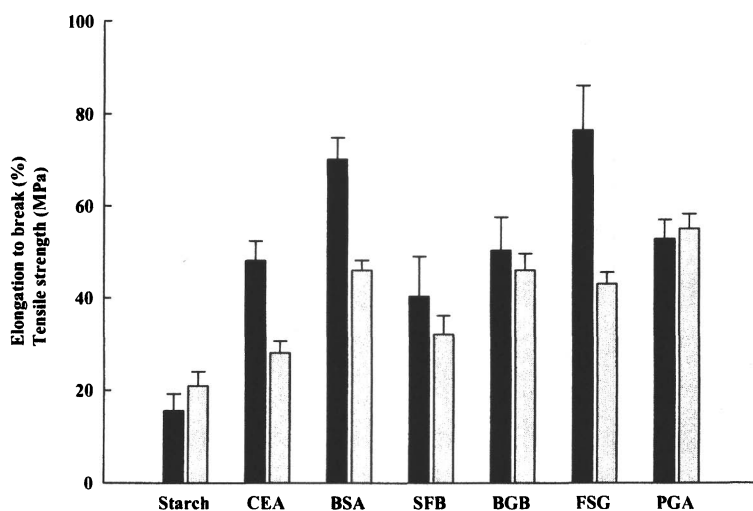


Figure 3. Effect of protein on maximal elongation (black bar) and tensile strength (gray bar) of pectin based composite films.

Physical properties of cross-linked pectin-protein films.

Pectin-protein composite films were further evaluated after reacting with glutaraldehyde, divinyl sulfone, or pectin-polyaldehyde. In this paper, we only report the results regarding the films treated with glutaraldehyde.

As shown in Table 2, the initial modulus (IM) increased by more than one order of magnitude after cross-linking. This was even seen after the films were equilibrated at 90% humidity. Large increase in IM could be attributed to the suppression of water adsorption on the films after cross-linking (data not shown). In contrast, glutaraldehyde treatment had no effect on pectin/starch films.

Table II. Effect of Cross-Linking on the Initial Modulus of Pectin Films

<i>Proteins</i>	<i>Initial Modulus (MPa)</i>			
	<i>A</i>	<i>B*</i>	<i>C</i>	<i>D*</i>
CEA	28(1.4)	990(155)	18(2.7)	657(11)
BSA	18(3.3)	1065(139)	13(3.3)	324(44)
BGB	19(4.5)	1354(194)	11(2.9)	637(27)
FSG	20(1.5)	1083(122)	14(1.5)	303(11)
PGA	17(2.8)	1400(108)	11(1.5)	613(530)
SBF	15(0.8)	627(33)	6(1.3)	327(34)
Control:				
Starch	22.15(0.23)	21.95(0.44)	14(0.4)	6(0.4)

Note: All films were equilibrated at 22% (A and B) or 95% (C and D) relative humidity. * Films were cross-linked with glutaraldehyde. Tests were triplicated and expressed as mean \pm (SD).

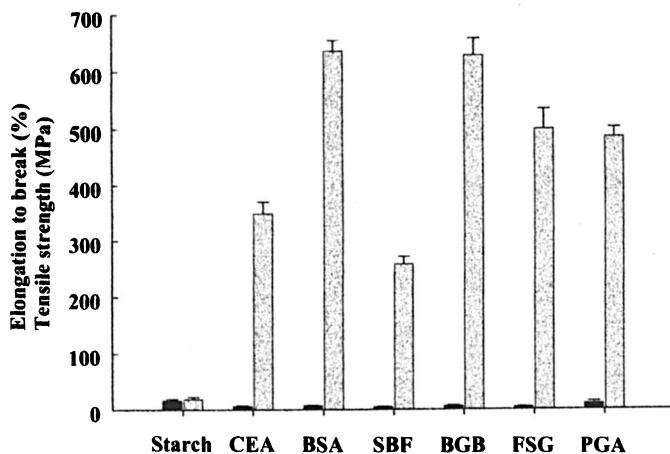


Figure 4. Effect of cross-linking on the maximal elongation (black bar) and tensile strength (gray bar) of pectin-protein composite films.

Furthermore, a dramatic increase in tensile strength and decrease in maximal elongation also were detected for all pectin-protein films after cross-linking (Fig. 4). Again, no changes in values of tensile strength or maximal elongation of pectin-starch films could be detected after cross-linking (Fig. 3,4).

Pectin-layered silicate nanocomposites: preparation and flame retardant property

Strategies to reduce the flammability of materials can be categorized as (I) modification of gas-phase oxidation chemistry by using halogenated flame retardants and (II) modification of the condensed-phase chemistry by incorporating inorganic additives into the materials (14). Often the second approach has been applied to reduce flammability and enhance thermal stability of existing polymeric materials. Nanoparticles or nanocomposite precursors have been used to fill or coat materials for this purpose. Among them, polymer-layered silicate nanostructures have been more widely investigated than nanoparticles fabricated from other materials because their intercalated and exfoliated (or delaminated) chemistry has been well studied (15). Research in polymer-layered silicate nanocomposites has been done mainly with synthetic polymers, such as polypropylene, polyethylene oxide, polyether sulfone, polyether ketone, polymethyl methacrylate, polystyrene, polyimide, and polyurethane. However, research related to incorporation of silicate nanoparticles into natural polymers has received less attention. In this study, pectin-layered silicate gels were prepared and coated on the surfaces of paper strips. The flame-retardant property of resultant materials was investigated. Considering the unique properties of pectin such as the film forming capability and adhesive activity, the pectin-layered silicate nanostructures may be useful in the manufacture of flame resistant papers, textiles and materials in daily life.

Preparation and characterization of paper strips coated with pectin-layered silicate nanocomposite.

Pectin-layered silicate gels were prepared in solution (16). The nanoparticles and the polymers were mixed in pure water; the entropy gained by water adsorption allows polymer chains to diffuse between the silica layers. The gels were coated on the surfaces of paper strips by dipping the strips into the gel-like mixtures. After evaporation of the solvent, an intercalated nanocomposite resulted. The strips were examined for structure by SEM and the inherent flame retardancy by a standard test method ASTM D 6413-99 using a specified test cabinet apparatus, which was originally designed for the test of textile flame

resistance. Afterflame time (AFT) and afterglow time (AFG) were measured. AFT indicates how long the fire could be continued after the flame is removed. AFG is the time glow continues after removing the ignition source and the cessation of flaming, respectively. The char length, the distance from the bottom of the paper to the furthest point of visible damage after 25 g tearing force is applied to the paper, also was recorded. The effect of pectin-layered silicate nanostructure on the mechanical properties of coated papers also was investigated by the method as described for the analysis of pectin-protein composite films.

Physical properties and flame retardancy of paper strips coated with pectin-silica gels.

SEM micrographs of the paper strips treated with pectin-layered silicate nanostructures are shown in Figure 5.

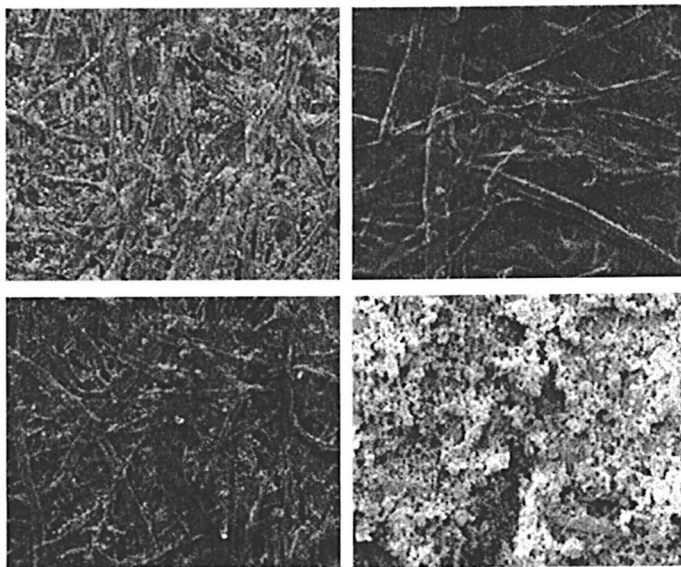


Figure 5. SEM images of paper strips (top right) and its derivatives coated with pectin gel (top left), silicate in solution (bottom left) and pectin-layered silicate (bottom right). Filed width, 10 μ m.

For the paper strips treated with pectin gels without silicate, a thin pectin film was formed on the paper surfaces, for the paper strips treated with pure water containing silicate nanoparticles, only a few silicate clouds could be found on the paper surfaces; for the strips treated with pectin-layered silicate gel, more silica particles were embedded in the pectin layer, which covered the entire paper surfaces. Table III shows the improvement of flame retardancy of the paper strips coated with pectin-layered silicate gels. Plain paper burned quickly; 8 seconds after being exposed to flame, no sample was left, thus no afterflame time and no char length could be measured. Paper pre-treated with pectin showed improved properties, it took about 12 seconds to burn the whole samples, indicating that pectin has some inherent flame resistant property, which may come from the combined thermal insulation and mass barrier effect. Specimens pre-treated with silica gel also show better flame resistance than the plain paper. The silica nanoparticles possess a huge surface area and are heat retardant materials. The silica pre-treated paper did not show expected flame resistance, because very little of the silica formulation adhered to the paper (Fig. 5). The specimens treated with pectin and silica formulation show the best results. After being exposed to the flame for 12 seconds, the flame was removed, the fire continued for an additional 9 seconds and stopped. About 2/3 of the paper remained undamaged (Fig. 6). In this study, we also found that the increase in coating thickness or the particle volume of the silicate fraction contributed to improved flame resistance (data not shown).

Table III. Flammability of Papers Treated with Pectin Formulations

Characteristics	Plain	+ Pectin	+ Silicate	+ Pectin-Silicate
Time required to burn the whole samples (s)	8	12	14	Not applicable
Char length (mm)	-	-	-	86
Afterflame time (s)	-	0	0	9
Afterglow time (s)	10	23	34	38

Table IV. Tensile Strength of Paper Strips Coated with Pectin-Layered Silicate Nanoparticles

Specimens	Tensile strength (MPa)	Modulus (MPa)	Elongation to break (%)
Plain Xerox paper	14.3	242.1	5.6
Pectin-silicate coated (1:1, w/w; 5.4 mg/cm ²)	14.1	269.4	4.9

With respect to paper functionality, the coating with pectin-layered silicate structures on the paper surfaces did not affect the basic functions of the paper, such as writing on it with ink or labeling with stickers (data not shown). The coating also did not alter the mechanical properties of the paper (Table IV).

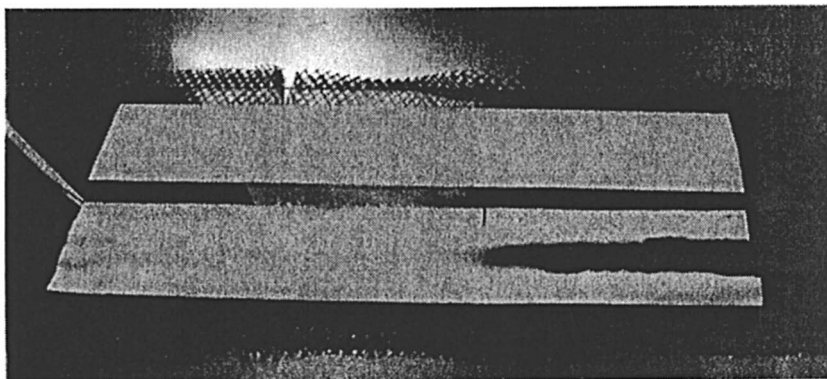


Figure 6. Images of papers coated with pectin-layered silicate before (top) and after (bottom) being exposed to flame. (See page 4 of color inserts.)

Summary

Based on the gelling, film forming and adhesive properties of pectin, a variety of naturally occurring polymers, such as proteins, or synthetic materials, such as silicate nanoparticles, could be integrated into pectin formulations. The resultant composite gels could be subsequently cast as a film with unique properties or layered on the surfaces of a matrix to introduce new characteristics to existing substrates. Proteins co-exist with polysaccharides to form organs and tissues with specific properties. Some are as hard as bone, some are as tough as skin. Some are as flexible as a blood vessel. Through controlling the types of interaction between the two components, the properties of pectin/protein composites could be altered to meet the demands of various applications. Silicate nanoparticles have demonstrated various utilities ranging from biomedical substitutes to engineering materials. Applications of silicate nanoparticles could be further expanded by formulating them with pectin gels.

This study explored the new strategies to broaden pectin applications. These strategies included forming composites or hybrids of pectin with organic or inorganic compounds.

* Mention of trade names or commercial products in this article is solely for the purpose of providing specific information and does not imply recommendation or endorsement by the U.S. Department of Agriculture.

References

1. Coffin, D. R.; Fishman, M. L. *J. Appl. Polym. Sci.* **1994**, *54*, 1311.
2. Fishman, M. L.; Coffin, D. R.; Unruh, J. J.; Ly, T. *J.M.S.-Pure Appl. Chem.*, **1996**, *A33(5)*, 639.
3. Fishman, M. L.; Coffin, D. R. *Carbohydr. Polym.* **1998**, *35*, 195.
4. Hotchkiss, A. T., Olano-Martin, E., Grace, W. E., Gibson, G. R. Rastall, R.A. Pectic Oligosaccharides as Prebiotics. In *Oligosaccharides in Food and Agriculture*; Eggleston, G. and Cote, G. L., Eds.; ACS Symposium Series 849, American Chemical Society: Washington, D.C. **2003**; p 54
5. Liu, L.S.; Fishman, M. L.; Kost, J.; Hicks, K. B. *Biomaterials*, **2003**, *24*, 3333.
6. Liu, L.S.; Won, Y. J.; Cooke, P.H.; Coffin, D. R.; Fishman, M. L.; Hicks, K. B.; Ma, P. X. *Biomaterials*, **2004**, *25*, 3201.
7. Liu, L.S.; Chen, G.; Fishman, M. L.; Hicks, K. B. *Drug Delivery*, **2005**, *12*, 149.
8. Hind, J.; Hopkins, W. U.S. Patent 4,129,134, 1978.
9. Kashiwagi, T., Shields, J. R., Harris, R. H., Davis, R.D. *J. Appl. Polym. Sci.*, **2003**, *87*, 1541
10. Motomatsu, M., Takahashi, T., Nie, H.-Y., Mizutani, W. H., Tokumoto, H. *Polymer*, **1997**, *38*, 177
11. Coffin, D. R.; Fishman, M. L. *J. Agric. Food Chem.* **1993**, *41(8)*, 1192.
Kester, J. J.; Fennema, O.R. *Food Technol.* **1986**, *12*, 47.
12. Schultz, T. H.; Miers, J. C.; Owens, H. S. *J. Phys. Colloid Chem.* **1949**, *53*, 1320.
13. Coffin, D. R.; Fishman, M. L. In *Polymers from Agricultural Coproducts*; Fishman, M.L.; Friedman, R. B.; Huang, S. J., Eds.; ACS Symposium Series 575, American Chemical Society: Washington, D.C. **1994**; p 82.
14. Kashiwagi, T., Shields, J. R., Harris, R. H., Davis, R.D. Jr. *J. Appl. Poly. Sci.* **2003**, *87*, 1541.
15. Gilman, J. W. *Apply. Clay Sci.* **1999**, *15*, 31.
16. Alexandre, M., Dubois, P. *Mater. Sci. & Eng.* **2000**, *28*, 1.

Hydrogels Constructed via β -Hairpin Peptide Self-Assembly

Bulent Ozbas¹, Joel P. Schneider², and Darrin J. Pochan¹

Departments of ¹Materials Science and Engineering, Delaware Biotechnology Institute and ²Chemistry and Biochemistry, University of Delaware, Newark, DE 19716

Rigid, physical peptidic hydrogels with controlled stiffness are formed via β -hairpin self-assembly. Intramolecular folding followed by consequent gelation can be triggered by pH, temperature and ionic strength. The magnitude of the stimulus governs the kinetics of self-assembly and final rigidity of the materials. Hydrogels preserve their rigidity when they are cooled below their formation temperature. In addition, these hydrogels recover their mechanical strength rapidly after cessation of high shear-rates. By altering the β -hairpin hydrophobicity, the folding transition, and, thus, gelation transition, can be tuned and made reversible. TEM and SANS data reveal that the network structure of the hydrogels is composed of dense fibrillar assemblies with monodisperse cross-sectional dimensions (~ 3 nm). Rheology and TEM shows that the fibrils are crosslinked to each other permanently by hydrogen bonding and hydrophobic interactions. Hydrogels are cytocompatible and non-toxic to fibroblast cells and promote proliferation.

Oligopeptides and polypeptides can undergo protein-like folding events via changes in environmental conditions, such as pH, temperature, ionic strength, or light, and self-assemble into hierarchical structures in different length scales with specific molecular and energetic interactions.¹⁻⁶ Moreover, these transitions and interactions can be controlled at the molecular level and one can engineer materials with different properties by altering the primary structure. The

responsive behavior of these molecules to a stimulus and their rich nano- and micro-scale self-assembled structures make peptide molecules excellent candidates for biomaterials applications, such as tissue engineering, drug delivery and microfluidics. Hydrogels, an important class of biomaterials, have extensive applications due to their viscoelastic properties, high surface area of network structure and their ability to alter mass transport.⁷ In our previous studies,⁸⁻¹⁰ we have introduced a peptide based, stimulus-responsive hydrogel formation strategy using β -hairpin peptides that undergo an intramolecular folding event followed by an intermolecular self-assembly process. This leads to formation of a network structure and a soft-solid, rigid, processible, physical hydrogel with dilute peptide concentrations (< 2 wt %) at a variety of environmental conditions including physiological pH, temperature and ionic strength. The folding of the molecules and, thus, their β -sheet formation and self-assembly transitions, can be altered via slight changes in the peptide sequence. At some physical conditions these transitions can also be reversible. The final materials properties, especially viscoelasticity, can be tuned by changing the rate of molecular self-assembly through variations in the magnitude and type of folding stimuli.

There are various examples in the literature of triggered gelation of biomacromolecules such as gelatin,¹¹ polysaccharides,¹² β -lactoglobulin,¹³ and synthetic peptides such as elastin-mimetic peptides¹⁴ and polypeptides with leucine zipper domains.¹⁵ In addition, peptides constituting hydrophobic and hydrophilic residues that form β -sheet and β -amyloid-like structures have been studied as biomimetic materials by a number of groups.¹⁶⁻¹⁸ Most of the β -amyloid like structures are not responsive to an external stimulus; random coil to β -sheet transitions are not reversible and they form high-order, insoluble, hierarchical structures.

Figure 1 shows the structure of the peptide Max1 and its reversible triggered-self-assembly mechanism. Max1 is a 20 amino acid β -hairpin with two β strands connected by a turn sequence. The strands are composed of alternating lysine and valine residues with high β -sheet propensity and the turn is a tetrapeptide sequence (Val-^DPro-^LPro-Thr) that is designed to adopt a type II' turn. While lysine has a hydrophilic character at acidic conditions, valine is a hydrophobic amino acid making Max1 locally amphiphilic. When Max1 is dissolved in aqueous media at slightly acidic pH conditions, it exhibits an unordered secondary structure due to the electrostatic repulsion of the protonated, positively charged lysine residues. If the pH of the solution is increased, for example to 9, some lysine residues deprotonate thereby decreasing interstrand electrostatic repulsion and the molecule intramolecularly folds into a β -hairpin conformation. This conformation is stabilized by intramolecular hydrogen bonding between strands. In the folded state, the molecule becomes facially amphiphilic; the lysine residues are positioned at one face of the molecule, while the valine residues are at the other face. The β -hairpin

undergoes further assembly with another molecule to bury their hydrophobic faces by bringing together their valine residues. As the triggered-folding and assembly proceeds, the low-viscosity, dilute peptide solution changes into a self-supporting, soft-solid, rigid, and clear hydrogel material.

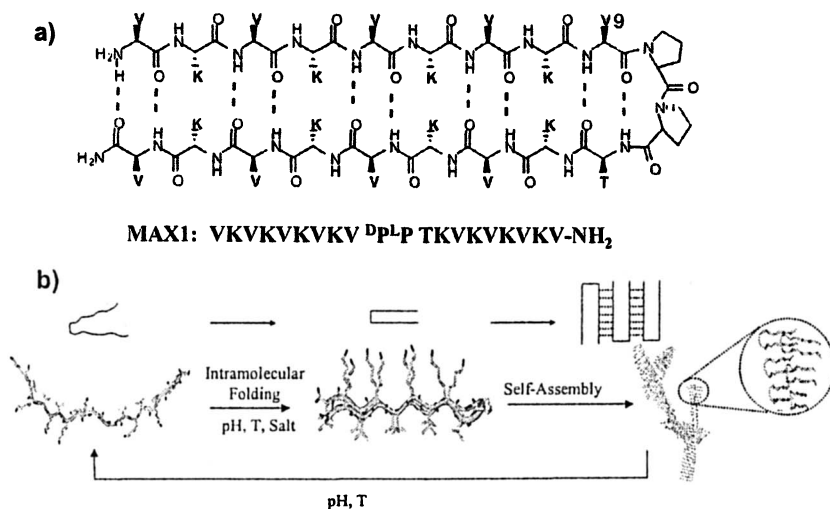


Figure 1. a) β -Hairpin structure and primary sequence of 20 residue Max1. b) Intramolecular folding and self-assembly mechanism.

Here, we describe the self-assembly of β -hairpin peptides that can be triggered by pH, temperature, or ionic strength. The changes in secondary structure and rheological behavior with application of the stimulus are discussed. The thermally responsive and reversible hairpins are reviewed. The characterization of hydrogel network and nanostructure is described using electron microscopy and neutron scattering. The rheological behavior of the hydrogels and the effect of kinetics of self-assembly on the viscoelastic properties is studied by dynamic oscillatory measurements. Finally, the cytocompatibility of the self-assembled β -hairpin peptide hydrogel surfaces are discussed.

Experimental

Peptide Synthesis and Sample Preparation: Peptides were prepared on Pal amide resin via automated Fmoc peptide synthesis employing an ABI 433A

peptide synthesizer and HBTU/HOBT activation. The details of the peptide preparation are given elsewhere.⁸ Peptide solutions were prepared by dissolving lyophilized peptide first in deionized water and the desired final solution conditions were achieved by the subsequent addition of buffer and salt containing solution.

Circular Dichroism: CD spectra of the solutions were collected using a Jasco J-810 spectropolarimeter. Temperature was controlled with a Peltier element. The mean residue ellipticity, $[\theta]$, was calculated from the equation $[\theta] = (\theta_{obs}/10lc)/r$, where θ_{obs} is the measured ellipticity in millidegrees, l is the length of the cell path, c is the concentration and r is the number of residues.

Rheology: Dynamic oscillatory measurements were performed in a strain-controlled Rheometrics ARES and stress-controlled Anton Paar Physica MCR500 instruments, using 25 mm diameter parallel plate geometry with 500 μm gap distance. Lyophilized peptide was dissolved in deionized water and buffer solution was added to peptide solutions at temperatures less than 15 °C to suppress the folding and self-assembly before the solutions is loaded to the instrument. For high temperature measurements, low-viscosity mineral oil was used to cover the sides of the sample to minimize water loss due to evaporation. Control experiments were performed to ensure that the results were unaffected.

Small-Angle Neutron Scattering: SANS experiments were performed on the 30-m instrument on beamline NG3 at NIST, Gaithersburg, MD. The data were corrected for background electronic noise and radiation, detector inhomogeneity, and empty cell scattering. Intensities were normalized to an absolute scale relative to main-beam transmission measurements through the sample. The samples were prepared by dissolving deuterio-chloride salt of lyophilized peptide in D_2O .

Transmission Electron Microscopy (TEM): Negative staining techniques were employed to improve the contrast of self-assembled structures. Hydrogels were first diluted with deionized water to prevent the formation of salt crystals and to image individual fibrils. 2 % (w/v) uranyl acetate aqueous solution was placed on the TEM-grid for negative staining and excess staining solution was blotted with filter paper. Bright field images of the samples were taken on a JEOL 2000-FX transmission electron microscope at 200 kV accelerating voltage with a Gatan CCD camera.

Laser Scanning Confocal Microscopy: LSCM images of hydrogels were collected by a Zeiss 510 NLO microscope with an ArKr laser (30 mW) at an excitation wavelength of 488 nm. Lipophilic fluorescent dye (DiO C_{18} , Molecular Probes) was incorporated into the hydrogel during the self-assembly of the peptide molecules.

Results and Discussion

Using spectroscopy and rheology techniques, it was shown that Max1 forms β -sheet rich, rigid hydrogels as the pH of the solution is increased from acidic conditions to around 9.⁸ As discussed earlier, the folding and self-assembly of Max1 is triggered via partially deprotonating lysine residues, thus decreasing the electrostatic repulsions of the β -hairpin strands. At physiological pH conditions, the electrostatic repulsions can alternatively be screened by additional ions in the solution and β -sheet formation and gelation of Max1 molecules can be triggered by increasing ionic strength. In our previous study, we have investigated the effect of ionic strength on the kinetics of assembly and final rigidity of hydrogels.¹⁰

In addition to pH and ionic strength, gelation can also be triggered thermally.⁹ Figure 2a shows the CD spectra of a 2 wt % Max1 solution at pH 7.4. The solution has 50 mM bis-tris-propane (BTP) as a buffer and no additional salt added. At 20 °C, the spectrum has a minimum at around 199 nm, indicating that Max1 has a random coil structure. As the temperature is increased to 50 °C, Max1 adopts β -sheet secondary structure, with a clear minimum in its spectrum at 216 nm. It can be concluded that when there is no additional salt in the solution, the β -sheet formation of Max1 molecules can be triggered via increasing temperature. This effect is similar to heat renaturation phenomena seen in some globular proteins. For Max1 molecules this transition is irreversible; they preserve their β -sheet structure when the solution is cooled back to 5 °C.

Figure 2b shows the dynamic time sweep data for a Max1 solution with the same conditions described for the CD spectra. While monitoring the changes in storage (G') and loss (G'') moduli of the hydrogel, first the solution temperature is kept at 25 °C for 2 hours and then it is suddenly increased to 60 °C. At 25 °C, G' values are very low (~2 Pa) and are close to G'' . Actually at that state, the solution flows like water and the sample is too weak to create significant torque in the instrument. When the temperature is 60 °C, the G' increases, exhibiting one order of magnitude greater values compared to G'' . The increase in the elasticity of the material is a clear indication of the self-assembly of the β -hairpin molecules and the rate of increase in G' values also lends insight to the kinetics of the assembly process.

Figure 3a shows the dynamic time sweep data for 2 wt % Max1 solution at pH 7.4 (50 mM BTP) with 150 mM NaCl at 20, 37 and 60 °C. The rate of self-assembly increases with temperature, providing the opportunity to obtain desired rigidity at identical peptide concentration by simply the magnitude of the stimulus. Similar tunability of rigidity through control of self-assembly kinetics was previously reported with salt-triggered self-assembly.¹⁰ As the kinetics of assembly increase, the number of crosslink points apparently increase leading to

more rigid hydrogels. The folding transition of Max1 is thermally irreversible; therefore, the hydrogels can be formed at relatively higher temperatures and their rigidity can be preserved at biologically relevant conditions. Figure 3b shows frequency sweep data at 37 °C for a hydrogel that was formed at 60 °C (see Figure 3a). It can be seen that cooling the material to a lower temperature compared to its formation temperature does not change the elasticity of the material.

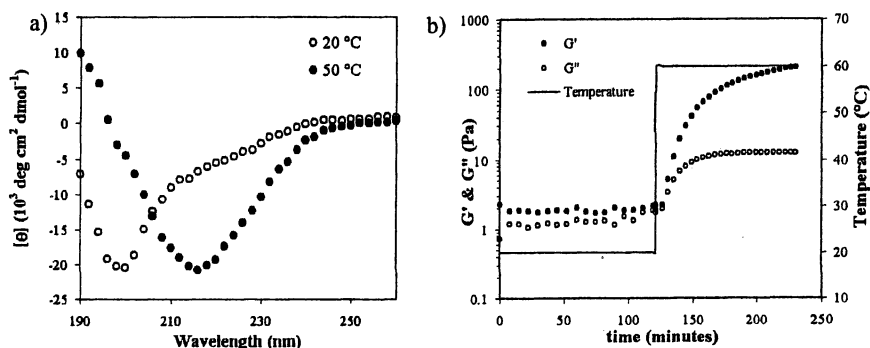


Figure 2. 2 wt % Max1 solution at pH 7.4 (50 mM BTP) with no additional salt (NaCl). (a) CD spectra at 20 and 50 °C. (b) Rheology: Dynamic time sweep at 25 and 60 °C.

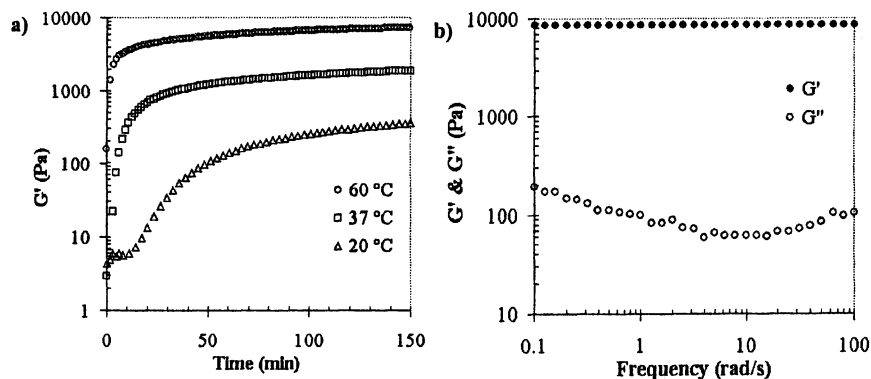


Figure 3. Rheology of 2 wt % Max1, at pH 7.4 (50 mM BTP) with 150 mM NaCl. (a) Dynamic time sweep measurements at 20, 37 and 60 °C. (b) Frequency sweep measurement: The hydrogel was formed at 60 °C and cooled to 37 °C

Frequency sweep data also reveal some physical information about the network structure. The G' is almost independent of the frequency, is an order of magnitude greater than G'' , and does not exhibit any crossover point with G'' within the studied frequency range. This type of a rheological response is similar to covalently crosslinked polymer gels. Although no chemical crosslinking strategy is employed in Max1 hydrogels, the rheological data suggest that the physical crosslink points in the network structure are permanent in nature. Max1 can also form self-supporting, rigid hydrogels at biologically relevant conditions, such as in DMEM cell-growth medium.^{10,21} Moreover, they are processible; they quickly recover their initial stiffness after shear-thinning due to external mechanical forces.¹⁰ We have shown that after hydrogels are formed, they shear-thin and easily flow when disturbed with mechanical forces. However, they quickly recover their initial rigidity after the cessation of shear. This recovery process is very rapid partially due to the peptide concentration (< 2 wt%) that allows faster diffusion of the self-assembled structures.

Thermally Reversible Hydrogels

Although the thermally induced folding transition of Max1 is irreversible, reversible systems can be designed by changing the primary sequence of Max1. It was shown that by replacing valine residues with threonine, isostructural with valine but less hydrophobic, the β -sheet transition was shifted to higher temperatures.⁹ Figure 4 shows the sequence of Max2 and Max3 peptides, with one and two threonine residues replacing existing valines of Max1. At 150 μ M peptide concentrations (pH 9, 125 mM Borate, 10 mM NaCl), the random coil to β -sheet transitions are around 25 °C for Max1, 40 °C for Max2, and 60 °C for Max3 peptides. In addition, the secondary structure transition is fully reversible for Max3 peptide with heating and cooling cycles.



Figure 4. Comparison of the sequences and hydrophobicity of Max1, Max2 and Max3 β -hairpin peptides.

Figure 5a shows the change in rigidity of a 2 wt % Max3 peptide solution at pH 9 on heating. The solution was heated in 5 °C increments with enough time given in each step to reach the equilibrium. Figure 5a shows that G' dramatically increased when the temperature reached 60 °C. The same folding transition temperature was also measured by CD spectroscopy. These experiments

demonstrate that folding of the β -hairpin is a prerequisite to self-assembly and gelation. Similar to the folding transition, reversible sol-gel transitions of Max3 hydrogel are also accessible. Figure 5b shows the change of G' in Max3 solution vs. time during heating and cooling cycles between 75 and 10 °C. When the temperature was suddenly jumped to 70 °C, the G' increased rapidly to values around 800 Pa. The G'' values (not shown) are always one order of magnitude less than the G' values and follow the same trend at any stage of the measurements. In the cooling cycle, at 10 °C, the self-assembled structure dissolved due to the unfolding of the peptide as also monitored by CD. The hydrogel gradually lost its rigidity and became a freely-flowing solution. As can be seen in the cooling cycles, there is an initial, almost order of magnitude jump in G' at the very early stages. We think that the sudden increase in rigidity with cooling is due to complexation of buffer species with the peptide that is subsequently destroyed due to peptide unfolding. This complexation effect can be permanent and controlled via solution conditions and it is being studied with Max1 peptide in more detail.

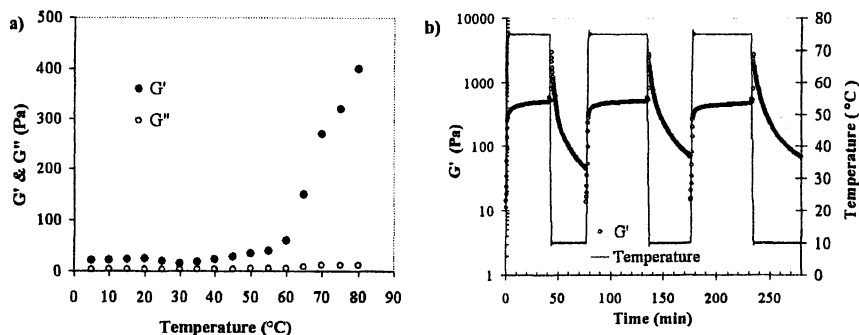


Figure 5. Rheology of 2 wt % Max3 solution at pH 9, (125 mM Borate) with 10 mM NaCl. (a) Temperature sweep between 5 and 80 °C. (b) Time sweep with heating (75 °C) and cooling (10 °C) cycles.

Network and Nanostructure of the Hydrogels

Figure 6a shows a TEM micrograph of negatively stained Max1 hydrogel. The network nanostructure is formed by fibrillar self-assembled structures (Figure 6b). The crosslinks can be seen at high dilutions suggesting that these junction points are permanent in nature. As discussed earlier, rheological experiments are also in accordance with this observation of permanent

crosslinks. We believe that these junction points are formed during the self-assembly process: valine face collapse can occur between hairpins orthogonal to one another (Figure 6c). Subsequent fibril growth can then occur along two different axes thus producing a fibril junction point. It is also possible that fibrils might have strong interactions via their surfaces that result in simple entanglements with long life-times. Figure 6b shows the proposed structure of the fibrillar assemblies. The cross-section consists of two β -hairpin molecules that assemble with each other via their valine rich, hydrophobic faces. The long axis of the fibrils corresponds to the hydrogen bonding direction and thus the growth direction. For the Max1 molecule the actual arm length is around 32 Å and the distance between two lysine faces is around 20 Å. Although staining effects at the edges cause uncertainties, the TEM micrographs reveal that the width of the fibrils is mono-disperse in size and around 3 nm, which is in good agreement with the molecular dimensions. This also suggests that there is no fibril lamination, which would otherwise cause two dimensional structures that have been observed in β -amyloid-like precipitates in the literature. The hydrogel fibrils are similar to amyloid structures, however no fibril twisting is observed in Max1 fibrils at the studied conditions.

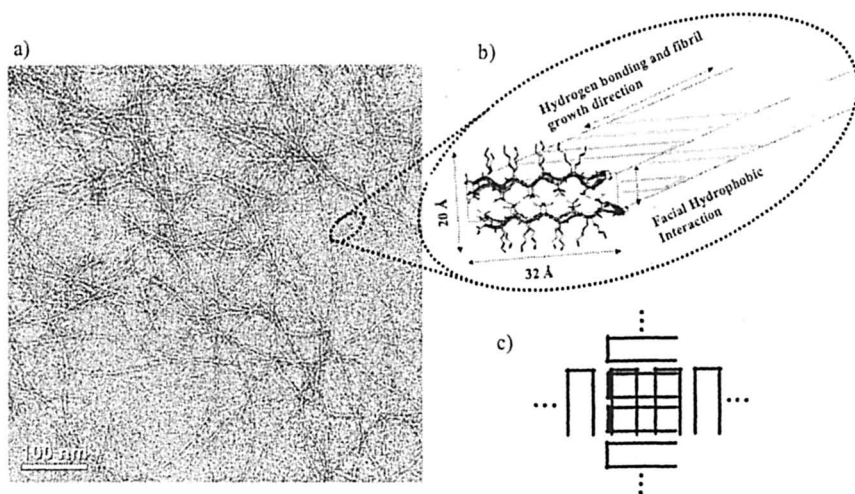


Figure 6. (a) Negatively stained (uranyl acetate) TEM images of fibrillar assemblies. (b) Proposed structure of β -hairpin molecules in a fiber. The long axis of the fibrils corresponds to the hydrogen bonding direction. (c) Schematic of self-assembled crosslink point.

To globally characterize the network structure of the hydrogels SANS measurements were employed. Figure 7a shows the SANS data for 2 wt% Max1 peptide solutions at pH 7.4 with 150, 400 and 600 mM NaCl concentrations. The -1 slope, indicative of a rigid rod behavior, for 150 mM NaCl solution at the intermediate q (scattering vector) regimes suggests that the network structure is globally formed of fibrillar aggregates. Quantitative analysis were also employed to SANS data, and it was shown that the SANS spectra are in good agreement with rigid-rod form factors.¹⁹ The -1 slope in the $\log(I)$ vs $\log(q)$ plot is sustained up to very low q values. This indicates that the persistence length of the fibrillar aggregates is large (up to 50 nm) resulting in semiflexible chain behavior. TEM micrographs also qualitatively support this observation. SANS data reveal that the slope in the intermediate q regime increases as the NaCl concentration increases in peptide solutions. The slopes between 0.007 \AA^{-1} and 0.07 \AA^{-1} , for 150, 400 and 600 mM NaCl are -1.02, -1.29, and -1.55, respectively. We believe that the increase in the slopes in this regime is due to increase in interparticle scattering. It was shown that Max1 solutions with same peptide concentration but with different salt content have different final rigidity because of faster kinetics of assembly. The faster kinetics apparently leads to formation of network structure with more permanent crosslink points and denser crosslinked regions leading to more heterogeneity. Figure 7b shows Guinier analysis for the 600 mM NaCl solution. For a rod-like particle with finite cross-section diameter, the form factor is approximated as $P(q) \sim [\exp(-qRc^2/2)]/q$, where Rc is the radius of gyration of the crosssection. When scattering data is plotted as $\ln [I(q) \times q]$ vs. q^2 , the slope of the linear region gives $-Rc^2/2$, then the rod radius (R) is calculated using $R=Rc \sqrt{2}$. The rod diameter is found as 30 Å for the fibrils in 600 mM NaCl solution and this value in agreement with TEM micrographs and the actual strand length of Max1. This diameter is also 3 nm for 150 mM and 400 mM NaCl solutions, which indicates that unlike the rigidity of the hydrogels and thus number of crosslink points within the network, the local fibrillar nanostructure is not affected by the kinetics of self-assembly.

Microstructure of the hydrogels was investigated using LSCM. Figure 8 shows a microscopy image of 0.5 wt % Max1 hydrogel at pH 9. The grey regions are the self-assembled peptide, while dark regions are the water channels. There is heterogeneity at the microscale constituted by hydrogel network structure permeated by interconnected water pores and channels. Previous studies, using ultra-small angle neutron scattering, also support the existence of a sharp interface between the self-assembled regions and water channels.⁸ Such heterogeneity at this length scale is desired for tissue engineering applications because of the available surface area at micrometer length scales and ease of transportation of solutes. In traditional, chemically crosslinked polymer hydrogels, however, this microscale heterogeneity is only possible through additional processing steps, such as freeze and thaw cycling.

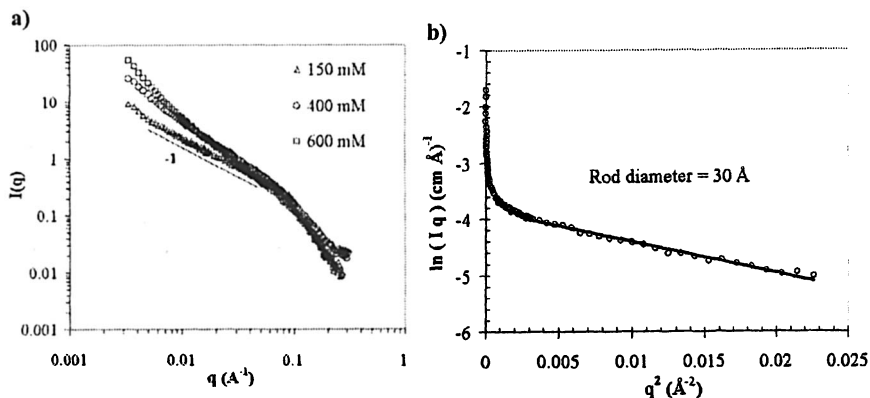


Figure 7. 2 wt % Max1 at pH 7.4 (50 mM BTP) (a) 150, 400 and 600 mM NaCl. (b) Guinier analysis for 600 mM NaCl solution.

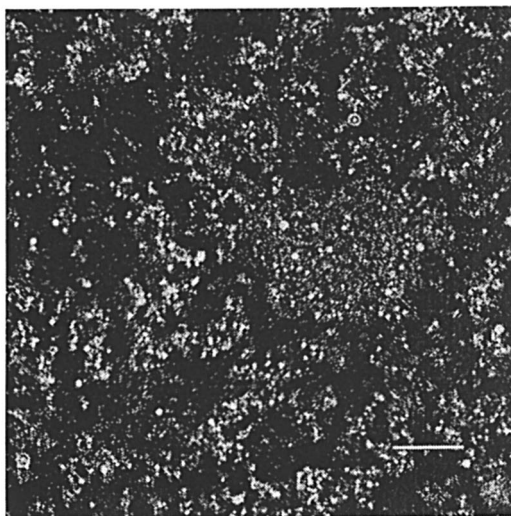


Figure 8 LSCM of 0.5 wt % Max1 (pH 9) hydrogel microstructure.

Effects of Strand Length

Semiflexible chain dynamics has been extensively studied in the literature both experimentally and theoretically in the context of biophysics.²⁰ For example, DNA and F-actin are semiflexible biomacromolecules and their functions and higher hierarchical assemblies are directly related to single chain

dynamics. SANS and rheological experiments suggested that Max1 fibrils are semiflexible chains.¹⁹ Using the scaling theory proposed by Mackintosh,¹⁴ the persistence length of Max1 fibrils was estimated to be around 50 nm by rheological measurements. The persistence length and thus the bending modulus of the chains are directly related to the chemical structure of the repeating units, their charge state, as well as the cross-sectional dimension of the chains. As it can be seen from Figure 6b, the cross-sectional dimension of the β -hairpin fibrils is governed by the strand length of the molecules. Assuming that the local nanostructure does not change (no fibril lamination), the dynamics of the network structure should be altered by varying the bending modulus of the fibrils, which simply can be changed with the number of residues on the strands of the β -hairpins. To test this hypothesis, peptides that have similar sequences of Max1 were synthesized with different number of residues. Figure 9 shows the dynamic frequency sweep experiment for a 16 amino acid long β -hairpin peptide. It can be seen that there is a drastic change in the frequency dependence of G' . The G' values decrease with decreasing frequency, suggesting the presence of a crossover point with G'' at lower frequencies. In addition, at the same solution conditions and peptide concentrations, Max1 molecules form almost one order of magnitude stiffer hydrogels. These results imply that there are faster relaxations in the network structure of the 16 amino acid hairpin compared to that of Max1. The difference in the dynamics of the network can be an indication of changes in the bending modulus of the fibrils or/and in the nature of crosslink points. The decrease in the strand length can lead to changes in the association of the hydrophobic faces of the β -hairpin molecules, which, in turn, disrupt the permanent crosslinking points formed during the assembly process. Our future studies are directed at understanding the ability of the strand length to alter the gelation kinetics and hydrogel behavior.

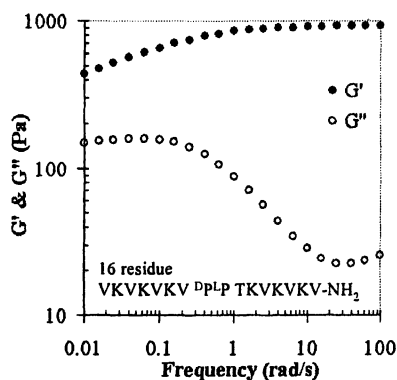


Figure 9. Frequency sweep of 16 residue peptide hydrogel (2 wt%, pH 9, 40 °C).

Cytocompatibility of the Hydrogels

The cytocompatibility of Max1 hydrogels were studied with fibroblast attachment and proliferation assays.²¹ It was shown that Max1 hydrogel surfaces highly promote NIH 3T3 cell attachments with and without serum protein. The attachment assays show that almost 15 minutes after seeding, more than 95 % of the cells were strongly attached to Max1 hydrogel surfaces, while for tissue culture treated polystyrene and bovine serum albumin coated polystyrene control experiments the attachments are around 85 and 15 %, respectively. In addition, using ³H-thymidine incorporation assay, it was shown that Max1 hydrogels promote fibroblast cells proliferation while maintaining their mechanical rigidity.

Conclusion

A peptide intramolecular folding event that is triggered by pH, temperature, or salt, is followed by a intermolecular self-assembly process that leads to formation of rigid, self-supporting hydrogels. The kinetics of the self-assembly, and, consequent final rigidity of the material, can be varied by the magnitude of the stimulus. Thermoreversible β -sheet formation and gelation are achieved by tuning the folding transition via alteration of the peptide sequence hydrophobicity. The network structure is composed of semiflexible fibrillar nanostructures that are monodisperse in width. The rheological behavior of the hydrogels is similar to covalently crosslinked polymer gels except the peptide gels can quickly reheel after shear disruption. The dynamics and nanostructure of the hydrogels can be altered with strand length and turn sequence of the β -hairpin molecules. The cytocompatibility studies suggest that these materials are possible candidates for biomaterials applications.

Acknowledgements

This work was supported by National Institutes of Health (P20-RR17716 and RO1) and National Science Foundation (CHE 0348323). We acknowledge the support of the National Institute of Standards and Technology, U.S. Department of Commerce, in providing the neutron research facilities used in this work. We acknowledge the W.M. Keck foundation for funding the College of Engineering Electron Microscopy Lab.

References

1. Rodriguez-Hernandez, J.; Lecommandoux, S. *J. Am. Chem. Soc.* **2005**, *127*, 2026-2027.
2. Bellomo, E.G.; Wyrsta, M.D.; Pakstis, L.; Pochan, D.J.; Deming, T.J. *Nature Materials*, **2004**, *4* 244-248.
3. Aggeli, A.; Bell, M.; Boden, N.; Keen, J.N.; Knowles, P.F.; McLeish, T.C.B.; Pitkeathly, M.; Radford, S.E. *Nature*, **1997**, *386*, 259-262.
4. Higuchi, M.; Minoura, N.; Kinoshita, T. *Colloid and Polymer Science*, **1995**, *273*, 1022-1027.
5. Collier, J.H.; Messersmith, P.B.; *Advanced Materials*, **2004**, *16*, 907-910.
6. Collier, J.H.; Hu, B.H.; Ruberti, J.W.; Zhang, J.; Shum, P.; Thompson, D.H.; Messersmith, P.B.; *J. Am. Chem. Soc.* **2001**, *123*, 9463-9464.
7. Lee, K. Y.; Mooney, D. *J. Chem. Rev.* **2001**, *101*, 1869-1879.
8. Schneider, J. P.; Pochan, D. J.; Ozbas, B.; Rajagopal, K.; Pakstis, L.; Kretsinger, J. *J. Am. Chem. Soc.* **2002**, *124*, 15030-15037.
9. Pochan, D. J.; Schneider, J. P.; Kretsinger, J.; Ozbas, B.; Rajagopal, K.; Haines, L. *J. Am. Chem. Soc.* **2003**, *125*, 11802-11803.
10. Ozbas, B.; Kretsinger, J.; Rajagopal, K.; Schneider, J. P.; Pochan, D. J. *Macromolecules*, **2004**, *37*, 7331-7337.
11. Nijenhuis, K. T. *Colloid and Polymer Science*, **1981**, *259*, 1017-1026.
12. Nijenhuis, K. T. In *Thermoreversible Networks*; Springer-Verlag Berlin: Berlin 33, 1997; Vol. 130, pp 1-12.
13. Tobitani, A.; RossMurphy, S. B. *Macromolecules*, **1997**, *30*, 4855-4862.
14. McMillan, R. A.; Conticello, V. P. *Macromolecules*, **2000**, *33*, 4809-4821.
15. Petka, W. A.; Harden, J. L.; McGrath, K. P.; Wirtz, D.; Tirrell, D. A. *Science*, **1998**, *281*, 389-392.
16. Aggeli, A.; Bell, M.; Carrick, L. M.; Fishwick, C. W. G.; Harding, R.; Mawer, P. J.; Radford, S. E.; Strong, A. E.; Boden, N. *J. Am. Chem. Soc.* **2003**, *125*, 9619-9628.
17. Caplan, M. R.; Schwartzfarb, E. M.; Zhang, S. G.; Kamm, R. D.; Lauffenburger, D. A. *Biomaterials*, **2002**, *23*, 219-227.
18. Goeden-Wood, N. L.; Keasling, J. D.; Muller, S. J. *Macromolecules*, **2003**, *36*, 2932-2938.
19. Ozbas, B.; Rajagopal, K.; Schneider, J. P.; Pochan, D. J. *Phys. Rev. Lett.* **2004**, *93*.
20. Mackintosh, F. C.; Kas, J.; Janmey, P. A. *Phys. Rev. Lett.* **1995**, *75*, 4425-4428.
21. Kretsinger, J.K.; Haines, L.; Ozbas, B.; Rajagopal, K.; Pochan, D. J.; Schneider, J. P. *Biomaterials*, **2005**, *26*, 5177-5186

Author Index

- Aguilar, Cristóbal N., 215
Atichokudomchai, Napaporn, 146
Barnes, Brian, 115
BeMiller, James N., 165
Brasch, Uwe, 185
Brown, Eleanor M., 36
Burchard, Walther, 185
Charles-Rodríguez, Ana V., 215
Chau, Hoa K., 201
Chen, Tianhong, 262
Coffin, David R., 201, 272
Contreras-Esquivel, Juan C., 215
Cooke, Peter H., 201, 272
Corredig, Milena, 115
Doyle, Jonathan P., 19
Eggleston, Gillian, 19
Espinoza-Pérez, Judith D., 215
Farrell, Harold M., Jr., 1, 52, 93
Finkenstadt, Victoria L., 256
Fishman, Marshall L., 201, 272
Gray, Jonathan A., 165
Han, Jung-Ah, 165
Hicks, Kevin B., 272
Hotchkiss, Arland T., Jr., 201
Huber, Kerry C., 165
Jane, Jay-lin, 146
Kim, Yookyung, 230
Lee, Chia C., 123
Liang, Hongquan, 123
Liu, LinShu, 272
Montanez, Julio C., 215
Mora-Gutierrez, Adela, 93
Mulvaney, Steven J., 123
Nothnagel, Eugene A., 243
Ozbas, Bulent, 284
Park, Jin-Hee, 146
Payne, Gregory F., 262
Pochan, Darrin J., 284
Qi, Phoebe X., 1, 52, 71
Rayas-Duarte, Patricia, 123
Renovato, Jacqueline, 215
Rodríguez-Herrera, Raúl, 215
Schneider, Joel P., 284
Stanley, Robert J., 137
Suh, Dong-Soon, 146
Tunick, Michael, 272
Uversky, V. N., 1, 52
Wicker, Louise, 115, 215, 230
Willett, J. L., 256
Yadav, Madhav P., 243

Subject Index

A

- Acidified milk dispersions
analysis methods, 117
elution profile of milk protein-pectin dispersions, 118
interactions with pectins, 121
materials and methods, 116–117
molecular weight distributions of pasteurized and non-pasteurized samples, 118, 121
molecular weight distributions of supernatants from centrifuged, non-pasteurized, and pasteurized, 120*f*
molecular weight of protein-pectin dispersions vs. pectin controls, 118, 119*t*
particle size data of centrifuged, homogenized, with varying pectin and heat treatment, 119*t*
pectin stabilization of, 116
sample preparation, 116–117
- Agars, interaction with galactomannans and glucomannans, 29–30
- Aggregation
carrageenans, 25–26
protein structure, 14
See also Acidified milk dispersions
- Alginates
egg-box model of gelation, 26*f*
structural polysaccharides, 26–27
- Amination. *See* Reductive amination of starch fragments
- Amyloid formation, casein secretion, 65–67
- Amylopectin
average branch chain-length distributions, 151*f*
branch chain-length distribution, 149–150
branch chain-length of, debranched with isoamylase, 155*t*
branch chain-length variation within starch granule, 152, 155
branch linkages' structures of A- and B-type, 150, 152
extra-long branch chains of, 155–156
high performance size exclusion chromatography (HPSEC) chromatogram of isoamylase-debranched, 156*f*
molecular weight, 147, 149
molecular weights and gyration radii of selected starches, 148*t*
proposed models for branching patterns, 153*f*
relationships between molecular weight and radius of gyration, 151*f*
scanning electron microscopy (SEM) of normal maize starch granules and surface-gelatinized starch, 154*f*
starch composition, 147
See also Starch granules
- Amylose, starch composition, 147
- Analytical ultracentrifugation, experiments with bovine β -casein, 76–77, 79*f*
- Anilino-8-naphthalenesulfonic acid (ANS), protein binding, 89–90
- Arabinogalactan-proteins (AGPs)
components of gum arabic, 245–246
hypothetical model of AGP structure, 246*f*
See also Gum arabic

Arbutin, chitosan and gel formation, 264

Atomic force microscopy (AFM)
gels from citrus pectins, 203–204,
210–213
polysaccharides, 24

B

Biological extraction, pectins, 217–
218

Biopolymers. *See* Chitosan;
Electroactive biopolymers

Bovine β -casein (β -CN)
analytical ultracentrifugation, 76–
77
analytical ultracentrifugation
analysis of, and β -CN-(f1–192),
79f

aniline-8-naphthalenesulfonic acid
(ANS) binding, 89–90

β -CN-(f1–192) preparation, 73

bulk solvent environment and
secondary structure of β -CN-
(f1–192), 85–89

CD (circular dichroism)
spectroscopy, 73–75

CD spectra of β -CN-(f1–192), 81f

CD spectra of β -CN-(f1–192) and
 β -CN in sodium dodecyl sulfate
(SDS) micelles, 89f

characterization of protein
fragment β -CN-(f1–192), 77–78

effect of temperature on secondary
structure of β -CN-(f1–192), 82–
85

electrospray ionization mass
spectrometry (ESI-MS) analysis
of molecular mass, 78t

ellipticity changes, 82, 83t

endothermic self-association, 72

fluorescence emission spectra of
ANS, and with β -CN and β -CN-
(f1–192), 90f

fluorescence spectroscopy, 75
materials, 73

nonlinear regression analysis,
75

reduction of self-association in β -
CN-(f1–192), 78, 80

SDS-PAGE gel electrophoresis of
chymosin cleaved products of,
74f

secondary structure analysis for CD
spectra of β -CN-(f1–192) and β -
CN, 87t

secondary structure comparison
between β -CN-(f1–192) and β -
CN, 80–82

temperature dependence of CD
spectra of β -CN-(f1–192) and β -
CN, 84f

See also κ -Carrageenan interaction
with caseins

Bovine collagen. *See* Collagen
networks

Bovine serum albumin (BSA)
confocal fluorescence image of
pectin-BSA composite films,
275f

pectin-protein composite films,
273–274

See also Pectin-protein composite
films

Branch structures. *See* Amylopectin

C

Caprine caseins. *See* κ -Carrageenan
interaction with caseins

Carbohydrates

linkage, 20

pyranose ring structure, 20f

See also Polysaccharides

κ -Carrageenan interaction with
caseins

calculated hydration products and
virial coefficient for bovine and

- caprine casein solutions with κ -carrageenan, 105*t*
- caprine and bovine caseins, 94–95
- casein distribution of bovine and caprine caseins by densitometry, 96*t*
- C α trace of backbone structure of α_{s2} -casein by modeling, 108*f*
- chloride intracellular channel (CLIC) molecules, 107, 108*f*
- comparing bovine α_{s2} -casein with human CLIC-proteins, 109*t*
- complex formation, 94
- dependence of ^{17}O nuclear magnetic resonance (NMR) transverse relaxation rates on bovine casein concentration, 104*f*
- homologous molecular model for α_{s2} -casein, 106–109
- hydration characteristics, 103, 105–106
- manipulation of Ala 116 for accessible hydrophobic central core, 108*f*
- materials, 95
- molecular modeling of bovine α_{s2} -casein, 99
- NMR hydration theory and data analysis, 98–99
- ^{17}O NMR transverse relaxation rate measurements, 97–98
- preparation of bovine and caprine caseins, 95
- preparation of samples for NMR measurements, 97
- pseudo-charge surface representation of model, 110*f*
- salt-induced insolubility and solubility of caseins and carrageenan mixtures, 102*t*
- solubility characteristics, 99–103
- solubility measurements, 96
- solubility of caprine and bovine caseins and κ -carrageenan-caseins, 101*f*
- solubility theory and data analysis, 96–97
- Carrageenans
- interaction with galactomannans and glucomannans, 29–30
- structural polysaccharides, 25–26
- See also* κ -Carrageenan interaction with caseins
- Casein (CN)
- amyloid formation and CN secretion, 65–67
- biological function, 67
- changes in calculated hydrated volumes with environmental changes, 63*t*
- classification of CNs among new intermediate states, 58–63
- composition profiling of α_{s1} -, α_{s2} -, β -, and κ -CNs, 58–59
- disorder predictions, 61*f*
- energy minimized 3D structures of α -, β -, and κ -, 55*f*
- environmental effects on CN monomer size and classification, 63–64
- historic views of structure, 53–54
- hydrated volumes for CNs from models and experiments, 62*t*
- hydration, 64–65
- intrinsic disorder, 59
- micelle formation, 66, 67*f*
- natively unfolded molecules, 60, 61*f*
- ordered and disordered proteins in CH space, 60
- persistent secondary structures and flexible elements, 62–63
- spaghetti plate analogy, 53
- synthesis and secretion of CN by mammary gland, 66, 67*f*
- three-dimensional models, 60, 62

- transmission electron micrograph
of negatively stained κ -CN and
reduced carboxymethylated κ -
CN, 66*f*
See also Bovine β -casein (β -CN);
 κ -Carrageenan interaction with
caseins; Protein structure
- Catechin
modified chitosan, 265
See also Chitosan
- Cavities. *See* Derivatization of starch
granules
- Cereal chemistry
rheology and, 124–125
See also Wheat gluten
- Channels
discovery of starch granule, 167,
169–170
See also Derivatization of starch
granules
- Charge modified citrus pectin
approach to charge distribution,
232–233
cumulative weight fraction vs.
molecular weight of
unfractionated pectin, 237*f*
de-esterification and
characterization, 234, 235*f*
degree of esterification of
unfractionated and fractionated
samples, 234, 236*f*
demethoxylation of esterified
pectins by pectin methylesterase
(PME), 231
ion exchange chromatography
elution profile, 235*f*
materials and methods, 233–234
molecular weight of original and
modified pectin, 234, 238
multiple PME isozymes, 231–232
pectin characterization, 234
PME isolation and pectin
modification, 233
PME variations (B-PME and U-
PME), 233
potential in food and
pharmaceutical industries, 232
reactive pectins from U-PME and
B-PME, 238
texture profile analysis data, 239*t*
unique charge distribution and gel
properties, 238
- Chemical extraction, pectins, 216–217
- Chemical modification. *See*
Derivatization of starch granules
- Chiroptical techniques, structures of
polysaccharides, 23
- Chitosan
arbutin and gel formation, 264
assembly of protein-chitosan
conjugates, 267–268
catechin-modified, 265
derivatizing, using tyrosinase, 263
description, 263
dihydroxyphenethylamine
(dopamine), 264, 265
directed assembly, 267–268
electrodeposition, 268
gallates for modifying chitosan
film, 264–265
grafting, backbone, 263
grafting chlorogenic acid to, 264
mechanism for electrodeposition,
268
tyrosinase-catalyzed modification,
264–265
tyrosinase-catalyzed modification
to peptides and proteins, 266–
267
- Chloride intracellular channel (CLIC)
molecules
comparing bovine α_{s2} -casein with
human CLIC-proteins, 109*t*
homologous model for α_{s2} -casein,
107, 108*f*
novel class of proteins, 107
- Chlorogenic acid, chitosan
modification, 264
- Chrome-tanning agent, leather
tanning, 38, 40

- Chymosin, cleavage of β -casein, 74*f*, 77–78
- Circular dichroism (CD)
 experiments with bovine β -casein, 73–74
 protein conformation, 40–41
 structures of polysaccharides, 23
- Citrus pectin. *See* Charge modified citrus pectin; Pectin
- Cluster
 term, 25
See also Pectin
- Collagenase resistance, crosslinking treatment, 47–48
- Collagen networks
 absorbance and circular dichroism (CD) spectra of acid-soluble bovine type I collagen, 42*f*
 biologically diverse family of proteins, 48
 biomaterial model, 44–48
 characteristics of fiber forming, 48
 collagenase resistance, 47–48
 collagen as raw material, 38, 40
 collagen structure, 37–38
 crosslinking studies, 44, 46–48
 effects of milling on collagen structure, 44, 45*f*
 electron micrographs of skin and fibril, 39*f*
 experimental tanning model, 40–43
 glycine, proline, and hydroxyproline content, 37
 melting profiles for soluble collagen under simulated tanning, 43*f*
 scanning electron micrographs (SEM) of crude, four- and seven-day milled collagen, 45*f*
 sodium dodecyl sulfate polyacrylamide gel electrophoresis (SDS-PAGE) of crude, 1, 4, and 7-day milled collagen, 44, 46*f*
 thermal stability, 41–43
- Composite films. *See* Pectin-protein composite films
- Composition profiling, caseins, 58–59
- Confocal laser scanning microscopy. *See* Reflectance confocal laser scanning microscopy (R-CLSM)
- Corn starch. *See* Derivatization of starch granules
- Crosslinking
 ball-milled collagen fibrils, 44, 46–48
 collagenase resistance, 47–48
 pectin-protein composite films, 277–279
- C-terminal region
 role in self-association process, 72
See also Bovine β -casein (β -CN)
- Cultivars. *See* Wheat gluten
- Cyclobutylpyrimidine dimers (CPDs)
 decay of reduced flavin adenine dinucleotide cofactor (FADH⁻) as control, 138–139
 dinucleotide kinetics, 141*f*
 fit of concerted and sequential models to transient absorption data, 143*f*
 kinetics for protein:pentameric substrate, 142*f*
 repair by DNA photolyase, 138–139
 target analysis to account for observations, 142–143
 transient absorption kinetics of photolyase:CPD complexes, 140*f*
- L-Cysteine, stress relaxation patterns of gluten with added, 133–134
- Cytocompatibility, peptide hydrogels, 296
- D**
- Deoxyribonucleic acid (DNA)
 photolyase (PL)

- binding and repairing
 cyclobutylpyrimidine dimers,
 138–139
See also Cyclobutylpyrimidine
 dimers (CPDs)
- Derivatization of starch granules
 anionic derivatives by scanning
 electron microscopy
 compositional backscattered
 electron imaging (SEM-BSE),
 172–173
 architecture of starch granule, 183
 complex structure of starch
 granule, 167
 discovery of starch granule
 channels, 167, 169–170
 effects of channels on granular
 reactions, 170–171, 183
 electron micrograph of thallium salt
 of partial 2-hydroxy-3-(thallium
 sulfonate)-propyl ether of waxy
 corn starch, 173*f*
 electron micrograph of thallium salt
 of POCl₃-treated hl sorghum
 starch granules, 172*f*
 fluorescence microscopy of hl
 sorghum and normal corn starch
 granules, 168*f*
 granule swelling and reactivity,
 178–179
 influence of reaction conditions,
 180–182
 methods for detecting reaction
 patterns, 172–178
 modification for industrial use, 166
 optical section of treated normal
 maize starch granule, 171*f*
 photomicrograph of hl sorghum
 and normal corn starch granules,
 168*f*
 potato starch, POCl₃-treated, by
 reflectance confocal laser
 scanning microscopy (R-
 CLSM), 174, 175*f*
 potato starch, unreacted, by R-
 CLSM, 174, 175*f*
 potato starch reacted with sodium
 3-chloro-2-hydroxy-1-
 propanesulfonate by R-CLSM,
 176, 177*f*, 178*f*
 R-CLSM method, 173–174
 uniqueness and heterogeneities of
 starches, 182
 waxy corn, reacted with sodium 3-
 chloro-2-hydroxy-1-
 propanesulfonate by R-CLSM,
 176, 177*f*
 waxy corn starch granules reacted
 with propylene oxide by R-
 CLSM, 176, 177*f*
 waxy corn starch reacted with
 sodium 3-chloro-2-hydroxyl-1-
 propanesulfonate by R-CLSM,
 181*f*
- Differential scanning calorimetry
 (DSC)
 α-lactalbumin (α-LA), 4, 5*f*
 polysaccharides, 24
- Dihydroxyphenethylamine, chitosan
 and gel formation, 264, 265
- Directed assembly, chitosan, 267–
 268
- Disordered proteins, caseins, 60
- Dopamine, chitosan and gel
 formation, 264, 265
- Dynamic light scattering, properties,
 200
- E**
- Egg-box model, gelation of alginates
 and pectin, 26*f*
- Electroactive biopolymers
 applications, 257*t*
 conductance vs. metal halide
 concentration for thermoplastic
 starch, 260*f*

- elongation vs. metal halide concentration for thermoplastic starch, 260*f*
- extrusion process, 258
- materials and methods, 257–258
- metal halide incorporation, 259, 261
- mobility of polymer chains in thermoplastic starch, 261
- moisture content and conductance, 259
- relationship of conductance to moisture for extruded thermoplastic starch, 259*f*
- resistance and ionic character, 259
- resistance measurements, 258
- resistance of native starches, 258*f*
- starches, 257
- Electrodeposition, chitosan, 268
- Electron microscopy
pectin structure, 203, 204–206
- polysaccharides, 24
- Ellipticity, β -casein protein fragment, 82–83
- Elongation
crosslinked pectin-protein composite films, 278*f*
- pectin-protein composite films, 276, 277*f*
- Emulsifiers
assay of emulsifying activity and stability, 248
- gum arabic, 244–245
- stabilization of oil droplets by, 244*f*
- See also* Gum arabic
- Energy landscape theory
minimally frustrated heteropolymer during protein folding, 57*f*
- new view of protein folding, 8–9
- Environmental effects, casein monomer size and classification, 63–64
- Enzyme digestibility, starch granules, 156–158
- Enzymes. *See* Charge modified citrus pectin; Chitosan
- Extraction
methods for pectins, 216–218
- See also* Pectin
- F**
- Films. *See* Pectin-protein composite films
- Flame retardancy, pectin-layered silicate nanocomposites, 279, 280–282
- Flavin adenine dinucleotide cofactor, decay as control for repair of cyclobutylpyrimidine dimers, 138–139
- Flours. *See* Wheat gluten
- Fluorescence microscopy, whole normal corn and hl sorghum starch granules, 168*f*
- Fluorescence spectroscopy, experiments with bovine β -casein, 75, 81*f*, 84*f*, 89*f*, 90*f*
- Functional self-association protein structure, 14
- G**
- Galactomannans
gelation of xanthan with, 30–31
- interactions of carrageenans and agars with, 29–30
- Gallates, modified chitosan films, 264–265
- Gelation
alginate, 26–27
- carrageenans, 25–26
- gellan, 28–29
- pectin, 232
- pectins, 27–28
- pH and ionic strength for hydrogels, 288–290

- reversible self-assembly
 mechanism of peptides, 285–286
- triggered, of biomacromolecules, 285
- xanthan with galactomannans and glucomannans, 30–31
See also Hydrogels by peptide self-assembly
- Gellan, extracellular polysaccharide, 28–29
- Geometry, linkage, of polysaccharides, 22
- Globular proteins, multi-state unfolding, 5–7
- Glucomannans
 gelation of xanthan with, 30–31
 interactions of carrageenans and agars with, 29–30
- Glutamine, content in casein, 58
- Gluten. *See* Wheat gluten
- Glycine, content in collagen, 37
- Glycosylphosphatidylinositol (GPI) lipid anchor
 arabinogalactan-protein (AGP), 246–247
 chemical treatments of AGPs in gum arabic, 250, 251*t*
 dephosphorylation cleavage of, 251*t*, 252
 emulsifying action of gum arabic, 252–253
 hypothesis on emulsifier activity of gum arabic, 247
See also Gum arabic
- Grafting. *See* Chitosan
- Gum arabic
 analysis of chemically treated sample, 251*t*
 arabinogalactan-proteins (AGPs), 245–246
 assay of emulsifying activity and stability, 248
 chemical analyses, 247, 249*t*
 chemical treatment, 247
 chemical treatment cleaving glycosylphosphatidylinositol (GPI) lipid anchors, 250
 composition, 245
 dephosphorylation cleavage of GPI linker oligosaccharide, 252
 emulsifiers, 244
 emulsifier activities and stabilities, 250*t*
 emulsifier activities and stabilities of, after chemical treatment, 251*t*
 GPI lipid anchor, 246–247
 GPI lipid anchors and emulsifying action, 252–253
 hypothesis, 247
 hypothetical model of structure of AGP, 246*f*
 materials and methods, 247–249
 model of, localization at oil-water interface, 245*f*
 separation of, subfraction, 248–249
 stabilization of oil droplets by emulsifiers, 244*f*
 uses, 244
- Gyration radii
 amylopectin, 148*t*, 149
 relationships between molecular weight and, of amylopectins, 151*f*
- ## H
- Hydrated volumes (V_h)
 caseins, 60, 62*t*
 changes in calculated, with environmental changes, 63*t*
- Hydration
 casein, 64–65
 newly defined partially folded states, 11
See also κ -Carrageenan interaction with caseins
- Hydrodynamic radius R_h

- conformational property, 188
See also Reductive amination of starch fragments
- Hydrogels by peptide self-assembly
 β -hairpin formation strategy, 285
 β -hairpin structure and primary sequence of 20 residue Max1, 285–286
- CD (circular dichroism) method, 287
- CD spectra of Max1 solution, 289*f*
- characterizing network structure by small-angle neutron scattering (SANS), 293, 294*f*
- conditions and protein-like folding events, 284–285
- cytocompatibility of hydrogels, 296
- dynamic time sweep data for Max1 solution, 288, 289*f*
- effects of strand length, 294–295
- experimental, 286–287
- frequency sweep data for max1 solution, 289*f*, 290
- frequency sweep of 16 residue peptide hydrogel, 295*f*
- intramolecular folding and self-assembly mechanism, 285–286
- laser scanning confocal microscopy (LSCM) method, 287
- literature of triggering gelation, 285
- microstructure of Max1 hydrogel by LSCM, 293, 294*f*
- network and nanostructure, 291–293
- peptide synthesis and sample preparation, 286–287
- pH and ionic strength, 288
- proposed structure of β -hairpin molecules in fiber, 292*f*
- rheology method, 287
- rheology of Max3 solution, 291*f*
- SANS method, 287
- sequences and hydrophobicity of Max1, Max2, and Max3 β -hairpin peptides, 290*f*
- TEM images of fibrillar assemblies, 292*f*
- TEM (transmission electron microscopy) method, 287
- temperature and time sweep data for Max3 solution, 291*f*
- thermal gelation, 288
- thermally reversible hydrogels, 290–291
- Hydroxyproline, content in collagen, 37
- I**
- Intrinsic disorder, caseins, 59
- Intrinsic disorder phenomenon, protein structure, 9–11
- Isoamylase, amylopectin debranched with, 155*t*
- J**
- Jicama pomace pectin yields, 221*t*
See also Pectin
- K**
- Kinetics. *See* Cyclobutylpyrimidine dimers (CPDs)
- L**
- α -Lactalbumin (α -LA)
 dependence of partial heat capacity on temperature for, 5*f*
- guanidine HCl induced unfolding, 4*f*
- molecular molding studies, 11–13
- molten globule state, 4–5

- Laser confocal scanning microscopy.
See Reflectance confocal laser scanning microscopy (R-CLSM)
- Leather, tanning processes, 38, 40
- Light scattering properties, static and dynamic, 200
- Lime
 pectin yields, 221*t*
See also Pectin
- Linear viscoelastic network strength index of wheat quality, 127
See also Wheat gluten
- Linkage geometry, polysaccharides, 22
- Loss modulus, pectin-protein composite films, 275–276
- Lysozyme, guanidine HCl induced unfolding, 3*f*
- M**
- Mango pomace
 pectin yields, 221*t*
See also Pectin
- Mark–Houwink plots, heating lime pectins during extractions, 208*f*, 210*f*
- Milk proteins
 pectin stabilization of acidified, 116
See also Acidified milk dispersions
- Milling, effects on collagen structure, 44, 45*f*, 46*f*
- Models
 biomaterial, 44–48
 experimental tanning, 40–43
 hydrated volumes for caseins from, 62*t*
 proposed, for branching patterns of starch granules, 153*f*
See also Molecular modeling
- Molecular modeling
 α_{s2} -casein, 99, 106–109
 chloride intracellular channel (CLIC) molecules, 107, 108*f*
 milk protein α -lactalbumin (α -LA), 11–13
See also κ -Carrageenan interaction with caseins
- Molecular weight, amylopectin, 147, 148*t*, 149
- Molten globule state (MG)
 α -lactalbumin (α -LA) and, 4–5
 new view of protein structure, 56, 58
See also Protein structure
- Monomer size, environmental effects on casein, 63–64
- Multi-state unfolding, globular proteins and pre-molten globule state, 5–7
- N**
- Nanocomposites. *See* Pectin-layered silicate nanocomposites
- Nanostructure, peptide hydrogels, 291–293
- Network formation
 carrageenans, 25–26
 peptide hydrogels, 291–293
See also Pectin
- Nopal pulp
 pectin yields, 221*t*
See also Pectin
- Nuclear magnetic resonance (NMR)
 polysaccharides, 24
See also κ -Carrageenan interaction with caseins
- O**
- Optical rotatory dispersion (ORD), structures of polysaccharides, 23
- Orange pectin. *See* Pectin
- Ordered proteins, caseins, 60

P

Partial denaturation, protein structure, 14

Partially folded states, hydration and stability of newly defined, 11

Pasteurization. *See* Acidified milk dispersions

Pectin

atomic force microscopy (AFM) method, 203–204

biological methods, 217–218

characterization, 223–224, 231

change in shape as function of heating time, 210*f*

chemical methods, 217

classification, 231

commercial use, 216, 272–273

composition, 116

conventional extraction, 217

effect of heating time on lime pectin properties, 207*f*

egg-box model of gelation, 26*f*

electronically thinned strands from phase images of gels, 212*f*

electron microscopy method, 203

experimental, 202–204

extraction and downstream processing, 219

extraction enzymes, 218

extraction method, 202–203

extraction methods, 217*f*

Fourier transform infrared (FTIR)

spectroscopy and molecular characterization of mango pectins, 219

FTIR spectra of non-traditional pectin polysaccharides, 225*f*

FTIR spectra of pomaces, 222*f*

gelling activity, 232

height and phase-shift of acid-gel from commercial citrus pectin, 211*f*

Mark–Houwink plots for lime pectin heated during extraction, 208*f*

materials and methods, 218–219

molar mass distributions for lime pectin by heating time, 207*f*

molecular characterization of mango, 224–226

molecular properties of, from lime and orange albedo, 209*t*

molecular weight distributions of citrus and mango pectins, 226*f*

network dried from water at high concentration, 206*f*

non-food applications, 273

physico-chemical properties of, in solution, 206–210

polysaccharide in cell walls of plants, 27–28, 202, 216, 272

pomace characterization by FTIR, 219–220

preparation of pomaces, 218–219

production, 216, 272–273

raw materials for commercial extraction, 216

rotary shadowed peach pectins dried and replicated, 205*f*

size exclusion chromatography (SEC) method, 204

stabilization of acidified milk proteins, 116

structure of pectin high methoxy sugar acid gels (SAG) by AFM, 210–213

structure visualized by electron microscopy, 204–206

yields from novel sources, 220–223

See also Acidified milk

dispersions; Amylopectin;

Charge modified citrus pectin;

Pectin-layered silicate

nanocomposites; Pectin-protein

composite films

Pectin-layered silicate nanocomposites flammability of treated papers, 281*t*

- images of coated papers before and after exposure to flame, 282*f*
- physical properties and flame retardancy of coated paper strips, 280–282
- preparation and characterization of coated paper strips, 279–280
- scanning electron microscopy (SEM) of paper strips and coated derivatives, 280*f*
- tensile strength of coated paper strips, 281*t*
- Pectin methylesterase (PME)**
- multiple isozymes, 231–232
- pectin modification, 232–233
- PMEs from Valencia for reactive pectins, 233, 238
- See also* Charge modified citrus pectin
- Pectin-protein composite films**
- confocal fluorescence image, 275*f*
- effect of crosslinking on initial modulus, 278*t*
- effect of crosslinking on maximal elongation and tensile strength, 278*f*
- effect of protein on maximum elongation and tensile strength, 276, 277*f*
- effect of proteins on $\tan \delta$, 276, 277*t*
- fabrication and characterization, 273–274
- physical properties, 275–276
- physical properties of crosslinked, 277–279
- storage modulus and loss modulus, 275–276
- structural properties, 274–275
- Peptides**
- tyrosinase-catalyzed modification, 266–267
- See also* Hydrogels by peptide self-assembly
- Phenols, chitosan modification, 264**
- Photolyase (PL)**
- binding and repairing cyclobutylpyrimidine dimers (CPDs), 138–139
- See also* Cyclobutylpyrimidine dimers (CPDs)
- Polymorphism, starch, 157**
- Polysaccharides**
- alginate, 26–27
- analysis of higher structures, 22–24
- carbohydrate pyranose ring structure, 20*f*
- carrageenans, 25–26
- chiroptical techniques, 23
- classification of structural organization, 20–21
- clusters and networks, 25–29
- differential scanning calorimetry (DSC), 24
- egg-box model for gelation of alginates and pectin, 26*f*
- electron microscopy, 24
- future outlook, 31–32
- gelation of xanthan with galactomannans and glucomannans, 30–31
- gellan, 28–29
- glycosidic bond between adjacent residues in carbohydrate chains, 21*f*
- interactions, 29–31
- linkage geometry, 22
- nuclear magnetic resonance (NMR), 24
- pectins, 27–28
- primary and secondary structures, 21–22
- rheological analysis of solutions or gels, 23–24
- schematic proposed for binding galactomannan to κ -carrageenan, 30*f*
- synergistic interactions of carrageenans and agars with

- galactomannans and glucomannans, 29–30
 - X-ray diffraction, 22–23
 - See also* Gum arabic
 - Pomaces
 - characterization by Fourier transform infrared (FTIR) spectroscopy, 219–220
 - FTIR spectra of, 222*f*
 - pectin yields, 220, 221*t*
 - preparation, 218–219
 - See also* Pectin
 - Potato starch. *See* Derivatization of starch granules
 - Pre-molten globule state (PMG)
 - multi-state unfolding, 5–7
 - new view of protein structure, 56, 58
 - See also* Protein structure
 - Prickly pear pomace
 - pectin yields, 221*t*
 - See also* Pectin
 - Primary structure, polysaccharide molecules, 21–22
 - Proline
 - content in casein, 58
 - content in collagen, 37
 - Protein folding
 - background, 2–3
 - energy landscape for minimally frustrated heteropolymer during, 57*f*
 - energy landscape theory, 8–9
 - new view of, 8
 - Proteins
 - chloride intracellular channel (CLIC) molecules, 107, 108*f*
 - tyrosinase-catalyzed modification, 266–267
 - See also* Pectin-protein composite films
 - Protein structure
 - background of protein folding, 2–3
 - dependence of partial heat capacity on temperature of α -lactalbumin (α -LA), 5*f*
 - energy landscape for minimally frustrated heteropolymer during protein folding, 57*f*
 - energy landscape theory, 8–9
 - features of new view and protein species, 56, 58
 - guanidine HCl induced unfolding of α -LA, 4*f*
 - guanidine HCl induced unfolding of lysozyme, 3*f*
 - implications of new view, 54, 56, 58
 - intrinsic disorder phenomenon, 9–11
 - α -LA and molten globule state, 4–5
 - molecular dynamics (MD)
 - simulated radius of gyration (R_g) values, 13*t*
 - molecular modeling studies, 11–14
 - molten globule state (MG), 56
 - multi-state guanidine HCl-induced unfolding of NAD⁺-dependent DNA-ligase, 6*f*
 - multi-state unfolding of globular proteins and pre-molten globule state, 5–7
 - newly defined partially folded states, 11
 - partial denaturation and aggregation vs. functional self-association, 14
 - pre-molten globule state (PMG), 56
 - randomness of random coil, 7–8
 - rapid MD simulations, 11–12
 - unfolded state (U), 56
 - See also* Casein (CN)
- Q**
- Quality, wheat, and linear viscoelastic network strength of gluten, 127

R

Radius of gyration R_g
 conformational property, 188
See also Reductive amination of starch fragments

Random coil, proteins, 7–8

Reductive amination of starch fragments
 alternative models, 195–198
 association by hydrogen bonding, 197
 calibration curves for reducing end-groups of saccharides by Somogyi/Nelson method, 190*f*
 Casassa–Holtzer plots from modified starch fragments, 194*f*
 change from flexibility to rigidity, 197–198
 covalent binding of aliphatic amines, 189
 diffraction patterns from powder of non-modified fragment, 196*f*
 evaluation of angular dependence of scattered light, 190–193
 experimentally observed facts, 193–194
 experimental parameters from asymptotic plateau height in Casassa–Holtzer plots, 192, 193*t*
 hydrodynamic radius R_h , 188
 inclusion complex, 195–196
 interpretation attempt, 195
 Kratky plots for samples with radius of gyration $R_g > 75\text{nm}$, 192*f*
 Kratky plots from starch fragments with $R_g > 70$, 189*f*
 light scattering properties, 200
 molar mass dependence of R_g and R_h , 188*f*
 possible model preventing contact of aliphatic chains with water, 198*f*

precursors by controlled acid degradation in alcohols, 186, 187
 radius of gyration, R_g , 188
 random cluster formation, 197
 reducing end-groups (CHO) determination by Somogyi/Nelson technique, 189–190
 structure properties of precursor, 187–189
 theoretical curves for star molecules, 193*f*

Reflectance confocal laser scanning microscopy (R-CLSM)
 detecting reaction patterns within starch granules, 173–174
 normal corn starch, treated, 174*f*
 potato starch, treated, 174*f*, 175*f*
 potato starch, untreated, 175*f*
 potato starch granules, treated, 176, 177*f*, 178*f*
 waxy corn starch, treated, 181*f*
 waxy corn starch granules, treated, 176, 177*f*
See also Derivatization of starch granules

Reversible network, contribution of, to viscosity of gluten, 132–133

Rheological analysis, polysaccharide solutions or gels, 23–24

S

Scanning electron microscopy
 compositional backscattered electron imaging (SEM–BSE)
 detecting reaction patterns within starch granules, 172–173
 sorghum starch granules, treated, 172*f*
 waxy corn starch, treated, 173*f*
See also Derivatization of starch granules

- Scanning electron microscopy (SEM)
 effect of milling on collagen
 structure, 44, 45*f*
 maize starch granules and surface-
 gelatinized starch, 154*f*
 paper strips coated with pectin-
 layered silicate nanocomposites,
 280*f*
- Secondary structure
 polysaccharide molecules, 21–22
See also Bovine β -casein (β -CN)
- Secretion, casein, 65–67
- Self-assembly
 chitosan, 267–268
See also Hydrogels by peptide self-
 assembly
- Self-association
 endothermic, of β -casein, 72
 microfibrils of fiber-forming
 collagens, 38, 39*f*
 partial denaturation and
 aggregation vs. functional, of
 proteins, 14
 reduction of, in β -casein protein
 fragment, 78, 80
See also Bovine β -casein (β -CN)
- Silicate nanocomposites. *See* Pectin-
 layered silicate nanocomposites
- Simulations, molecular dynamics
 (MD) of α -lactalbumin, 11–13
- Size exclusion chromatography (SEC)
 effect of heating time on pectin
 structure, 204, 206–210
 high performance SEC
 chromatogram of isoamylase-
 debranched amylopectin, 156*f*
- Sodium dodecyl sulfate
 polyacrylamide gel electrophoresis
 (SDS-PAGE)
 chymosin cleaved products of
 bovine β -casein, 74*f*
 effect of milling on collagen
 structure, 44, 46*f*
- Solubility. *See* κ -Carrageenan
 interaction with caseins
- Sorghum starch. *See* Derivatization of
 starch granules
- Spaghetti plate analogy, casein
 structure, 53
- Stability, newly defined partially
 folded states, 11
- Starch. *See* Electroactive biopolymers;
 Thermoplastic starch
- Starch granules
 amylopectin and amylose, 186
 amylopectin branch chain-length
 variation with, 152, 155
 amylopectin molecular weights and
 gyration radii, 148*t*
 amylose content, 157–158
 amylose content of starch, 157–158
 biosynthesis and enzymes, 147
 composition, 147
 confocal laser-light scanning
 micrographs of, 160*f*, 161*f*
 enzyme digestibility, 149, 156–158
 internal structures of, with different
 polymorphisms, 158–159, 162
 molecular weights and gyration
 radii, 148*t*
 organization and properties, 156–
 158
 polymorphism, 157
 proposed models for branching
 patterns, 153*f*
 relative enzyme digestibility of
 uncooked, 157*f*
 scanning electron micrographs of
 normal maize, and surface-
 gelatinized starch, 154*f*
 schematic of cross-section of
 normal maize starch granule,
 159*f*
See also Amylopectin;
 Derivatization of starch
 granules; Reductive amination
 of starch fragments
- Static light scattering, properties, 200
- Storage modulus, pectin-protein
 composite films, 275–276

Stress relaxation
 glutens with added L-cysteine,
 133–134
See also Wheat gluten

Structure
 analysis of, of polysaccharides, 22–
 24
 casein (CN), 53–54
 collagen, 37–38
See also Amylopectin; Bovine β -
 casein (β -CN); Polysaccharides;
 Protein structure

Supramolecular structure, starch, 186

T

Tanning processes
 absorbance and circular dichroism
 (CD) spectra of bovine type I
 collagen, 42*f*
 collagen matrix of hide, 38, 40
 experimental tanning model, 40–43
 melting profiles for soluble collage,
 43*f*
 thermal stability, 41–43
 vegetable, 38

Tejocote pomace
 pectin yields, 221*t*
See also Pectin

Temperature
 effect on secondary structure of
 bovine casein, 82–85
 effect on stress relaxation
 parameters for glutens, 130–132
 heating during pectin extraction,
 206–210
See also Wheat gluten

Tensile strength
 crosslinked pectin-protein
 composite films, 278*f*
 paper strips coated with pectin-
 layered silicate nanocomposites,
 281*t*

pectin-protein composite films,
 276, 277*f*

Thermal stability, tanning process,
 41–43

Thermoplastic starch
 conductance vs. metal halide, 260*f*
 elongation vs. metal halide, 260*f*
 ionic character and resistance, 259
 metal halide incorporation, 259,
 261
 mobility of polymer chains and
 conductivity, 261
 moisture content and conductance,
 259
 relationship of conductance to
 moisture content, 259*f*
See also Electroactive biopolymers

Three-dimensional models, caseins,
 60, 62

Transmission electron microscopy
 (TEM), negatively stained κ -CN
 and reduced carboxymethylated κ -
 CN, 66*f*

Tyrosinase. *See* Chitosan

U

Ultracentrifugation, analytical,
 experiments with bovine β -casein,
 76–77, 79*f*

Unfolded state (U)
 new view of protein structure, 56,
 58
See also Protein structure

V

Valencia
 pectin methylesterases (PMEs)
 from, 233, 234
 PMEs from, for reactive pectins,
 238

See also Charge modified citrus pectin

Vegetable tanning, dried hides, 38

Viscoelasticity. *See* Wheat gluten

Viscosity, contribution of reversible network to, of gluten, 132–133

W

Water solubility, polymers, 187

Waxy corn starch. *See* Derivatization of starch granules

Wheat gluten

addition of L-cysteine, 133–134, 135

cereal chemistry and rheology, 124–125

contribution of reversible network to viscosity of, 132–133

effect of temperature on linear viscoelastic viscosity of, 132*f*

effect of temperature on stress relaxation parameters, 130–132

gluten strength, 124

high molecular weight glutenin subunits (HMW-GS), 124–125

HMW-GS and wheat quality, 125–127

linear viscoelastic network strength, 127, 135

materials and methods, 128

parameterization of gluten stress relaxation curves, 129–130

protein content of flours and HMW-GS for three cultivars, 128*t*

stress relaxation patterns for glutens with different L-cysteine levels, 134*f*

viscoelastic materials, 124

wheat quality, 127

X

Xanthan, gelation with galactomannans and glucomannans, 30–31

X-ray fiber diffraction, structures of polysaccharides, 22–23

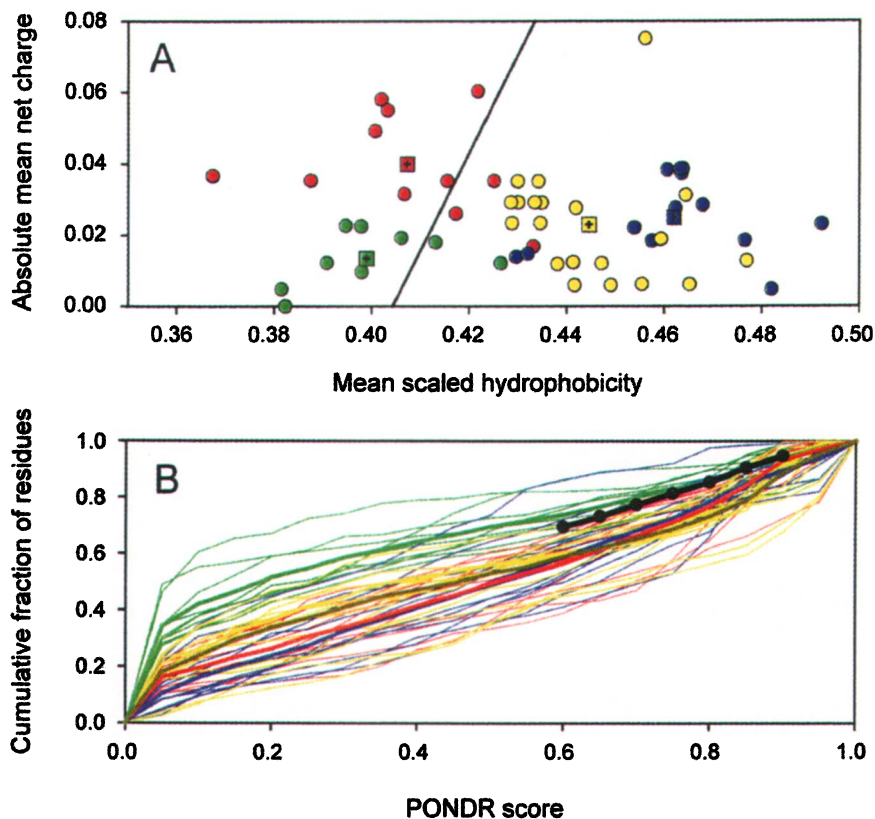


Figure 4.4. Disorder predictions on 11 α_{S1} -CNs (red symbols and lines), 9 α_{S2} -CNs (green symbols and lines), 13 β -CNs (blues symbols and lines), and 20 κ -CNs (yellow symbols and lines). **A.** CH-plot (28). The black line represents the order-disorder boundary calculated according to Oldfield et al. (30). Crossed squares correspond to the "averaged" α_{S1} -, α_{S2} -, β - and κ -CNs, for which charge and hydrophobicity values were averaged over corresponding CN subclasses. **B.** CDF analysis (29). The order-disorder boundary is plotted as black line with circles. Bold lines correspond to the "averaged" α_{S1} -, α_{S2} -, β - and κ -CNs, for which cumulative fractions of residues were averaged over corresponding CN subclasses. These calculations were performed PONDR[®] CDF and CH algorithms. Access to PONDR[®] is provided by Molecular Kinetics (www.molecularkinetics.com).

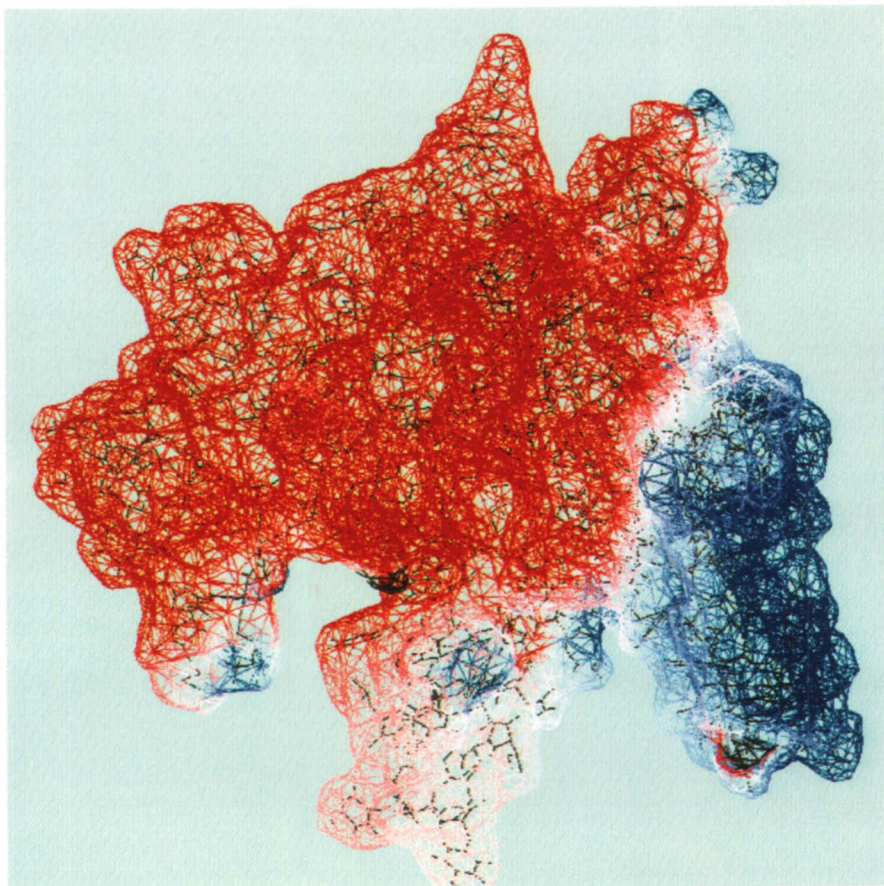


Figure 6.4. Pseudo-charge surface representation of the model of Figure 3 B. The negative charges on the top left (red) are due to the two anionic sections of the molecule. The positively charged C-terminal is on the top right (blue); this surface region would serve as a site for reaction with poly anions such as κ -carrageenan. The region of the molecule extending from the center to 6 o'clock represents the central hydrophobic core region; it is lightly colored and could react with other caseins as suggested for κ -casein (52).

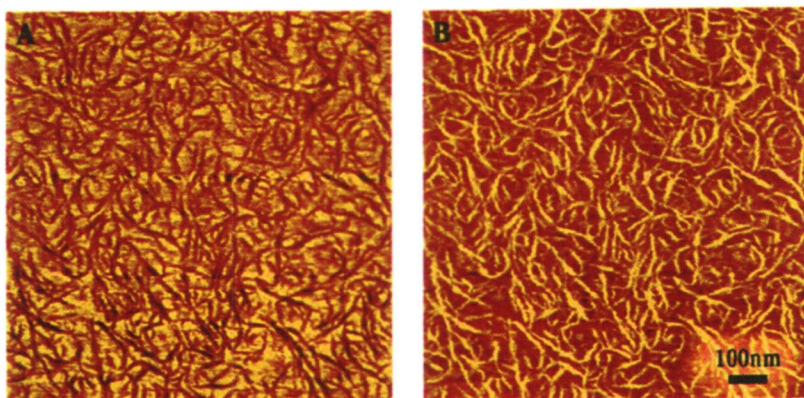


Figure 13.7. Matching images of (A) height and (B) phase-shift of an acid-gel made from commercial citrus pectin (CCP). The organization of thin clefs or depressions in the surface of the gel in (A) corresponds to the arrangement of phase-shifted or adhesive areas in (B). (Reproduced from reference 9).

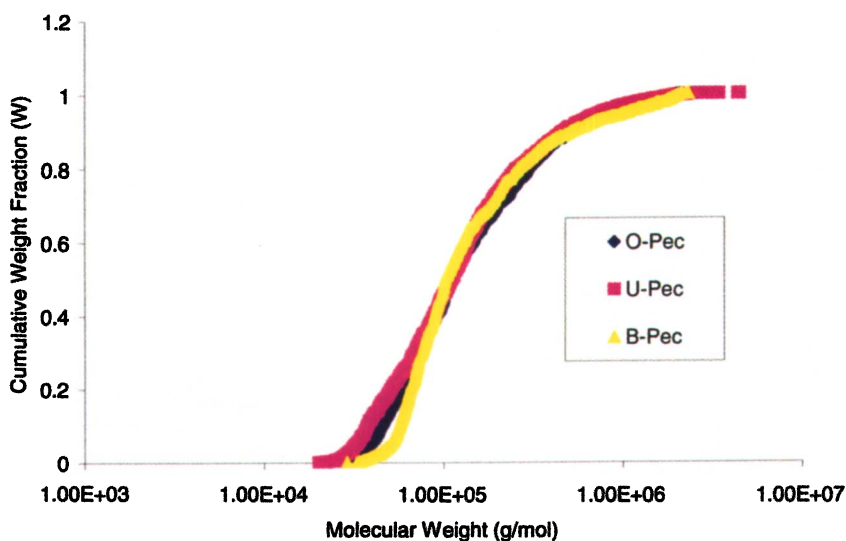


Figure 15.3. Cumulative weight fraction plotted against molecular weight of unfractionated pectin samples. (O-Pectin): original pectin. (B-Pectin): SP-unbound and HP bound pectin. (U-Pectin): SP-unbound and HP unbound pectin. Pectin modification is as described by Kim et al. {Kim, 2005 #4625}

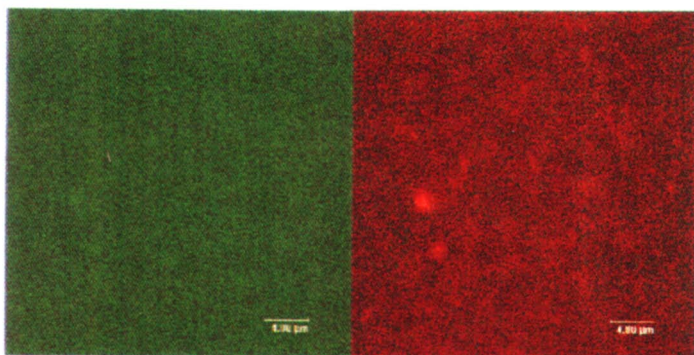


Figure 19.1. Averaged confocal fluorescence image of pectin-BSA composite films
 Left: pectin networks, ex/em, 425/475nm; right: BSA networks, 640/666 nm.

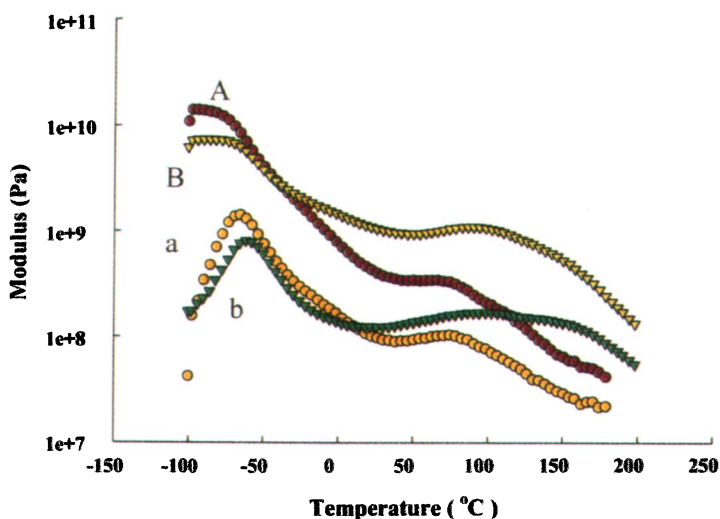


Figure 19.2. Effect of the substitution of starch (B, b) with CEA (A, a) on storage modulus (A, B) and loss modulus (a, b) for pectin composite films.

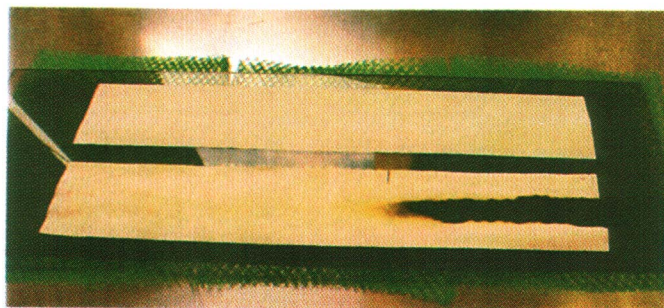


Figure 19.6. Images of papers coated with pectin-layered silicate before (top) and after (bottom) being exposed to flame.